The Electrospinning of Blended Polyaniline Nano-fibres and their Application in an Ion-Selective Electrode

by

Nathan James Newman, BAppSc (Honours)

Submitted in fulfilment of the requirements for the Degree of

Doctor of Philosophy

University of Tasmania, October 2007

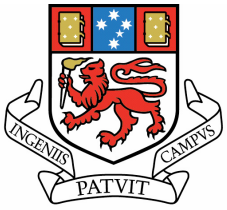

UNIVERSITY OF TASMANIA

Declaration

This thesis contains no material which has been accepted for a degree or diploma by the University or any other institution, except by way of background information and duly acknowledged in the thesis. To the best of the candidate's knowledge and belief, no material previously published or written by another person is included in the text of the thesis except where due acknowledgment is made.

Nathan James Newman

October, 2007

Authority of Access

This thesis may be made available for loan and limited copying in accordance with the *Copyright Act 1968*.

Nathan James Newman

October, 2007

Statement of Authorship

The following people contributed to the publication of the work undertaken as part of this thesis

1. *Fabrication of Nanofibers Containing Carbon Nanotubes*

   Nathan J Newman (35%), Trevor W Lewis (10%), Yong Liu[1,2] (30%), Violeta Misoska[1,2] (10%) Gordon G Wallace[1,2] (10%)

   [1]ARC Centre for Nanostructured Electromaterials, University of Wollongong

   [2]Intelligent Polymer Research Institute, University of Wollongong

   In preparation

Trevor Lewis assisted with guidance and general supervision in all aspects of producing the manuscripts

I agree with the above "proportion of work" undertaken for each of the above submitted peer-reviewed manuscripts contributing to this thesis.

_____

Dr. Trevor Lewis (Supervisor)

October, 2007

Acknowledgements

Without the professional and personal support of the following people, I would not have had the opportunity to undertake this project.

- Dr. Vahid Mottaghitalab for assistance with rheological analysis, Dr. Phil Witten for assistance with tensile testing Dr. Simon Moulton and Dr. Peter Innis for assistance with Raman spectroscopy, and Prof. Gordon Wallace for assistance in travel/accommodation, the beer and access to your laboratories and equipment (Intelligent Polymer Research Institute, University of Wollongong).

- Dr. David Steele and Dr. Jim Hutton for assistance with SEM (Central Science Laboratory, University of Tasmania)

My thanks and appreciation to the staff and fellow students at the University of Tasmania for their knowledge, assistance and support during the past eight years.

A sincere and heartfelt thankyou to Dr. Trevor Lewis for the support, guidance and supervision you have offered me. Without your efforts this work would never have reached this level, nor would have I. Thankyou.

Lastly, my thanks and gratitude to family and friends for their love and support throughout this work, and with all my endeavours. Yes Phyllis, I have got my work done.

Abstract

Polyaniline (PAni) is a conducting polymer that has shown promise in the field of composite sensors, including ion-selective and biomedical sensors. Sub-micron fibres of PAni/poly(vinyl chloride) (PVC) and PAni/poly(acrylonitrile) (PAN) have been electrospun from THF/DMF and DMSO/DMF respectively. Quaternary ammonium salts (QAS) were incorporated into these polymer blends in an attempt to produce electrospun solid-state conducting polymer ion-selective electrodes for the detection of nitrate in aqueous solutions.

The electrospinning process relies on a number of different parameters for successful fibre production, including solution viscosity, solution surface tension and solution conductivity. The role of these parameters on the electrospinning of PVC from THF/DMF solution and PAN from DMSO/DMF solution, both with and without the addition of PAni and QAS, was studied. In addition to this study, the morphology of the resultant fibres was determined by Scanning Electron Microscopy (SEM). SEM morphology and fibre-sizing analysis revealed significant changes in the morphological properties of the electrospun fibres, including bead formation and alteration of the fibre diameters with varying solution viscosity, solution surface tension and solution conductivity. It is believed this is the first time that the influences of the conducting properties of PAni on these essential electrospinning parameters have been documented.

Electrospun fibrous mats of conducting and non-conducting blends, in addition to blends incorporating QAS were analysed by Raman spectroscopy to determine the degree of doping of PAni, the influence of QAS on the chemical properties of the electrospun fibres and also the degree of dispersion of PAni throughout the electrospun

fibres. PAni was found to be relatively well dispersed throughout the underlying fibre mat. Raman spectra of PAni/PAN electrospun fibres indicated that PAN influenced the doping of PAni significantly. It produced characteristic peaks similar to those observed in the 'secondary doping' of PAni associated with increases in free-charge carriers and changes in the PAni chain conformation. This phenomenon also occurred for PAni/PVC electrospun fibres in the presence of the QAS, tetradodecylammonium bromide (TDAB) and triallylethylammonium bromide (TAEAB). It is believed that this is the first time that 'secondary doping' of PAni was induced by the normally electro-inactive species PAN or TDAB. If this is so, it indicates a strong interaction between PAni and these species which is not based on the use of dopant solvents for 'secondary doping'.

Mechanical strength measurements of electrospun fibres of these polymer blends were also carried out, indicating that the support polymer, the degree of orientation and also the components of the polymer blend significantly influence the tensile strength of these materials. However the overall tensile strength of these samples was relatively low compared with literature values for other electrospun fibres.

Cyclic voltammetry (CV) analysis of electrospun composite PAni fibres showed that PAni retains its electroactivity and produced the characteristic oxidation/reduction responses expected of PAni. It is believed that this is the first time electrochemical responses have been recorded for fibres electrospun from PAni/PVC and PAni/PAN blends. Amperometric responses for nitrate, chloride and tetrafluoroborate were observed, indicating that whilst these fibre mat electrodes were sensitive to changes in solution composition, they were not selective towards nitrate in solution, regardless of the QAS employed.

Glossary of Terms

2-NPOE	2-Nitrophenyloctylether
CSA	Camphorsulfonic Acid
CV	Cyclic Voltammetry
DBSA	Dodecylbenzenesulfonic Acid
DMF	Dimethylformamide
DMSO	Dimethylsulfoxide
ICP	Inherently Conducting Polymer
ISE	Ion Selective Electrode
MWNT	Multi-wall Carbon Nanotube
PAni	Polyaniline
PAN	Polyacrylonitrile
PEO	Poly(ethylene oxide)
PVC	Poly(vinyl chloride)
SEM	Scanning Electron Microscope
SWNT	Single-wall Carbon Nanotube
TAEAB	Triallylethylammonium Bromide
TDAB	Tetradodecylammonium Bromide
THF	Tetrahydrofuran
TOAB	Tetraoctylammonium Bromide

Table of Contents

List of Equations

List of Figures

List of Tables

Chapter 1 - General Introduction

"The most exciting phrase to hear in science, the one that heralds new discoveries, is not 'Eureka!' (I found it!) but 'That's funny ...' "

Isaac Asimov (1920 – 1992)

1.1 The Conducting Polymer Polyaniline

1.1.1 Background of Polyaniline

Inherently conducting polymers (ICPs), also termed synthetic metals, have attracted much interest since the discovery in 1977 of conducting polyacetylene by Alan MacDiarmid, Alan Heeger and Hideki Shirakawa, and the awarding of the Nobel Prize in Chemistry to these individuals in 2000 [1-3]. Since that time there has been a significant increase in the research of ICPs, initially in synthesis and characterisation, followed by the development of new materials and applications using these compounds [4].

The first recording of conducting polyaniline (PAni) was in 1862 in the United States where a partially conductive compound was discovered by the oxidation of aniline with sulphuric acid. However it was not until 1980 that the true electrochemical properties of PAni was made clear by Diaz and Logan [5], three years after the discovery of polyacetylene [4]. Since that time PAni has been studied, and in some cases employed in rechargeable batteries [4, 6], capacitors [4, 7-10], textile coatings [6, 11], corrosion protection [6, 12-15], electromagnetic shielding [15], anti-static materials [15], light emitting diodes (LEDs) [6], chemical sensors [6, 16-24], electrochromic displays [6] and separation membranes [25, 26].

1.1.2 Polymerisation of Polyaniline

Polyaniline can undergo both chemical and electrochemical polymerisation in an aqueous medium [6, 27].

The electrochemical synthesis of PAni requires that the polymerisation solution be strongly acidic to allow solubilisation of the aniline monomer, and is required to produce the conducting form of PAni. Generally the potential is held constant, or cycled within the potential range of -0.2 and +0.70 V vs. SCE to avoid overoxidising the resultant PAni film, which can lead to decreased conductivity [1, 28]. According to Yoneyama et al. and Stilwell and Park in Pud [29], this overoxidation leads to the hydrolysis of PAni due to nucleophilic attack by water in the aqueous solution, in turn converting the quinoid units to *p*-benzoquinone units. However, overoxidation also produces cross linking of PAni chains which leads to a decrease in the conductivity of PAni and reduces its solubility in aqueous solution [27, 29].

The sequence of events for PAni electrochemical polymerisation follows the scheme in Wallace et al. [1] presented in Figure 1.1. The initiation step is the rate-determining step of the process, followed by coupling of the radical cations, where a radical N or the radical in the para position are the most likely to couple. However, this is not always the case as -N=N- and para-para coupling occur with increases in pH. Furthermore, other mechanisms have been suggested that depend on the solvent, applied potential and pH [27].

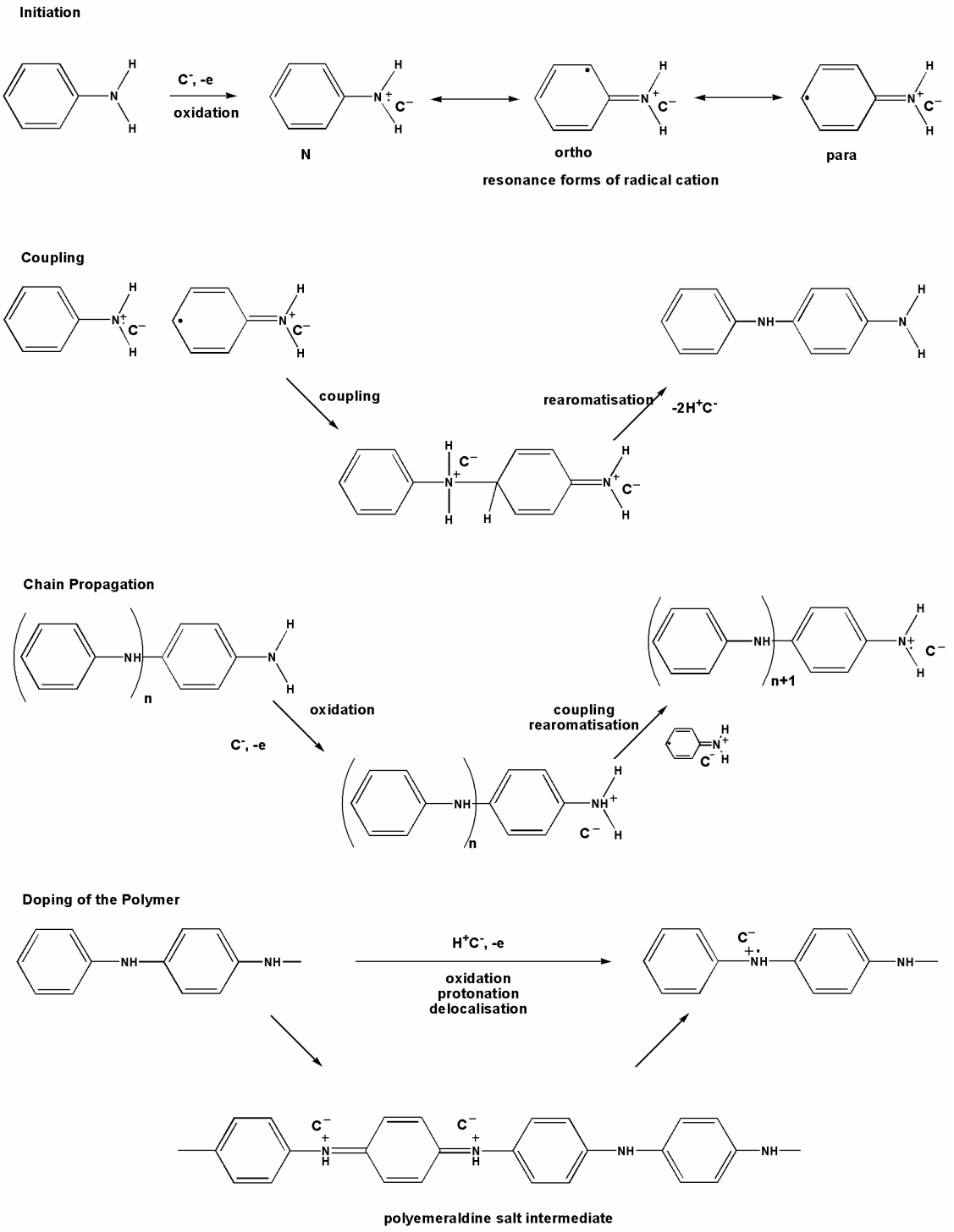

Figure 1.1 Reaction steps in the electrochemical polymerisation of polyaniline [1]

Oxidation of the oligomer form is necessary to induce chain propagation by reintroducing the radical, in turn leading to further coupling. Wallace et al. [1] note that this propagation of the chain is self-catalysing. Continued oxidation eventually produces the doped form of PAni with a positively charged nitrogen radical, also termed a

'polaron', which is delocalised over two aniline units per single charge. The introduction of a suitable counter-ion balances the positive charges along the backbone. According to MacDiarmid [30] the chemical synthesis of PAni is slightly different in that the pernigraniline form of PAni is first produced, followed by emeraldine. Pernigraniline (given in Figure 1.2) is formed due to the high oxidation potential of an ammonium peroxodisulphate/HCl mixture, which is sufficiently high to oxidise any emeraldine-state PAni. The pernigraniline product then actively oxidises any excess aniline to the emeraldine state, which is followed by the pernigraniline reducing to the emeraldine oxidation state [30-32]. Adams and Monkman [33] also observed this process and indicated that it was likely to be the result of the complete addition of the oxidant to solution in one step, as well as a low reaction temperature. It is also important to note that the type of oxidant employed and pH also affect the final properties of the PAni powder, including conductivity, yield, molecular weight and the production of other compounds [34-36].

1.1.3 Doping, Protonation and Conductivity of Polyaniline

PAni exists in one of three specific oxidation states; leucoemeraldine, emeraldine and pernigraniline, and these can exist as either a base form or a salt. The relationship between these states and structures is presented in Figure 1.2.

PAni is unique amongst ICPs as the conductivity can be controlled both chemically and electrochemically [15]. In addition PAni has the unique ability to be doped by protonation simply by the addition of an aqueous acid, as well as p-doping and n-doping of the π-system of the polymer backbone observed for other ICPs [28, 30, 37]. The terms p-doping and n-doping are derived from the doping of inorganic semiconductors. However, in the case of ICPs they refer to the oxidation or reduction, respectively, of

the insulating neutral polymer to form an ionic polymer, together with the inclusion of a suitable counter-ion to balance the charge [38]. These forms of doping change the number of π electrons along the polymer chain [39].

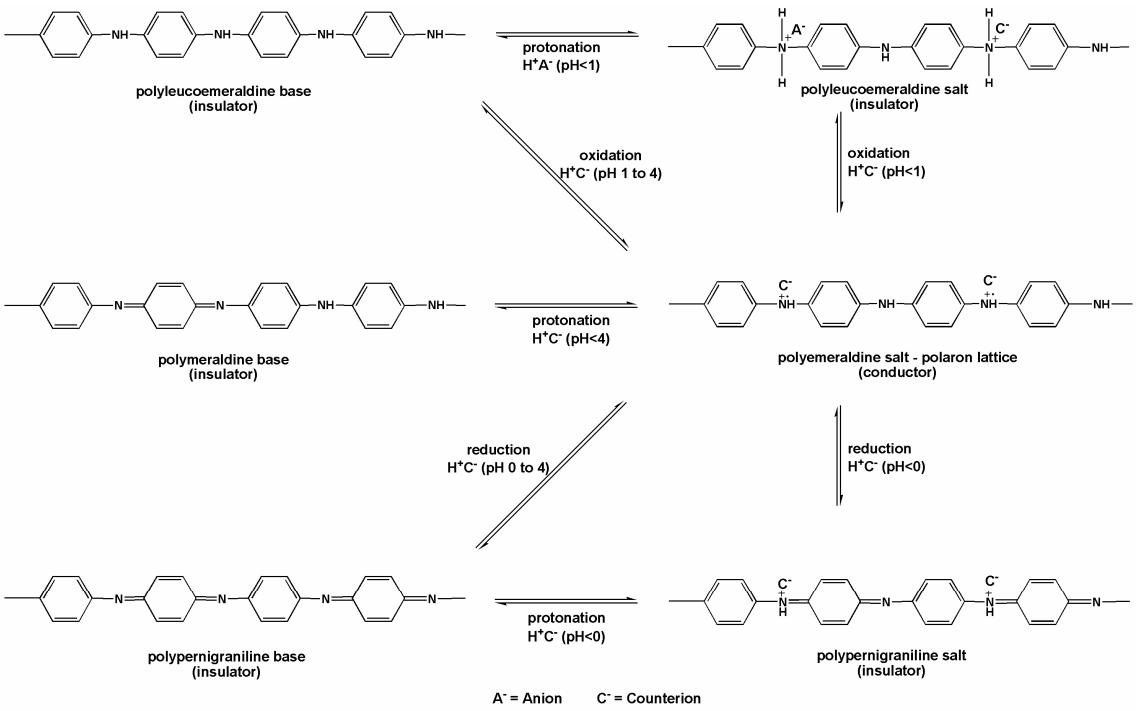

Figure 1.2 Chemical formation and redox relationships between PAni [1]

The conducting form of PAni is the emeraldine salt and requires p-doping or n-doping from the leucoemeraldine or pernigraniline states respectively, or protonation from the emeraldine base form [1]. Electrochemically, the conductive emeraldine salt form exists within a potential range of +0.20 to +0.60 V vs. Ag/AgCl, depending on pH. The non-conducting forms of leucoemeraldine and pernigraniline exist below and above this range respectively [1]. However, the rates of doping are dependent on the size, concentration and charge of the anions in the supporting electrolyte, as well as the PAni film thickness [40]. Chemically the oxidation state of PAni can also be altered through the use of various oxidants. It is important to note that actual production of pure pernigraniline is difficult. According to Kang et al. [34] pernigraniline is too unstable to

be collected in the dry state, and instead reduces slightly to produce a compound between emeraldine and pernigraniline termed nigraniline. This is also true for electrochemical treatment of PAni where electrochemical p-doping does not produce pernigraniline, but only 75% of the polymer chain is oxidised, forming nigraniline. Further increases in the applied voltage leads to hydrolysis of PAni.

The addition of a suitable acid leads to the protonation of the imine nitrogen groups on the emeraldine base, forming the conducting emeraldine salt [39, 41]. This protonation leads to the partial de-population of the π system, and the formation of a nitrogen base salt, rather than a carbonium ion seen for other ICPs. This structure is responsible for the relatively high stability of PAni [1, 37]. In the case of emeraldine, a pH greater than 4 will inhibit the ability of PAni to form emeraldine salt [1]. Ping et al. [41] note that doping of the emeraldine base commences at a pH of 6, however the doping level increases significantly at pH 4 and remains relatively constant after pH 2. However, other studies have observed the redox activity of PAni and PAni derivatives at pH greater than 4 [22, 42], and in some cases up to pH 9 [43]. The maximum doping level has been reached where 50% of the nitrogen atoms along the chain have been protonated, consistent with the doping of the imine nitrogens that make up 50% of the emeraldine structure [1, 30, 39, 41]. According to Wallace et al. [1] and Epstein et al. [44], the protonation of these imine groups produces a bipolaron structure that dissociates to form a delocalised polaron lattice. This scheme is presented in Figure 1.3.

The conductivity of PAni is due to the π delocalisation and conjugation along the polymer backbone in a form that produces an equivalent resonance structure along the chain, presented in Figure 1.4 [28].

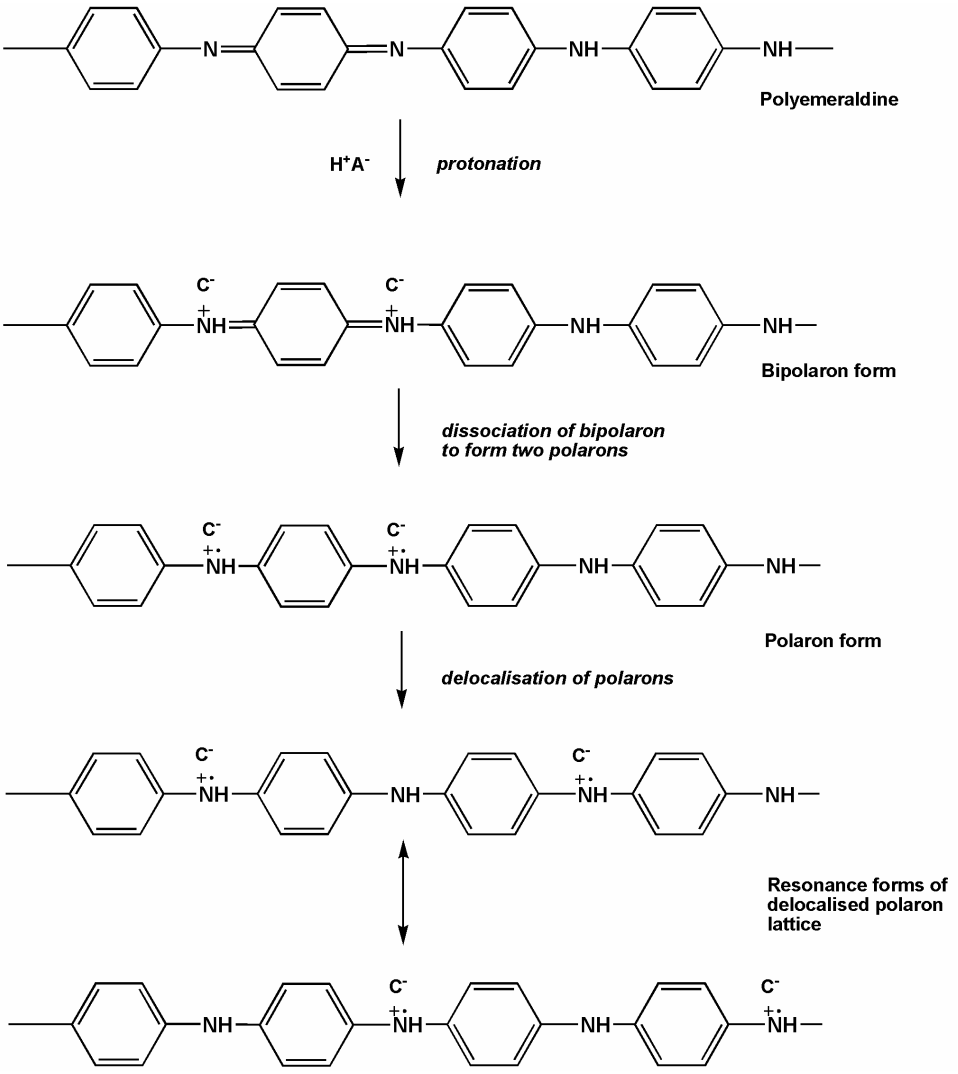

Figure 1.3 Protonation of PAni [1].

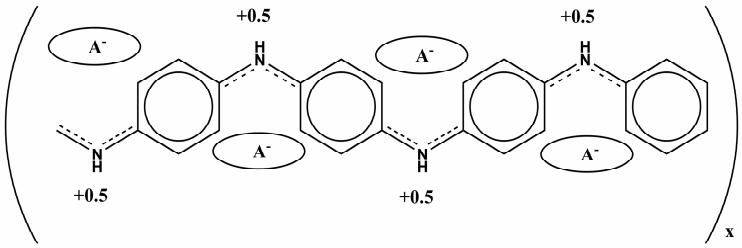

Figure 1.4 Structure of delocalised PAni [28]

Thus, alternate charged radical nitrogens are delocalised over the structure, imparting the equivalent of half a charge on each individual aniline group, and producing a polysemiquinone radical cation [28, 30]. This structure would be anticipated to impart extra stability within the polymer chain [28]. In terms of energy bands, the presence of

polarons leads to the reorganisation of the electronic structure and formation of overlapping polaron states, in turn forming half-filled polaron conduction bands that allow the promotion of electrons to unfilled bands [1, 30, 45].

Wallace et al. [1] state that the presence of the polaron conduction bands are insufficient to account for the high conductivity observed in PAni, and that intrachain and interchain charge transport mechanisms also occur. Focke et al. [46] outline a mechanism for both of these processes, with the first presented in Figure 1.5. Here deprotonated emeraldine does not offer any intrachain charge transport as the quinoidal structures cannot alter in structure; however in the protonated form intrachain transport is possible by valence resonance. This transport occurs over a large number of rings, but is prevented by defects in the structure or any deprotonated imines or protonated amines [46].

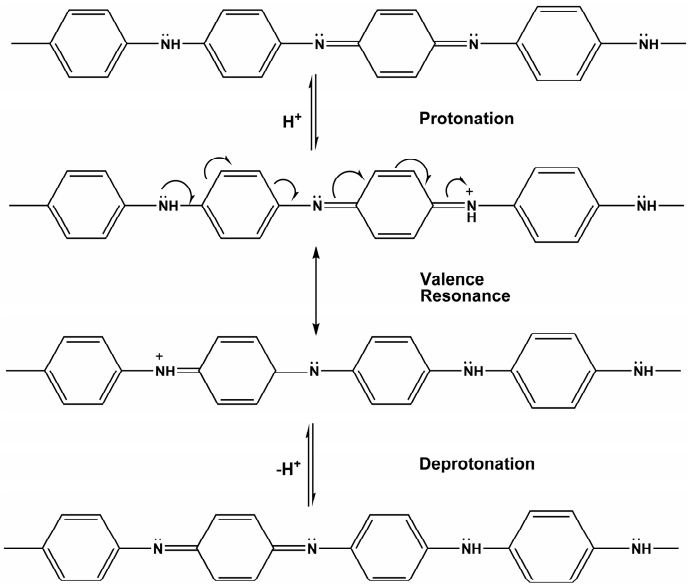

Figure 1.5 Schematic representation of intrachain transport in PAni [46]

Interchain charge transport incorporates electron transfer between the chains in addition to protonation/deprotonation similar to the intrachain transport. Initially protonation is required to form the radical cations [46]. This can be seen in Figure 1.6.

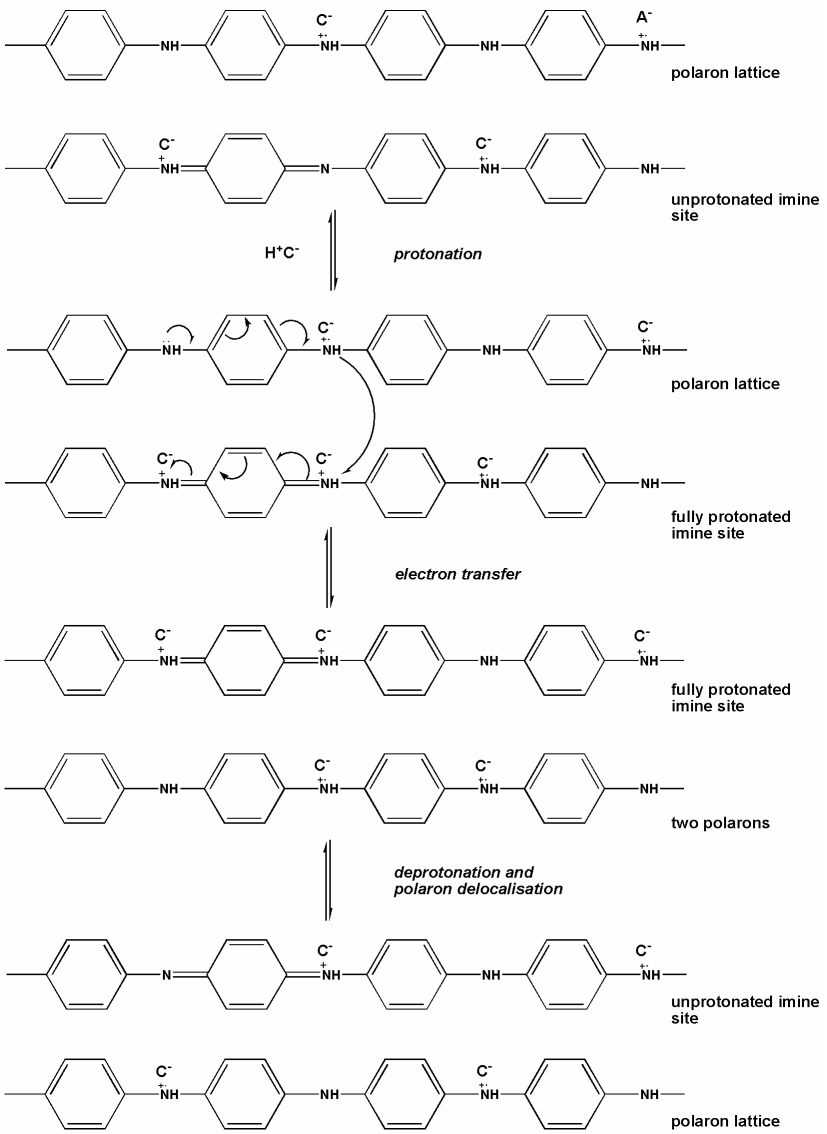

Figure 1.6 Schematic representation of interchain transport in PAni [1]

1.1.4 Factors Affecting the Conductivity of Polyaniline

According to Wallace et al. [1] the conductivity of PAni is affected by a number of factors including temperature, water content, the counter-ion, functional groups, and the preparation conditions.

Properties associated with conductivity are dependent on the granularity of the PAni where heterogeneous islands the controlling factor in the conductivity of PAni [47]. At lower temperatures there is insufficient energy to allow hopping between 'islands' of

crystalline PAni, whilst higher temperatures lead to scattering of the charge carriers by phonons [47-49].

Focke et al. [46] indicate that an increase in humidity, and hence water content, increases the conductivity of PAni. However, this is affected by the pH of the solution in that a lower pH will induce a lower resistance in the presence of moisture, whilst a higher pH will produce a higher resistance under the same conditions. However, in both cases the resistance decreases with increasing percentage of moisture. The interchain and intrachain transport mechanisms for conductivity rely on the presence of moisture for proton transport and also the presence of protic solvents for proton exchange. Focke et al. [46] also reported that the type of anion employed makes a difference to the conductivity of PAni. Using Cl^- as a counter-ion, PAni had the lowest resistance at pH 2 and at 0.28 V vs. SCE, whilst the resistance slightly increased for other anions. However, a Hydrion® buffer (tartaric, phosphoric and phthalic acid) did increase the resistance by 60% compared with the HCl/KCl solution [46]. Whilst the counter-ions employed appear to only slightly alter the conductivity of PAni, the mobility of the ions significantly influences the capacitance of PAni [50].

The preparation conditions of PAni have also been identified as a major factor in the conductivity of PAni. Stejskal and Gilbert [51] observed a standard deviation of 40% for PAni conductivity based on a standard method and using 59 samples from various research groups. In addition, they state that this is comparable with 35 samples prepared by a single individual who observed a standard deviation of 39%.

1.1.5 Surfactant Counter-ions and Polyaniline Blends

Cao et al. [52, 53] studied the use of different protonic acids to assist the dissolution of PAni in various solvents. They observed that some acids possessing an organic functional group actively assist dissolution of PAni in non-polar or weakly polar solvents, with the acid component protonating the PAni and the negatively-charged component acted as a counter-ion. In essence, the organic functional group acted as a surfactant within the solvent, increasing the ability of PAni to dissolve. The conductivity of the PAni was dependant on the choice of counter-ion and the solvents, and this conductivity could be increased beyond those of ordinary PAni powder. Such functionalised protonic acids include camphorsulfonic acid (CSA) and dodecylbenzenesulfonic acid (DBSA).

The benefit of using these functionalised protonic acids is to enhance processing of PAni, with a particular view towards PAni blends with non-conducting polymers, such as poly(vinyl chloride) (PVC). Processing PAni in this way, PAni can be dissolved in previously unsuitable solvents. This in turn expands the blends of PAni/commodity polymer possible, and in turn increases the processability of these blends [53].

Kaiser [48] studied the conductivity of PAni dispersed throughout non-conducting support polymers. The blended PAni was similar to non-blended PAni in terms of the metallic behaviour, however the overall conductivities were lower compared to non-blended PAni, and they exhibited a trend towards zero conductivity at a temperature of absolute zero. One interesting observation was that the protonation of PAni in the poly(methyl methacrylate) (PMMA) blend using an organic acid led to conductivity higher than the unblended PAni. According to Subramaniam et al. and Wessling et al. in Kaiser [48], this was due to a reduction in the barriers surrounding PAni particles.

Another benefit that has been observed from the use of functionalised protonic acids to assist dissolution is the concept of 'secondary doping' of PAni. Avlyanov et al. [54] observed that the use of CSA in poor solvents, that is those that offer little polymer/solvent interaction, will lead to a compact coil conformation of PAni. Conversely, the use of a good solvent, that is those that offer a greater polymer/solvent interaction, will lead to an expanded coil formation by solvating both the positive charges on the PAni chain, and the negative charges from the CSA counter-ion. This expanded coil leads to an increase in the linearity of the PAni chain, and hence an increase in the conductivity through a reduction in chain defects associated with twisting [54, 55].

1.2 Electrospinning

Electrospinning was first patented by Formhals in 1934 who electrospun cellulose acetate from acetone [56]. Initially he encountered difficulties in collecting dry fibres, but later developed the process further to overcome these problems [57]. With the re-discovery of electrospinning there has been in increase in the research incorporating electrospinning as a technique in the last fifteen years [58]. The applications cover a wide array of fields and include chemical sensors [59-63], biosensors [64-66], tissue scaffolding [67-70], drug delivery systems [70-73], optical sensors [74-76], molecular electronics and other electronic devices [77-79].

The basic premise of electrospinning is the application of an electric potential between a polymer solution held within a capillary-type structure, such as a syringe or pipette, and a metallic 'target' (Figure 1.7). This applied potential overcomes the surface tension of the polymer blend by charging the surface of the fluid and ejecting a jet from the apex of the polymer droplet. As this jet traverses the air gap between the capillary and the

target, the solvent evaporates and a polymer fibre forms, eventually depositing on the electrically grounded target [57, 65, 80-82]

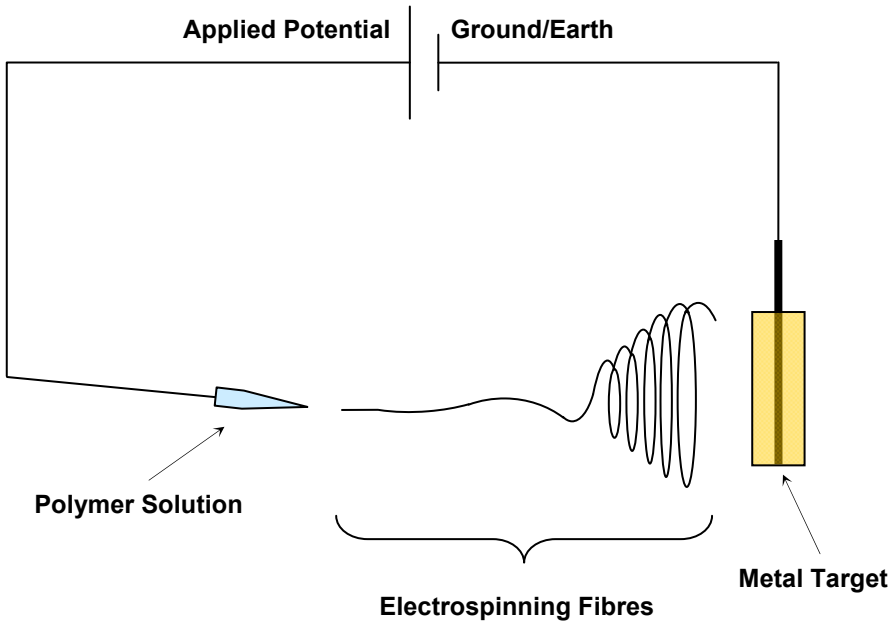

Figure 1.7 Basic apparatus for electrospinning

1.2.1 Jet Initiation and Stretching

Sessile and pendant droplets of polymer will attain stable shapes with the application of a potential, provided that this potential does not exceed a critical value. According to Yarin et al. [83] the droplet will form these shapes due to the equilibrium of electrical forces and the surface tension of the solution. At the critical potential the droplet will form a conical shape with a critical half angle of 49.3^{o}. This initial droplet at the end of a pipette or syringe in electrospinning is also often referred to as a Taylor cone [57]. However, Yarin et al. [83] state that in an elastic or unrelaxed viscoelastic fluids the critical half angle is closer to 33.5^{o} due to both elastic forces and surface tension. After this critical potential, the equilibrium between the electrical forces and surface tension will cease as the charge overcomes the stabilising affect of the surface tension, and a

liquid jet will form corresponding to observations made by Raleigh over 100 years ago with regards to charged liquid droplets [65, 83, 84].

Hayati [85] noted axisymmetric circulation of the solution inside the solution cone due to interfacial shear stresses. These shear stresses are observed in solutions where the surface can support charge, and are the result of an electric field tangential to the direction of flow for a fluid. The shear stresses attempt to stabilise the jet surface by evening out disturbances on the surface of the polymer droplet. The surface charge is a result of the electric field directing free charges in the solution to the surface of the cone, whilst the solution must possess semi-conductivity to produce a potential drop between the base of the cone at the edge of the pipette/syringe and the tip of the solution cone. This potential drop generates the tangential electric field, creating the shear stresses on the surface of the cone and in turn producing the axisymmetric circulation. Highly conducting solutions, such as water, do not exhibit these shear stresses as the potential drop is negligible, preventing conducting liquids from producing stable sprays. Jet formation in these semi-conducting solutions results in stripping the solution from the drop surface, rather than the ejection of a polymer stream that is often identified in literature [85]. It is this shearing of polymer from the cone that leads to more concave cone shapes rather than a Taylor cone [80].

Scuador et al. [86] observed that the critical potential required for jet formation was dependant on the viscosity, surface tension, conductivity and dielectric constant of the fluid. Shin et al. [80] noted that altering the protrusion of the syringe in a uniform electric field can increase the effect of the electric field and lower the initial potential required for jet initiation. Fong and Reneker [65] also observed that the potential for jet initiation is higher than the potential required to maintain jet flow. Furthermore, they

also reported that the conical-shaped droplet will relax and convert to a spherical structure after jet initiation for poly(ethylene oxide) (PEO) dissolved in water.

During stretching of the polymer jet, the transient extensional viscosity increases as the polymer chains uncoil, termed strain hardening. If a steady stretching rate is achieved the elongational viscosity can decrease or increase, leading to extension thinning or thickening, respectively. These processes affect the ultimate production of fibres due to the axial tensile strength of the jet resisting stretching. In addition the presence of strain hardening suppresses stretching further along the jet, in turn producing fibres with a larger diameter [81].

It is important to note that whilst a single syringe or pipette is most often used as a container for jet formation, other approaches have been taken. Wang et al. [75] utilised two pipettes that enabled concurrent electrospinning of two separate solutions, allowing cross linking of the polymers and to overcome problems associated with jet initiation. Madhugiri et al. [77] used a dual syringe method to electrospin composite molecular sieve fibres to overcome mechanical strength issues encountered when spinning molecular sieves. Fibres have also been electrospun without the use of any capillary-type structure. Yarin and Zussman [87] employed a magnetic fluid that was influenced by a magnetic field. This produced a number of vertical spikes of magnetic suspension that disturbed the surface of the polymer solution. In turn the application of a potential produced multiple jet filaments from the polymer, electrospinning towards a counter electrode. The benefit of this design was an increase in the production of nanofibres and a reduction in the problems associated with capillary blockage.

1.2.2 The Whipping Jet

The second stage of electrospinning is the development of a non-axisymmetric bending instability, also referred to as the whipping instability that produces bending and stretching of the polymer jet after initiation [81].

Hohman et al. [82, 88] and Shin et al. [89] quantified this whipping instability. They stated there were three different types of instabilities affecting a polymer jet. The first was the *Rayleigh mode* where axisymmetric extension occurs based on the Rayleigh instability. This is the break-up of a liquid cylinder into droplets as a result of solution surface tension. This instability is suppressed when the applied electric field and the surface charge density exceeded a threshold value based on the surface tension and the dielectric constant of the jet. It is important to note that this instability develops faster for polymer jets; however extensional stresses stabilise and compete with this instability to prevent break-up of the jet. The second instability identified by Hohman et al. [82, 88] and Shin et al. [89] was an *axisymmetric conducting mode* that is present in a high electric field, and the third was a non-axisymmetric *whipping conducting mode*. The axisymmetric conducting mode is a product of the finite conductivity of the solution, whilst the whipping mode is the product of the dipole charges within the jet that interact with the external electric field, in turn bending the jet by the application of a twisting force.

Additionally, the repulsion of charges on the jet surface can also lead to bending of the jet [82, 88-90]. This charge repulsion affect has also been identified by Fridrikh et al. [91] who stated that this was the major contributor to the whipping instability, and that the wavelength and growth rate of the instability are controlled by the inertia of the jet,

the charge repulsion and the shear viscosity of the solution. The charge repulsion model is given in Figure 1.8.

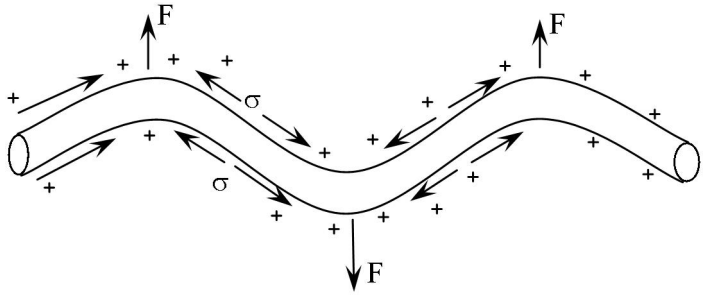

Figure 1.8 Whipping instability and the surface charge repulsion [91]

The two conducting modes are independent of surface tension, but instead are enhanced with an increasing electrical field and surface charge density. The type of instability that occurs is dependent on the viscosity, dielectric constant and conductivity of the solution [82]. For example, a solution exhibiting high conductivity with no static charge density on the jet will exhibit the axisymmetric conducting mode, whilst a solution with a large static charge density will exhibit the whipping mode. The Rayleigh mode is suppressed in both cases due to the high surface charge [88]. Furthermore, Zuo et al. [92] note that a high applied potential suppresses both the Rayleigh and conducting axisymmetric modes whilst the whipping mode is enhanced.

Reneker et al. [93] and Fong and Reneker [65] noted three stages of the bending instability in a PEO/water solution. The first stage was the uniform jet developing a number of bends in its structure. This was followed by the second stage where the jet elongates and develops spiralling, concentric loops. Lastly, as these loops increased in diameter the cross-sectional diameter of the jet decreased and the conditions for the first step recurred, producing a secondary instability on these large loops in which the jet again bends and loops. Thus, the elongation and decrease in the diameter of the jet

continued for as long as there was sufficient force from the applied potential to induce the whipping instability and to overcome the surface tension and viscoelastic forces [65, 93].

Both reports note a high area reduction ratio. For example, in a jet with 50 μm diameter and final fibre diameter of 500 nm, there was an area reduction ratio of 10,000 [65, 93]. According to Fong and Reneker [65] the evaporation of the solvent accounts for a factor of 16, the initial elongation of the straight jet accounts for a factor of 5 and the whipping jet accounts for a factor of 125. Furthermore, it was anticipated that the polymer chains were elongated and orientated axially during electrospinning.

In addition, Fridrikh et al. [94] note that the fibre diameter produced from a whipping jet is determined by the surface tension and the surface charge repulsion, and can be controlled by flow rate, electric current and the surface tension of the solution.

It has been widely reported that the jet splits into many smaller jets as it travels towards the target [69, 75, 95-98]. Other literature indicates that the fibre is a single jet that whips and rotates at a rate sufficiently fast to give the appearance of multiple filaments splitting from a main fibre [80, 99-101]. However the electrospinning jet can exhibit both this splitting of the jet (termed ‘splaying’) and whipping, whereby the secondary splaying fibres will eject from the main whipping jet [93, 102, 103].

1.2.3 Fibre Collection

The collection of electrospun fibres requires an earthed or grounded target to ensure completion of the electrical circuit. This target can consist of a sheet of metal or a metal mesh screen, both of which can be covered with a fabric to collect the fibres, a coagulation bath, or a rotating collection target [57, 99-101, 104].

Liu and Hsieh [96] indicated that the type of target used can affect the morphology and fibre density of the collected fibres. Specifically, electrically conducting targets will allow a greater density of fibres to be collected as the target will dissipate electrical charges, in turn reducing the repulsion of incoming charged fibres. However Reneker and Chun [104] note that dry fibres with low electrical conductivity may be slow to dissipate the electrical charge to the underlying target. Non-conductive targets will produce a lower density and greater porosity throughout the fibrous surface. In addition Liu and Hsieh [96] observed that fibres of cellulose acetate collected on paper connected to an electrically grounded target were smoother in appearance, offered more uniformity in the fibre diameter and fewer defects.

Theron et al. [100] used a rotating disc to collect electrospun fibres; however the edge of the disc was the target and not the planar side. They observed the whipping jet expanded in a helical and concentric spiral in a similar manner to the observations other literature [65, 80, 88, 99, 101, 105], followed by a contraction in this concentric spiral. The edge of the disc affected the electric field set up in electrospinning process, such that this field converged towards the edge of the disc, in turn directing the whipping jet towards the edge of the disk. In addition, this rotation led to the alignment of the electrospun fibres in a uniform orientation [100].

1.2.4 Electrospinning of Non-Conducting Polymers

A significant number of commodity plastics have been shown to electrospin and produce fibres [71, 96-98, 105-127], or have been blended with other materials to produce composite electrospun fibres [59, 69, 72, 76-78, 84, 116, 122, 128-140].

Formhals [56] patent in 1934 is the first documented attempt at electrospinning polymer solutions, in this case the spinning of cellulose acetate solutions and cellulose derivatives. However, according to Norris et al [58] it is only during the last decade that the interest in electrospinning has grown, sparked by Doshi and Reneker's paper in 1995 on the electrospinning of poly(ethylene oxide) (PEO) [141]. A review by Subbiah et al. [57] outlined 24 different polymer or co-polymer solutions and five composite polymer solutions that had been successfully electrospun, including poly(vinyl chloride) (PVC) from tetrahydrofuran (THF)/dimethylformamide (DMF) [142], polyacrylonitrile (PAN) from DMF [143], polycaprolactone (PCL) from acetone [105], polyurethane (PU) from DMF [107], poly(methyl methacrylate) (PMMA) from DMF[119] and polystyrene (PS) from THF/DMF [144].

Composites of electrospun fibres have also been successfully electrospun and include conducting polymers [16, 58, 78, 79, 129, 131, 140, 145-147], chitosan and PEO composites from acetic acid [69, 72], gelatine and PCL from 2,2,2-trifluoroethanol (TFE) [139], nylon and montmorillonite (MMT) from hexafluoroisopropanol and DMF [130], and a solution of PU and organically modified MMT from N,N-diemthyl acetamide (DMAc) and THF [134].

1.2.5 Electrospinning of Conducting Polymers

There have been only limited studies on the electrospinning of neat PAni or of PAni/polymer blends. Reneker and Chun [104] successfully electrospun PAni fibres from concentrated H_2SO_4 without the need for a support polymer, and this was also emulated by MacDiarmid et al. [79] who reported an average fibre diameter of 139 nm. Other research centred on the electrospinning of PAni/PEO electrospun fibres by Norris et al. [58] and MacDiarmid et al. [79], although difficulties were encountered in

achieving true nanofibres with diameters below 100 nm for this blend. These fibres exhibited a lower electrical conductivity, measured by a four-point probe method, but according to MacDiarmid et al. [79] this was attributed to difficulties in the measuring process, and also the porous nature of the electrospun fibres compared with a film possessing the same composition. However, MacDiarmid et al. [79] did electrospin PAni/PS fibres with an average fibre diameter of 43 nm.

Other PAni/polymer composites have also been electrospun since then, including sulfonated PAni and PU from DMF, and sulfonated PAni and PAN from DMF [78], PAni/PMMA fibres from various solvents [129, 148], PAni/polycarbonate (PC) from chloroform [146], PAni/nylon-6 from formic acid [149], superhydrophobic PAni/PS from DMF [150], PAni/gelatin from 1,1,1,3,3,3-hexafluoro-2-Propanol (HFP) [151], and PAni doped with 2-acrylamido-2-methyl-1-propanesulfonic acid and electrospun into an acetone bath [152].

1.3 Nitrate

1.3.1 Nitrate Contamination and Health

The four main sources of nitrate in the environment are: human and animal waste, plant residues, fertilisers and the fixation of atmospheric nitrogen. In Australia these sources can include human waste water effluent, landfills, farm/feedlot animal wastes, influence of clearing/stocking, and degradation of natural vegetation [153]. Additionally, the concentration of free nitrate within the soil increases with respect to the application of fertiliser [154]. According to Eichler and Schulz [155] almost half of all nitrogen compounds in Germany were derived from agricultural sources, followed by transport, industrial processes and wastewater, with 59% of the nitrogen from these sources discharged into the atmosphere.

The processes that nitrate undergoes in the soil include mineralisation, nitrification and denitrification. Mineralisation is the conversion of organic nitrate forms, such as bacterial amino acids, to inorganic nitrate forms by aerobic bacteria. Nitrification is the conversion of the ammonium ion to nitrate via nitrite, which allows the nitrogen to become more mobile throughout the soil structure and can lead to nitrate migration through to groundwater. Denitrification is the removal of nitrogen from the soil and groundwater by the reduction of nitrate to gaseous nitrogen by anaerobic organisms [156].

In terms of human health, nitrate is associated with the condition of methaemoglobinaemia whereby haemoglobin is oxidised to methaemoglobin, reducing the ability of blood to carry oxygen. This process is a result of the reduction of nitrate to nitrite in the gut, and nitrite then causes methaemoglobinaemia [156]. According to *Nitrates: An Environmental Assessment* prepared for the United States Environmental Protection Agency, it is the nitrite form that is toxic to humans rather than the nitrate form, however microbial activity produces the nitrite form in the gut [157].

There has also been an interest in nitrate as a precursor to the production of carcinogenic nitrosamine compounds with studies carried out on the relationship between these compounds and human cancer rates. However, at this point there is no conclusive evidence to indicate that ingested nitrate can cause cancer [157]. This is also the case for other conditions possibly induced by nitrate exposure, including type-1 diabetes [158], hypertension, birth defects of the central nervous system and increased infant mortality [156, 157].

In conjunction with other nutrients, the addition of nitrate to river systems and watercourses can lead to eutrophication [156, 157]. In essence this is enrichment of water systems with nutrients, leading to the rapid growth of biota such as toxic algae blooms, a decrease in algae diversity, decreases in the diversity of flora and fauna, and a decrease in the dissolved oxygen within the system [157].

1.3.2 Current Methods of Nitrate Analysis

Nitrate can be analysed using various techniques, however there are problems associated with each technique that limits the accurate determination of nitrate concentration [157].

Nitrate can be directly analysed by UV spectroscopy at 220 nm in aqueous samples without any prior treatment. However, samples for this analysis require that there is little organic material in the sample. Organic matter can also absorb at this wavelength, but can be corrected for by a second measurement at 275 nm where nitrate does not absorb. This correction is only suitable when the organic matter is constant in terms of properties and concentration. Other interferents include surfactants, nitrite, chromium (VI), and in some cases chlorite and chlorate. Furthermore, other processes can be incorporated with spectroscopy to determine nitrate, including the reduction of nitrate to nitrite by cadmium reduction or hydrazine reduction [159].

Ion chromatography can also be used in the detection of nitrate in aqueous samples and is the most common method for the determination of nitrate in water. However, there are problems associated with co-eluting contaminants or high concentrations of other anions in solution that can limit the detection and resolution of the nitrate response [156, 159].

Another popular technique is the use of nitrate-selective electrodes to determine nitrate concentration in solution by potentiometry. However, some interference occurs in the presence of other ions such as Cl^-, as well as requiring the test solution to be buffered for pH and ionic strength. This is necessary as the activity of nitrate, rather than the direct concentration is analysed [156, 157, 159].

1.3.3 Theory of Ion-Selective Electrodes

According to Horvai et al. [160] the first ion-selective electrode (ISE) was the glass electrode used for pH measurement in the early 1900s. Work by Nicolsky on ion exchangers in the 1930s initiated the research into suitable membranes for ISEs, however it was not until the 1960s that this field began to expand [160, 161]. Since then further study into ISEs have looked at miniaturisation, development of electrode arrays and the production of biosensors [160].

The type of electrode used for analysis can vary and include glass membranes for cations, homogeneous and heterogeneous solid state membranes and liquid membranes for cations and anions [162, 163]. In terms of operation, the glass electrode relies on the formation of a potential difference between the inner surface of the membrane in contact with an internal solution, and the outer surface of the membrane in contact with the test solution. The inner solution has a constant ion activity such that an ion-exchange equilibrium between H^+ ions in the internal solution and Na^+ ions in the glass membrane at the internal boundary occurs. Such an equilibrium also occurs for the external test solution and the external boundary, however this varies according to the concentration of the analyte. It is this difference in association/dissociation between the two solutions that leads to the formation of a potential difference across the glass membrane, in turn allowing the measurement of the concentration of the analyte [163].

Solid state electrodes can sometimes vary in the mechanism of response towards the detection of a species in solution. For example, silver sulfide electrodes can detect both silver and a halide, depending on the composition of the electrode. The silver sulfide electrode dissolves slightly such that the film of liquid next to the electrode becomes saturated and forms an equilibrium with the external test solution. The solubility of the silver sulfide is dependent on the concentration of the silver or sulfide species in solution. Due to the insolubility of this material it is unlikely that both will be present in solution together. Again boundary potentials develop at the internal and external surfaces due to this equilibrium, in turn corresponding to the concentration of the analyte [163].

Modern liquid membrane electrodes rely on the immobilization of ion exchangers in plastic membranes, such as PVC, that separates the test solution from an internal reference solution. The mechanism and response is analogous to a glass membrane electrode. In this case a potential difference exists across the polymeric membrane between the internal surface in equilibrium with an internal reference solution and the external surface in equilibrium with the test solution [163]. These ion exchangers vary according to the specific analyte to be analysed and include quaternary ammonium salts (QAS), basic dyes, complex cations with 1,10-phenanthroline, quaternary phosphonium, quaternary arsonium, derivatives of tetraphenylborate, aromatic nitrocompounds, and aromatic sulfonates [164]. According to Johnson and Bachas [165], plasticisers are often employed in polymer ISEs to lower the glass transition temperature to below room temperature. This results in membranes that possess suitable conductivity and mechanical properties, and allow the diffusion of species through the membrane. In addition it has been reported that changes in the composition and concentration of the plasticiser alter the response to test species in solution [164]. For example, Akl et al.

[166] observed that incorporating the Cr^{3+} ionophore dibenzo-18-crown-6 (DB18C6) with 2-nitrophenyloctylether (2-NPOE) and bis(ethylhexyl)sebacate (DOS) produced PVC membranes with Nernstian responses. However, the responses for PVC membranes with blends of DB18C6 with dioctyl phthalate (DOP) and didecyl phthalate (DDP) were sub-Nernstian, indicating the type of plasticiser employed can affect the response of the ISE. According to Johnson and Bachas [165] these differences are a result of the polarity of the plasticisers, and there may be some relationship between the rigidity of the polymer membrane and the selectivity of the ISE.

Current ISEs do have problems associated with the operation and determination of species in solution. Most potentiometric ISEs respond to the activity of the ion in solution, rather than the concentration. This activity is directly related to the concentration of the species of interest via the activity coefficient [167]. Interfering ions can lead to a deviation from the Nernstian response of an electrode giving a false increase in the activity of the test ion, while the presence of an ion with opposite charge can lead to a decrease in the Nernstian response of the ISE [160].

1.3.4 Ionophores

1.3.4.1 Quaternary Ammonium Salts (QAS) as Ionophores in ISEs

According to Johnson and Bachas [165] quaternary ammonium salts (QAS) are generally employed in ISE membranes when a cationic site is required for anionic reception. These salts vary in structure, thermal stability, lipophilicity (to prevent solubility in the aqueous phase), compatibility with other components of the membrane and the selectivity towards species of interest. The ion-exchanging quaternary ammonium salts themselves are limited in selectivity and the response is based on the lipophilicities of the anions according to the Hofmeister selectivity series [164, 165].

Feng [164] notes that ion exchangers that deviate from the Hofmeister selectivity series are termed second generation ion-exchangers. In addition, various factors influence the ion association with quaternary ammonium salts, including the ionic mobility in solution and in the membrane, and the hydration energy of the ions. Structural effects of the quaternary ammonium salts also contribute to the degree of association and are influenced by electrostatic interaction, hydrogen bonding and steric factors. As a result the selectivity towards species in solution can be altered through altering the structure of the salts [164].

Braven et al. [168], and Ebdon and Braven [169, 170] observed selectivity towards nitrate for a number of triallylalkylammonium bromide salts within hot-pressed acrylonitrile-butadiene membranes. Braven et al. [168] reported that the limit of detection and the selectivity coefficient with respect to Cl^- could be improved with increasing alkyl chain length up to 10 carbon atoms. This phenomenon was also observed by Nielsen and Hansen [171] for a range of tetraalkylammonium nitrate QAS, including tetraheptylammonium nitrate (THAN), tetraoctylammonium nitrate (TOAN), and tetradodecylammonium nitrate (TDDAN). In addition they state the selectivity coefficients remain relatively constant at longer chain lengths, such that alkyl chain lengths greater than 12-14 carbon atoms offer no major benefits, and that the synthesis of longer chain QAS is significantly more difficult.

Quan et al. [172] observed changes in the selectivity of nitrate with changes in the composition of the polymeric membrane possessing a quaternary ammonium salt. These electrodes consisted of the conducting polymer polypyrrole (PPy), tetraoctylammonium bromide (TOAB), PVC and 2-nitrophenyloctylether (2-NPOE). Increasing the mass of TOAB and PVC, and keeping the mass of 2-NPOE constant, led to a decrease in the

sensitivity of the electrode towards nitrate, and also slightly changed the selectivity series of the membrane. Shishkanova et al. [20] also observed responses inconsistent with the Hofmeister series for a range of anions, including F^-, Cl^-, $H_2PO_4^-$, Br^-, NO_3^- and ClO_4^-. These species were analysed by electrodes consisting of tridodecylmethylammonium chloride (TDDMACl), PVC and PAni. According to Shishkanova et al. [20], the presence of the conducting polymer PAni significantly influenced the potentiometric response towards these solution anions in the presence of the QAS, with the PAni facilitating the movement of anionic species through to the PVC matrix, and in the case of highly solvated ions such as F^- and $H_2PO_4^-$, increasing the sensitivity of the sensor.

1.3.4.2 2-Nitrophenyloctylether (2-NPOE)

2-NPOE has been used as a plasticiser in PVC-based ISEs incorporating different ion exchange species [166, 169, 170, 172-175]. Arada Perez et al. [173] observed that the incorporation of 2-NPOE produced ISEs with lifetimes greater than 6 months, and in combination with membrane components, offered good selectivity towards nitrate. As mentioned in Section 1.3.3, Akl et al. [166] observed good Nernstian responses for PVC membranes incorporating the Cr^{3+}-selective ionophore DB18C6, and 2-NPOE as the plasticising agent, compared with other plasticisers. The structure of 2-NPOE is presented in Figure 1.9.

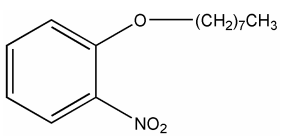

Figure 1.9 Chemical Structure of 2-nitrophenyloctylether (2-NPOE)

It is important to note that significant concentrations of 2-NPOE are used in devices reported in the literature, often in the order of 2:1 w/w ratio compared with PVC to induce the mechanical and chemical properties required [165]. For example Santos et al. [174] prepared electrodes containing 66% w/w 2-NPOE and 33% w/w PVC dry weight, whilst Quan et al. [172] utilised compositions of 91% w/w 2-NPOE and no lower than 75% w/w dry weight.

1.3.4.3 Tetraoctylammonium Bromide (TOAB)

As mention in Section 1.3.4.1, Quan et al. [172] fabricated an amperometric nitrate selective electrode incorporating PPy, PVC, 2-NPOE and TOAB. The structure of TOAB is presented in Figure 1.10.

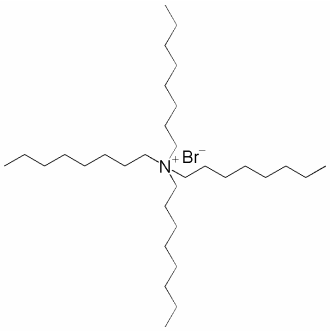

Figure 1.10 Chemical structure of tetraoctylammonium bromide (TOAB)

The use of TOAB was also reported by Santos et al. [174], however in this case TOAB was employed to alter the lipophilicity of the membrane, stabilise the ionophores of tin(IV)-porphyrins, influence the selectivity of the membrane, and prevent the formation of a negatively charged membrane due to binding of phthalate anions with the neutral tin porphyrins. It was observed that TOAB was necessary to achieve an optimal potentiometric response. In addition the selectivity profiles of the membranes tested showed that selectivity towards nitrate remained relatively constant throughout the

blends containing TOAB. However, the electrodes were more selective towards salicylate and thiocyanate than nitrate, but less selective towards NO_2^-, Cl^- and CH_3COO^-.

1.3.4.4 Tetradodecylammonium Bromide (TDAB)

TDAB has been previously utilised as an additive for the production of a potentiometric nitrate ISE by Lu et al. [176]. They prepared this membrane by dissolving PVC as the support structure, TDAB as the ion sensitive species, and dioctyl phthalate as the plasticiser in THF. They produced an ISE with a Nernstian response in the range of 5 x 10^{-1} to 5 x 10^{-6}, however ClO_4^-, I^-, Br^- and NO_2^- were interferents. The structure of TDAB is presented in Figure 1.11.

Baro-Roma et al. [177] also employed TDAB in a PVC matrix with 2-NPOE as the plasticiser in the detection of sodium laurylsulfate and sodium dodecylbenzenesulfonate. Whilst this membrane was sensitive to these species, they did observe that nitrate and perchlorate were interfering species in the analysis, indicating some affinity for nitrate.

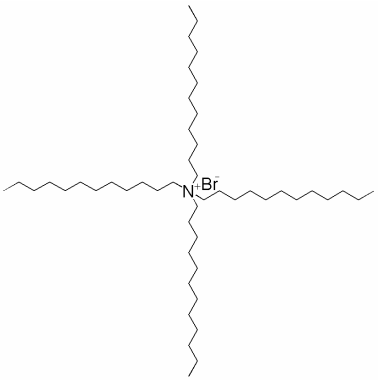

Figure 1.11 Chemical structure of tetradodecylammonium bromide (TDAB)

Wegmann et al. [178], referenced by Fluka [179], reported the use of membranes prepared from PVC and tetradodecylammonium chloride for the potentiometric analysis of chloride in solution. They noted that by incorporating the test ion as the counter-ion within the QAS (i.e. Cl^- to produce TDACl, Br^- to produce TDAB), the response is Nernstian, with variable responses to other ions in solution. They conclude that the sensitivities of these liquid-membrane electrodes were controlled by the Hofmeister series, but the selectivity can be influenced by utilising species that interact more directly with the test analyte.

1.3.4.5 Triallylethylammonium Bromide (TAEAB)

Ebdon and Braven [169, 170] synthesised TAEAB, as well as triallylbutylammonium bromide (TABAB), triallyloctylammonium bromide (TAOAB) and triallyldodecylammonium bromide (TADDAB), and prepared both solvent-cast and hot pressed acrylonitrile-butadiene membranes for the analysis of nitrate in solution. The structure of TAEAB and TAOAB are given in Figure 1.12.

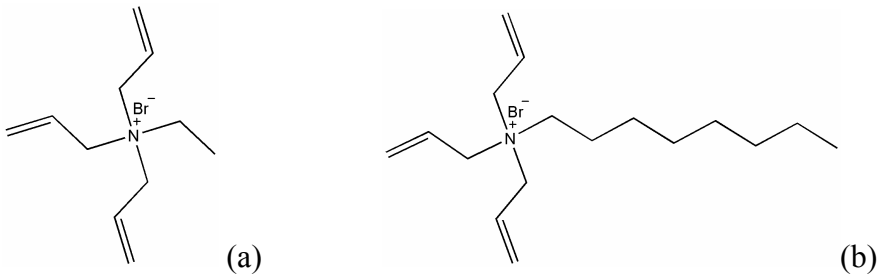

Figure 1.12 Chemical structure of (a) triallylethylammonium bromide (TAEAB) and (b) triallyloctylammonium bromide (TAOAB)

These QAS were immobilised by covalent cross-linking to the polymer through free-radical reaction. Ebdon and Braven reported that the selectivity coefficients, with respect to chloride, were significantly better than those offered by commercial nitrate-

selective electrodes. Specifically a commercial PVC nitrate-selective electrode employed by Ebdon and Braven recorded a selectivity coefficient of 8.0 x 10^{-3} during testing. All TAEAB and TABAB sensors prepared recorded lower coefficients, with the lowest value of 1.1 x 10^{-3} recorded for TABAB plasticised with 2-NPOE, and 1.3 x 10^{-3} in the case of a TAEAB sensor plasticised with 2-NPOE. Furthermore the limits of detection for these two membranes were 2 x 10^{-5} M and 6.3 x 10^{-5} M respectively. The TAOAB membrane produced a Nernstian response after more than 500 days and registered a limit of detection of 6.3 x 10^{-5} M after this time.

1.4 Support Polymers

1.4.1 Poly(vinyl chloride) (PVC)

PVC is a thermoplastic amorphous polymer with a structure consisting of chlorine atoms on alternate carbon units along the length of the chain. The structure of PVC is given in Figure 1.13.

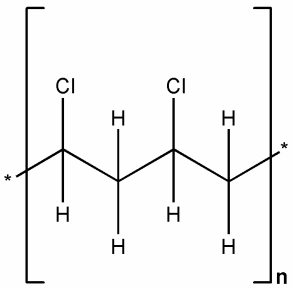

Figure 1.13 Chemical structure of poly(vinyl chloride) (PVC) [180]

The chlorine atoms influence the strength of PVC, creating strong dipole attractions that lead to strong cohesive forces throughout the chain. These forces make PVC resistant to acids and bases, as well as non-polar solvents, in addition to making it relatively flame resistant [180]. These properties make PVC particularly useful in chemical sensors,

specifically the compatibility of PVC with various solvent mediators, the entanglement of the PVC chains reducing the leaching of active components within the membrane or matrix, and the ease in fabricating ISEs based on PVC membranes [181].

1.4.2 Polyacrylonitrile (PAN)

PAN possesses the same ethylene backbone as PVC, however the chlorine atoms are replaced with cyano groups (-C≡N). The structure of PAN is presented in Figure 1.14.

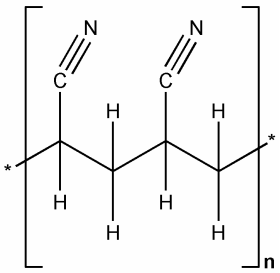

Figure 1.14 Chemical structure of polyacrylonitrile (PAN) [182]

This structure leads to the presence of strong dipole attractions that allow PAN to behave as a thermosetting plastic rather than a thermoplastic. These interactions are so strong that the energy required to break these attractions are greater than the energy required to break apart the ethylene backbone. Thus PAN will not flow like other thermoplastics with the application of heat, but instead degrades [182]. Similar to PVC, PAN is also resistant to chemical attack, as well as degradation from exposure to sunlight and ageing. According to Miles and Briston [180], PAN can also be modified to change its tensile strength. Fibres produced by extrusion result in an amorphous structure, but by stretching these fibres the orientation of the chains shift in the direction of the fibre axis, resulting in an increase in the crystallinity of the polymer and the tensile strength.

1.5 Project Aims

1.5.1 Electrospinning

The technique of electrospinning is influenced by a number of factors including the viscosity, surface tension and conductivity of the electrospinning solution. These techniques will be investigated to determine the affect of these parameters on the morphology, chemical composition and tensile strength of electrospun fibres derived from solutions comprised of non-conducting support polymers and conducting PAni/support polymer blends.

1.5.2 Nitrate Ion-Selective Electrode

This work aims to fabricate a selective, sensitive nitrate electrode incorporating the conducting polymer polyaniline (PAni) as the conductive component, an inert support polymer and an ion-selective quaternary ammonium salt as an ionophore. This electrode will be prepared using the physico-electrical technique of electrospinning, and evaluated to determine its selectivity and sensitivity towards nitrate, compared to chloride and tetrafluoroborate as interferents in solution.

Chapter 2 - Analysis of Polymer Solution Properties

"If a man is offered a fact which goes against his instincts, he will scrutinize it closely, and unless the evidence is overwhelming, he will refuse to believe it. If, on the other hand, he is offered something which affords a reason for acting in accordance to his instincts, he will accept it even on the slightest evidence. The origin of myths is explained in this way."

Betrand Russell (1872 – 1970)

2.1 Introduction

The electrospinning of polymer solutions and subsequent production of ultra-fine fibres has been found to be dependant on number of factors, including: viscosity [57, 65, 69, 84, 88, 91, 107, 112], surface tension [65, 78, 84, 96, 141, 142, 183, 184], solution conductivity [65, 84, 102, 112, 141, 184, 185], distance between origin and collector [57, 141], applied potential [102, 107, 141, 142] and the solvents employed [96, 142, 186].

Due to the lack of specific detail in the literature focusing on the effects of solution properties and electrospinnability of polymer solutions, viscosity, surface tension, conductivity and the particle size of the spinning solution are reported. Additionally, the correlation between these parameters, electrospinnability and fibre morphology and PAni dispersion will be reported in this chapter, Chapter 3, and Chapter 4. Such changes to the solution properties will comprise the addition of salt, changes in solution composition and polymer concentration, and the addition of MWNT to commodity plastic solutions of PVC in THF/DMF, and PAN in DMSO/DMF. These polymers were chosen based on their proven ability to electrospin and produce sub-micron diameter fibres [126, 142], the ionophores were chosen due to literature indicating selectivity towards nitrate [168-170, 172], while the MWNT were employed as an alternative charge carrier for these electrospun fibres, in place of PAni [128].

There is also very little information on changes in solution properties with the addition of PAni. It is anticipated this work will provide a starting point to show how the addition of PAni alters the viscosity, surface tension and conductivity with respect to PVC in THF/DMF and PAN in DMF/DMSO, leading to changes in the electrospinnability of these solutions, and the morphology of the electrospun fibre mats.

Furthermore, the addition of ionophores and the plasticiser 2-NPOE will also be analysed to determine the effect of these materials to the solution properties.

2.1.1 Viscosity of Polymer Solutions

A suitable concentration of a polymer in solution is required for the successful initiation and formation of electrospun fibres. As viscosity is a derivative of solution concentration with respect to the solvent, a suitable polymer concentration is required to achieve a desired viscosity [57]. If the viscosity of a polymer solution is too low, droplets are formed [57, 102, 144]. This is due to the capillary break-up of the initial solution jet due to surface tension and lack of molecular entanglements [65, 121, 183]. This process is also known as electrospraying and is used widely in other industries [102].

Electrospinning is also inhibited by high viscosity due to limitations in initiation of the solution jet. Deitzal et al. [102] reported that a viscosity greater than 2000 centipoise (cP) for 10% blend of PEO in water could not be electrospun from a pressured syringe, and the flow rate was unstable. Lee et al.. [144] also supports this by stating that a high polymer concentration prohibits a continuous flow required for jet formation. Doshi and Reneker [141] found that a high-viscosity solution would dry at the tip of a glass capillary, blocking the flow of polymer solution. Thus both minimum and maximum viscosities exist (dependant on both the solvent and polymer properties) for electrospinning to be successful.

The introduction of new components into a polymer solution will also affect the viscosity of the solution. For example Seoul et al. [122] added SWNT (single wall carbon nanotubes) to a blend of poly(vinylidene fluoride) (PVDF) in DMF. The

viscosity of the solution increased from 1200 to 1800 cP by increasing SWNT from 0.002% to 0.004%, with the viscosity tapering after 0.004%. Though a direct rheological relationship between the addition of PAni to a polymer solution has not been reported, Jain and Gregory [187] report changes in the rheological nature of PAni in both N,N'-dimethylpropylene urea (DMPU) and N-methyl-2-pyrrolidinone (NMP). They observed non-Newtonian shear thinning at low shear rates and Newtonian characteristics at high shear rates for PAni/DMPU. The same was observed for PAni in NMP at a concentration of 7.5%, though when the concentration was increased the solution produced a pseudoplastic fluid at all shear rates studied. This may have been due to PAni forming a thixotropic gel for this solution whereby the increased shear rate disturbed the associations within the gel, thus lowering the viscosity [187].

In ternary polymer blends (polymer/polymer/solvent), viscosity may alter due to interactions between the polymers. This may lead to an increase or decrease in viscosity depending on the interaction between the polymers. Changes in the polymer conformation by repulsive forces may lead to lower viscosities than anticipated, whilst attractive forces will increase polymer interaction, and hence viscosity [188]. This may apply to a PAni/polymer blend where the presence of a dopant, such as camphorsulfonic acid (CSA), a quaternary ammonium salt (QAS) plus a bi-solvent system would be expected to further alter these interactions.

The charges on the doped PAni backbone may also affect the viscosity as a result of polymer-polymer interaction, and hence conformation of the polymer chains. That is, electrostatic repulsions between charged segments of the backbone may lead to straightening of the chains. This is dependent on the counter-ion employed and whether the counter-ion is sufficiently close to balance the localised charge on the chain.

According to Avlyanov et al. [54], solvation of the PAni chain and the counter-ion could lead to an increase in distance between the charged segment of the chain and the counter-ion. This in turn would lead to electrostatic repulsion on the PAni chain and a change in conformation to an expanded-coil structure, increasing the viscosity of the solution. Other inter- and intrachain effects within PAni also exists that can lead to changes in solution viscosity. Yang and Mattes [189] studied the use of 2-methylaziridine (2MA) as an additive together with N-methyl-2-pyrrolidone (NMP) to inhibit gel formation in high concentration solutions of high-molecular weight PAni. They found that the PAni, in the form of emeraldine base, complexes with 2MA, providing a 'dielectric shield' that improved the solubility of PAni by inhibiting PAni aggregation, and hence lowering viscosity. The 2MA in essence, acts as a proton donor, forming hydrogen bonds with the imine nitrogens of PAni. This results in 2MA and NMP combining to overcome intra- and interchain hydrogen bonding in high concentrated solutions of PAni.

2.1.2 Surface Tension of Polymer Solutions

The surface tension of polymer solutions is also an important factor in fibre formation and morphology. Liu and Hsieh [96] state that the surface tension of polymer solutions is highly dependant on the solvent itself, and not the polymer concentration. They observed a doubling of cellulose acetate concentration from 10% to 20% in a 2:1 acetone/dimethylacetamide blend produced only an increase of 0.5 mN m^{-1} (milli-Newton/metre) change in surface tension. However changing the solvent composition from 2:1 to 1:2 substantially increased the surface tension from 26 to 30 mN m^{-1} [96].

This is partially supported by Lee et al. [84] as they too reported the surface tension altered with differing solvent composition. It was also found that a change in the

polymer composition for a two-polymer, two-solvent system also significantly altered the solution surface tension. However, Lee et al. also state that that the surface tension is a product of the interaction between the polymer and solvent, or between polymers in the case of multiple-polymer blends [84]. Additionally Son et al. [185] noted that the polyelectrolyte poly(acrylic acid sodium salt) (PAA) slightly decreased the surface tension of a PEO solution, whilst Lin et al. [184] observed changes in the surface tension of polystyrene dissolved in THF/DMF after the addition of QAS, with these QAS acting as surfactants.

Though there would appear to be no specific literature on the relationship between the addition of PAni and surface tension in a polymer solution, Lee et al. [84] report that changes in surface tension would be expected from altering the composition of a ternary polymer blend [84].

The introduction of SWNT into a polymer solution also affects the surface tension. Seoul et al. [122] reported a significant decrease in the surface tension of a poly(vinylidene fluoride) (PVDF)/DMF solution with the addition of 0.1% SWNT. The surface tension of the solution decreased from approximately 35 mN m^{-1} to approximately 22 mN m^{-1} [122].

2.1.3 Conductivity of Polymer Solutions

Conductivity has been linked to the charge density on the polymer jet. This influences the elongation of the jet during the electrospinning process with a higher charge density leading to an increased elongation of the polymer jet [190]. This is significant in the electrospinning process as the dominant jet instability largely relies on this charge density. The ‘non-conducting’ axisymmetric instability competes with the conducting

instabilities during electrospinning. Furthermore the conducting axisymmetric instability competes with the whipping non-axisymmetric instability, dominating at a low static charge density, whilst the whipping instability dominates at high static charge density [82, 88, 89, 92].

Li and Hseih [121] report that the higher dielectric constant of water leads to a higher solution conductivity compared with DMF solutions of the same composition. The addition of ionic salts such as NaCl to polymer solutions of poly(acrylic acid) and poly(2-acrylamido-2-methyl-1-propane sulfonic acid) (PAMPS), and the subsequent increase in conductivity has also been documented [121, 135]. Li and Hsieh [121] observed an eight-fold increase in conductivity of PAA in water with the addition of 8 wt% NaCl whilst Kim et al. [135] reported a ten-fold increase in the conductivity of PAMPS with an increase in NaCl from 0.01 mol% to 0.1 mol%. The addition of these salts led to an increase in the free-ion concentration, in turn affecting the charge density of the solution [190, 191]. According to Son et al. [185] solvents with higher dielectric constants have a higher net charge density, in turn affecting the net charge density of the polymer solution, the subsequent electrospinning process and the morphology of the fibres. Furthermore, Fong et al. [183] presented data where the conductivity of a poly(ethylene oxide) (PEO) solution altered with the addition of ethanol to the blend, leading to a decrease in the solution conductivity and net charge density of the jet. Conversely, Zuo et al. [92] observed an increase in conductivity for a poly(hydroxybutyrate-co-valerate) (PHBV)/$CHCl_3$ blend after the addition of ethanol. However a decrease in conductivity was observed with the addition of tetrachloromethane to the PHBV/$CHCl_3$ blend.

Lee et al. [84] varied the composition of poly(vinyl chloride) (PVC)/polyurethane (PU) resulting in a decrease in the conductivity with decreasing PVC concentration. Furthermore Jun et al. [112] reported that the addition of pyridinium formate (PF) to poly-L-lactide (PLA) significantly increased the conductivity of the resultant solution.

Addition of insoluble components have also been reported to increase overall solution conductivity. Seoul et al. [122] observed an increase in conductivity by orders of magnitude with the addition of small amounts of SWNT to a solution of PVDF in DMF [122].

Composite solutions containing PAni would be expected to alter the conductivity of the solution depending on whether the PAni is present in the conducting emeraldine salt form or not. However, there has been very little data as to the affect that the introduction of conducting PAni has on polymer solutions. One way to view PAni is as a polyelectrolyte when in the doped form [54]. Son et al. [185] stated that the polyelectrolytes poly(allylamine hydrochloride) (PAH) and poly(acrylic acid sodium salt) (PAA) significantly increased the conductivity of PEO dissolved separately in chloroform, ethanol, DMF and water. The conductivity of PAni relates back to the conformation of the chain discussed by Avlyanov et al. [54] where the conductivity is enhanced by an expanded–coil conformation leading to a decrease in defects in the π-region of the conjugation due to less ring-twisting along the PAni chain.

2.1.4 Background on Particle Size Analysis

PAni particles also exhibit a tendency to aggregate due to hydrogen bonding [192]. Xia and Wang [192] stated that decreasing the size of PAni particles can assist doping and support interchain and intrachain interaction.This aggregation may be reduced by the

introduction of plasticisers to overcome PAni-PAni adhesion or may be assisted by various dopants [193].

The ability to use carbon nanotubes in materials is limited by the ability to produce suitable dispersions [194]. One of the most effective methods for dispersing particles or dissolving materials with low solubility is sonification. This is particularly pertinent to carbon nanotubes that are difficult to disperse predominantly due to the attractive forces between the nanotubes, termed van der Waals forces, but also due to entanglement of the nanotubes. This may be reduced by introducing surfactants or functionalising the nanotubes themselves [195]. Jin et al. [196] state that during sonification of multi-wall carbon nanotubes (MWNT) the solvent will interfere with the nanotubes and break them apart. This allows polymer molecules to interact with the MWNT and produce dispersed MWNT 'micelles'. That is, the polymer acts to form a micelle solution and encloses the MWNT within it.

2.2 Reagents and Materials

2.2.1 Materials

Polyacrylonitrile (PAN, MW 97 000), poly(vinyl chloride) (PVC, MW 62 000), 2-nitrophenyl octyl ether (2-NPOE), tetraoctylammonium bromide (TOAB) and tetradodecylammonium bromide (TDAB) were obtained from Sigma-Aldrich. Tetrahydrofuran (THF, AR) and dimethylformamide (DMF, AR) were obtained from BDH Chemicals. Dimethylsulfoxide (DMSO,LR) was obtained from AJAX chemicals. D-camphor-10-sulfonic acid (CSA, LR), concentrated ammonia solution (AR), concentrated HCl (AR), ammonium peroxodisulphate (APS, AR) and aniline (AR) was obtained from BDH chemicals. Multi-wall carbon nanotubes (MWNT, 95%+, OD/ID

10-20/5-10 nm) were obtained from Nanostructure and Amorphous Materials. All chemicals were used without further purification.

Polyaniline (PAni) was synthesised from aniline distilled over the range of 182-183^{o}C. Distilled aniline was sealed under nitrogen and stored in a freezer until use. 100 mL 0.2 M APS in 2 M HCl was placed in an ice bath with stirring. Over the course of 1 hour 100 mL 0.2 M aniline in 2 M HCl was added dropwise to the APS solution and left to stir for a further 12 hours. The resulting green, protonated PAni precipitate was filtered using No. 1 Whatman filter paper and then washed with distilled water until a consistent pH was obtained. The solid was mixed with 300 mL of concentrated ammonia solution to deprotonate it to emeraldine base. The mixture was allowed to stir for 1 hour after which the product was again filtered with No. 1 Whatman filter paper and then collected. The product was then freeze-dried, sealed and stored in a freezer until required.

2.2.2 Synthesis of Ionophores

2.2.2.1 Synthesis of triallylethylammonium bromide (TAEAB)

This synthesis was based on King [197], and was altered slightly based on Ebdon et al..[169]

Approximately 25 g (31.7 mL, 0.26 mol) of diallylamine was placed in a 3 neck flask with 25 mL of distilled water. To this 28 g (19.2 mL, 0.26 mol) of bromoethane was added dropwise followed by 40 mL of a 10 M NaOH solution. This mixture was stirred and heated at 70^{o}C for 4 hours. The top oily layer was separated from the aqueous layer and dried over KOH pellets overnight. Employing a vigreux side arm and a 4-connection vacuum receiver adapter, the oily layer was then purified by distillation. Two fractions were collected, with the first small fraction appearing between 60 – 80^{o}C

and the second major fraction corresponding to diallylethylamine collected between 123 – 125°C.

Allylbromide (3.4 mL, 4.9 g, 0.04 mol) was added dropwise to a stirred solution of 7.9 g diallylethylamine in 5 mL of acetone. This solution was allowed to stir for 3 hours and then placed in a dry, sealed container and stored in the freezer for one week. The liquid was decanted off and the resultant crystals were washed three times with 6 mL aliquots of dry THF. The crystals were then dissolved in, and recrystallised from 10 mL of hot acetone and absolute ethanol solution (9:1) by vacuum to remove any residual solvent or moisture. The crystals were subsequently stored under vacuum.

2.3 Preparation of Samples

2.3.1 Calculations

To allow comparisons between various electrospinning solutions, the solutions were made up on a w/w basis according to the following equations:

$$\text{Final Solution Weight (g)} = \left[\frac{\text{Solvent Weight (g)}}{\text{\% of Solvent (w/w)}}\right] \times 100$$

Equation 2.1 Final solution weight of polymer solutions

$$\text{Solvent Weight (g)} = \text{Solvent Density (g/mL)} \times \text{Solvent Volume (mL)}$$

Equation 2.2 Solvent weight of an individual solvent within solvent blend

$$\text{Percentage of Solvent (w/w)} = \left[\frac{\text{Solvent Weight (g)}}{\text{Total Solvent Weight (g)}}\right] \times \text{Overall Solvent Percentage (w/w)}$$

Equation 2.3 Percentage of solvent based on the overall solvent contribution

$$\text{Polymer Weight (g)} = \left[\frac{\%\ \text{Polymer (w/w)}}{100} \times \text{Final Solution Weight (g)} \right]$$

Equation 2.4 Weight of polymer based on percentage in solution

$$\text{PAni Weight (g)} = \left[\frac{\%\ \text{PAni (w/w)}}{100} \times \text{Final Solution Weight (g)} \right]$$

Equation 2.5 Weight of polyaniline based on percentage in solution

$$\text{Solvent Volume (mL)} = \left[\frac{\%\ \text{Solvent (v/v)}}{100} \times \text{Final Volume (mL)} \right]$$

Equation 2.6 Volume of solvent based on percentage in solvent blend.

$$\text{Ionophore Weight (g)} = \left[\frac{\%\ \text{Ionophore (w/w)}}{100} \times \text{Final Solution Weight (g)} \right]$$

Equation 2.7 Weight of ionophore based on percentage solution

$$\text{Ionophore Volume (mL)} = \frac{\text{Ionophore Weight (g)}}{\text{Ionophore Density (g/mL)}}$$

Equation 2.8 Volume of ionophore based on ionophore weight

$$\text{CSA Weight Factor} = \left[\left(\frac{1}{\text{Molecular Weight of Aniline (g/mol)}} \right) \times \left(\frac{\text{Molecular Weight of CSA (g/mol)}}{2} \right) \right] \times 100$$

Equation 2.9 CSA weight factor required to dope polyaniline

$$\text{CSA Weight (g)} = \left[\frac{\text{CSA Weight Ratio}}{100} \times \text{PAni Weight (g)} \right]$$

Equation 2.10 Weight of CSA based on weight of polyaniline

$$\text{MWNT Weight (g)} = \left[\frac{\%\,\text{MWNT (w/w)}}{100} \times \text{Final Solution Weight (g)} \right]$$

Equation 2.11 Weight of MWNT based on percentage in blend

Equation 2.2, 2.3 and 2.4 were used to determine the final polymer solution weight based on the solvent weight and the percentage of solvent with respect to the total solvent contribution of the 100% w/w polymer blend. These were originally derived from the v/v composition of the solvents. Using the final solution weight, the polymer and PAni weight were determined by Equations 2.5 and 2.6 respectively. The solvent volume (Equation 2.6) was determined by the v/v relationship and by the amount of solution required for an adequate-sized sample as noted in Equation 2.4.

The required weight or volume of the ionophore, or other additives such as 2-NPOE and the organic salt tetrabutylammonium perchlorate, were determined by Equations 2.8 and 2.9, based on the final solution weight.

The CSA weight factor in Equation 2.10 is necessary to ensure PAni is doped from the emeraldine base to emeraldine salt. PAni has been found [52, 53] to be more soluble in a number of solvents by utilising a functionalised protonic acid, such as CSA. In such a case the proton from the organic acid is reported to dope the PAni from the emeraldine form to the emeraldine salt form, while the deprotonated sulfonate group would be an ideal counter-ion. The organic functional group act as solvating groups, increasing the solubility of the PAni in organic solvents [52, 53]. Equation 2.11 determines the weight of CSA required for a given mass of PAni to ensure the full protonation of PAni.

As blends incorporating MWNT rather than PAni did not require CSA, Equations 2.10 and 2.11 were removed from the calculations and the weight of MWNT determined by Equation 2.12.

2.3.2 Dissolution of PVC

The calculated amount of PVC was dissolved in THF/DMF by magnetic stirring and stirred overnight in a 20 mL scintillation vial.

2.3.3 Dissolution of PAN

The calculated amount of PAN was dissolved in DMSO/DMF by magnetic stirring and stirred overnight in a 20 mL scintillation vial.

Previous work [78, 116, 126, 133] had relied on DMF as the sole solvating agent for PAN. However, it was found that a mixture of DMF and DMSO was a much better solvent for PAN and this mixture was used throughout this work.

2.3.4 Dissolution of PAni / Polymer Blends

Due to limitations of its solubility [52, 58, 78, 129, 145], all PAni solutions were made up to be 1% w/w PAni.

The calculated mass of CSA was weighed into a 20 mL scintillation vial and suitable volumes of solvents were added. After dissolution of the CSA, PAni was added slowly. The PAni was allowed to dissolve with vigorous magnetic stirring for a period ranging between 8-24 hours, depending on visual determination of dissolution. The commodity plastic was then added and mechanically stirred until it had dissolved.

2.3.5 Dissolution of PAni/Polymer/Additive Blends

If further materials were to be added (e.g. the quaternary ammonium salts (QAS) TOAB, TDAB, TAEAB), the correct mass or volume was added and competely dissolved in the solvent blend before the addition of PAni.

2.3.6 Dissolution/Dispersion of MWNT/Polymer Blends

MWNT (0.5% w/w) was weighed into a 5 mL or 20 mL scintillation vial and the volumes of solvents, calculated as discussed earlier, were added. MWNT were dispersed by sonicating for 1 hour in a Vibra Cell VC-505 sonicator (Amplitude: 35%, Pulse: 2s on / 2s off) in an ice bath during sonification to prevent solvent evaporation. The commodity plastic was then added and mechanically stirred until it had dissolved.

2.3.7 Special Note on Naming Conventions of Spinning Solutions and Electrospun Samples

Throughout this work reference will be made to the composition of the polymer solutions and electrospun fibres. The composition of solutions is in the form of % w/w in solvent. For simplicity, this convention will also be employed for the electrospun fibres, such that actual composition of the dry electrospun fibres will not be employed, but the original spinning solution composition. Additionally, and to avoid repetitiveness, the unit w/w will not be expressed for the remainder of the thesis. For example, the term PAni 1% PVC 5% will be used instead of PAni 1% PVC 5% w/w.

Furthermore, in the case of solutions and electrospun fibres containing PAni, all reference is to PAni doped with camphorsulfonic acid (CSA) unless otherwise stated.

2.3.8 Analysis of Samples – Viscosity

Samples were analysed on a Brookfield RVDV-II+ viscometer using a Din 85 type spindle with results collected on Rheocalc software Version 2.4. The temperature of the solutions was kept constant using a thermostatted water bath at 20 ± 0.3^{o}C. Viscosity was calculated by the Rheocalc software (V 2.4) over the shear rate range.

2.3.9 Analysis of Samples – Surface Tension

Bulk densities of the solutions were estimated by the calculation of weight change after the removal of 1.00 mL of solution from blend, thus giving an estimate for bulk density in g mL^{-1}.

The surface tension of the polymer solutions were analysed by a Dataphysics OCA 20 Contact Angle System (Goniometer) with single electronic syringe dosing attachment and Live Feed CCD video camera. Samples were analysed using the pendant drop method fitted with the Young-Laplace equation.

Samples were mechanically withdrawn into a specialised syringe and ejected to form pendant drops at the end of the syringe. Snapshots of the pendant drop were taken and the Young-Laplace equation applied, providing a value for surface tension.

2.3.10 Analysis of Samples – Solution Conductivity

The blends were analysed using a Solartron SI 1260 Impedance / Gain-Phase Analyser interfaced through a Solartron SI 1287 Electrochemical Interface to a PC running ZView 2 and ZPlot 2 Software. The conductivity was estimated by using an [R_S(CPE – R_P)] model fitted to a Z' versus Z'' plot, where R_P is the polarisation resistance, and R_S

is the solution resistance. Cell potential (V) and air temperature (^{o}C) are noted in Tables 2.6 and 2.7 for PAN and PVC blends, respectively. .

2.3.11 Analysis of Samples – Particle Size Analysis

Samples were prepared as previously described in Section 2.3. The solutions were added to a square glass cuvette and analysed by a Zetasizer Nano (Malvern Instruments) at 25^{o}C. Data was analysed and recorded using Dispersion Technology Software (DTS, Version 4.10). The results for particle analysis of PAni/PAN and PAni/PVC solutions are given in Table 2.8 and 2.9, respectively.

2.4 Results and Discussion - Viscosity

It is generally accepted that polymer solutions exhibit non-Newtonian flow. This is due to the large polymer molecules transferring the energy from flow more so than Newtonian solutions [198]. However, it was necessary to confirm these observations for both PAN and PVC solutions. In addition it was also necessary to observe if changes take place with the addition of other components to the original solutions. The values for rheological analysis are given in Table 2.1 for PAN, and Table 2.2 for PVC solutions.

2.4.1 PAN Solutions

PAN has previously been identified as a pseudoplastic polymer in solutions of DMF [199, 200] and DMSO [200]. Figure 2.1 is a plot of shear stress vs. shear rate that displays the pseudoplastic nature of a solution of PAN 7% in DMSO/DMF, exhibited by the shear stress deviating from linearity with increasing shear rate. It is important to note that this uniform deviation from linearity was not observed in lower concentrations

of PAN in DMSO/DMF as the determined shear stress values were relatively low for the given shear rate.

That is, the flow graphs for PAN 1%, 3% and 5% were restricted due to the maximum shear rate possible with the viscometer and also the limits of accurate detection. This is typified by PAN 1% in Figure 2.2 which shows significant variation in response due to these limitations. As a result all viscosity data was determined with respect to the shear rate of 50 sec^{-1}. This allowed the data to be correlated, accounting for the pseudoplastic properties of the solutions.

PAN in DMSO/DMF					
[PAN] (% w/w)	**Viscosity (mPa.s)**	**Speed (RPM)**	**% Torque**	**Shear Stress (mPa)**	**Shear Rate (1 s^{-1})**
1	7.24	38.76	2.30	3.62	50.00
3	44.26	38.76	4.70	2.21	50.00
5	165.74	38.76	17.60	8.29	50.00
7	619.64	38.76	65.80	30.98	50.00
PAni 1% PAN in DMSO/DMF					
[PAN] (% w/w)	**Viscosity (mPa.s)**	**Speed (RPM)**	**% Torque**	**Shear Stress (mPa)**	**Shear Rate (1 s^{-1})**
1	7.87	38.76	2.50	3.93	50.00
3	73.02	38.76	23.20	36.51	50.00
5	262.88	38.76	8.40	131.44	50.00
7	935.73	38.76	29.90	467.87	50.00
MWNT 0.5% PAN in DMSO/DMF					
[PAN] (% w/w)	**Viscosity (mPa.s)**	**Speed (RPM)**	**% Torque**	**Shear Stress (mPa)**	**Shear Rate (1 s^{-1})**
3	98.88	38.76	10.50	4.94	50.00
5	323.00	38.76	34.30	16.15	50.00
7	947.35	38.76	100.60	47.37	50.00

Table 2.1 Viscosity results for PAN solutions

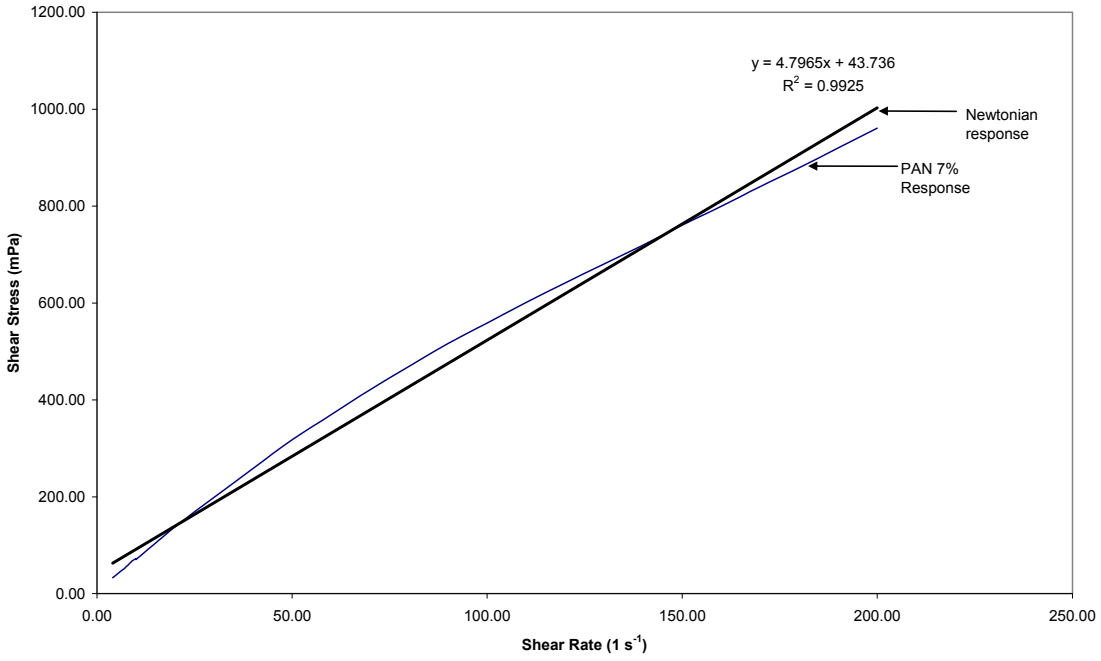

Figure 2.1 Shear rate vs. shear stress for a solution of PAN 7% in DMSO/DMF

It can be observed that there was a significant shift in the apparent viscosity of the solution above 5% PAN (Figure 2.3). This was also apparent in solutions containing PAni and MWNT. However, PAni appeared to impact much more on the underlying PAN solution than did MWNTs by the greater slope of the PAni/PAN line after 5% PAN. This may have been the result of intermolecular polymer chain associations, similar to observations by Abu-Sharkh et al. [201]. The deviation of the PAni/PAN and MWNT/PAN viscosity curves from the 'baseline' PAN curve, with increasing PAN concentration, indicates both MWNT and PAni contribute to the increased viscosity, possibly through further intermolecular interaction with the PAN.

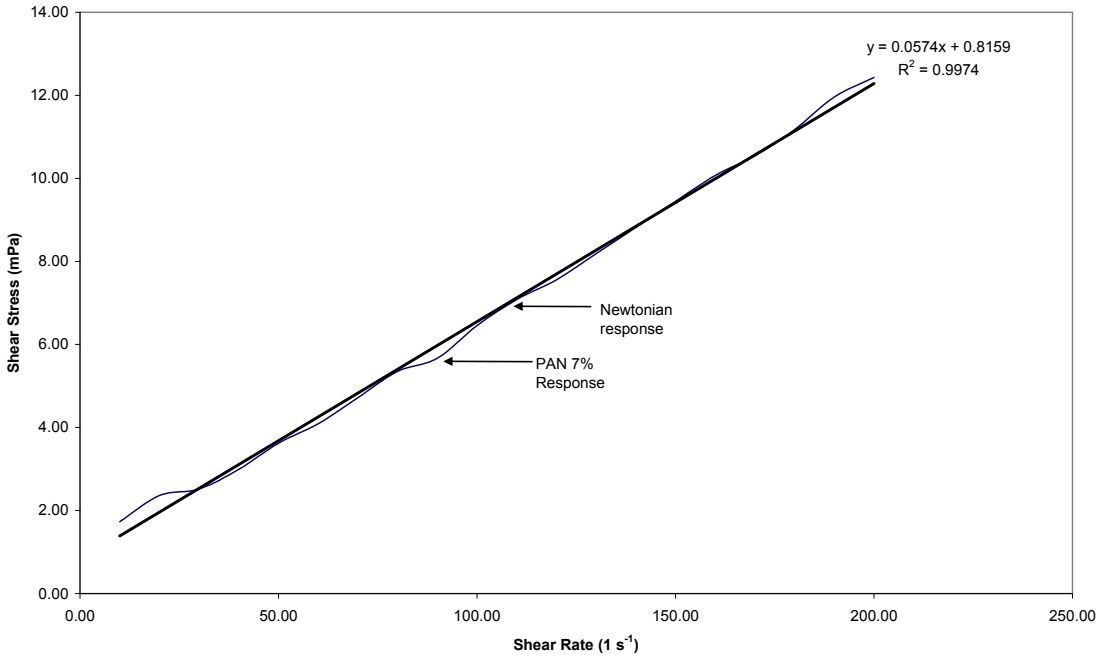

Figure 2.2 Shear rate vs. shear stress for a solution of PAN 1% in DMSO/DMF

It was previously discussed that the introduction of PAni would affect the overall viscosity of the solution, similar to other ternary polymer solutions. One possible explanation is that the viscosity alters with the addition of a further polymer to a polymer/solvent system, according to the degree of interaction between the second polymer and other components in the solution. A second possibility is that the solvation of the both counter-ion and PAni alters the conformation of the PAni chain. As postulated by Avlyanov et al. [54], an increase in solvation may lead to an increase in the distance between doped PAni and the counter-ion. As a result, electrostatic repulsion from the charged segments of the PAni chain unfold the chain and increase the overall viscosity of the solution. Either of these processes may contribute to the increase in viscosity for the PAni/PAN solutions.

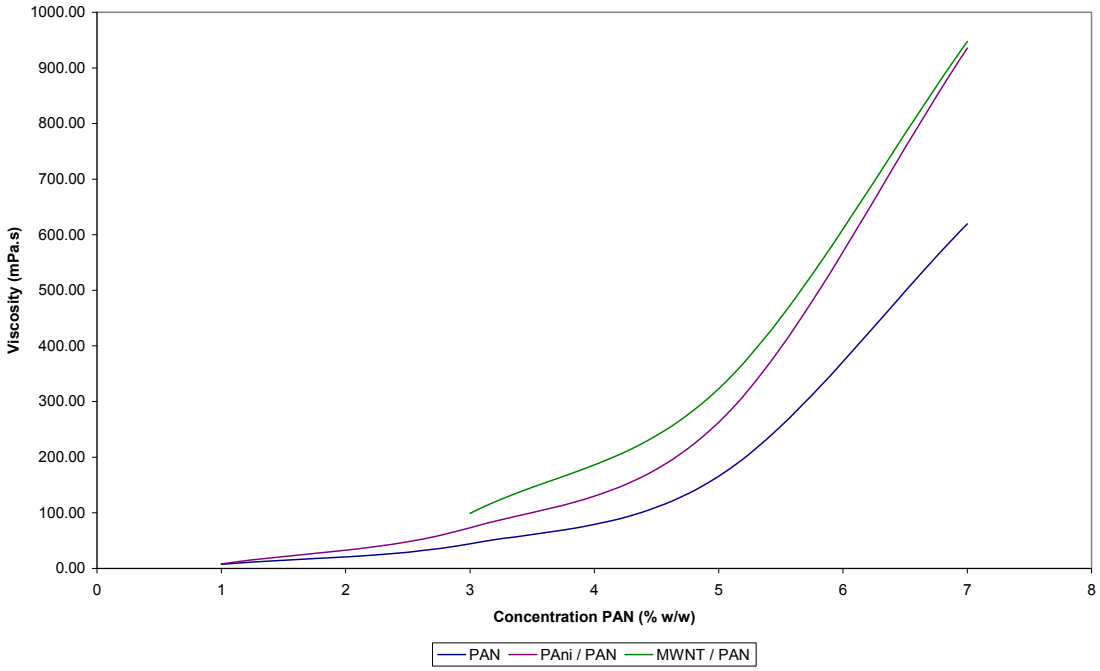

Figure 2.3 Viscosity of PAN, PAni 1%/PAN and MWNT 0.5%/PAN solutions at a shear rate of 50 s^{-1}

A third possible contribution may be that the ethylene PAN backbone interacted with the camphor group of CSA, whilst the negative sulfonate ion counters the positive charge on the radical nitrogen of the PAni backbone, leading to an ionic 'bond' of sorts. This possible interaction is presented in Figure 2.4.

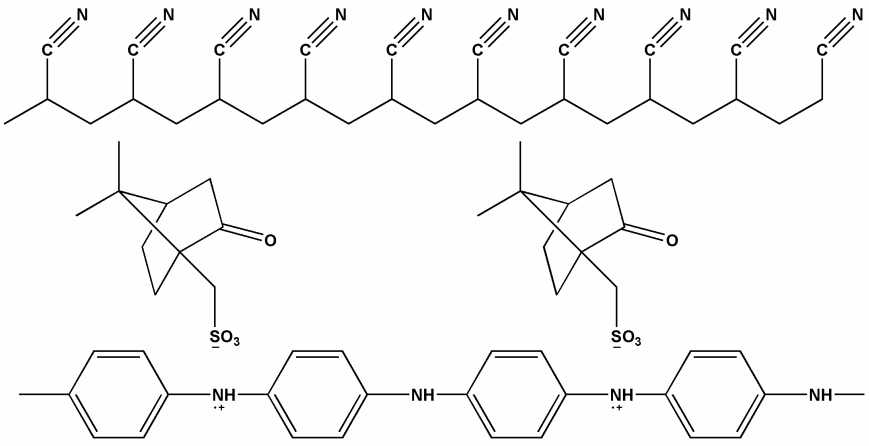

Figure 2.4 Possible chemical arrangement of PAni/PAN in solution

One interesting observation was the significant increase in viscosity of the MWNT/PAN blend compared with the PAN solution. Seoul et al. [122] observed significant increases in the viscosity of a PVDF solution with the addition of only small amounts of SWNT, almost doubling after the addition of 0.014% SWNT [122]. It was surmised that the SWNT were 'entangling'. Whilst an increased in viscosity was observed in the MWNT/PAN solution, it was not as great as that observed by Seoul et al.. This may be due to the inherent differences between SWNT and MWNT, the quality of the MWNT employed (Section 4.3.10) or perhaps the degree of dispersion of the MWNT within the polymer solution. Regardless, an interaction between the PAN and MWNT is observed due to the change in the slope of the line away from the original PAN solution.

2.4.2 PVC Solutions

PVC is also a polymer that has previously exhibited pseudoplastic properties in solution [202, 203]. Specifically Merrill in Fredrickson [202] classes PVC as a random-coiling non-electrolytic macromolecule in solution. Merrill also grouped PVC as an aggregate of macromolecules. These groups are two of the five different classes of polymeric non-Newtonian materials outlined by Merrill that provide a basis for the correlation between molecular structure and rheological properties.

To confirm this pseudoplastic nature, plots of shear stress vs. shear rate of PVC in THF/DMF were analysed at concentrations of 5%, 10%, 15% and 20% PVC, with results given in Table 2.2. Results quite similar to PAN were observed, specifically non-Newtonian characteristics were not observed at lower PVC concentration, where a linear relationship existed between shear rate and shear stress, but pseudoplastic behaviour was observed at 20% PVC in THF/DMF, evident by the shear stress deviating from linearity with increasing shear rate. This can be seen in Figure 2.5 as can the comparison plot of PVC 5% shear stress vs. shear rate in Figure 2.6. Again the

limitations of the instrument and the relatively low shear rates employed made it difficult to determine the true characteristics of the PVC solution. Only at higher viscosities was the pseudoplastic trend observed.

PVC in THF/DMF					
[PVC] (% w/w)	**Viscosity (mPa.s)**	**Speed (RPM)**	**% Torque**	**Shear Stress (mPa)**	**Shear Rate (1 s^{-1})**
5	7.53	38.76	0.80	0.38	50.00
10	22.60	38.76	2.40	1.13	50.00
15	94.17	38.76	10.00	4.71	50.00
20	635.30	38.76	20.30	317.65	50.00
PAni 1% PVC in THF/DMF					
[PVC] (% w/w)	**Viscosity (mPa.s)**	**Speed (RPM)**	**% Torque**	**Shear Stress (mPa)**	**Shear Rate (1 s^{-1})**
5	11.30	38.76	1.20	0.57	50.00
10	45.01	38.76	14.30	22.51	50.00
15	250.36	38.76	8.00	125.18	50.00
20	605.51	38.76	64.30	302.76	50.00
PAni 1% PVC 10% TDAB in THF/DMF					
[PVC] (% w/w)	**Viscosity (mPa.s)**	**Speed (RPM)**	**% Torque**	**Shear Stress (mPa)**	**Shear Rate (1 s^{-1})**
0	45.01	38.76	14.30	22.51	50.00
0.5	121.17	46.51	46.20	72.70	60.00
5	102.43	46.51	39.05	61.46	60.00
10	233.83	46.51	89.15	140.30	60.00
MWNT 0.5% PVC in THF/DMF					
[PVC] (% w/w)	**Viscosity (mPa.s)**	**Speed (RPM)**	**% Torque**	**Shear Stress (mPa)**	**Shear Rate (1 s^{-1})**
5	25.43	38.76	2.70	1.27	50.00
10	202.47	38.76	21.50	10.12	50.00
15	32.96	38.76	3.50	1.65	50.00

Table 2.2 Viscosity results for PVC solutions

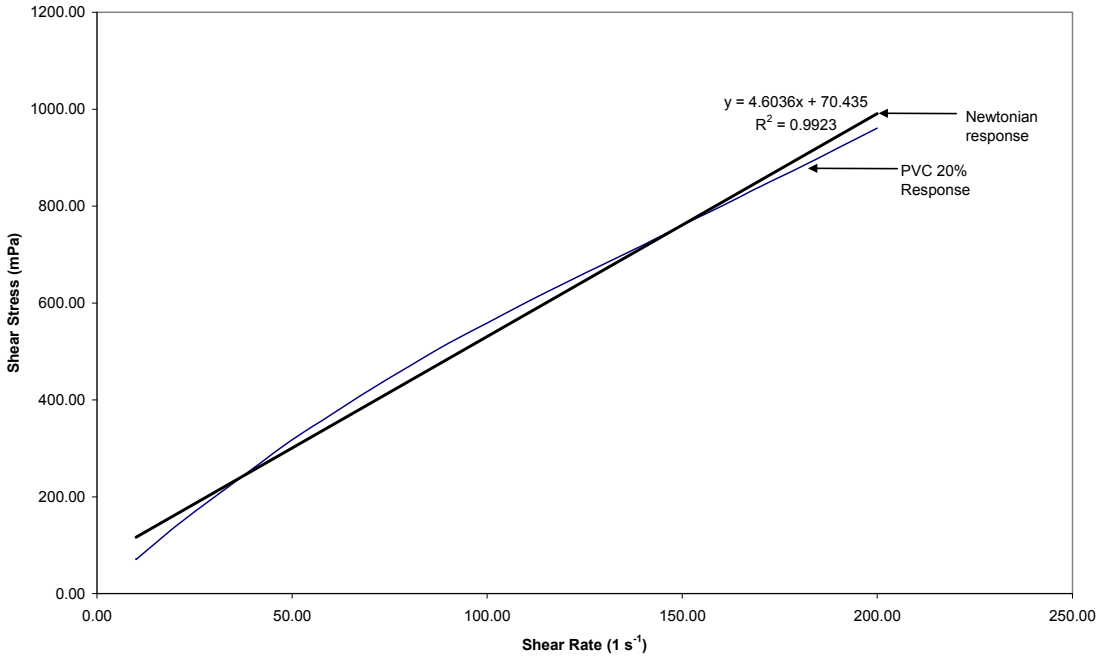

Figure 2.5 Shear rate vs. shear stress for a solution of PVC 20% in THF/DMF

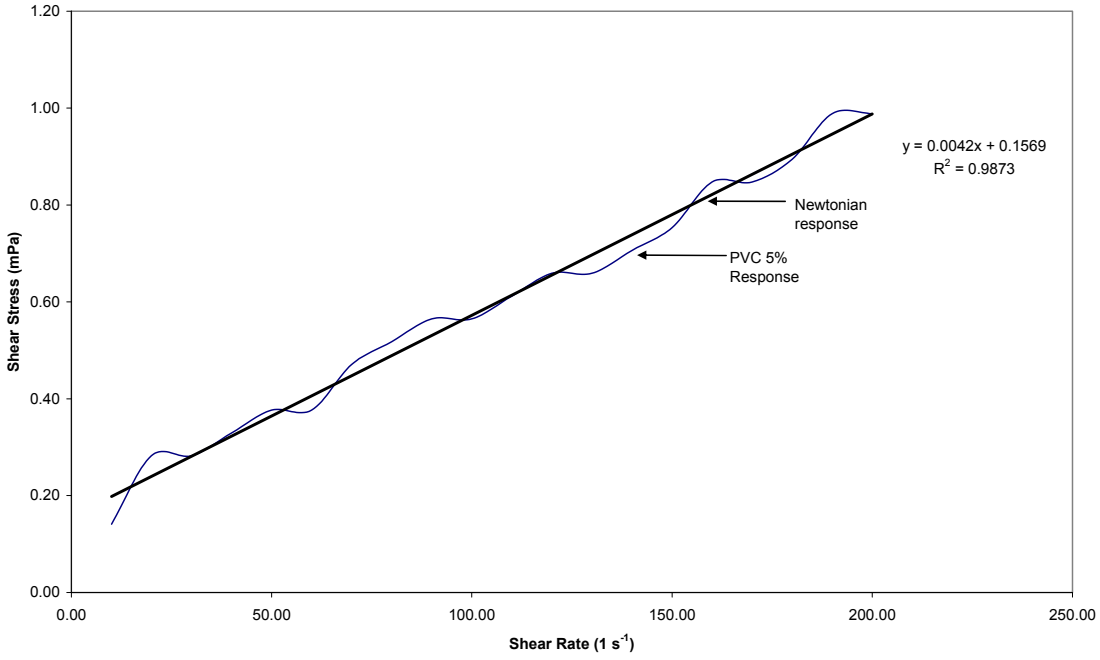

Figure 2.6 Shear rate vs. shear stress for a solution of PVC 5% in THF/DMF

PVC again had similar characteristics to PAN in terms of viscosity changes with increasing PVC concentration, and can be seen in Figure 2.7. There is a noticeable

increase in the solution viscosity between PVC 15% and PVC 20%. As discussed previously, this was most likely a result of intermolecular attractions of polymer chains within the solution as the concentration of PVC increased above a critical point.

Again, the viscosity of PAni/PVC solutions deviated from the PVC trend, though in this instance the deviation begun as low as PAni 1% PVC 8%. Compare this with PAni/PAN blend that exhibited a far more gradual deviation, where this deviation first appeared at 5% PAN. Initially, it appears that PAni interacts far more strongly with the PVC solution than with PAN solution, increasing the viscosity even at lower concentrations of PVC. However, the interaction between the PAni and PVC appears to decrease with increasing PVC concentration to the point where the viscosity of the PAni/PVC solution was lower at PVC 20% compared with the corresponding PVC solution. This indicates that the either PVC was reducing interaction between charged PAni molecules at PVC 20%, through shielding or screening, or that PAni, or CSA, was actively lubricating or interfering with the PVC chains, in turn reducing their molecular entanglements. This is important for it may lead to a decrease in the ability of the PAni to carry charge throughout the polymer blend due to limitations in interaction with other PAni molecules. This screening effect was not observed in the PAN solutions and provides further evidence that the more polar nature of the PAN backbone significantly altered the PAni chain conformation, leading to a significantly larger increase in viscosity within the PAni/PAN solutions.

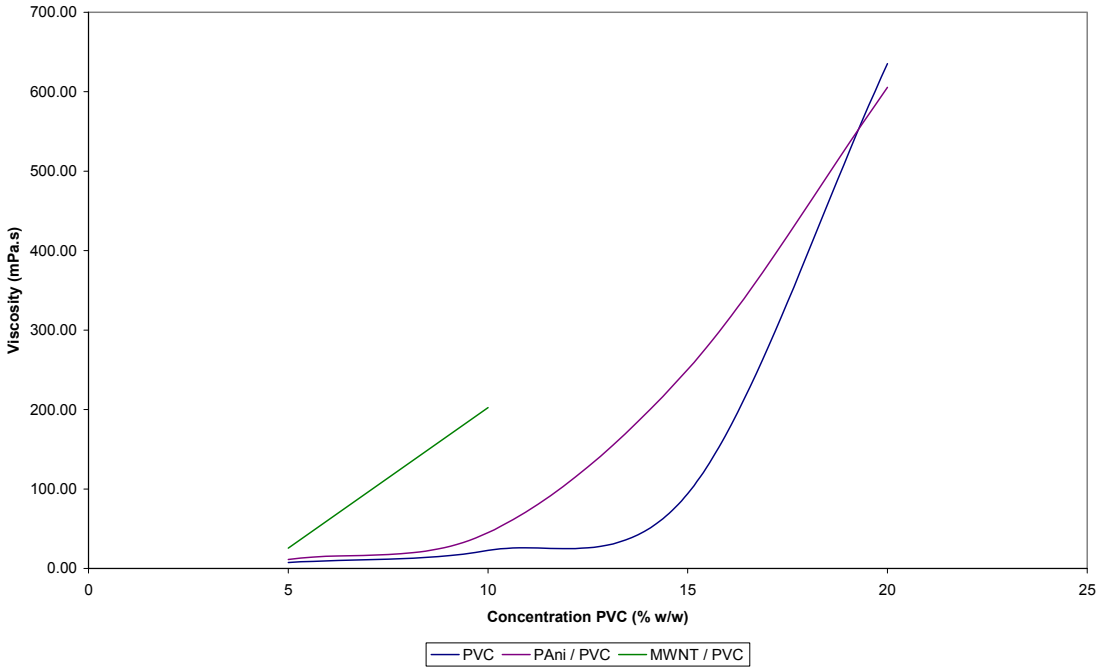

Figure 2.7 Viscosity of PVC, PAni 1%/PVC and MWNT 0.5%/PVC solutions at a shear rate of 50 s^{-1}

The addition of the nitrate ionophore tetradodecylammonium bromide (TDAB) to the solution of PAni 1% PVC 10% led to a significant increase in the viscosity. For a 0.5% addition of TDAB the viscosity increased from 45.01 mPa.s to 121.17 mPa.s. Further addition of TDAB to 5% in PAni 1% PVC 10% led to a decrease in the viscosity to 102.43 mPa.s, whilst the final TDAB concentration of 10% increased the solution viscosity to 233.83 mPa.s. However, this final value is dubious as the TDAB solution became saturated and the ionophore recrystallised from the PAni/PVC solution.

The graph of these points, presented in Figure 2.8 shows significant variation in the viscosity which may imply that the value for 10% TDAB was not in error. However there was some indication the viscosity for 0.5% TDAB was, and excluding this point presents a trend similar to increases in the polymer concentration observed for both PVC and PAN. Thus whilst there was some uncertainty in the results, a significant

increase in the viscosity did occur, indicating that a significant change took place within the solution. This change may have been due to the ionic structure of the ionophore interacting with ionic structure of PAni, or to some extent the PVC, leading to an increase in the viscosity of the polymer system by changes in the conformation of the polymer chains.

According to Lin et al. [184] these QAS act as cationic surfactants. In aqueous solutions the non-ionic polymer chains expand as they interact and wrap around the ionic surfactants. Furthermore Benrraou [204] notes that electrostatic interactions between polyelectrolytes and surfactants are quite strong, and as a result determine as to whether a polymer/surfactant interaction occurs. Thus this interaction may also apply to organic solutions whereby these QAS may alter the nature of the polyelectrolyte PAni chains and the chain conformation.

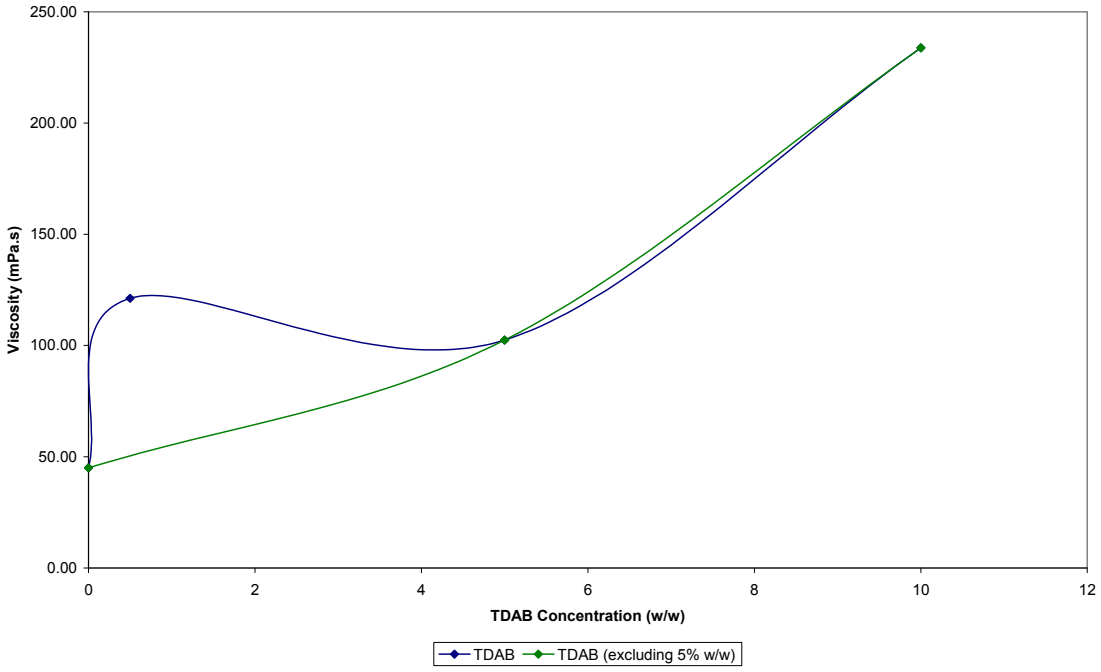

Figure 2.8 Viscosity of PAni 1% PVC 10% TDAB solutions at a shear rate of 60 s^{-1}

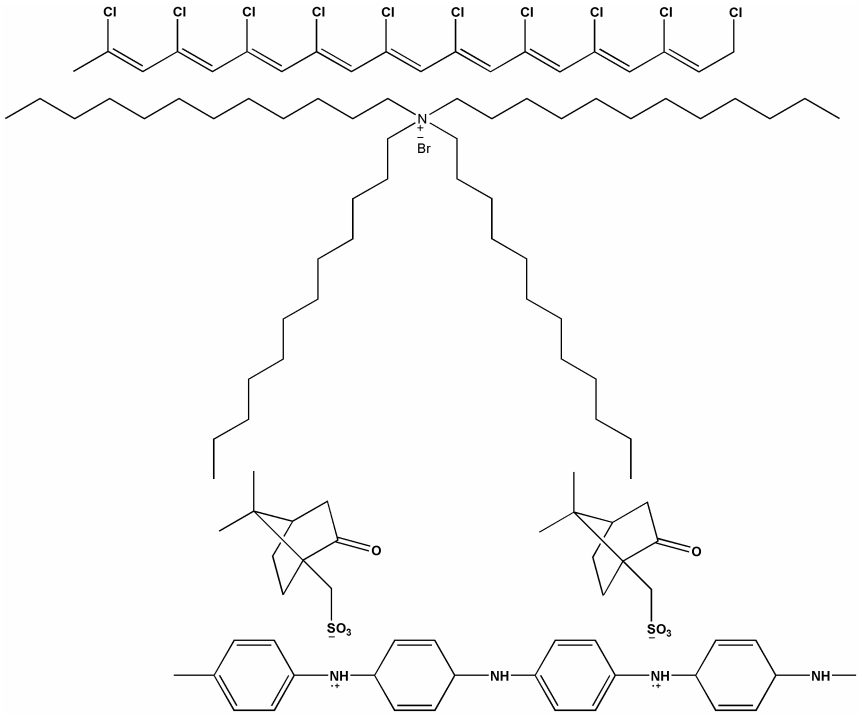

Figure 2.9 Possible chemical arrangement of PAni/PVC/TDAB in solution.

Another possibility is that the large alkyl chains on TDAB interact with the camphor group of CSA and also the PVC. This possible arrangement is presented schematically in Figure 2.9. If this were the case it would be expected the combination of TDAB and PVC would provide some structural support, leading to an uncoiled PAni chain, and in turn a higher viscosity.

MWNT/PVC solutions for 5% and 10% PVC highlighted an interesting point. There was a slight increase in the viscosity of MWNT 0.5% PVC 5% solution compared with the PVC 5% solution, followed by a significant increase for the MWNT 0.5% PVC 10% solution. This large increase in viscosity is similar to that observed by Seoul et al. [122] for SWNT in a solution of PVDF, though it would be expected that a similar increase would have been observed for both PAN and PVC solutions due to the same concentration of MWNT employed. Considering that MWNT 0.5% PVC 10% solution produced a significantly higher increase in viscosity then that observed for the

MWNT/PAN blend, it appears that again the two polymers strongly, but differently, influenced the viscosity in the presence of other additives. This difference does not support the Seoul et al. [122] observation that the increase in viscosity is due to entanglement of nanotubes. Thus the MWNT have influenced the entanglement and/or interaction of the polymer chains within the solution, though this interaction was strongly dependent on the type of polymer employed.

MWNT 0.5%/PVC 15% solutions were tested, but the results were discarded due to suspected water contamination.

2.5 Results and Discussion – Surface Tension

As surface tension of the electrospinning solution has been identified as an important parameter in electrospinning [84, 96, 185] it is necessary to study its effects with changes in polymer concentration, polymer and non-polymeric additives, and solvent composition.

The surface tension results for PAN solutions are given in Table 2.3, whilst results for PVC solutions are given in Tables 2.4 and 2.5

2.5.1 PAN Solutions

The surface tension of PAN 3% in DMSO/DMF increased from 42.5 mN m^{-1} (milliNewton per metre) to 44.6 mN m^{-1} as the level of PAN was increased to 5%. A further increase in polymer concentration to PAN 7% led to a decrease in surface tension to 43.1 mN m^{-1}. These large shifts in surface tension were unexpected as Liu and Hsieh [96] reports that the surface tension of a solution of cellulose acetate (CA) in

acetone and dimethylacetate only increased by 0.5 mN m^{-1} when the concentration of CA was doubled from 10% to 20%.

PAN 3% in DMSO/DMF				PAN 5% in DMSO/DMF			
Run	**IFT (mN m^{-1})**	**Error (mN m^{-1})**	**Volume (µl)**	**Run**	**IFT (mN m^{-1})**	**Error (mN m^{-1})**	**Volume (µl)**
1	42.4	0.5	5.9	1	44.5	0.3	5.8
2	42.1	0.6	6.1	2	45.0	0.5	6.1
3	43.0	0.7	6.2	3	44.6	0.2	5.7
4	42.2	0.4	6.1	4	44.7	0.5	5.3
5	42.9	0.7	6.3	5	44.4	0.3	5.6
Average	**42.5**	**0.6**	**6.1**	**Average**	**44.6**	**0.4**	**5.7**
St. Dev	**0.4**	**0.1**	**0.1**	**St. Dev**	**0.2**	**0.1**	**0.3**
PAN 7% in DMSO/DMF				**PAni 1% PAN 1% in DMSO/DMF**			
Run	**IFT (mN m^{-1})**	**Error (mN m^{-1})**	**Volume (µl)**	**Run**	**IFT (mN m^{-1})**	**Error (mN m^{-1})**	**Volume (µl)**
1	43.5	0.2	4.9	1	44.7	0.8	5.8
2	43.2	0.7	6.6	2	44.7	0.9	6.0
3	43.0	0.2	5.2	3	45.4	0.8	6.2
4	42.9	0.9	6.1	4	44.6	0.8	6.1
5	43.2	0.7	6.5	5	44.6	0.8	6.1
Average	**43.1**	**0.5**	**5.8**	**Average**	**44.8**	**0.8**	**6.1**
St. Dev	**0.2**	**0.3**	**0.8**	**St. Dev**	**0.3**	**0.0**	**0.1**
PAni 1% PAN 3% in DMSO/DMF				**PAni 1% PAN 5% in DMSO/DMF**			
Run	**IFT (mN m^{-1})**	**Error (mN m^{-1})**	**Volume (µl)**	**Run**	**IFT (mN m^{-1})**	**Error (mN m^{-1})**	**Volume (µl)**
1	43.6	0.9	6.0	1	47.2	1.0	7.0
2	44.1	0.8	4.9	2	47.5	1.3	7.1
3	43.8	0.9	6.2	3	47.0	2.5	8.3
4	43.5	0.7	5.8	4	46.5	1.5	7.3
5	42.9	0.6	5.7	5	47.8	1.5	6.8
Average	**43.6**	**0.8**	**5.7**	**Average**	**47.2**	**1.5**	**7.3**
St. Dev	**0.4**	**0.1**	**0.5**	**St. Dev**	**0.5**	**0.6**	**0.6**
PAni 1% PAN 1% TBACIO4 1% in DMSO/DMF				**PAni 1% PAN 3% TBACIO4 1% in DMSO/DMF**			
Run	**IFT (mN m^{-1})**	**Error (mN m^{-1})**	**Volume (µl)**	**Run**	**IFT (mN m^{-1})**	**Error (mN m^{-1})**	**Volume (µl)**
1	42.4	0.4	5.7	1	43.6	1.5	7.3
2	43.1	0.2	5.7	2	43.4	0.6	6.2
3	42.3	0.2	5.7	3	43.5	0.5	6.3
4	43.0	0.2	5.7	4	43.4	0.3	6.1
5	42.2	0.2	5.6	5	43.2	0.3	6.1
Average	**42.6**	**0.3**	**5.7**	**Average**	**43.4**	**0.7**	**6.4**
St. Dev	**0.4**	**0.1**	**0.1**	**St. Dev**	**0.2**	**0.5**	**0.5**

Table 2.3 Surface tension results for PAN solutions

One possible explanation is the evaporation of solvent from the pendant drop. These droplets were exposed to normal atmospheric conditions, thus the evaporation of solvent from the high surface area droplets would have occurred to some extent. This could possibly lead to the formation of a polymer skin over the droplet, altering the profile and thus altering the final results. In addition, it would be expected that the effect would be greater at higher solute concentrations where a small amount of evaporation would alter the polymer/solvent composition significantly, and this affect would be variable depending on the extent of evaporation and changes in the drop profile. However, this still does not account for the higher surface tension observed for PAN 5% compared to both 3% and 7% PAN solutions. The droplet profile error for all PAN solutions was relatively low and consistent between the samples. This error value provides a measure of the fit of the droplet profile to the Young-Laplace equation and indicates the accuracy of the results. This may indicate that the PAN 5% result was in error, possibly as a result of solution preparation.

The introduction of PAni 1% into the PAN solution did not significantly affect the solution surface tension of the solution. The addition of PAni 1% to PAN 3% solution increased the surface tension from 42.5mN m^{-1} to 43.6 mN m^{-1}. A much larger increase of 2.6 mN m^{-1} was recorded for PAni 1% PAN 5% compared to the PAN 5% solution, however this droplet profile error was relatively high, indicating a poor fit. Thus there appears to be little change in polymer/solvent or polymer/polymer interaction in the presence of PAni. The surface tension of the PAni 1% PAN 7% solution could not be determined due to the high solution viscosity preventing droplet formation and hence, analysis.

The surface tension of solutions containing tetrabutylammonium perchlorate ($TBAClO_4$), added to alter solution conductivity (see Section 2.6.5), were also determined. From these results it would appear that there was no shift in the surface tension, with the slight change observed well within experimental error. Thus it appears the organic salt makes little contribution to the surface tension at this concentration in these solutions.

2.5.2 PVC Blends

The increase in concentration of PVC did not appear to significantly alter the surface tension of the solution, however closer inspection of Tables 2.4 and 2.5 shows some uncertainty in the results. The standard deviation of the drop profile error for PVC 10% solution was extremely large, indicating that the analyses were of poor quality. The values for PVC 15% offered a better profile fit, however the standard deviation between the droplet profile errors was still quite large compared with both PVC 5% and the previous PAN solutions. PVC 20% in THF/DMF continued this trend in large droplet profile errors with a standard deviation of 3.57 for these values. Thus it is difficult to determine whether the surface tension of the solutions has altered with increasing PVC concentration. Assuming the surface tension values are correct, regardless of the drop profile errors it appears that the surface tension was reasonably consistent between PVC 5%, PVC 10% and PVC 15% solutions.

These large drop profile errors were a direct result of evaporation of the solvent, especially the volatile THF components, and formation of a polymer film on the droplets. This was consistently observed in these blends during ejection with the formation of non-uniform droplets, and the reduction in the size of the droplet over a short time.

With the addition of PAni 1% to PVC THF/DMF solutions the surface tension appears to have increased for all solutions. Again the standard deviation places these results with the values obtained for PVC-only solutions, indicating that any increases were not really significant. This can be clearly seen as the average for PAni 1% PVC 5% was 34.5 mN m^{-1} with a standard deviation of 0.6 mN m^{-1}, whilst the average for PVC 5% was 33.5 mN m^{-1} with a standard deviation of 0.9 mN m^{-1}. Furthermore the PAni 1% PVC 10% solution recorded an average of 34.2 mN m^{-1} with a standard deviation of 2.6 mN m^{-1}, compared with PVC 10% which recorded an average of 33.6 mN m^{-1} and standard deviation of 0.5 mN m^{-1}.

PVC 5% in THF/DMF				**PVC 10% in THF/DMF**			
Run	**IFT (mN m^{-1})**	**Error (mN m^{-1})**	**Volume (µl)**	**Run**	**IFT (mN m^{-1})**	**Error (mN m^{-1})**	**Volume (µl)**
1.0	33.1	0.4	4.3	1.0	33.2	4.6	6.4
2.0	34.4	0.5	5.2	2.0	33.8	4.4	5.9
3.0	33.6	0.3	5.2	3.0	34.3	1.6	5.9
4.0	34.0	0.4	5.4	4.0	33.3	0.4	4.8
5.0	32.2	0.7	5.3	5.0	-	-	-
Average	**33.5**	**0.4**	**5.1**	**Average**	**33.6**	**2.8**	**5.8**
St. Dev	**0.9**	**0.1**	**0.4**	**St. Dev**	**0.5**	**2.1**	**0.7**
PVC 15% in THF/DMF				**PVC 20% in THF/DMF**			
Run	**IFT (mN m^{-1})**	**Error (mN m^{-1})**	**Volume (µl)**	**Run**	**IFT (mN m^{-1})**	**Error (mN m^{-1})**	**Volume (µl)**
1	34.7	0.7	5.3	1	36.6	10.6	6.7
2	32.8	0.3	5.1	2	41.0	5.4	6.9
3	34.5	1.4	6.1	3	42.0	3.8	6.6
4	33.4	1.2	5.9	4	37.8	3.6	6.5
5	34.4	3.4	6.7	5	44.1	0.9	4.8
Average	**34.0**	**1.4**	**5.8**	**Average**	**40.3**	**4.9**	**6.3**
St. Dev	**0.8**	**1.2**	**0.7**	**St. Dev**	**3.1**	**3.6**	**0.9**
PAni 1% PVC 5% in THF/DMF				**PAni 1% PVC 10% in THF/DMF**			
Run	**IFT (mN m^{-1})**	**Error (mN m^{-1})**	**Volume (µl)**	**Run**	**IFT (mN m^{-1})**	**Error (mN m^{-1})**	**Volume (µl)**
1	34.7	0.7	5.1	1	35.6	2.2	7.0
2	33.6	0.5	4.7	2	36.2	0.9	6.3
3	35.2	0.8	5.4	3	29.7	0.3	5.3
4	34.2	0.4	5.2	4	34.7	4.7	7.0
5	34.6	0.6	5.0	5	34.7	4.4	7.5
Average	**34.5**	**0.6**	**5.1**	**Average**	**34.2**	**2.5**	**6.6**
St. Dev	**0.6**	**0.2**	**0.3**	**St. Dev**	**2.6**	**2.0**	**0.8**

Table 2.4 Surface tension results for PVC solutions

PAni 1% PVC 15% in THF/DMF				PAni 1% PVC 10% $TBAClO_4$ 1% in THF/DMF			
Run	**IFT (mN m^{-1})**	**Error (mN m^{-1})**	**Volume (µl)**	**Run**	**IFT (mN m^{-1})**	**Error (mN m^{-1})**	**Volume (µl)**
1	34.7	0.8	5.4	1	35.6	2.8	6.2
2	36.7	0.8	5.9	2	35.1	2.3	6.0
3	38.0	0.5	5.8	3	36.2	3.5	7.3
4	37.1	0.8	5.2	4	33.3	2.3	5.1
5	36.2	0.7	6.0	5	35.7	0.7	5.4
Average	**36.5**	**0.7**	**5.7**	**Average**	**35.2**	**2.3**	**6.0**
St. Dev	**1.2**	**0.1**	**0.3**	**St. Dev**	**1.1**	**1.0**	**0.8**

PAni 1% PVC 10% TDAB 0.5% in THF/DMF				PAni 1% PVC 10% TDAB 5% in THF/DMF			
Run	**IFT (mN m^{-1})**	**Error (mN m^{-1})**	**Volume (µl)**	**Run**	**IFT (mN m^{-1})**	**Error (mN m^{-1})**	**Volume (µl)**
1	40.1	0.5	5.8	1	39.7	0.4	5.1
2	40.4	0.4	5.6	2	38.1	0.8	4.9
3	40.3	0.3	5.6	3	38.8	0.3	5.4
4	40.4	0.4	5.6	4	39.2	0.6	5.0
5	40.2	0.3	5.7	5	38.8	0.7	5.2
Average	**40.3**	**0.4**	**5.7**	**Average**	**38.9**	**0.6**	**5.1**
St. Dev	**0.1**	**0.1**	**0.1**	**St. Dev**	**0.6**	**0.2**	**0.2**

MWNT 0.5% PVC 10% in THF/DMF			
Run	**IFT (mN m^{-1})**	**Error (mN m^{-1})**	**Volume (µl)**
1	33.4	2.1	5.0
2	34.9	2.2	4.8
3	36.6	2.5	5.2
4	36.8	0.9	4.5
5	36.3	1.6	4.5
Average	**35.6**	**1.8**	**4.8**
St. Dev	**1.4**	**0.6**	**0.3**

Table 2.5 Surface tension results for PVC solutions (continued)

The addition of 0.5% tetradodecylammonium bromide (TDAB) to PAni 1% PVC 10% in THF/DMF increased the surface tension by approximately 6 mN m^{-1}, from 34.2 mN m^{-1} for PAni 1% PVC 10% to 40.3 mN m^{-1} for PAni 1% PVC 10% TDAB 0.5%. This was a notable increase and would be expected to influence the morphology of the electrospun fibres to be discussed in Chapter 3. The surface tension of the PAni 1% PVC 10% TDAB 5% solution (38.9 mN m^{-1}) though slightly lower than the 0.5% blend, was also notably higher than the corresponding PAni 1% PVC 10% solution. This decrease in the surface tension compared with the TDAB 0.5% blend is intriguing, especially considering the drop profile was good and the individual results from

analyses were consistent. Thus, changes in the solvent interactions with both the polymer and the increased amount of quaternary salt may have affected the surface tension of the solutions.

Whilst the presence of TDAB altered the surface tension of the PAni/PVC solution, the introduction of $TBAClO_4$ had little affect on the surface tension of the blends, taking into account the error of the measurements. It is possible the shorter alkyl chains of $TBAClO_4$ may have interacted with the polymer chains to a lesser degree than the longer TDAB chains, thus producing little affect on the solution surface tension.

Lin et al. [184] did observe a 2 mN m^{-1}decrease in surface tension with an increase in concentration of dodecyltrimethylammonium bromide (DTAB) in a solution of polystyrene (PS) in THF/DMF, stating that this was due to a polymer/surfactant interaction. A solution of tetrabutylammonium chloride (TBAC) in PS initially increased 0.5 mN m^{-1} and subsequently decreased by 0.5 mN m^{-1} with an increase in the concentration of TBAC from 0.3 mmol to 3 mmol, indicating no polymer/surfactant interaction. As mentioned in Section 2.4.2 QAS can interact with, and wrap around polymer chains. This may change the interaction of the polymers with a solvent, which could possibly lead to a change in the solvation characteristics and in turn, surface tension. As the surface tension increased for PAni/PVC/TDAB, it may indicate the presence of both TDAB and PAni led to an increase in the solution surface tension. Consider that the solutions outlined by Lin et al. contained a non-ionic polymer and an ionic QAS, whilst these solutions contain a non-ionic polymer (PVC), QAS and an ionic polymer (PAni). The presence of PAni alone may have been sufficient to disrupt the solvation characteristics of the solution by interacting with the QAS, similar to Figure 2.9, leading to an increase in the intermolecular attractions of the solvents with the ionic

species, and in turn increasing the surface tension of the solution. Furthermore, considering $TBAClO_4$ is also a QAS, it appears that this interaction is directly influenced by the long alkyl chains of TDAB which would be expected to wrap around the polymer chains to a greater extent than $TBAClO_4$.

Finally, the addition of 0.5% MWNT to PVC solution slightly increased the surface tension of the polymer solution compared with PVC 10%. However, taking into account the error in the results, this increase was not significant. This observation is quite different to those reported by Seoul et al. [122] who observed a large decrease in the surface tension of a PVDF/DMF solution after the addition of 0.1% SWNT. This may imply that SWNT exert a different influence on the solution properties compared with MWNT, or that the SWNT could interact with PVDF far more than MWNT interacts with PVC, and in such a way as to reduce the solution surface tension.

2.6 Results and Discussion - Conductivity

2.6.1 PAN Solutions

The solution conductivity of a number of PAN/DMSO/DMF solutions varied considerably, as can be seen in Table 2.6.

From this table it can be seen that as the concentration of PAN increases, the conductivity of the solution also increases, covering the range of 0.11 mmhos for PAN 1% in DMSO/DMF through to 0.23 mmhos for PAN 5%. A plot of solution conductivity vs. [PAN] is given in Figure 2.10.

PAN Polymer Solutions	Cell Potential (V)	Air Temp (°C)	Average Rs (ohms)	Conductivity (mmhos)
PAN 1% in DMSO/DMF	-0.06	27	9380	0.11
PAN 3% in DMSO/DMF	-0.02	25	5790	0.17
PAN 5% in DMSO/DMF	0.01	27	4295	0.23
PAni 1% PAN 1% in DMSO/DMF	0.10	27	209	4.78
PAni 1% PAN 3% in DMSO/DMF	0.02	26	239	4.19
PAni 1% PAN 5% in DMSO/DMF	-0.04	27	228	4.38
PAni 1% PAN 1% $TBACIO_4$ 1% in DMSO/DMF	-0.01	27	90	11.10
PAni 1% PAN 3% $TBACIO_4$ 1% in DMSO/DMF	0.00	27	75	13.28

Table 2.6 Conductivity results for PAN solutions

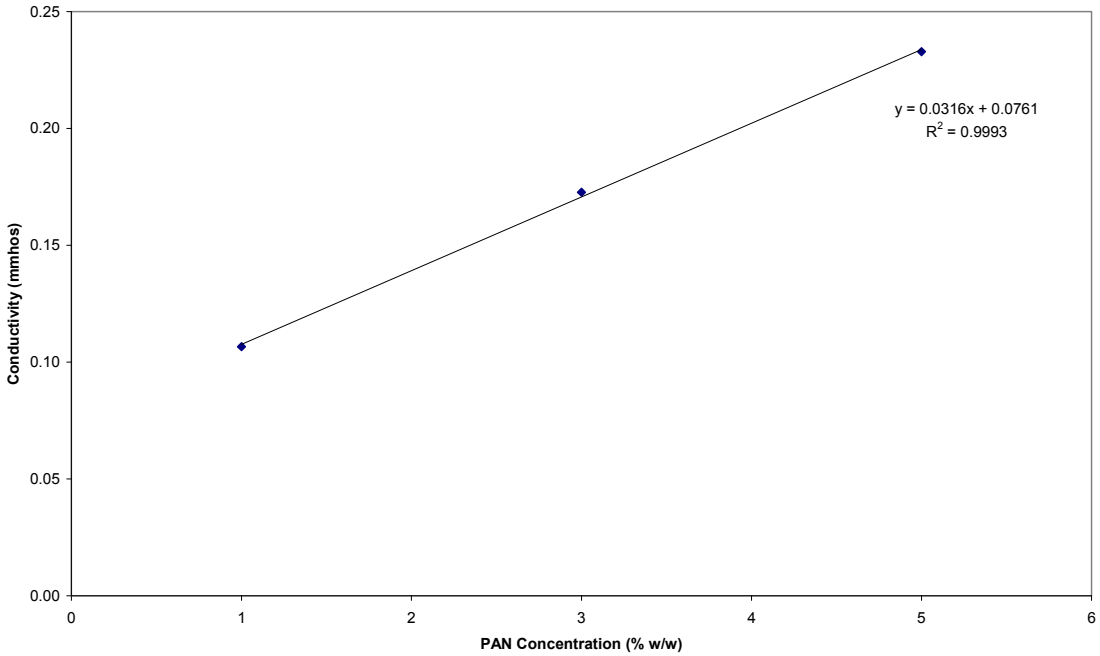

Figure 2.10 Conductivity of PAN in DMSO/DMF solutions with increasing PAN concentration

Theron et al. [101] previously observed increases in conductivity of PEO in an ethanol/water solution with increasing polymer concentration. They indicate that the solution conductivity is mainly the result of impure solvents due to the low conductivity values recorded, but do not detail as to why the conductivity increases with increasing

PEO concentration. This increase in conductivity of PEO solutions has also been observed by other authors [69, 183] with neither offering an explanation for the increase in conductivity. The same observation was recorded by Jun et al. [120] using poly(vinyl alcohol) (PVA) solutions in water with increases in conductivity with an increase in PVA concentration. However, Choe et al.. [205] observed that an increase in PAN concentration led to a significant decrease in conductivity in ethylene carbonate.

It has been shown [205-207] that the PAN chain interacts with lithium salts for polymer-based electrolytes. Among these Croce [206] suggests that the interaction takes place on the polar polymer backbone, specifically the C≡N group. It was also noted by Choe et al. [205] that the composition of ethylene carbonate (EC), propylene carbonate (PC) blend in a PAN based-Li salt electrolyte can influence the conductivity of the electrolyte due to a number of factors including the dielectric constant of the solvents, suppression of polymer crystallisation, viscosity and the solvation ability of the solvents. Specifically higher conductivities were observed with higher concentrations of EC, due to the higher dielectric constant of EC (89.6) compared with PC (64.4) that produced higher concentrations of charge carriers in EC-rich electrolytes. The viscosity for EC was lower (1.91 cP @ 40.0^{o}C) compared with PC (2.53 cP @ 40.0^{o}C), which also allows greater ionic mobility. It is therefore possible that other ions could also interact with the PAN chain in other solvents, altering the overall conductivity of the polymer blend, provided that the properties of the solvents are suitable.

It is also known that solvents contribute to conductivity of a solution due to polarity [121, 185]. Both DMSO and DMF have relatively high dielectric constants of 47 and 38 respectively. However, if the solvents influenced the solution conductivity of a polymer solution, it would be expected the conductivity would decrease with increasing polymer

concentration as the solvent contribution to the blend decreases, and ionic mobility also decreases [205]. However, this was not the case (Table 2.6 and Figure 2.10), as an increasing PAN concentration led to increased solution conductivity.

It is possible that the interaction between the solvents and PAN, along with the unique properties of PAN, affected the solution conductivity. Iovleva et al. [208] state that dilute solutions of PAN in DMF have low association; however PAN in DMSO shows strong association. This leads to differences in both the size and shape of the PAN coils in these solvents. However in concentrated solutions this association does not occur [208].

It would be expected that a mixture of these solvents would impart both low and high association, with respect to the solvent contribution. This may possibly lead to a conformation change to allow any contaminating species in the original polymer to interact with the polymer backbone, with negligible effect from the increased viscosity of the solution. In essence the PAN would be acting as a polymer electrolyte, with an ionic impurity from the original polymer powder, or solvents. It is equally likely that the solvent interacts more closely with the PAN, in turn increasing the polarity and hence increasing overall solution conductivity, such that the higher the PAN concentration, the greater the ability of PAN to carry charge.

2.6.2 PVC Solutions

As opposed to the case of PAN, it was found the conductivity of a PVC solution decreases with increasing concentration in THF/DMF, and this is presented in a plot of solution conductivity vs. [PVC] in Figure 2.11.

PVC Polymer Solutions	Cell Potential (V)	Air Temp (°C)	Average Rs (ohms)	Conductivity (mmhos)
PVC 5% in THF/DMF	0.03	27	12498	0.08
PVC 10% in THF/DMF	0.07	27	19490	0.05
PVC 15% in THF/DMF	-0.01	26	29400	0.03
PAni 1% PVC 5% in THF/DMF	0.03	27	1054	0.95
PAni 1% PVC 10% in THF/DMF	0.01	27	1052	0.95
PAni 1% PVC 15% in THF/DMF	0.03	26	1006	0.99
PAni 1% PVC 10% TDAB 0.5% in THF/DMF	0.05	26	244	4.10
PAni 1% PVC 10% TDAB 5% in THF/DMF	-0.07	26	75	13.28
PAni 1% PVC 10% $TBACIO_4$ 1% in THF/DMF	0.00	27	105	9.50
MWNT 0.5% PVC 10% w/w in THF/DMF	0.03	26	14520	0.07

Table 2.7 Conductivity results for PVC solutions

From both Table 2.7 and Figure 2.13 it can be seen that the increase in the concentration of PVC from 5% to 15% produced a decrease in the conductivity from 0.08 mmhos to 0.03 mmhos. This is consistent with other researchers who have observed decreases in the conductivity in a solution with increasing polymer concentration [101, 112, 209]. Pornsopone et al. [209] showed changes in conductivity for three different methacrylate-based copolymers (E-RLPO, E-L100 and E-EPO) dissolved in ethanol. The conductivity of E-RLPO increased followed by a plateau, E-L100 increased significantly and then began to decrease whilst E-EPO increased conductivity slightly followed by a large decrease. Again no inference was made as to the reasons for the changes in conductivity with changing polymer concentration. However it is most likely due the reduction in solvent contribution, with an increase in the resistive polymer component.

Another observation from both Table 2.7, and Figures 2.10 and 2.11, was that the conductivity of the PAN/DMSO/DMF solutions were an order of magnitude greater

than with PVC/THF/DMF solutions. The solvents may have contributed to some of the variation in conductivity of the solutions, but it is also likely that the significant difference in conductivity was a result of the different electrical properties of the two polymers. This is to be expected due to the ionic interaction of PAN discussed previously. This significant difference in conductivity may lead to significant differences in the morphology of electrospun fibres that will be discussed in Chapter 3.

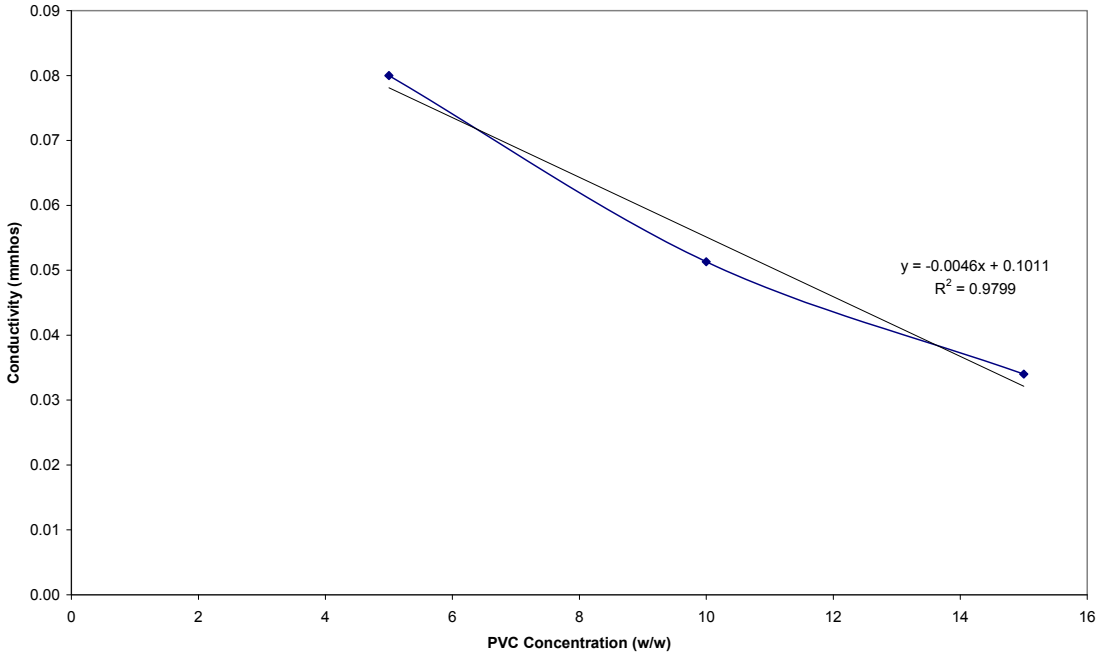

Figure 2.11 Conductivity of PVC in THF/DMF solutions with increasing PVC concentration

There is little data on the conductivity of PVC in organic solutions, making comparison of conductivity difficult. Lee et al. [84] reported changes in conductivity in a PVC/PU solution with altering polymer composition based on a 13% total polymer content. For 100% PVC polymer component at 13% concentration in a solvent blend of THF/DMF, they give a conductivity of approximately 0.10 mS m^{-1}. In comparison, a matching PVC concentration based on Figure 2.11 would produce a conductivity value of 0.04 mmhos.

This is less than half the conductivity compared with Lee et al. [84] indicating that the conductivity may vary significantly between blends depending on the purity, composition, type and brand of polymer and solvents.

2.6.3 PAni/PAN Solutions

Surprisingly, there is little information on the conductivity of organic polymer solutions containing PAni as a conductive component as mentioned previously. As anticipated, there was a significant change in the conductivity of a polymer solution with the introduction of CSA-doped PAni into the blend. Both PAni/PAN solutions and PAni/PVC solutions gave significant increases in the conductivity of the solutions, consistent with an increase in the number of charge-carriers within solution, comprising both PAni and the dopant, CSA.

From Table 2.6 it can be seen that the introduction of PAni 1% into the PAN 1% solution in DMSO/DMF increased the conductivity by more than an order of magnitude, from 0.11 mmhos to 4.79 mmhos. This also occurred for PAni 1% PAN 3% and PAni 1% PAN 5% solutions with the addition of 1% PAni (4.19 and 4.38 mmhos respectively) compared with PAN 3% and PAN 5% (0.17 and 0.23 mmhos).

The PAni 1% PAN 1% solution gave a noticeably higher conductivity than both PAni 1% PAN 3% and PAni 1% PAN 5% solutions while the conductivity for PAni 1 % PAN 3% was lower than the PAni 1% PAN 5% blend. These trends can be observed in a plot of conductivity vs. PAN concentration presented in Figure 2.12.

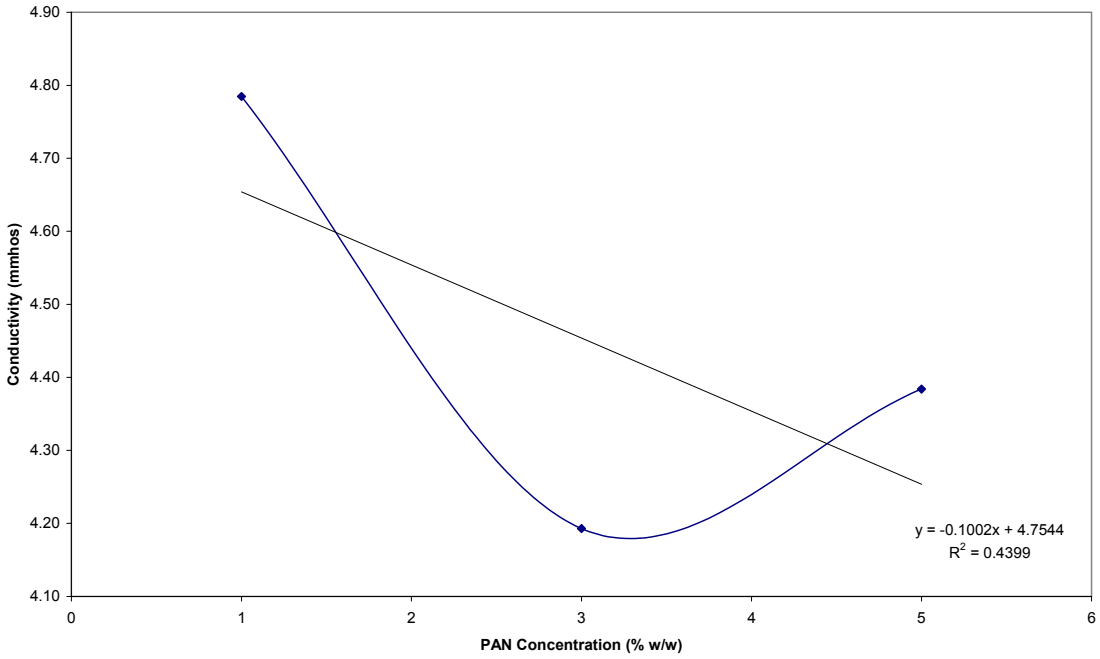

Figure 2.12 Conductivity of PAni/PAN in DMSO/DMF solutions with increasing PAN concentration

This indicates at least two things. Firstly the solution conductivity recorded after the addition of PAni was not significantly dependant on the conductivity of the original PAN solutions. Secondly, the conductivity of PAni 1% PAN solutions appear to have altered significantly with only slight changes in PAni addition. It has been noted [53] that conductivity of a PAni/poly(methyl methacrylate) (PMMA) blend increases logarithmically with linearly increasing PAni levels at low concentrations. Thus any error in the solutions in terms of PAni concentration may be magnified, leading to significant discrepancies in the results. Furthermore, increasing the concentration of PAN in a PAni blend may possibly reduce the mobility of the charge carriers, decreasing the conductivity of the solutions. Another issue with regards to the treatment of the PAni-polymer solutions was identified in solution dispersion, and will be discussed later in Section 2.7.

2.6.4 PAni/PVC Solutions

In contrast, the introduction of PAni into the PVC solutions increased the conductivity of all PVC solutions. As recorded in Table 2.7 and Figure 2.13, the addition of 1% PAni to PVC in THF/DMF solution increased the conductivity by at least an order of magnitude. For example, 1% PAni added to PVC 5% in THF/DMF increased the conductivity from 0.08 to 0.95 mmhos.

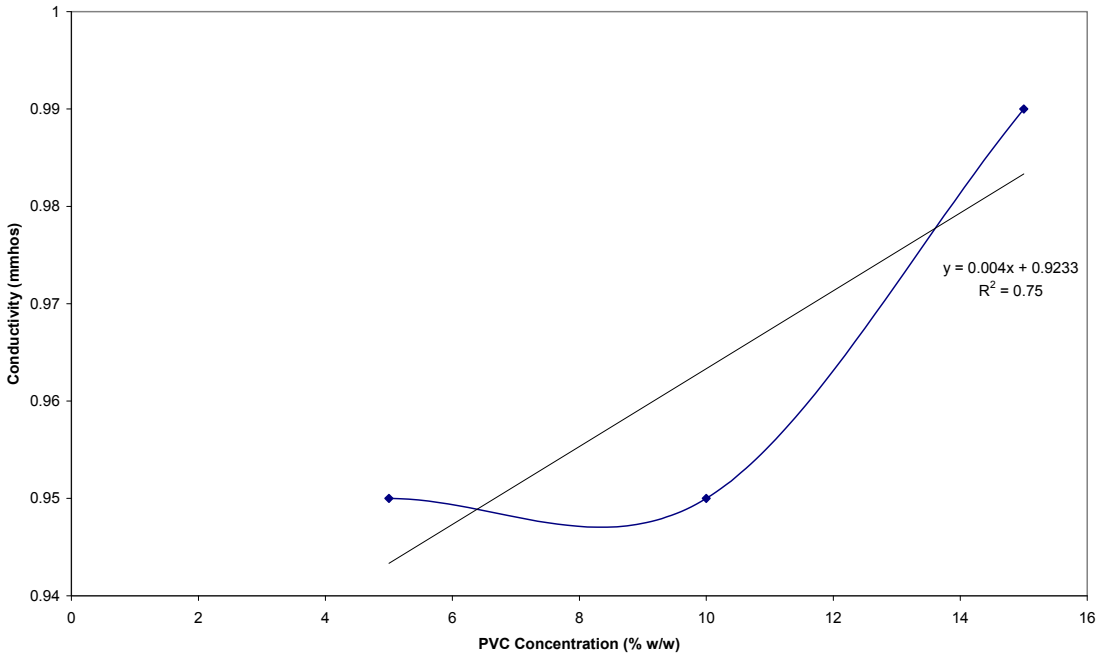

Figure 2.13 Conductivity of PAni/PVC in THF/DMF solutions with increasing PVC concentration

This increase in conductivity for PAni 1% PVC 5% may be a result of the influence of the addition of PAni to conductivity postulated in the PAni/PAN discussion: slight differences in the PAni concentration within the solution produced a significant change in the conductivity response of the solutions. Additionally, it would be expected that with increasing PVC concentration, the mobility of the charge carriers would decrease. Thus it is likely the experimental error in preparing 1% PAni solutions may have

contributed to these differences in conductivity, and they were not the result of an inherent change in the solution properties.

2.6.5 PAni/Polymer/TBAClO4 Solutions

The addition of 1% $TBAClO_4$ to PAni/PAN and PAni/PVC solutions produced some interesting data. For PAni 1% PAN 1% in DMSO/DMF a significant increase in the conductivity of the solution was observed, from 4.79 mmhos to 11.10 mmhos. PAni 1% PAN 3% and PAni 1% PVC 10% also increased conductivity by factors of over 3 and nearly 10 respectively. Obviously the introduction of $TBAClO_4$ increased the concentration of conducting species in solution, especially considering that only 1% $TBAClO_4$ was added to the solution. This supports other observations about the affect of salts on the conductivity of polymer solutions [112, 121, 183, 185]. Again the lower overall conductivity of the PAni/PVC solution compared with PAni/PAN may have been a result of the higher PVC content in the solution. However, the increase in conductivity between the two solutions after the addition of 1% $TBAClO_4$ was disproportionate with PVC increasing by an order of magnitude, but PAN only doubling in conductivity, indicating that the solution conductivity in the presence of $TBAClO_4$ was dependent on the polymer solution composition.

2.6.6 Addition of an Ionophore to PAni/PVC Blend

TDAB has been identified as a possible nitrate-selective ionophore for the use in nitrate-selective electrodes [210, 211].

From Table 2.7, the addition of 0.5% TDAB to a solution of PAni 1% PVC 10% in THF/DMF led to a four-fold increase in the conductivity of the solution from 0.95 mmhos for PAni 1% PVC 10% to 4.10 mmhos for PAni 1 PVC 10% TDAB 0.5%, and

to 13.28 mmhos for PAni 1% PVC 10% TDAB 5%. Further addition of TDAB led to saturation of the solution and it was unsuitable for analysis. However, from Figure 2.14 it is clear that the conductivity increased linearly with increasing TDAB up to the solubility limits of the QAS in solution.

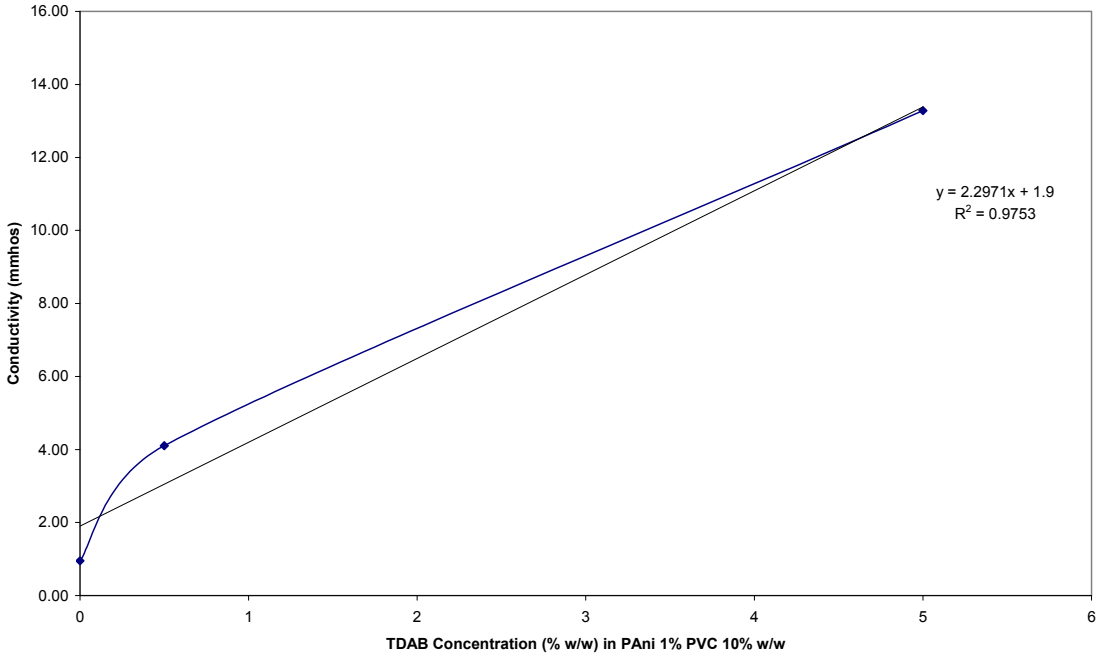

Figure 2.14 Conductivity of PAni/PVC/TDAB in THF/DMF solution with increasing TDAB concentration

According to House, Feng and Peet [212] tetraalkylammonium halide salts have been previously used in THF and DMF as supporting electrolytes. Thus, the change in conductivity follows the same reasoning as for the addition of $TBAClO_4$ to PAni/Polymer solutions, namely free ionic species in the solution acting as charge carriers. Though comparable with TDAB, it appears $TBAClO_4$ induced a greater change in conductivity with respect to the percentage added. A 1% addition of TDAB, according to Figure 2.14 would have a conductivity of approximately 5 mmhos, whilst the addition of 1% TBAClO4 would lead to a value of 9.50 mmhos. Thus different

tetraalkylammonium halide salts influence the solution conductivity to a different extent.

2.6.7 MWNT/PVC

The addition of MWNT to PVC 10% in THF/DMF produced only a slight increase in the conductivity of the solution, from 0.05 mmhos for a PVC 10% solution to 0.07 mmhos for MWNT 0.5% PVC 10% solution. However, even though nanotubes are recognised as having high electrical conductivity [213], and have been used as electrically conductive fillers in polymer composites [214], ionic conductivity was being measured here. As MWNT are non-ionic, the conductivity will be dependent on the charge carriers within solution and their mobility.

Seoul et al. [122] observed an increase in solution conductivity by more than three orders of magnitude, from 5 x 10^{-6} S cm^{-1} to approximately 4 x 10^{-3} S cm^{-1}, for an increase in SWNT from 0.000 to 0.014 wt % in a solution of poly(vinylidene fluoride) (PVDF) in DMF. This concentration is significantly lower than the concentration of MWNT employed in the PVC blend. It is possible the charge mobility throughout the solution was limited due to the polymer matrix, however this was not reported by Seoul et al. [122]. Though it is also possible aggregations of MWNT may have persisted, limiting the overall conductivity of the composite. This will be discussed further in Section 2.7. Another possibility is that the quality of the MWNT was low, with a large proportion of impurities and other products which would not contribute to an increase in solution conductivity.

MWNT/PAN solutions were not analysed for conductivity due to the volume required, the cost of raw MWNT and access to instrumentation.

2.7 Results and Discussion – Particle Size Analysis

2.7.1 PAni/PAN Solutions

The PAni/PAN solutions presented a wide array of particle sizes, given in Table 2.8. Most notable is the high Z-Average for PAni 1% PAN 1% $TBAClO_4$ 1% in DMSO/DMF, having a value of 1900 nm. Compare this with the solution containing PAni 1% PAN 3% $TBAClO_4$ 1% in DMSO/DMF with a value of 461 nm. It would be expected that the results would be similar as the only factor that has changed is the concentration of PAN. It is possible the support polymer is actively influencing the particle size.

PAN Polymer Solution	Z-Average (d.nm)	Size Quality Report
PAni 1% PAN 1% w/w in DMSO/DMF	437	Presence of large and segmenting particles Sample fluorescence Sample absorbance (coloured samples) Sample is very polydisperse Sample contains large particles/aggregates/dust
PAni 1% PAN 3% w/w in DMSO/DMF	223	Presence of large and segmenting particles Sample fluorescence Sample absorbance (coloured samples)
PAni 1% PAN 5% w/w in DMSO/DMF	119	Presence of large and segmenting particles Sample fluorescence Sample absorbance (coloured samples)
PAni 1% PAN 1% TBAClO4 1% in DMSO/DMF	1900	Presence of large and segmenting particles Sample fluorescence Sample absorbance (coloured samples)
PAni 1% PAN 3% TBAClO4 1% in DMSO/DMF	461	Presence of large and segmenting particles Sample fluorescence Sample absorbance (coloured samples)

Table 2.8 Particle size results for PAni/PAN solutions

This also appears to follow for all the PAni/PAN solutions. The particle size decreased from 437nm for PAni 1% PAN 1% to 223 nm for PAni 1% PAN 3%, followed by a particle size of 119 nm for the PAni 1% PAN 5% solution. Thus, the higher the concentration of PAN the lower the particle size, indicating PAN actively reduces the

average particle size in the PAni/PAN solutions. This would support the hypothesis that there is a strong interaction between PAni and PAN. As the concentration of PAN increases it helps solubilise PAni, breaking down the particle size.
Again MWNT/PAN solutions were not analysed due to cost and access to instrumentation.

2.7.2 PAni/PVC Solutions

The values for PAni/PVC are less consistent (Table 2.9). For example the solution of PAni 1% PVC 5% had a smaller particle size (119 nm), compared with the remaining PAni/PVC blends and the MWNT 0.5% PVC 15% solution. All these remaining PVC solutions had particle sizes around 600-700 nm, which indicates that neither the concentration of PVC nor QAS made appreciable difference to the particle size.

However, the support polymer concentration had some influence on particle size, similar to observations for PAni/PAN, except in this case an increase in the support polymer led to an increase the particle size. This may be due to PAni or MWNT aggregations within the PVC solution due to the higher support polymer content, and further evidence that the interaction between PAni and PVC was not particularly strong. Nonetheless, the average diameters are extremely large considering that electrospun fibres will produce widths below 100nm, which will be discussed in Section 3.4.
Whilst there appears to be some relationship, all Z-Average values should be treated carefully. Consistently there were large particles within the solutions along with sample fluorescence and absorbance. Whilst the values may not be absolute and offer little in definitive results, the quality report indicates that the solutions are not well dispersed and aggregations have either existed or formed since preparation. This is significant for the production of electrospun fibres that are homogenous. The morphology of the

electrospun fibres will be examined in Chapter 3 and the particle size analysis will be related to the quality of PAni and MWNT fibres produced.

PVC Polymer Solution	Z-Average (d.nm)	Size Quality Report
PAni 1% PVC 5% w/w in THF/DMF	119	Presence of large and segmenting particles Sample fluorescence Sample absorbance (coloured samples)
PAni 1% PVC 10% w/w in THF/DMF	744 656 (Rpt)	Presence of large and segmenting particles Sample fluorescence Sample absorbance (coloured samples) Sample is very polydisperse Sample contains large particles/aggregates/dust
PAni 1% PVC 10% TDAB 0.5% in THF/DMF	696	Presence of large and segmenting particles Sample fluorescence Sample absorbance (coloured samples) Sample is very polydisperse Sample contains large particles/aggregates/dust
PAni 1% PVC 10% TDAB 5% in THF/DMF	690	Presence of large and segmenting particles Sample fluorescence Sample absorbance (coloured samples) Sample is very polydisperse Sample contains large particles/aggregates/dust
PAni 1% PVC 10% TBAClO4 1% in THF/DMF	647	Presence of large and segmenting particles Sample fluorescence Sample absorbance (coloured samples) Sample is very polydisperse Sample contains large particles/aggregates/dust
MWNT 0.5% PVC 10% w/w in THF/DMF	565	Presence of large and segmenting particles Sample fluorescence Sample absorbance (coloured samples)

Table 2.9 Particle size results for PAni/PVC solutions

2.8 Conclusions

Both PAN and PVC solutions exhibited a pseudoplastic trend, as well as comparable increases in viscosity with increased polymer concentration. It was found that the presence of PAni in solutions of PAN in DMSO/DMF and PVC in THF/DMF exhibited significantly different solution properties. The presence of PAni altered the rheological response of both PAN and PVC solutions, providing evidence that these two support polymers interact with PAni, and by different means. It was postulated that the strong dipole interactions of the cyano-groups on PAN may interact more directly with PAni in solution or provide a strong support structure, whereas this did not appear to be the case with PVC, which appears to screen or lubricate the PAni chains. The presence of TDAB in PAni 1% PVC 10% significantly increased the viscosity of the solution, indicating that the solution properties had altered. It was surmised that TDAB had produced a support structure, similar to PAN, which had led to the uncoiling of polymer chains within solution, and a subsequent increase in viscosity.

The addition of MWNT to both PAN and PVC provides further evidence that these two polymers are inherently different in solution. The presence of MWNT in a PVC solution increased the viscosity significantly, whilst this also occurred with MWNT in PAN, it did so to a lesser extent. Thus these two polymers interact with solution additives to a different extent, in turn directly influencing the rheological properties of the solution.

Surface tension values of PAN and PVC solutions were markedly different. However, the higher surface tension for PAN solutions compared with PVC solutions appears to be a result of the solvent composition more so than the polymer composition. The addition of PAni or $TBAClO_4$ to these solutions did not alter the surface tension

significantly and was accounted for by error within the analyses. The only major change in surface tension arose from the addition of TDAB to PAni/PVC. It is believed these changes arose from TDAB directly interacting with polymer chains, in turn altering the solvation characteristics of the chains, and hence the surface tension of the solution. Furthermore this response appears to be directly related to the length of the alkyl chains on TDAB, as $TBAClO_4$ recorded no change in surface tension.

The addition of MWNT did not significantly increase the surface tension of a PVC solution. Other literature has observed a decrease in surface tension in a SWNT/PVDF solution, implying MWNT interacts with polymers differently, or not at all, or that the other solution components predominately determine the degree of interaction with the MWNT.

It was found that PAN was far more conductive in solution than PVC, and this solution conductivity increased with increasing concentration of PAN. It was postulated that contaminants within the solution were interacting with the cyano-groups of PAN and leading to PAN acting as a polymer electrolyte, similar to PAN-Li^+ blends, or that the overall solution conductivity was a product of solution polarity. The addition of PAni to these polymer solutions significantly increased the conductivity by an order of magnitude for both polymers. The solution conductivities indicated that only small changes in PAni composition can lead to a significant change in the conductivity of the solution. The addition of both TDAB and $TBAClO_4$ led to further increases in solution conductivity, such that these species were acting as free-charge carriers.

The presence of MWNT only slightly increased the solution conductivity of a PVC solution. Considering nanotubes have been recognised as having good electrical

properties this was a surprising result, and indicates that the MWNT were not sufficiently separated, or there was a large amount of non-conductive impurities within the MWNT powder.

Particle size analysis indicated that large particles of undispersed or undissolved matter were present in the solution, but more importantly the size of these particles was dependent on the concentration of the support polymer. An increase in the PVC concentration led to an increase in the size of the particulate matter, indicating that this support polymer assists in the formation of aggregate material within solution. Conversely, when PAN was employed as a support polymer, increasing its concentration decreased the size of the particulate matter, indicating that this support polymer either helps solubilise PAni or disperse PAni and/or MWNT.

Chapter 3 - Fibre Morphology

'To the complaint, 'There are no people in these photographs,' I respond,

'There are always two people: the photographer and the viewer.'

Ansel Adams (1902 – 1984)

3.1 Introduction

Viscosity has been identified as affecting not only the spinning of electrospun polymer fibres, but also the resultant fibre morphology including diameter and structure. A number of studies indicate that generally an increase in the viscosity of the spinning solution will lead to an increase in the fibre diameter [67, 68, 84, 96, 97, 107, 112, 119, 120, 190]. It has also been noted that fibre morphology alters significantly with changes in surface tension, both directly and indirectly, whilst fibre diameter has been shown to decrease with an increase in the conductivity of the spinning solution [84, 104, 183-185].

However, contradictions arise as to the effect that these parameters contribute to electrospinning and fibre morphology. There is also limited information in the literature where conducting polymers are included in combination with these commodity plastics. This chapter will provide an analysis of the commodity plastics PVC and PAN, and the inclusion of both the conducting polymer PAni, and ionophores, and identify the relationship between these parameters and fibre morphology, including fibre diameter and the visual appearance.

3.1.1 Viscosity & Fibre Morphology

It was reported by Fong et al. [183] that significant changes in the fibre diameter as a function of viscosity occurs for poly(ethylene oxide) (PEO) fibres electrospun from water. The diameters ranged from <80 nm to 250 nm as the viscosity increased from 13 cP to over 1800 cP [183].

In contrast, Fong and Reneker [65] reported in a later study that fibre diameter was not affected significantly by altering the viscosity of the PEO solution. This is also

supported by Lee et al. [142] who studied the electrospinning of 15% w/w poly(vinyl chloride) (PVC) in various compositions of a tetrahydrofuran (THF) and dimethylformamide (DMF) solution to alter the viscosity of the solution. Though the resultant fibre diameter varied, increased viscosity did not necessarily correspond to increased fibre diameters. In fact, the highest viscosity was observed for a solution of PVC in 100% DMF, which in turn produced the lowest fibre diameter. On the other hand, the solution exhibiting the lowest viscosity produced fibre diameters that were similar to blends with four different solvent compositions of THF/DMF [142].

The relationship between the fibre diameter and solution viscosity can be unpredictable as the viscosity of the solution is not always directly related to the extensional viscosity, a parameter used to provide a measure of the elasticity of the electrospinning jet [215]. According to Yu et al. [216], it is this elasticity that influences jet formation during electrospinning, and hence, the resultant fibre morphology. In some cases this extensional viscosity can be an order of magnitude higher than the shear viscosity used to determine solution viscosity [215].

In general, it is expected that lower viscosity solutions will stretch to a greater degree due to the reduced cohesive forces and less chain entanglement associated with lower polymer concentration, in turn leading to thinner electrospun fibres [209]. Conversely, the greater the viscosity the greater the cohesive forces and chain entanglement, which in turn leads to fibres with a greater diameter. Whilst this may not be always the case, the fibre morphology is dependent on the polymer concentration of the solution [98, 119].

3.1.2 Surface Tension and Fibre Morphology

There has been much debate about the formation of spherical structures along fibres and how these relate to surface tension. Fong and Reneker [65] and Fong et al. [130] state that these spherical structures, or 'beads', are a result of the partial collapse of fibres due to the surface tension of the polymer solution. The surface tension leads to the capillary break-up of the jet, forming droplets, with the remaining jet forming fibres. The solvent then evaporates leaving behind the corresponding beads and fibres. Lee et al. [144] indicated that bead formation was, in fact, a result of viscosity more so than surface tension, whilst Entov and Shmaryan [217] indicated that beads were a result of the jet instability. Shawon and Sung [98] partially support Lee et al. [144] by stating that the viscoelastic forces from polymer solutions overcome the affect of surface tension as the viscosity of the polymer solution increases [98].

Thus an increase in polymer concentration leads to a decrease in bead formation as the viscoelastic properties cancel out the effects of the surface tension [65, 183]. Alternatively, a decrease in the surface tension of a polymer solution can also lead to a reduction in the occurrence of beads [183]. According to Zuo et al. [92] this is also related back to the jet instabilities, discussed in Section 1.2.2, whereby enhancement of the axisymmetric instabilities leads to bead formation, whilst the whipping instability suppresses bead formation. The applied potential, surface tension and the surface charge density play key roles in the generation of these instabilities [92].

However, Jaeger et al. [103] offered two alternate explanations for the 'beads-on-string' morphology that do not mention surface tension. The first is that the solution flows along the jet, or liquid cylinder, into evenly spaced droplets along the main fibre backbone. The second rationale is that these beads are a result of the draw-resonance

phenomenon. That is the jet becomes unstable when the ratio of stretching exceeds some critical point leading to the production of beads. This instability occurs more slowly for solutions exhibiting a higher viscosity [103, 218].

3.1.3 Conductivity and Fibre Morphology

A significant decrease in fibre diameter was reported by Tan et al. [190] in the electrospun fibre diameter of poly(L-lactid acid-co-caprolactone) (PLLA-CL) by adding pyridine to dichloromethane (DCM) in a 50/50 wt% ratio. They indicated that this decrease in fibre diameter was a direct result of an increase in the conductivity of the solution from 0 to 13.1 $\mu S\ cm^{-1}$, leading to a diameter decrease from approximately 310 to 110 nm. According to Tan et al. [190] this was due to an increase in the charge density of the solution and polymer jet, such that this extra charge density led to increased elongation of the jet during electrospinning. Lin et al. [184] observed significant decreases in the fibre diameter of solutions of polystyrene (PS)/dodecyltrimethylammonium bromide (DTAB) and tetrabutylammonium chloride (TBAC) electrospun from THF/DMF. These cationic surfactants led to an increase in conductivity of the solution. The increase in conductivity, and hence charge density, led to an increase in the whipping instability observed during electrospinning which elongated the jet [184].

On the other hand, Li and Hseih [121] observed an increase in the conductivity of poly(acrylic acid) (PAA) solution with the addition of NaCl, however there was no discernable decrease in the diameter of the fibres. This was due to the increased entanglement of PAA molecules in the solution which negated the anticipated fibre diameter decrease [121].

In terms of bead production, Jun et al. [112] reports that the addition of an organic salt (which increased the conductivity of the solution but did not significantly alter the viscosity or surface tension) reduced the presence of beads in electrospun fibres. This supports the statements from Tan et al. [190] that bead production may be a symptom of low conductivity solutions, leading to the formation of beads due to reduced jet elongation and uniform fibre production. This relationship is also supported by Frenot and Chronakis [99] who state that bead production is directly related to the charge density, surface tension and viscosity of a solution [99]. Furthermore Son et al. [185] report that the dielectric properties of the solvents also affect the conductivity of the polymer solutions, leading to the production of beads-on-string morphology from solutions comprised of solvents having low dielectric constants.

3.2 Preparation of Samples

3.2.1 Polymer Solution Preparation

The appropriate amount of PVC or PAN was dissolved in THF/DMF or DMSO/DMF respectively and magnetically stirred overnight to prepare a homogeneous polymer solution.

3.2.2 PAni/Polymer Solution Preparation

All PAni/polymer solutions utilised 1% PAni due to previously recognised limitations in its solubility [52, 58, 78, 129, 145]. Camphorsulfonic acid (CSA) was weighed into a scintillation vial, and suitable volumes of solvent were added. After CSA had dissolved, PAni was added slowly and stirred on a magnetic stirrer until dissolved. Following this the commodity plastic was added and mechanically stirred until dissolved.

3.2.3 Other Polymer Solutions

If other additives were required, such as quaternary ammonium salts (QAS), this material was weighed and added to the solutions prior to the addition of PAni. It is important to note that a small amount of THF was added to assist in the dissolution of the TDAB in PAni/PAN blends prior to the addition of PAni due to insolubility of TDAB in DMSO/DMF. In the case of MWNT solutions, MWNT (0.5%) was weighed and added to a scintillation vial, following the addition of the solvents. The MWNT were dispersed by sonification, after which the support polymers were added to the solution and left to dissolve by magnetic stirring.

Further details of solution preparation can be found in Section 2.3 Preparation of Samples.

3.2.4 Electrospun Fibres

A Gamma High Voltage Power Supply (ES50P-10W/DAM) was employed for all electrospinning. The polymer solutions were drawn into a 100 μL Eppendorf micropipette tip which was then removed and placed on a 50 mm length of platinum wire attached to the end of the high voltage coaxial cable. This was tilted at an angle from horizontal to obtain a steady droplet at the end of the pipette tip. A potential was applied to obtain a constant production of electrospun fibres. These electrospun fibres were collected on 45 mm x 10 mm gold-coated Mylar® targets (see Figure 3.1) rotated at 400 rpm for PAN solutions and 600 rpm for PVC solutions on a Janke & Kunkel, Eurostar Digital overhead stirrer. The electrospinning was carried out at suitable potentials for steady fibre formation (8-9 kV for PAN, 12-13 kV for PVC) at a distance of approximately 12 cm from the target. Three separate aliquots of 100 μL of polymer solution were used for each electrospinning sample.

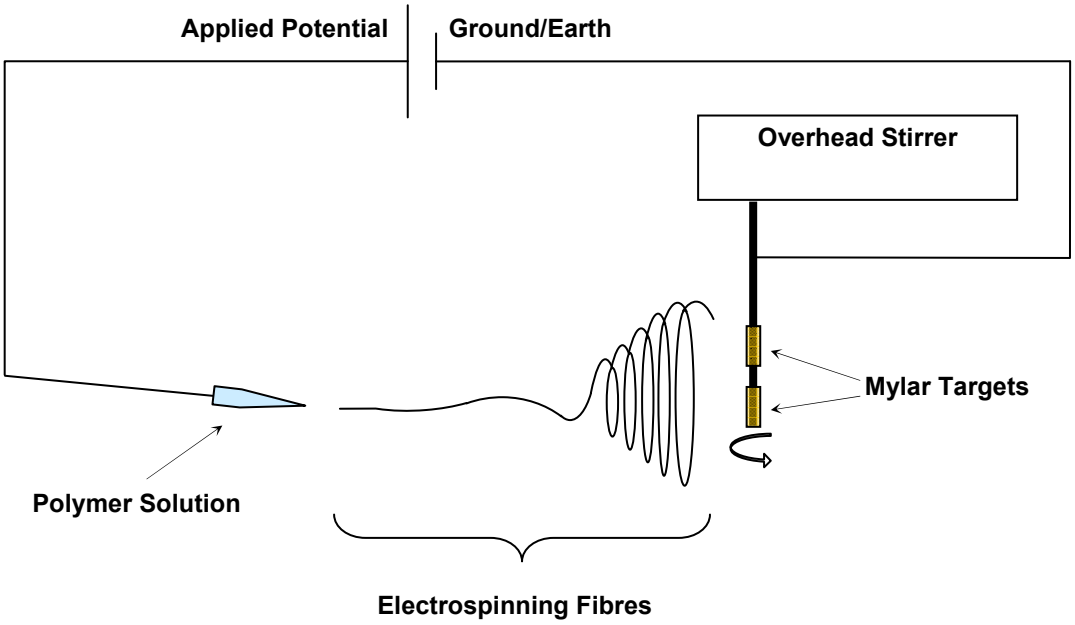

Figure 3.1 Electrospinning Apparatus

3.2.5 Analysis of samples

Samples were attached to metallic stubs before being gold-coated on a Bal-Tech Sputter Coater (Model 050) and then analysed on an ElectroScan ESEM (Model 2020) scanning electron microscope, a Leica Stereoscan SEM (Model 440) or an FEI ESEM (Quanta 600). Fibre size analysis was carried out using the University of Texas Health Science Center at San Antonio ImageTool (Version 3).

3.3 Results and Discussion – Scanning Electron Microscopy

3.3.1 PVC Electrospun Fibres

It was not possible to electrospin fibres from PVC 5% in THF/DMF as the viscosity was too low to enable jet initiation, instead the solution electrosprayed fine polymer droplets. Fibres were successfully electrospun from PVC 10% in THF/DMF and studied by scanning electron microscopy (SEM). These fibres exhibited a significant number of

beads and globules throughout the fibrous mat, and can be observed in Figures 3.2 (a) and (b).

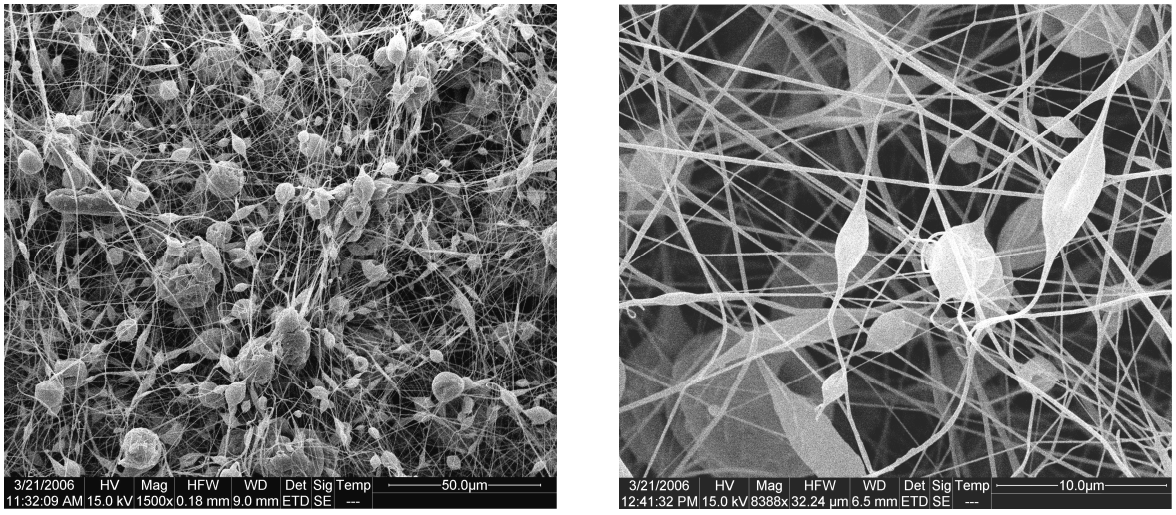

(a) (b)

Figure 3.2 SEM micrographs of fibres electrospun from PVC 10% in THF/DMF (a) Mag: 1,500X, (b) Mag: 8,388X

These beads and globules differed throughout the blend showing both spherical and ellipsoidal shaped beads, as well as large globules that appear to be the result of electrospraying of the PVC solution. This indicates that the viscosity of the solution, and hence the concentration of the polymer may have been too low, or the surface tension may have been too high to electrospin the solution adequately. There was also no significant orientation of the electrospun fibres which may indicate the rotation speed of the target was lower than required to produce orientated fibres.

As can be seen in Figures 3.3 (a) and (b), the number of beads and globules decreased dramatically for fibres electrospun from PVC 15% in THF/DMF compared with the PVC 10% fibres. Thus an increase in PVC concentration has led to a decrease in the number of non-fibre structures throughout the sample. This was not due to a change in the surface tension of the polymer solution as the surface tension did not change

significantly with increases in the polymer concentration (Section 2.5.2). However, the solution conductivity did decrease (as noted in Section 2.6.2), but this would be expected to increase the number of beads [190]. Consequently, it appears that the increased concentration of PVC directly reduced bead production and electrospraying. This is supported by Shawon and Sung [98] who state that the increased viscoelastic properties from increasing polymer concentrations overcame the influence of the surface tension on bead production, thus reducing bead numbers.

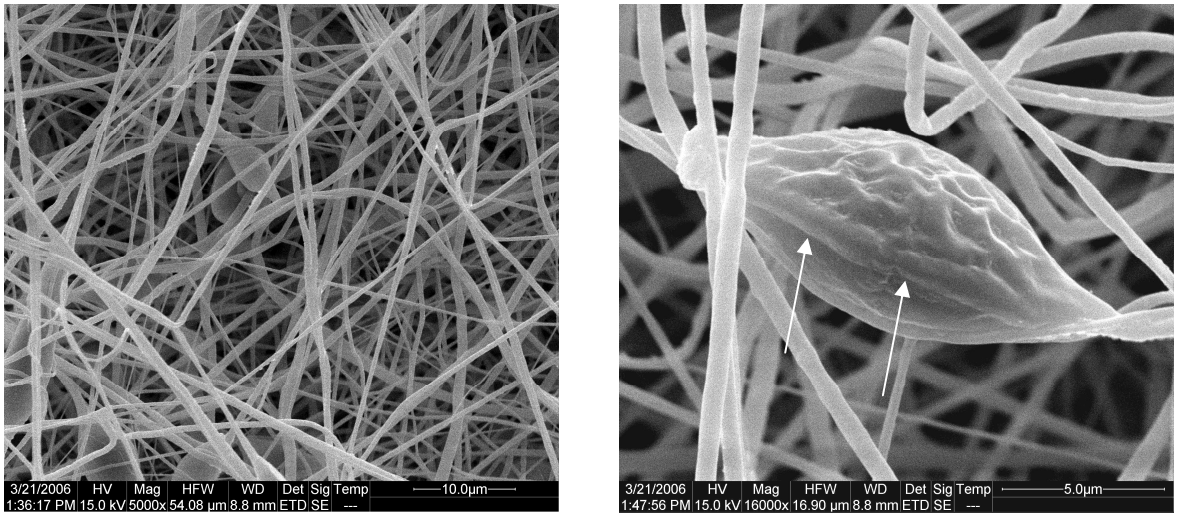

(a) (b)

Figure 3.3 SEM micrographs of fibres electrospun from PVC 15% in THF/DMF (a) Mag: 5,000X, (b) Mag: 16,000X; arrows indicate underlying fibre

Figure 3.3 (b) presents a closer look at one of the beads/globules present in the fibres. This image is interesting in that the feature is consistent with the 'beads-on-string' morphology. However, it appears that the bead/globule is attached to the surface of the electrospun fibre (indicated by the arrows), rather than being an expanded part of the fibre. Furthermore, it appears that the beads are not solid polymer as the dimples on the surface indicate that there was some evaporation of solvent.

Increasing the concentration further led to a decrease in the overall uniformity of the electrospun fibres. Figure 3.4 (a) provides an overview of the fibrous mat showing that the electrospun fibres were not orientated in any one direction, but instead electrospun in the form of a non-woven mat. Again this indicates that the rotation speed of the target was insufficient to produce orientated fibres. This lack of orientation may decrease the tensile strength of the electrospun fibres if the fibres are not stretched in the direction of their individual orientation, instead relying only on fibres that are orientated in the direction of stretching.

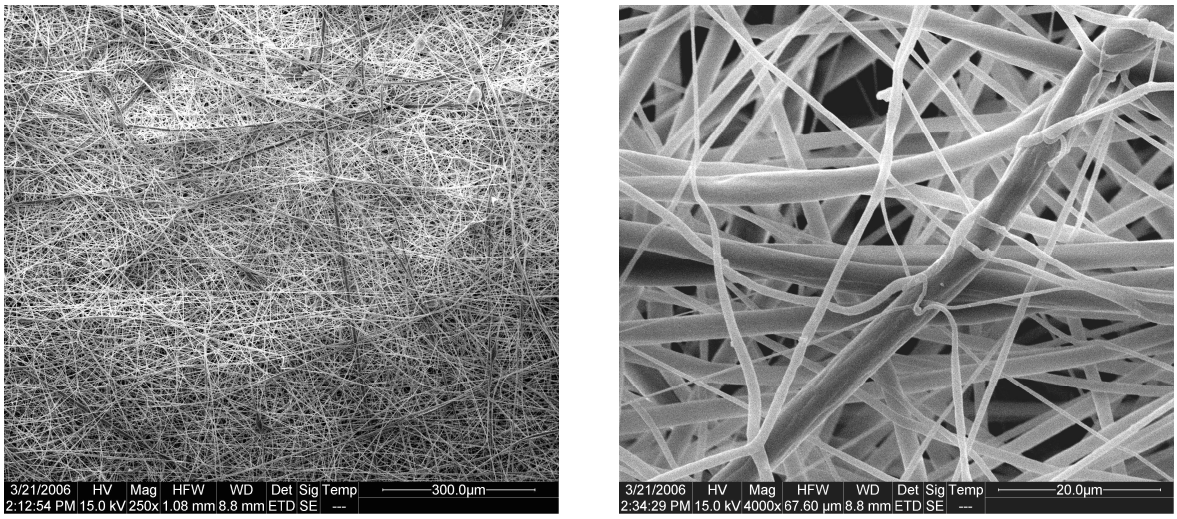

(a) (b)

Figure 3.4 SEM micrographs of fibres electrospun from PVC 20% in THF/DMF (a) Mag: 250X, (b) Mag: 4,000X

Figure 3.4 (b) shows significant differences in the size of the fibres from this blend. The actual fibre diameters of a representative sample of each mat were determined and will be discussed later in this chapter (Section 3.4). These larger fibres exhibit grooves in the surface which may be indicative of evaporation of the solvent either during or after electrospinning. It is also possible that these large fibres were originally smaller fibres that twisted and bundled together during electrospinning to form large diameter fibres before complete evaporation of the solvent.

3.3.2 PAN Electrospun Fibres

It was not possible to electrospin fibres from PAN 1% in DMSO/DMF, again due to the low viscosity of the solution limiting jet formation. Electrospinning of PAN 3% from DMSO/DMF produced quite different fibres in comparison to PVC. Whilst there appears to be the presence of globules in Figure 3.5 (a), these are actually bundles of fibres that coalesced, as detailed in Figure 3.5 (b), indicating solvent was retained in these fibres after electrospinning. The fibres also appear to have very little uniformity throughout the fibrous mat with the presence of small, large and broad fibres. Furthermore there was no indication of beads along the fibres.

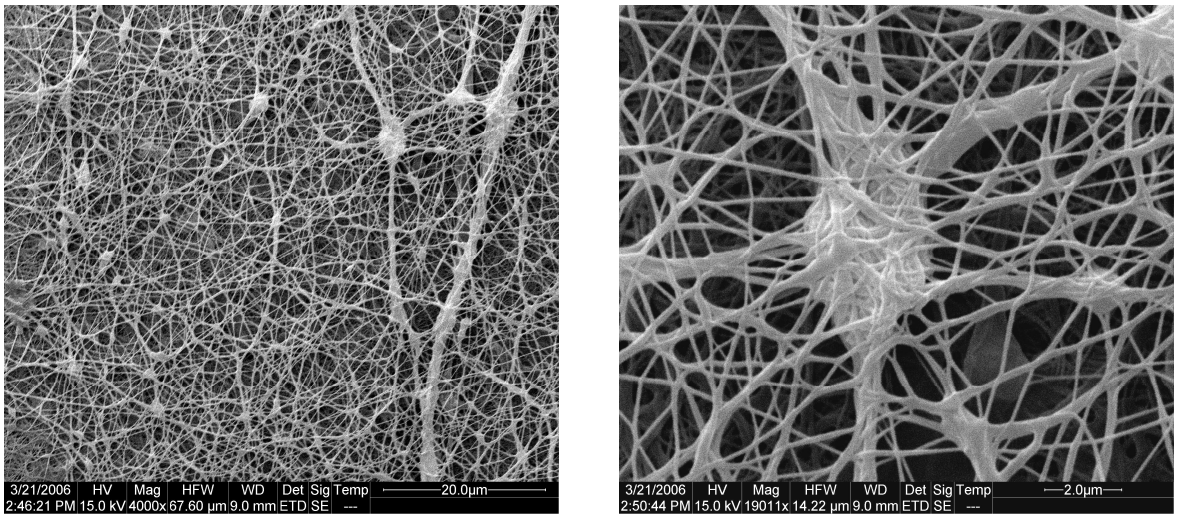

(a) (b)

Figure 3.5 SEM micrographs of fibres electrospun from PAN 3% in DMSO/DMF (a) Mag: 4,000X, (b) Mag: 19,011X

This lack of bead formation is interesting. In previous work [219] PAN was electrospun from both DMSO and DMF individually, and both exhibited spherical and ellipsoidal bead structures at 3%. The combination of the two solvents appears to have had a significant affect on the morphological properties of the fibres, and most likely an affect on the properties of the spinning solution. This is of even more importance considering

that the surface tension results from the solution of PAN 3% in DMSO/DMF in Section 2.5.1 was significantly higher compared with that of the PVC solutions. It was previously noted that surface tension plays a major role in the 'bead-on-string' morphology [65, 98, 183].

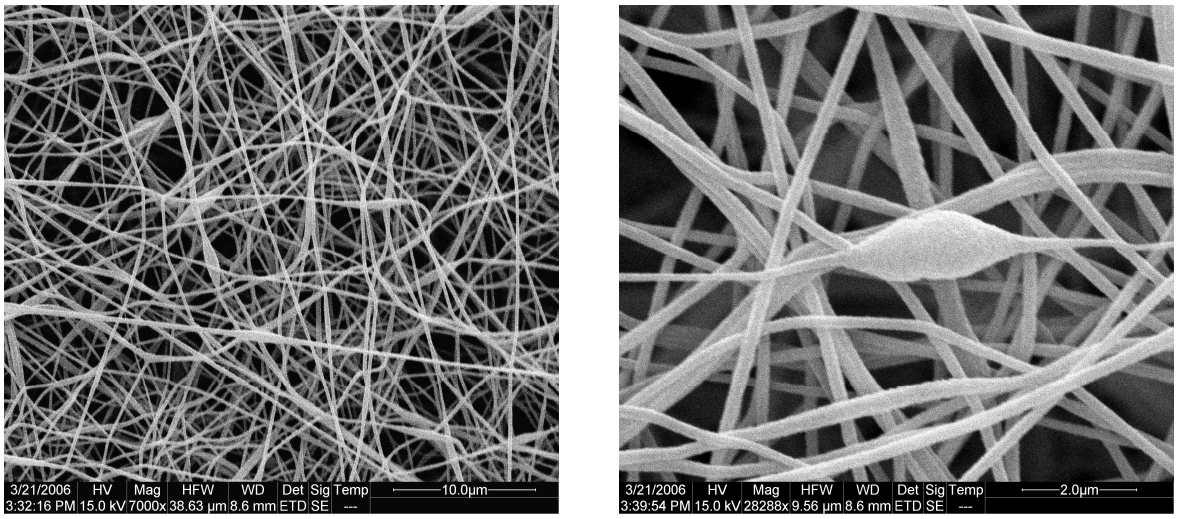

(a) (b)

Figure 3.6 SEM micrographs of fibres electrospun from PAN 5% in DMSO/DMF (a) Mag: 7,000X (b) Mag: 28,288X

Increasing the concentration of PAN produced far more uniform fibres, and the presence of some beads as can be seen in Figures 3.6 (a) and (b). Along with an increase in the uniformity of structure, Figure 3.6 (a) shows fewer intersections where the fibres 'point-bonded' or coalesced into other fibres during, and/or after, electrospinning in comparison to PAN 3%. This further supports the statement that the fibres from the PAN 3% solution still contained solvent after electrospinning, possibly due to the higher solvent contribution in the PAN 3% blend, or that the fibres intertwined and bonded during the electrospinning process rather than during electrospinning.

Figure 3.6 (b) shows one of the few beads present in this electrospun mat while Figures 3.7 (a) and (b), which show that there are no beads present in fibres spun from PAN 7% DMSO/DMF. This indicates that the increase in polymer concentration led to an increase in the viscoelastic effects in the blend, in turn reducing the occurrence of beads.

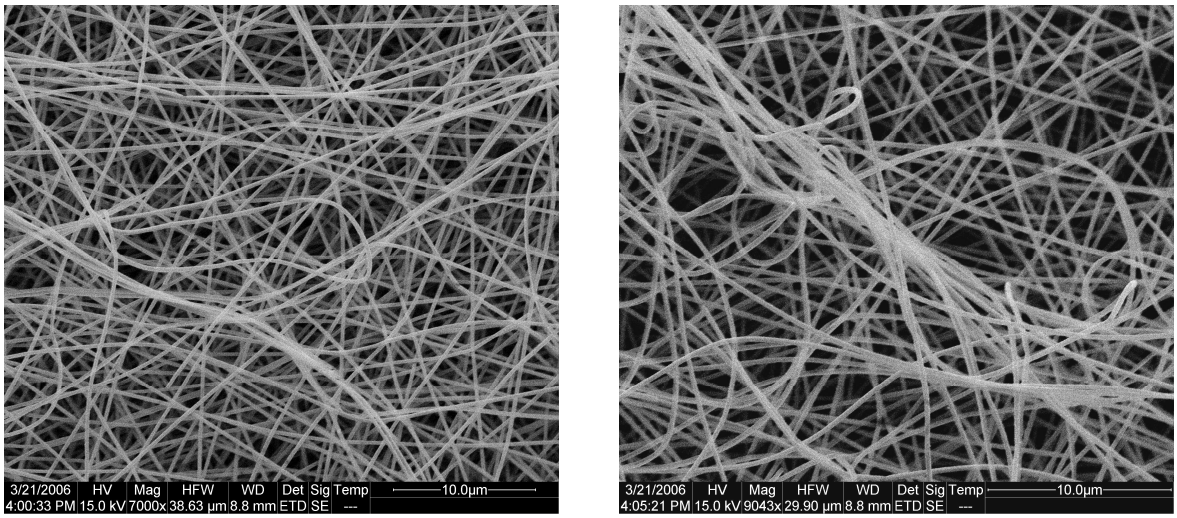

(a) (b)

Figure 3.7 SEM micrographs of fibres electrospun from PAN 7% in DMSO/DMF (a) Mag: 7,000X, (b) Mag: 9,043X

In addition, Figure 3.7 (b) presents a bundle of intertwined electrospun fibres. There is no indication that the fibres have coalesced and point-bonded as was observed from PAN 3%, and to some extent, PAN 5%. Thus it appears the higher concentration of polymer, and in turn the lower amount of solvent has reduced the ability of fibres to overtly bond together.

3.3.3 PAni/PVC Electrospun Fibres

Having studied the morphology of neat PVC and PAN electrospun fibres, the effects of adding the intrinsically conducting polymer (ICP) PAni and its dopant, CSA, to the blend were studied using SEM. Fibres could not be electrospun from a solution of PVC

5% in THF/DMF as it electrosprayed onto the gold-coated Mylar® target. The introduction of PAni into the PVC 5% solution allowed the successful production of electrospun fibres [Figures 3.8 (a) and (b)]. Thus the presence of PAni offered some improvement in the viscoelastic properties of the polymer blend. This is also supported by the viscosity results covered in detail in Section 2.4 where it was observed that the PAni/polymer solutions produced an increase in the shear viscosity compared with the polymer solutions not containing PAni. Whilst the increase in viscosity of PVC 5% solution compared with the PAni 1% PVC 5% solution was relatively small, this indicates that the minimum shear viscosity for successful electrospinning this blend occurs within this range of 7.53 mPa.s to 11.30 mPa.s detailed in Table 2.2 in Chapter 2.

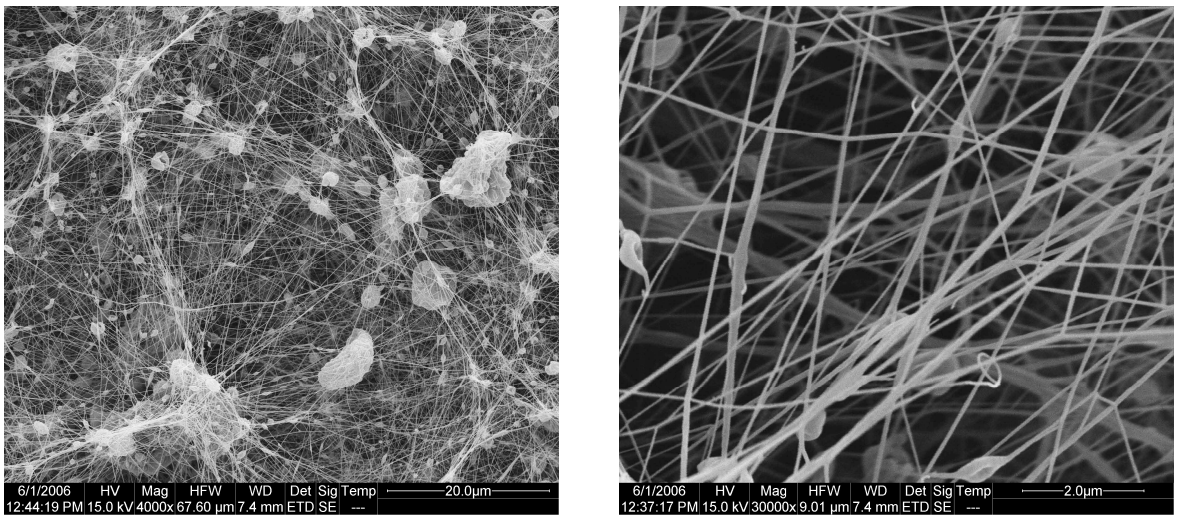

(a) (b)

Figure 3.8 SEM micrographs of fibres electrospun from PAni 1% PVC 5% in THF/DMF (a) Mag: 4,000X, (b) Mag: 30,000X

From Figure 3.8 (a) it can be seen that a significant amount of electrospraying occurred in conjunction to electrospinning, further evidence that the minimum shear viscosity for successful electrospinning for this blend is close to the viscosity of this solution. There was also the presence of the 'beads-on-string' morphology, but more importantly, the

beads and globules occurred far more in the PVC 10% electrospun fibres [Figure 3.2 (a)] than this sample, and that the size of the particles were much larger in the PVC 10% fibres.

This possibly indicates two things. The first is that the PAni provided a large contribution to the viscoelastic properties of the polymer blend, in turn reducing the presence of beads and globules throughout the mat. The second is the contribution from conductivity. The presence of PAni decreased the electrical resistance of all the polymer solutions by an order of magnitude, as outlined in Section 2.6. Both Jun et al. [112] and Tan et al. [190] reported that the presence of beads in an electrospun fibre can be attributed to the conductivity of the polymer solution whereby a lower conductivity reduces the jet elongation during electrospinning . Thus the presence of PAni will increase the conductivity, and also contribute to the viscoelastic properties of the polymer solution.

Increasing the concentration of PVC to 10% in the spinning solution led to the production of more uniform fibres consisting of less beads and globules. This can be observed in Figures 3.9 (a) and (b). Whilst there were a number of large globules present in the electrospun mat, these were slightly less in magnitude and number compared with PAni 1% PVC 5% fibres, however the structure was consistent between the two. It is possible that these globules were the same large particles identified in Section 2.7.2, rather than electrosprayed polymer solution. Furthermore the number of beads along the fibres decreased substantially compared to the electrospun fibres from PVC 10% solution, a result of the increased viscoelastic properties of the polymer blend due to the increased concentration of PVC. However, it is important to note that the conductivity of the PAni 1% PVC 10% blend was 0.95 mmhos compared with the 0.05

mmhos for the PVC 10% solution, and also 0.95 mmhos for the PAni 1% PVC 5% blend (Table 2.7). Thus whilst the conductivity of the solution may have played a role in producing uniform and beadless fibres, it appears the main contributor was the increase in concentration of PVC from 5% to 10%.

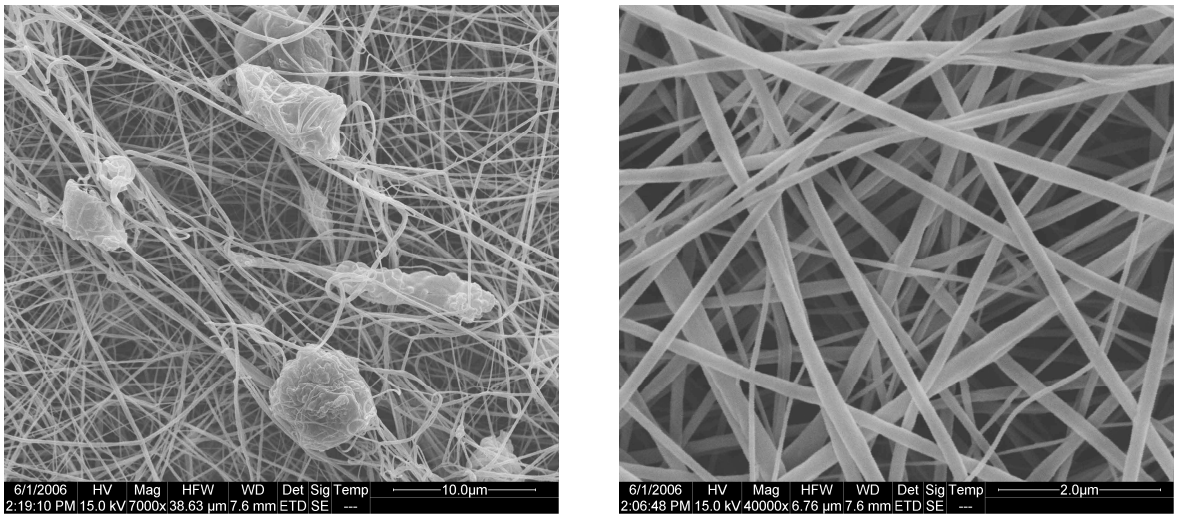

(a) (b)

Figure 3.9 SEM micrographs of fibres electrospun from PAni 1% PVC 10% in THF/DMF (a) Mag: 7,000X, (b) Mag: 40,000X

A further increase in the concentration of PVC to 15% in the PAni/PVC spinning solution did decrease the presence of particles appreciably throughout the fibrous mat [Figure 3.10 (a) and (b)]. From Figure 3.10 (a), the increased concentration of PVC to 15% reduced the presence of globules significantly compared with the PAni 1% PVC 10% solution, indicating that the increase polymer concentration has reduced the electrospray from the solution. It also indicates that the particulate matter, identified in Section 2.7.2, does not appear to have had a major affect on the final fibre morphology. According to the detail in that chapter, increased PVC concentration led to an increase in particulate size in PAni/PVC solutions. Furthermore, this increased PVC concentration appears to have slightly increased point-bonding of fibres, as in Figure

3.10 (b) it appears two of the fibres combined to form one large fibre, as indicated by the arrows.

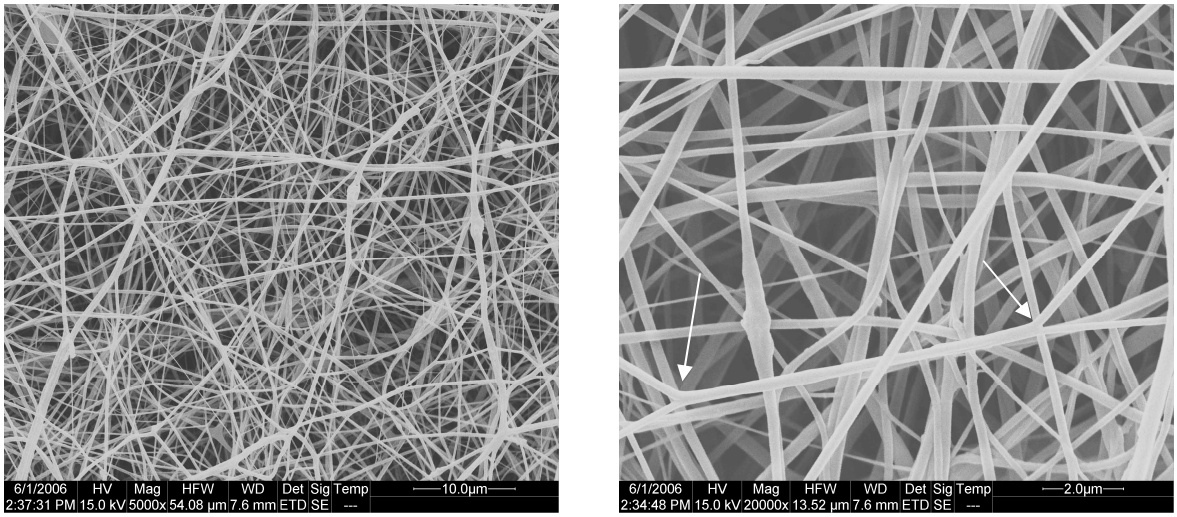

(a) (b)

Figure 3.10 SEM micrographs of fibres electrospun from PAni 1% PVC 15% in THF/DMF (a) Mag: 5,000X, (b) Mag: 20,000X; arrows indicate point-bonding

Electrospinning of PAni 1% PVC 20% was by far the most difficult PAni/PVC blend to electrospin. This sample required a significantly higher potential to initiate electrospinning and overcome the higher viscoelastic forces. As a result the fibres produced [Figures 3.11 (a) and (b)] were not uniform in diameter, consisting of a wide array of fibre diameters, which will be discussed later in Section 3.4. The fibres have electrospun in a loop-type orientation. This may have been a result of the increased viscoelastic forces associated with the increased PVC concentration reducing the ability of the polymer jet to whip in a large circular motion and instead whipping in smaller concentric circles. It is also possible that the higher potential required for electrospinning has contributed to this by increasing the whipping rotation of the polymer jet. One interesting aspect of this is that there were no globules of electrosprayed polymer throughout the blend, but only fibres, further supporting the

statement that the particle size (Section 2.7.2) did not affect the final fibrous mat morphology.

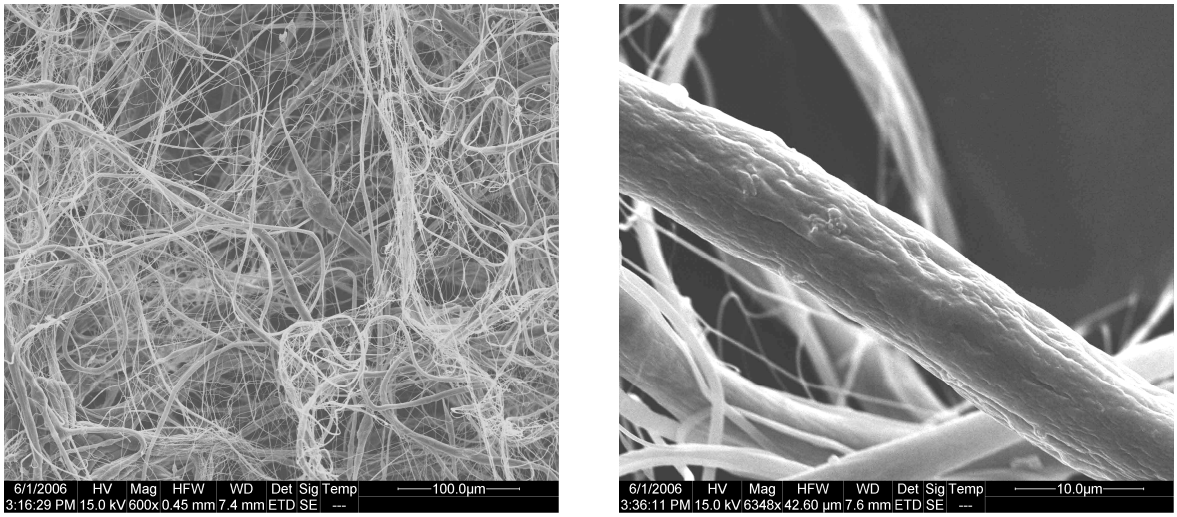

(a) (b)

Figure 3.11 SEM micrographs of fibres electrospun from PAni 1% PVC 20% in THF/DMF (a) Mag: 600X, (b) Mag: 6,348X

Figure 3.11 (b) presents a fibre electrospun from PAni 1% PVC 20% in THF/DMF. The size of this fibre is extremely large compared with previous blends. In addition the morphology of the fibre itself is not uniform. The surface of the fibre consists of grooves and pits, indicative of solvent evaporation. Thus this fibre was not a product of individual smaller fibres bundling to form a larger one. From this, the viscoelastic forces of the polymer blend would appear to be too high to prepare uniform electrospun fibres. Therefore, the upper viscosity limit for the production of such fibres lies between 250 and 600 mPa.s (Table 2.2) corresponding to the viscosity values for PAni 1% PVC 15% and PAni 1% PVC 20% solutions, respectively.

3.3.4 PAni/PAN Electrospun Fibres

Blending PAni with PAN produced significantly different fibres compared with PAni/PVC and also with the original PAN electrospun fibres. Again, it was found that PAni made some contribution to the viscoelastic forces of the polymer blend similar to the observations for PAni/PVC.

From the micrographs of fibres electrospun from PAni 1% PAN 1% in DMSO/DMF [Figure 3.12 (a) and (b)] it can be seen that the fibres produced were of poor quality, bundling together instead of coating the Mylar®. Furthermore, the fibres intertwined on the surface of large particles, indicating that whilst some electrospinning occurred, there was also the presence of electrosprayed products, possibly the particulate matter identified in Section 2.7.1.

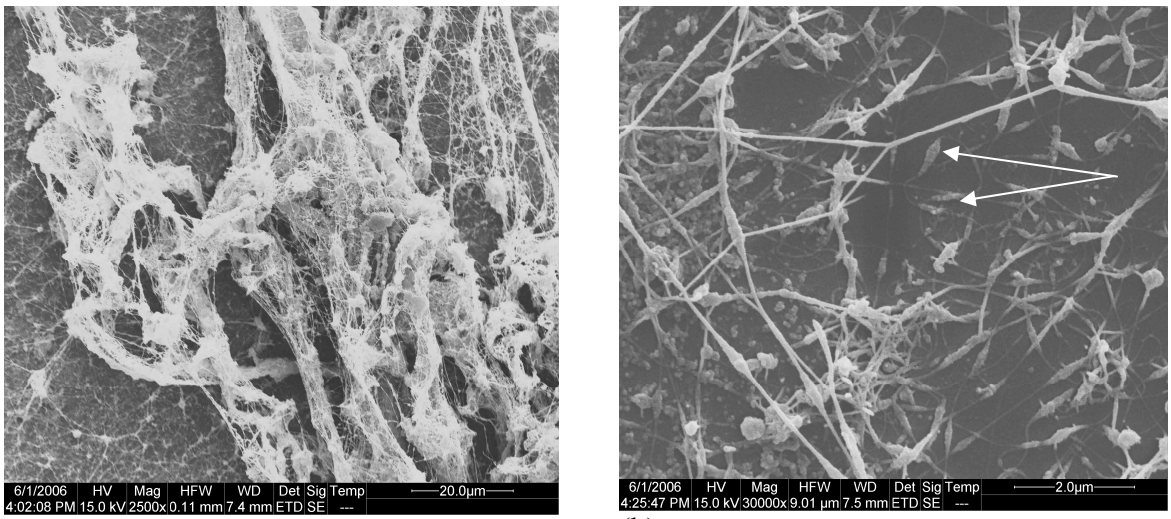

(a) (b)

Figure 3.12 SEM micrographs of fibres electrospun from PAni 1% PAN 1% in DMSO/DMF (a) Mag: 2,500X, (b) Mag: 16,000X; arrows indicate beads

The 'beads-on-string' morphology was also observed for this blend. Figure 3.12 (b) shows that these beads were not uniform. Instead both ellipsoidal and spherical type

structures formed, similar to observations for PAN 3% in DMF or DMSO noted previously [219]. It is important to mention that this blend of PAni 1% PAN 1% possessed a relatively high conductivity of $4.8x10^{-4}$ mhos compared with $1.1x10^{-5}$ mhos for PAN 1% (Table 2.6). Thus this may have also contributed to fibre formation, however in this case the higher conductivity did not prevent the formation of beads and other particles. The surface tension of the solution was comparable to neat PAN blends indicating that there was no significant affect on the surface tension due to the presence of PAni, however at this low PAN concentration the surface tension most likely contributed the most to the formation of beaded fibres.

Increasing the concentration of PAN produced far more uniform fibres, with noticeably different morphology to straight PAN 3% fibres. SEM micrographs of fibres electrospun from PAni 1% PAN 3% in DMSO/DMF [Figures 3.13 (a) and (b)] show the presence of electrosprayed droplets of polymer amongst the fibrous mat. These particles are significantly less in number than those found in PAni 1% PAN 1% fibres, indicating the higher concentration of PAN increased the viscoelastic properties of the polymer solution, in turn reducing the propensity for the solution to electrospray. As mentioned for the PAni/PVC blends, the presence of larger particulate matter (Section 2.7.1) in the PAni/PAN blend did not led to the formation of a number of large beads and globules throughout the sample. The viscosity of the PAN 3% blend was 44.26 mPa.s whilst the PAni 1% PAN 3% blend had a viscosity of 73.02 mPa.s at a shear rate of 50.00 s^{-1} for both solutions (Table 2.1).

Whilst this significant difference in viscosity would have contributed to the difference in appearance of the fibre mats, the increase in PAN viscosity did not translate to a decrease in the number of beads along the fibres. Figure 3.13 (b) shows that these beads

were largely elliptical in appearance, although the degree of this ellipsoidal structure varies, and had quite rough textures, a result of the evaporation of solvent. In addition there was no significant agglomeration of fibres on beads or beads on beads, indicating that this evaporation occurred during electrospinning and not after coating the Mylar® target.

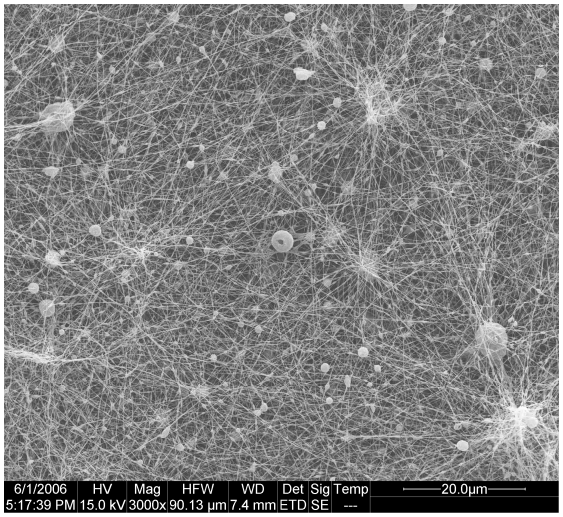

(a)

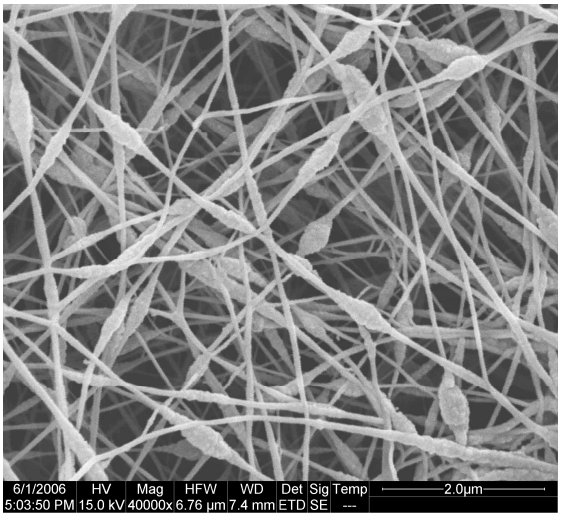

(a)

Figure 3.13 SEM micrographs of fibres electrospun from PAni 1% PAN 3% in DMSO/DMF (a) Mag: 3,000X, (b) Mag: 40,000X

The fibres did not coalesce or bond together to the same extent as observed for straight PAN 3% fibres. In fact, there is very little point-bonding of fibres at crossover points and minimal entanglement. It was previously postulated that the PAN 3% solution produced fibres that contained residual solvent after electrospinning, leading to bonding and coalescence of fibres due to the ability of the polymer fibre to flow. As this PAni/PAN blend had more polymer and less solvent contribution, it may be that there was insufficient solvent retained to allow the bonding and coalescence of fibres. Thus the structure of these electrospun fibres differ quite markedly compared with neat PAN 3% fibres.

Further increasing the concentration of PAN in the PAni/PAN blends altered the electrospinning process and also the microscopic properties of the fibres. Figures 3.14 (a) and (b) are images of PAni 1% PAN 5% fibres electrospun from DMSO/DMF. Figure 3.14 (a) shows that the majority of PAni 1% PAN 5% electrospun fibres were no longer orientated randomly, but instead coated the Mylar® in one general direction, as expected with a rotating target. This had not occurred for any previous PAN or PAni/PAN blends and may indicate that the presence of PAni, in conjunction with the higher PAN concentration, slowed the rate of fibres coating the Mylar surface such that the rotation of the target was the dominant parameter in fibre orientation.

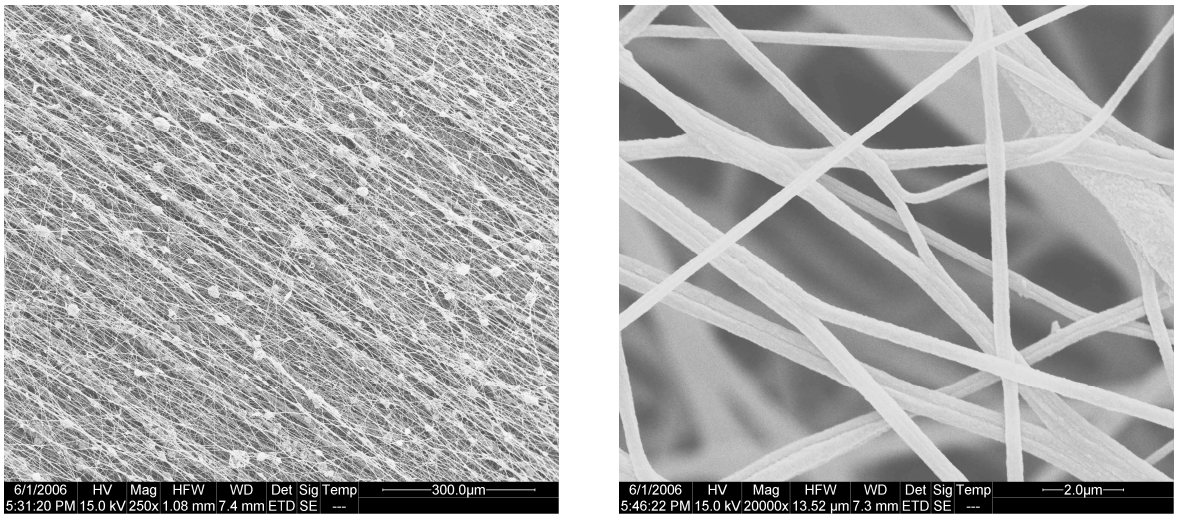

(a) (b)

Figure 3.14 SEM micrographs of fibres electrospun from PAni 1% PAN 5% in DMSO/DMF (a) Mag: 250X, (b) Mag: 20,000X

From Figure 3.14 (b), these fibres did not exhibit beads-on-string morphology due to greater amounts of PAN in the blend, implying the large particles or globules were due to electrospraying of the polymer solution. These may possibly be the solution particles reported in Section 2.7.1, though their effects were not seen in lower concentrations of PAN and the PAni/PVC solutions. From Table 2.1, the shear viscosity of the PAni 1% PAN 5% solution was approximately 100 mPa.s higher than the PAN 5% blend, while

the conductivity of the former was an order of magnitude higher than that of the latter, and their surface tensions averaged 47.19 mN m^{-1} and 43.14 mN m^{-1}, respectively. Thus, considering both higher solution viscosity and conductivity produce more uniform fibre mats, the increase in surface tension may have been responsible for the solution electrospraying.

If the surface tension was responsible for the electrospray then it appears the increased viscoelastic properties of the solution limited the production of beads along the fibres. The cause of the increased surface tension remains unclear, considering it was relatively constant for other blends of PAni/PAN. Possibly the higher PAN concentration led to changes in the polymer/solvent interaction, in turn increasing the surface tension of the polymer solution. Regardless, the observation that the fibres intertwined linearly, bonded and bundled together, and orientated indicates that a change in the electrospinning process occurred, brought about by a change in solution viscosity and/or surface tension, and that the fibres interacted significantly during flight.

Increasing the concentration of PAN to 7% in DMSO/DMF in the PAni/PAN blend led to the production of smaller secondary fibres presented in Figures 3.15 (a) and (b). It is possible that the smaller fibres in the PAni 1% PAN 7% sample were a result of splaying of the main jet, or evidence of the main electrospinning jet undergoing a secondary instability to produce secondary fibres. As discussed in Section 1.2.2, splaying involves the splitting of the main whipping jet during electrospinning, producing individual polymer filaments. These secondary fibres also possessed hook type structures along the length of the fibre at various intervals. The cause of these hook structures is unclear, however it may have been the beginning of a tertiary fibre splaying off from these secondary fibres.

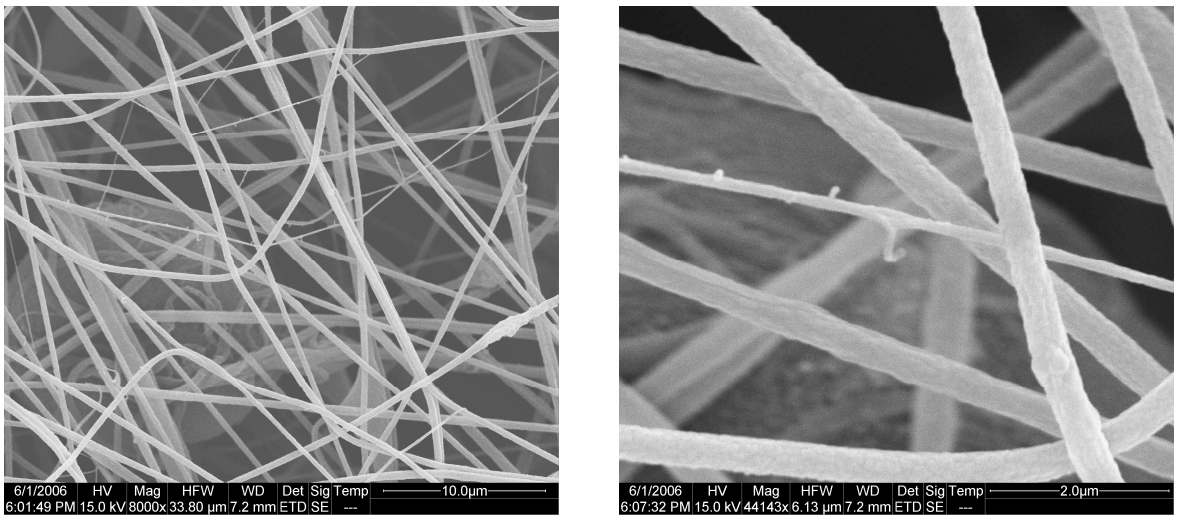

(a) (b)

Figure 3.15 SEM micrographs of fibres electrospun from PAni 1% PAN 7% in DMSO/DMF (a) Mag: 8,000X, (b) Mag: 44,143X

Thus, at this concentration the fibres, whilst smooth, did not possess uniform diameters. Furthermore, large globule like structures were present throughout the fibrous mat, indicating that again there has been some electrospraying of the polymer blend or that the particles identified in Section 2.7.1 were also electrospinning. Neither of these were observed in the fibres electrospun from PAN 7% solution, indicating that that presence of PAni and/or CSA has altered the solution properties, consistent with the other PAni/PAN blends.

These differences between the PAni/PAN fibres and those produced for PAN alone may have been a result of changes in the conductivity, surface tension and/or viscosity. It was noted previously that an increase in the conductivity will generally lower the bead numbers through a fibrous mat [190]. Increases in the viscosity would indicate that the viscoelastic forces would have also increased, affecting the morphology, however this is not always the case [98, 119, 209]. As the surface tension did not appreciably change from one solution to the next, apart from the PAni 1% PAN 5% blend, this would not have influenced these differences in morphology.

3.3.5 PAni/PVC/2-NPOE Electrospun Fibres

Electrospinning of PAni 1% PVC 10% 2-NPOE 5% (2-nitrophenoloctylether, a commercial plasticiser and solvent mediator) from THF/DMF produced fibres possessing a greater degree of intertwining [Figures 3.16 (a) and (b)] than those of any other blend. The fibres bundled together more closely, and point-bonding of fibres with one another (indicated by the arrows in Figure 3.16 (b)) also occurred. There were no beads produced along the fibres, however the mat itself was slightly different to fibres produced from PAni 1% PVC 10% solution.

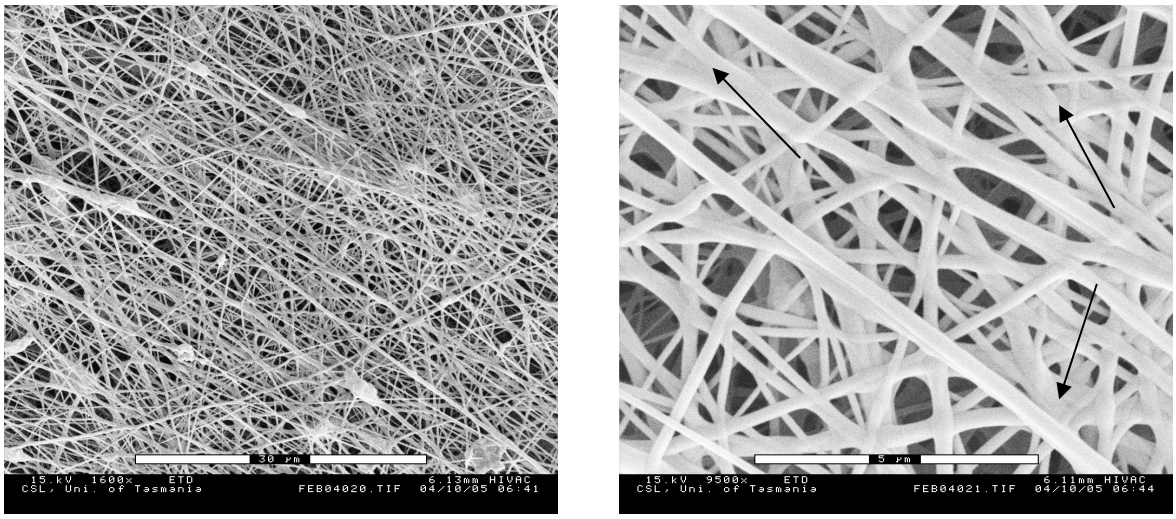

(a) (b)

Figure 3.16 SEM micrographs of fibres electrospun from PAni 1% PVC 10% 2-NPOE 5% in THF/DMF (a) Mag: 1,600X, (b) Mag: 9,500X; arrows indicate point-bonding

The presence of 2-NPOE possibly led to retention of solvent within the fibres, or decreased the glass-transition temperature (Tg) of the blend, such that when the fibres coated the target they point-bonded with underlying fibres to a large degree. However, this bonding was not as significant as the case of fibres from PAN 3% solution [Figure 3.5 (b)]. Thus whilst bonding between fibres did occur, it did not have an adverse effect on the overall structure of the electrospun fibres. In fact this bonding may have been

useful in terms of creating greater pathways for PAni to conduct throughout the sample. However, a further increase in the concentration of 2-NPOE to 20% in solution led to the formation of a film as opposed to a filament [Figures 3.17 (a) and (b)].

It would appear that the fibre structure collapsed as the polymer had sufficient mobility to flow, either through solvent retention or a decrease in Tg, or a combination of both, leading to the formation of a film. The resultant pores throughout the sample occurred where the flowing polymer solution had not covered gaps between the fibres. This creates a problem as the majority of PVC-based ISEs possess a plasticiser to aid ionic mobility, solvent mediation and structural properties. From these results it is apparent the use of a plasticiser to alter the properties of PVC negated the process of electrospinning, leading to the collapse in fibre structure and instead, the formation of a polymer film.

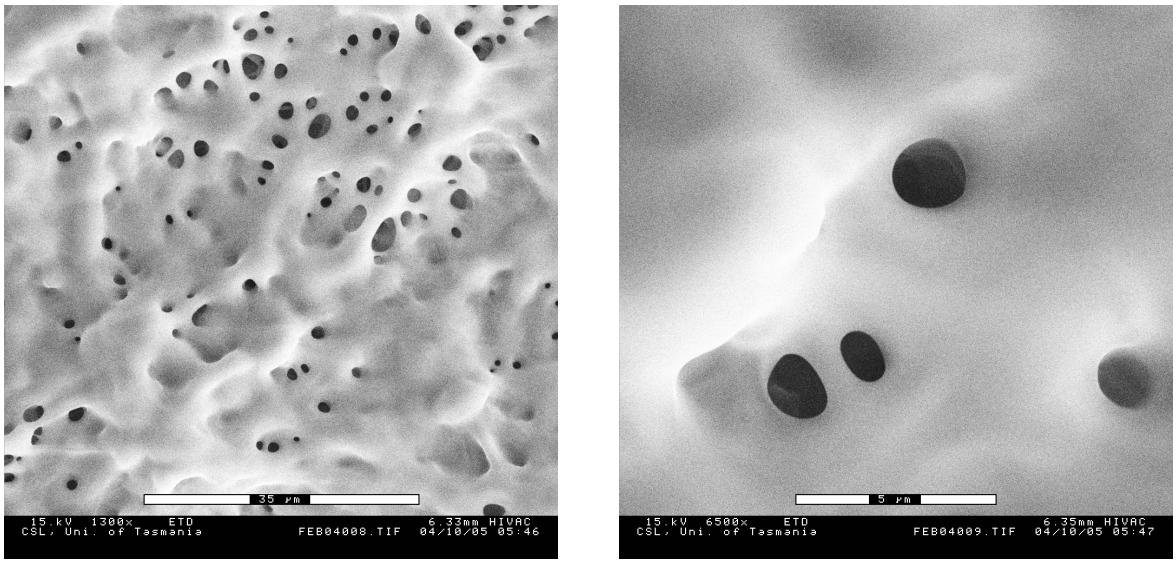

(a) (b)

Figure 3.17 SEM micrographs of fibres electrospun from PAni 1% PVC 10% 2-NPOE 20% in THF/DMF (a) Mag: 1,300X (b) Mag: 6,500X

3.3.6 PAni/PAN/2-NPOE Electrospun Fibres

The introduction of 2-NPOE 5% into a PAni 1% PAN 3% blend led to the formation of electrospun fibres [Figures 3.18 (a) and (b)] similar to those observed for PAN 3% [Figure 3.5 (b)], although the fibres were less densely packed. This similarity indicates that the presence of 5% 2-NPOE overcame the viscoelastic and electrical influences of PAni in this blend.

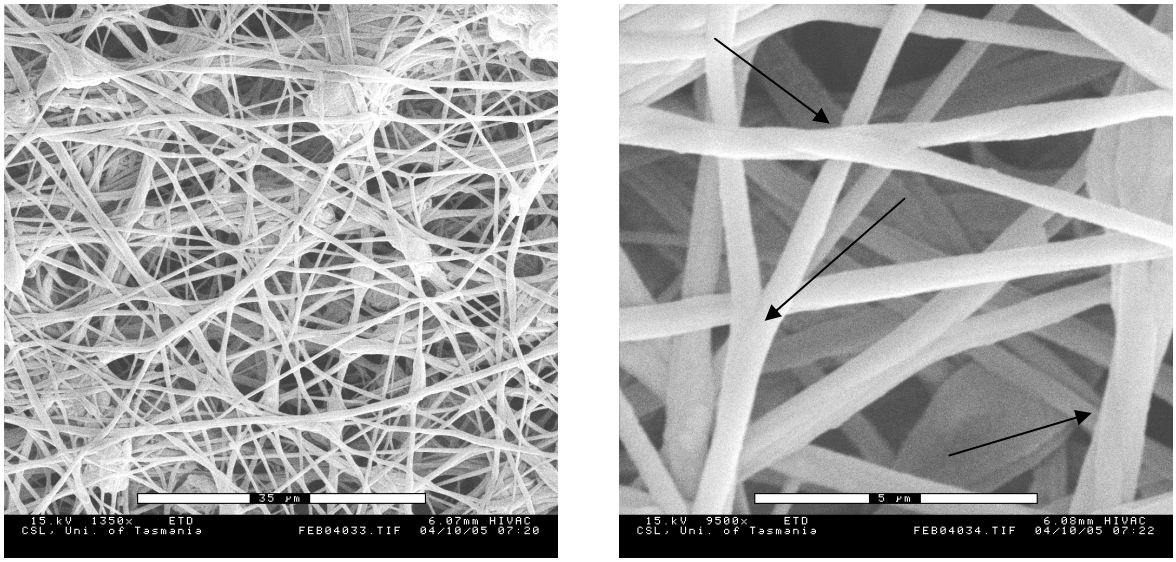

(a) (b)

Figure 3.18 SEM micrographs of fibres electrospun from PAni 1% PAN 3% 2-NPOE 5% in DMSO/DMF (a) Mag: 1,350X, (b) Mag: 9,500X; arrows indicate point-bonding

It was previously observed [Figure 3.13 (b)] that the presence of PAni changed the structure of the electrospun fibres compared with PAN 3%. Thus, the similar morphology of this blend and the PAN 3% fibres appears to be the result of the influence of 2-NPOE. Previously it was discussed that the differences between the PAni 1% PVC 10% 2-NPOE 5% fibres and fibres from the PAni 1% PVC 10% solution came about due to the retention of the solvent in the former blend. This also appears to be the case for PAni/PAN/2-NPOE 5% fibres. The benefit was the reduction in the number of beads along the electrospun fibres, but again there was a significant intertwining and

point-bonding of electrospun fibres due to this solvent retention, noted by the arrows in Figure 3.18 (b), as well as the presence of electrospraying.

Again, after increasing the concentration of 2-NPOE to 10% complete collapse of the fibre structure occurred, similar to that observed for PAni 1% PVC 10% 2-NPOE 20%. This can be observed in Figures 3.19 (a) and (b). However, whilst solvent retention or a decrease in Tg is likely, another contributor may have been a decrease in the surface tension of the polymer solutions. The reduction in the occurrence of beads in moving from PAni 1% PAN 3% to PAni 1% PAN 3% 2-NPOE 5% supports this..

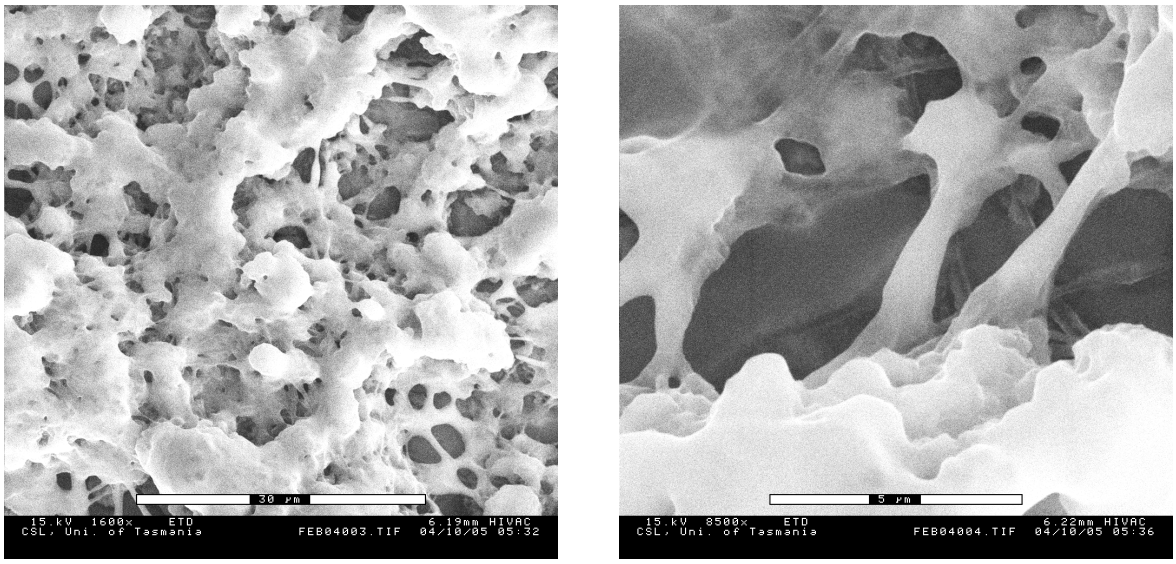

(a) (b)

Figure 3.19 SEM micrographs of fibres electrospun from PAni 1% PAN 3% 2-NPOE 20% in DMSO/DMF (a) Mag: 1,600X (b), Mag: 8,500X

Thus, it is possible that 2-NPOE altered the surface tension of both PAni/PVC and PAni/PAN blends. It is important to note that the surface tension of 2-NPOE polymer solutions was not measured due to availability of instrumentation and cessation of consideration of this ionophore. From the point of view of fabrication of a nitrate selective electrode, to be discussed in Chapter 5, 2-NPOE was deemed unsuitable, thus

solution analyses of this blend did not proceed. As a result, literature-based information and results in this thesis based on other blends have been used to identify reasons for the collapse of the fibre structure and other fibre properties.

3.3.7 PAni/PVC/TOAB Electrospun Fibres

The inclusion of tetraoctylammonium bromide (TOAB), a commercial ionophore, led to the production of a fibrous mat similar to that observed for fibres electrospun from a PAni 1% PVC 10% 2-NPOE 5% solution, however the orientation of the electrospun fibres changed [Figures 3.20 (a) and (b)]. This blend produced tighter looping of the whipping jet as the fibres themselves form tight loops with substantial point-bonding. On closer inspection in Figure 3.20 (b), these fibres were less uniform in structure and diameter than those of PAni 1% PVC 10% 2-NPOE 5%, and possessed a greater tendency to point-bond and bundle into groups of fibres.

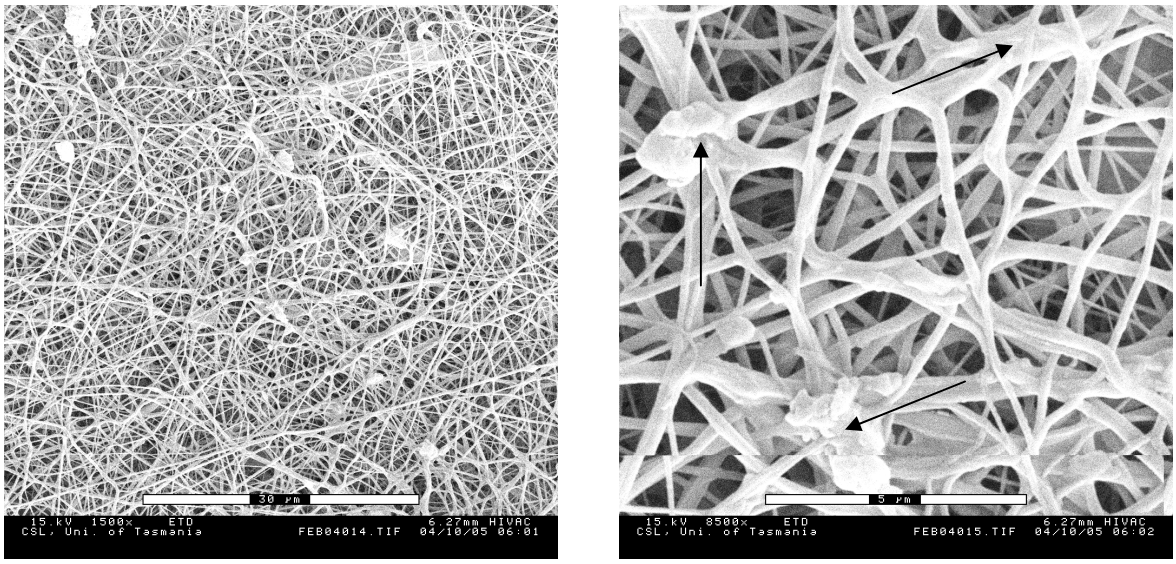

(a) (b)

Figure 3.20 SEM micrographs of fibres electrospun from PAni 1% PVC 10% TOAB 5% in THF/DMF (a) Mag: 1,500X, (b) Mag: 8,500X; arrows indicate bead-like structures

Furthermore, there appeared to be bead-like structures on the surface of these fibres, outlined by arrows in Figure 3.20 (b), but not along the fibre. It is unclear how these structures formed. It may be that these are small droplets of electrosprayed material that attached to the jet/fibres during electrospinning and bonded together, however it would be expected that this would have been observed in previous samples. It is also possible that these bead-like structures were made up of ionophore, or ionophore packets that were held within the fibre. If this is true, then the ionophore did not disperse throughout the blend, possibly due to their solubility in THF/DMF, their interaction with the other polymers or perhaps even the charging effect from the applied potential.

Increasing the concentration of the ionophore to 20% led partial coalescing of the fibre, however this was not as significant as that observed in the PAni 1% PVC 10% 2-NPOE 20% electrode [Figures 3.21 (a) and (b)].

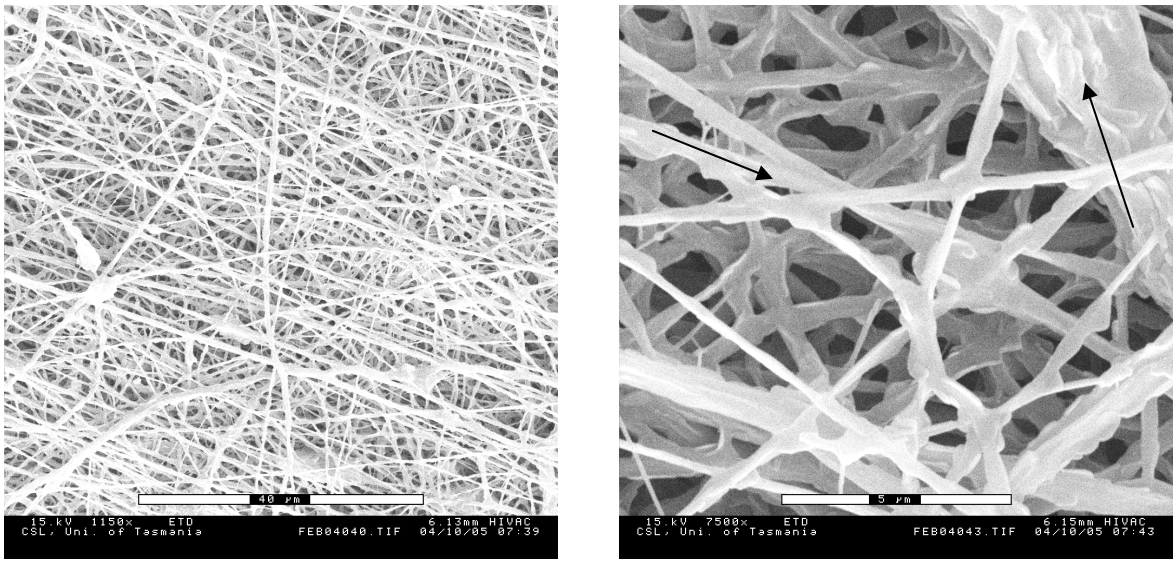

(a) (b)

Figure 3.21 SEM micrographs of fibres electrospun from PAni 1% PVC 10% TOAB 20% in THF/DMF (a) Mag: 1,150X, (b) Mag: 7,500X; arrows indicate bundling and point-bonding

Whilst the fibre structure was retained, they were not uniform, exhibiting an irregular form, consistent with the fibres partially collapsing [Figure 3.21 (b)], and an increase in the bundling and point-bonding of the fibres compared to the PAni 1% PVC 10% TOAB 5% fibrous mat. Whilst the skeleton fibre structure remained, the extent of bonding and intertwining of the fibres would limit the surface area of the fibrous mat, in essence producing a highly porous film rather than a fibrous mat. However these greater connections throughout the fibres may have led to an increase in the conducting PAni network.

Similar to the postulation put forward for the 2-NPOE blends, the ionophore may have increased the solvent retention of the fibres leading to an increase in polymer flow and subsequent collapse of the fibre structure, or a decrease in the surface tension of the solution. Due to instrument access and unsuitability of the ionophore for use in a sensor, the surface tension of TOAB blends was also not analysed. Thus postulations are based on other blends and literature values.

3.3.8 PAni/PAN/TOAB Electrospun Fibres

The addition of TOAB to the PAni/PAN spinning solution slightly altered the structure of fibres electrospun from PAni 1% PAN 3% TOAB 5% in DMSO/DMF compared with PAni 1% PAN 3% electrospun fibres. This can be observed in Figures 3.22 (a) and (b).

The number and shape of beads appears consistent in comparison to the PAni 1% PAN 3% fibrous mat, and while the beads were still ellipsoidal, they often exhibited a rough surface. In addition, there was the presence of the globules on the fibres similar to those observed for the PAni 1% PVC 10% TOAB 5% fibres. Both the beads and globules can

be seen in Figure 3.22 (b) with the bead the lower structure and the smooth globule the top structure. Considering that both of these samples possessed smooth globules, it would seem reasonable to conclude that these are due to the ionophore. They may have been either globules of ionophore or small electrosprayed droplets that have attached to the fibres during electrospinning, as postulated in Section 3.3.7.

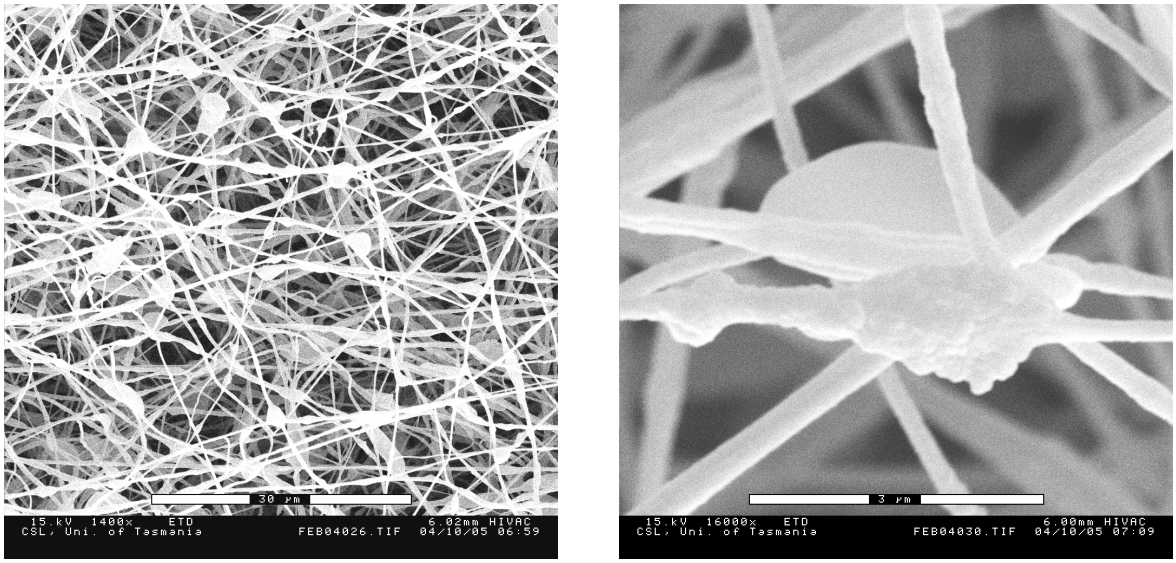

(a) (b)

Figure 3.22 SEM micrographs of fibres electrospun from PAni 1% PAN 3% TOAB 5% in DMSO/DMF (a) Mag: 1,400X, (b) Mag: 16,000X

Increasing the concentration of TOAB increased the number of globules significantly. This is clearly seen in Figures 3.23 (a) and (b). The increase in the number of, and variation in the size of, globules along the fibres indicates that the surface tension of the polymer solution had been affected. In some cases these globules appear to be situated on top of the electrospun fibre, as indicated in Figure 3.23 (b), indicating some degree of electrospraying had occurred. In turn this increase in the number of globules led to an increase in the agglomeration of fibres into bundles rather than free-standing fibres. This differs significantly from the morphology of PAni 1% PVC 10% TOAB 20% fibres indicating that the blend was not suitable for this ionophore.

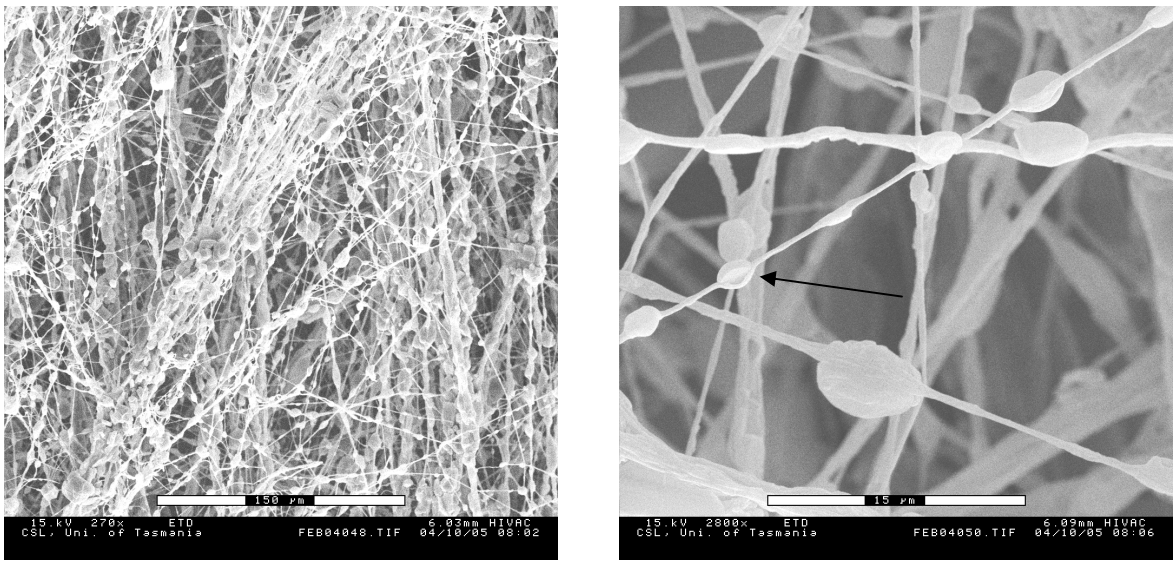

(a) (b)

Figure 3.23 SEM micrographs of fibres electrospun from PAni 1% PAN 3% TOAB 20% in DMSO/DMF (a) Mag: 2,70X, (b) Mag: 2,800X; arrow indicates bead

3.3.9 PAni/PVC/TDAB Electrospun Fibres

Replacing TOAB with TDAB 0.5% (tetradodecylammonium bromide, a commercial nitrate ionophore) in a PAni/PVC blend produced fibres that possessed very similar properties as straight PAni 1% PVC 10% electrospun fibres [Figures 3.24 (a) and (b)].

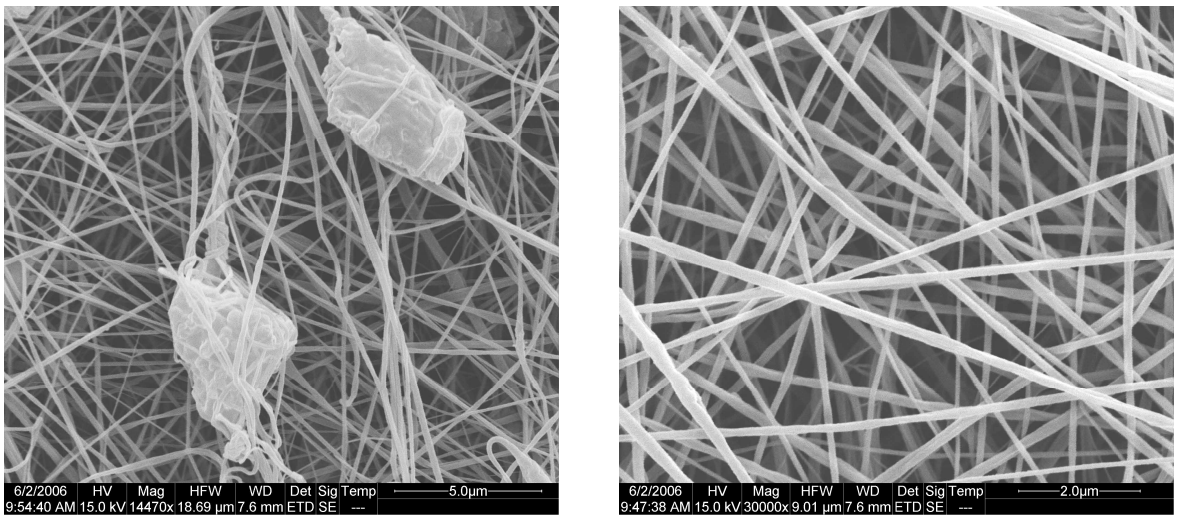

(a) (b)

Figure 3.24 SEM micrographs of fibres electrospun from PAni 1% PVC 10% TDAB 0.5% in THF/DMF (a) Mag: 14,470X, (b) Mag: 30,000X

The fibre structure was similar to the PAni 1% PVC 10% electrode in terms of orientation, and the appearance of the fibres, and the presence of particles from electrosprayed polymer. Whilst there was no change in fibre morphology compared with PAni 1% PVC 10% fibres, this does not necessarily mean that the ionophore is suitable for this blend. The concentration of the ionophore was much lower compared to previous PAni/PVC/ionophore blends, and its contribution may only be insignificant or inconsequential at this low concentration.

Increasing the TDAB composition from 0.5% to 5% did lead to a change in the morphology of the electrospun fibres. These changes can be observed in Figures 3.25 (a) and (b).

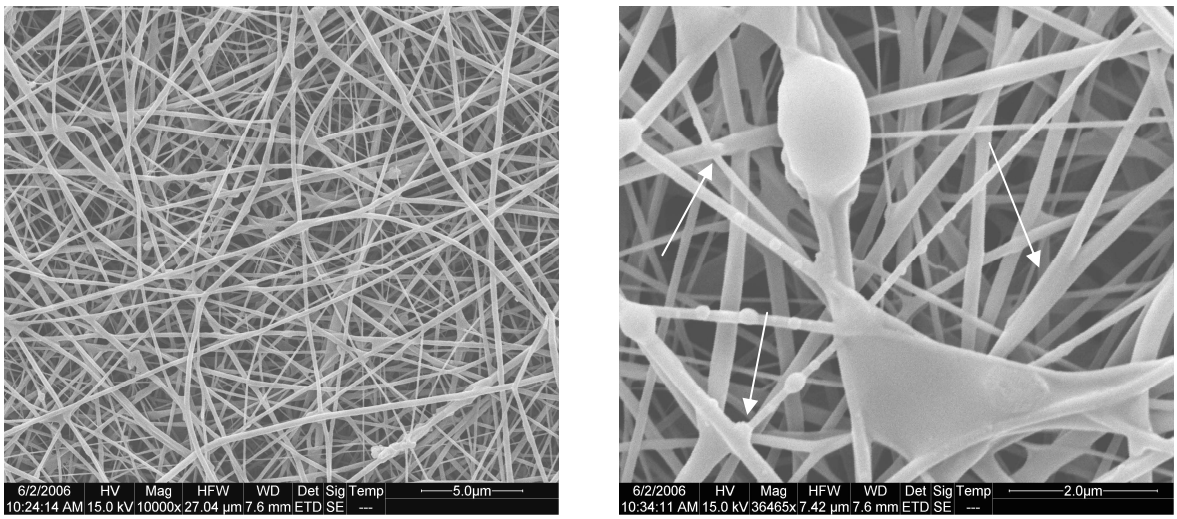

(a) (b)

Figure 3.25 SEM micrographs of fibres electrospun from PAni 1% PVC 10% TDAB 5% in THF/DMF (a) Mag: 10,000X, (b) Mag: 36,465X; arrows indicate spherical structures

The fibres point-bonded together during or after electrospinning, in a similar manner, but to a lesser extent, than both 2-NPOE 5% and TOAB 5% blends with PAni/PVC. A closer inspection of these fibres in Figure 3.25 (b) revealed the presence of spherical

structures on the fibres and areas where the polymer formed a film connecting fibres. The formation of film between the fibres supports the idea that the surface tension has decreased, allowing droplets of polymer to merge into films. However, according to results in Section 2.5.2 the surface tension of this solution increased significantly in the presence of TDAB compared with PAni/PVC solutions. Thus, the ionophore instead may have assisted in solvent retention leading to an increase in the mobility of the polymer, in turn leading to the formation of film-segments.

The spherical structures along the fibres were previously observed on fibres of PAni/PVC/TOAB as well as PAni/PAN/TOAB. Again, these may have been the result of surface tension changes caused by the addition of ionophore leading to electrospraying of smaller droplets. On the other hand they may have been regions of concentrated ionophore bound in polymer.

The significant increase in conductivity of the polymer solution in the presence of TDAB by two orders of magnitude over the original PAni/PVC blends, detailed in Section 2.6, did not affect bead production. Firstly, there were few if any beads in fibres electrospun from either the original PAni 1% PVC 10% fibres or PAni 1% PVC 10% TDAB 0.5%. Secondly, if the few structures which are present along the fibres are droplets of electrosprayed polymer then the increased conductivity has decreased the droplet size compared to those globules present in PAni 1% PVC 10% electrospun fibres [Figure 3.9 (a)]. This latter observation was similar to those of Chen et al. [220] and Kaufman et al. [221] who observed decreases in the size of electrosprayed droplets with an increase in the conductivity of the solution.

Increasing the concentration of TDAB further to 10% produced some similarities in morphology compared to PAni 1% PVC 10% TOAB 20% fibres in Section 3.3.7 [Figure 3.21 (a) and (b)]. Micrographs of fibres electrospun from PAni 1% PVC 10% TDAB 10% in THF/DMF are given in Figures 3.26 (a) and (b).

The fibres exhibited a little electrospraying in the form of particles on the fibrous mat, in addition there appears to be wide variation in fibre diameters as can be seen in Figure 3.26 (a). Closer inspection of the sample in Figure 3.26 (b) shows the fibres point-bonded with underlying fibres and appeared to possess characteristics of broadening, although not to the same extent as fibres from PAni 1% PVC 10% TOAB 20% THF/DMF.

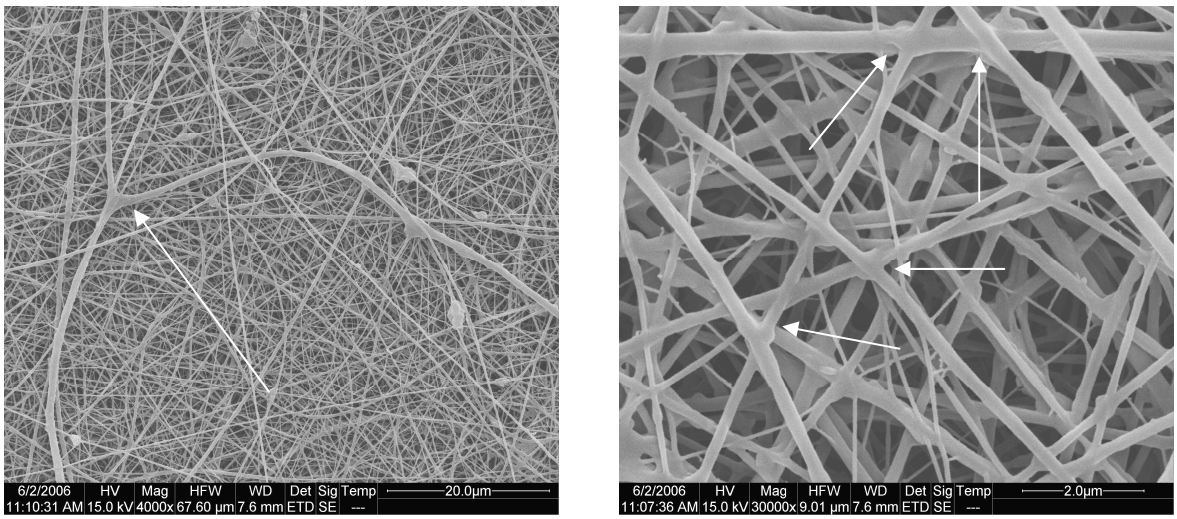

(a) (b)

Figure 3.26 SEM micrographs of fibres electrospun from PAni 1% PVC 10% TDAB 10% in THF/DMF (a) Mag: 4,000X, (b) Mag: 30,000X; arrows indicate point-bonding

This property of point-bonding appears to be due to the presence of the ionophore within the polymer blend as it was consistently observed in previous blends of PAni/polymer/ionophore containing higher concentrations of ionophore. Again this

appears to be a result of solvent retention of the fibres leading to the partially dissolved polymer point-bonding with other fibres.

The presence of fibres with much smaller diameters throughout the mat can also be clearly seen in Figure 3.26 (b). These may be a result of splaying of the whipping jet mentioned for PAni 1% PAN 7% fibres and previously discussed in Section 1.2.2. It is also possible the increased solution conductivity, also noted in Section 2.6.6, produced a secondary charge-repulsion on the whipping jet, leading to secondary jet ejection.

3.3.10 PAni/PAN/TDAB Electrospun Fibres

As was observed for PAni 1% PVC 10% fibres, the addition of low concentrations of TDAB did not alter the morphology of PAni 1% PAN 3% electrospun fibres significantly [Figures 3.27 (a) and (b)]. It is important to note that a small amount of THF was added to assist in the dissolution of the TDAB in PAni/PAN blends prior to the addition of PAni due to insolubility of TDAB in DMSO/DMF.

It is also important to note that the solution conductivity, surface tension and viscosity for PAni/PAN/TDAB solutions were not measured due to the high cost and low availability of TDAB required to produce suitable volumes of solutions for analysis. However, considering that a substantial increase in the solution conductivity was observed for the PAni/PVC/TDAB 0.5% solution compared with the PAni/PVC solution in Section 2.6.6, it would be expected that the conductivity of the PAni/PAN/TDAB 0.5% solution would also have increased in comparison with the PAni/PAN solution. Though the conductivity almost certainly would increase, this increase did not translate into a decrease in the presence of beads throughout the fibrous

mat as anticipated, based on literature [112, 190]. Thus this increase in the number of beads is likely the result of an increase in the surface tension of the solution.

As discussed in Section 3.3.9, PAni/PVC/TDAB solutions exhibited a significant increase in surface tension compared to PAni/PVC solutions, however this increase did not lead to bead formation in the PAni/PVC/TDAB blends. Assuming this change in surface tension was also true for PAni/PAN/TDAB blends, the increase in the conductivity associated with the addition of TDAB may have been countered by an increase in the surface tension of the solution. Considering the relatively high initial surface tension of the PAni/PAN solutions it was likely that this was this case, leading to no significant change in fibre morphology.

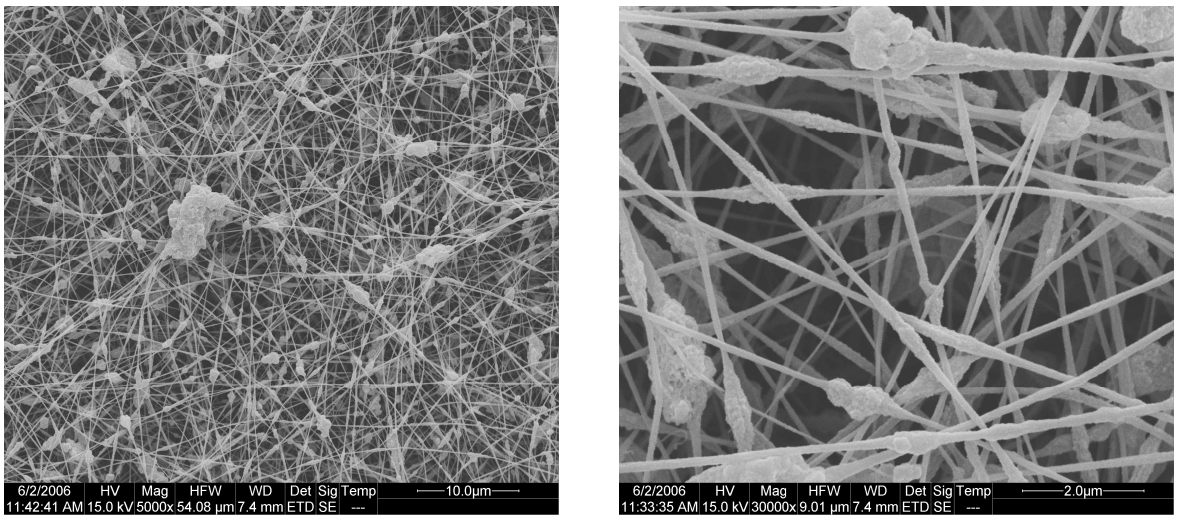

(a) (b)

Figure 3.27 SEM micrographs of fibres electrospun from PAni 1% PAN 3% TDAB 0.5% in DMSO/DMF/THF (a) Mag: 5,000X, (b) Mag: 30,000X

A further increase in the concentration of TDAB to 5% slightly altered the morphology of the electrospun fibres, changing the shape of the beads slightly to less ellipsoidal while increasing the presence of globules throughout the mat, given in Figures 3.28 (a) and (b). These globules appear to have interacted with the electrospun fibres during

electrospinning due to the diverse shapes ranging from spherical to cylindrical. The increase in globule numbers can be clearly observed by comparing Figure 3.13 (a) from electrospun PAni 1% PAN 3% fibres and Figure 3.28 (a). Again this indicates that the properties of the solutions changed dramatically with the introduction of 5% TDAB, reducing the ability of the electrospinning process to produce uniform fibres. Furthermore, the fibres appear to have bonded to the globules, with a small degree of intertwining during electrospinning.

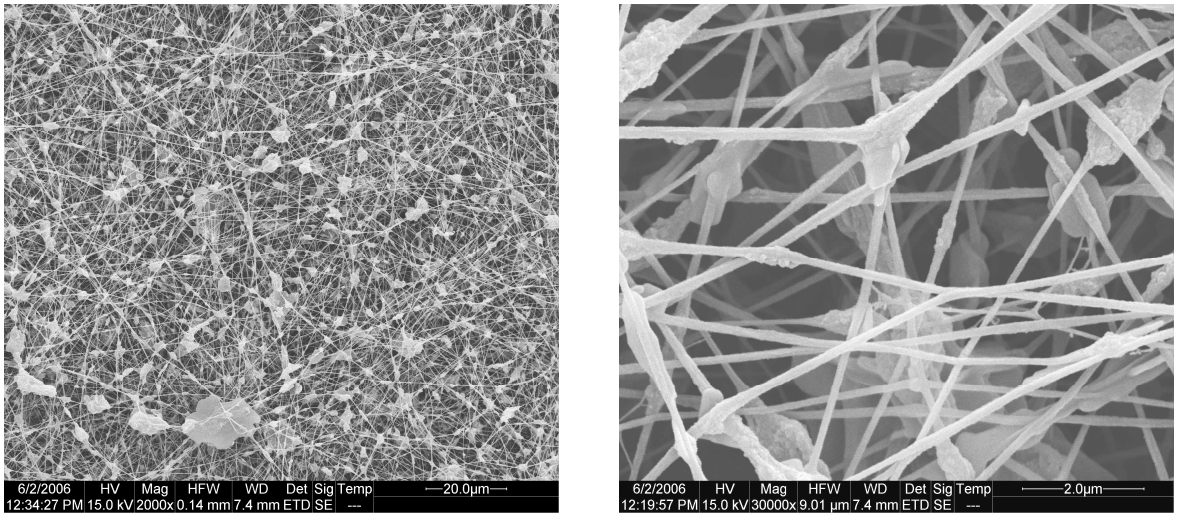

(a) (b)

Figure 3.28 SEM micrographs of fibres electrospun from PAni 1% PAN 3% TDAB 5% in DMSO/DMF/THF (a) Mag: 2,000X, (b) Mag: 30,000X

Increasing the concentration of TDAB further to 10% in PAni 1% PAN 3% produced far more globules and beads throughout the blend. This can be clearly observed in Figures 3.29 (a) and (b). Again, based on PAni 1% PVC 10% TDAB 5% results which recorded a negligible change in the surface tension of the solution with in increase in TDAB concentration, reported in Section 2.5.2, it could be assumed that any change in the surface tension of the PAni/PAN/TDAB solution was also negligible at concentrations of TDAB greater than 0.5%. However, PAni/PAN blends differ appreciably from PAni/PVC in that PAni and PAN are both highly polar. In this case

the ionophore, being an ionic species, may disturb the relationship between the solvents and the polymers far more in this blend than that surmised for PAni/PVC/TDAB (Chapter 2). Based on these observations, the influence of TDAB may have been greater, significantly increasing the surface tension of PAni/PAN/TDAB blends more so than PAni/PVC/TDAB blends with increasing concentration, in turn leading to the electrospraying of globules.

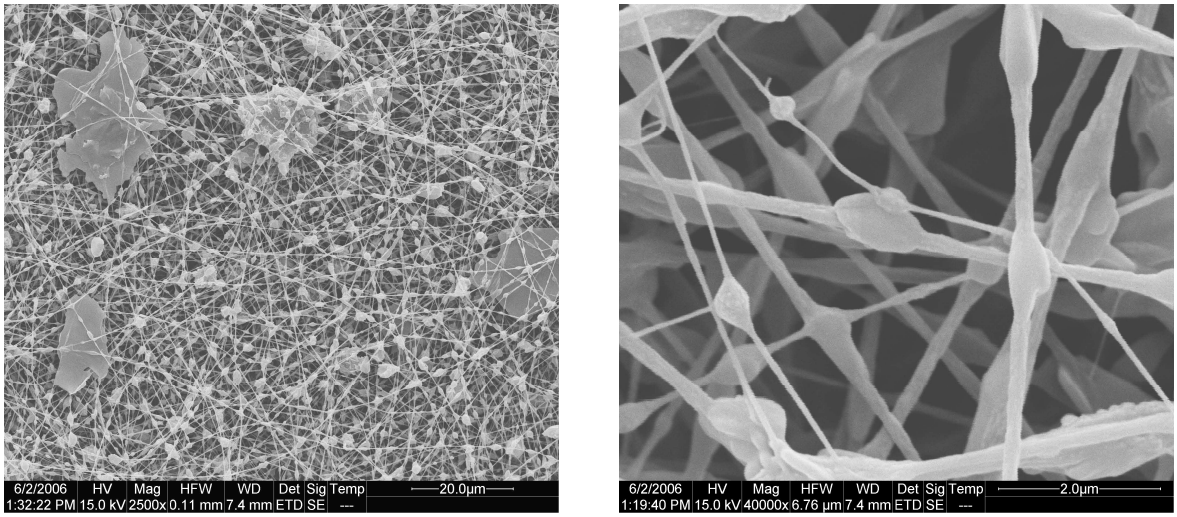

(a) (b)

Figure 3.29 SEM micrographs of fibres electrospun from PAni 1% PAN 3% TDAB 10% in DMSO/DMF/THF (a) Mag: 2,500X, (b) Mag: 40,000X

Closer inspection of the Figure 3.29 (b) reveals some degree of binding between globules with increasing TDAB concentration. It was also revealed that the globules and beads were becoming smoother and more spherical in appearance and secondary fibres also existed. These characteristics indicate that the properties of the polymer solution did change significantly after TDAB was added to the blend. This is further supported with the significant increase in viscosity for PAni/PVC solutions after the addition of TDAB, as noted in Section 2.4.2. It is important to note that Lin et al. [184] did not observe any significant increase in viscosity with the addition of TBAC and DTAB to PS in THF/DMF. From this it is reasonable to assume an overall increase in the

viscosity of the PAni/polymer solutions with the addition of TDAB indicates that there was a significant change in the PAni/polymer/solvent/ionophore interactions, not previously reported.

3.3.11 PAni/PVC/TAEAB Electrospun Fibres

Blending triallylethylammonium bromide (TAEAB), a documented nitrate ionophore, with PAni/PVC did not produce any significant change in the fibre morphology compared with PAni 1% PVC 10% electrospun fibres. Micrographs of PAni 1% PVC 10% TAEAB 0.5% fibres electrospun from THF/DMF are presented in Figures 3.30 (a) and (b).

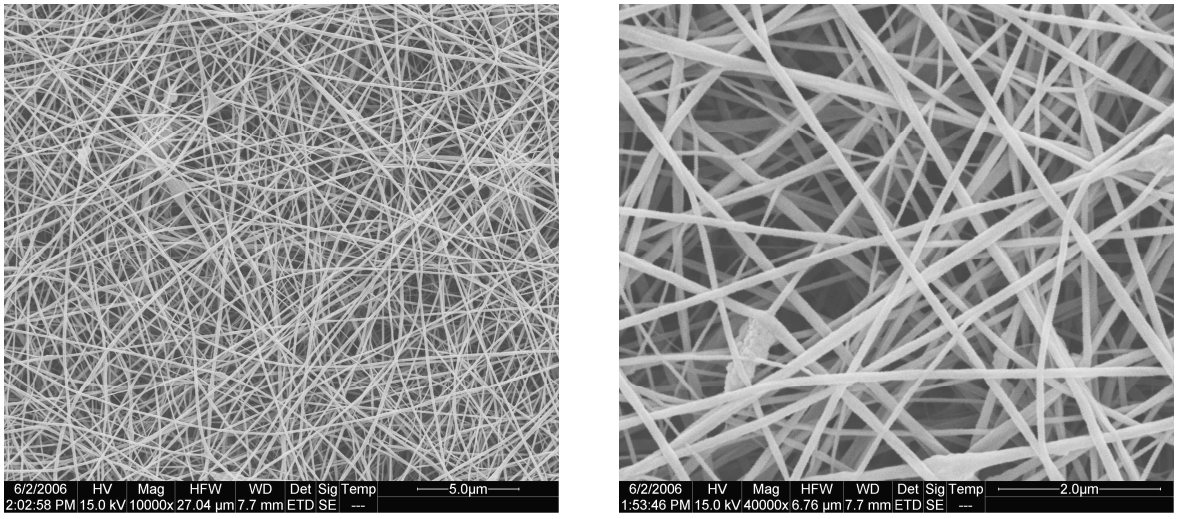

(a) (b)

Figure 3.30 SEM micrographs of fibres electrospun from PAni 1% PVC 10% TAEAB 10% in THF/DMF (a) Mag: 10,000X, (b) Mag: 40,000X

Whilst the morphology of the electrospun fibres themselves are identical to PAni 1% PVC 10%, there appears to have been a decrease in the presence of large globules from electrospraying. This may indicate that TAEAB increased the viscoelastic properties of the polymer solution, in turn decreasing the degree of electrospraying. However, this

was difficult to quantify as higher concentrations of the ionophore would not dissolve in the THF/DMF solvent, most likely due to the relatively low polarity of this solvent blend. This decrease in globule numbers may also have been a product of an increase in the conductivity after the addition of TAEAB to the polymer solution, similar to previous observations. The solution characteristics of viscosity, surface tension and conductivity of polymer/TAEAB solutions were not determined due to the insufficient quantities of ionophore synthesised, the time of synthesis, and due to the significant volumes of solution required for analysis.

3.3.12 PAni/PAN/TAEAB Electrospun Fibres

The addition of TAEAB 0.5% to PAni 1% PAN 3% spinning solution resulted in less beads when compared with PAni 1% PAN 3% fibres, as can be seen in Figures 3.31 (a) and (b).

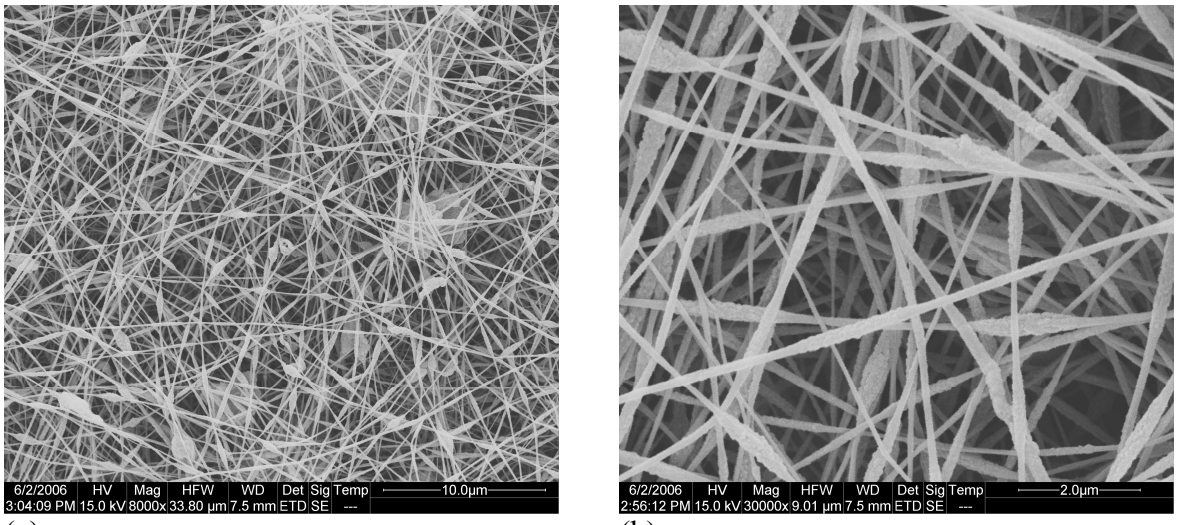

(a) (b)

Figure 3.31 SEM micrographs of fibres electrospun from PAni 1% PAN 3% TAEAB 0.5% in DMSO/DMF (a) Mag: 8,000X, (b) Mag: 30,000X

The beads along the fibres appeared ellipsoidal and the surfaces of these beads appeared quite rough compared with the PAni/PAN micrograph. It is clear the addition of TAEAB has led to a change in fibre properties, and hence solution properties. As noted in Section 3.3.11, the solution characteristics of viscosity, surface tension and conductivity of polymer/TAEAB solutions were not determined.

Increasing the concentration of TAEAB to 5% in the spinning solution changed the morphology of the fibrous mat substantially such that there was an increase in electrosprayed particles and changes in fibre point-bonding [Figures 3.32 (a) and (b)]. Whilst the blend produced particles over the entire fibrous mat there was also the presence of orientated and agglomerated particles, possibly indicating that the electrospinning jet interacted with electrosprayed droplets during flight, or that these agglomerated particles are electrosprayed material.

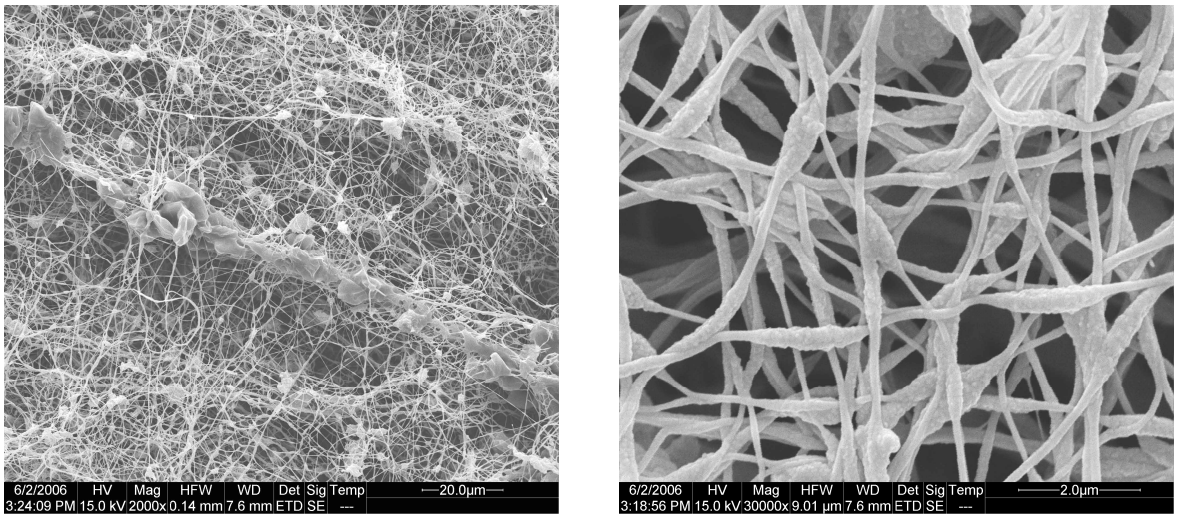

(a) (b)

Figure 3.32 SEM micrographs of fibres electrospun from PAni 1% PAN 3% TAEAB 5% in DMSO/DMF (a) Mag: 2,000X, (b) Mag: 30,000X

Closer inspection of Figure 3.32 (b) reveals similarities to both PAN 3% and PAni 1% PAN 3% electrospun fibres in Figures 3.5 (b) and 3.13 (b). The major similarity with

PAni 1% PAN 3% fibres was the structure of the beads along the fibres retaining the characteristic ellipsoidal structure and the rough surface texture. However, the fibres intertwined and bonded to other fibres in a manner similar of PAN 3%, albeit to a lesser degree. Thus, unlike the addition of TDAB 5% to PAni/PAN fibres, where there was a change in the bead structure as well as the fibre properties, it appears that the addition of TAEAB has led to retention of solvent within the fibres.

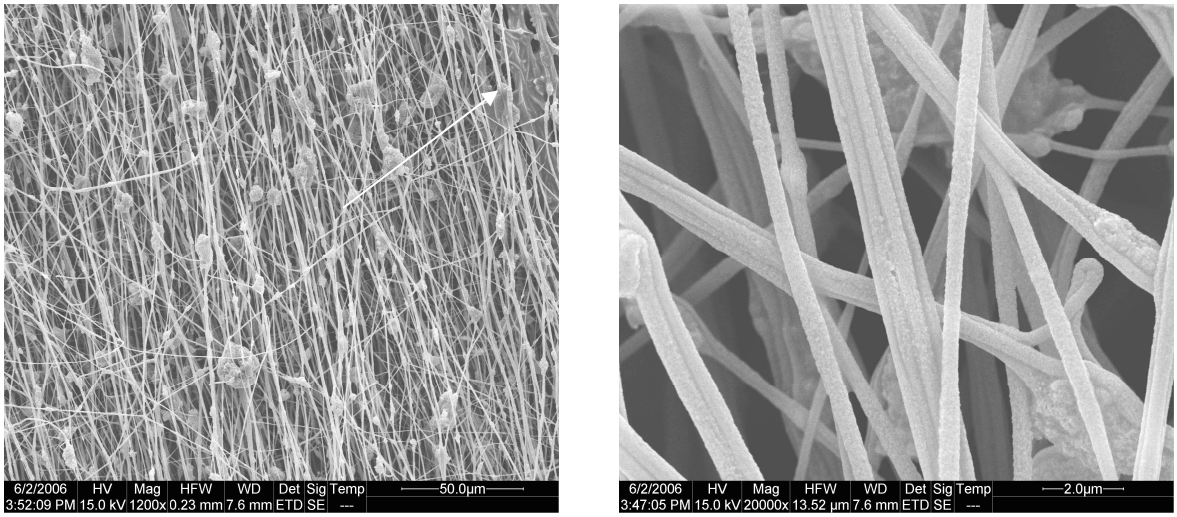

(a) (b)

Figure 3.33 SEM micrographs of fibres electrospun from PAni 1% PAN 3% TAEAB 10% in DMSO/DMF (a) Mag: 1,200X, (b) Mag: 20,000X

Increasing the TAEAB composition to 10% produced notable changes in the orientation of the electrospun fibres. Micrographs of fibres electrospun from PAni 1% PAN 3% TAEAB 10% in DMSO/DMF are given in Figures 3.33 (a) and (b). This change in orientation is similar to the observations for PAni 1% PAN 5% electrospun fibres [Figures 3.14 (a) and (b)] which are also orientated in one direction. This may indicate that the higher concentration of TAEAB led to a change in the solution properties, such as solution conductivity, solution surface tension and viscosity of the sample, in turn altering the electrospinning process and the resultant fibre morphology. Furthermore individual fibres possessed a tendency to bond together linearly. Again this may

indicate that in combination, the fibres and ionophore retained solvent more so than previously. This is further supported from the section of film-like surface in Figure 3.33 (a) in the upper right hand corner, which may be a product of electrosprayed polymer solution coating the previously electrospun fibres. Thus, TAEAB influences the morphological properties of the PAni/PAN electrospun fibres by influencing the solution properties of the blends, and in turn the electrospinning process.

3.3.13 MWNT/PVC Electrospun Fibres

Incorporating MWNT into PVC produced significantly different fibres compared to PVC 10%, with far less globules and beads present, with more similar characteristics to PAni 1% PVC 10% electrospun fibres. Micrographs of fibres of MWNT 0.5% PVC 10% are given in Figures 3.34 (a) and (b).

This result indicates that MWNT induces some structural support for the formation of electrospun fibres. Previously in Figures 3.2 (a) and (b) for PVC 10%, it was observed that the concentration of PVC was not sufficiently high to produce a uniform fibrous mat, instead producing a significant number of globules from electrospraying. It was also detailed in Section 2.6.7 that the presence of MWNT did not significantly increase the conductivity, or alter the surface tension of a PVC 10% solution (Section 2.5.2). However, the viscosity did increase notably compared to PVC 10%, which has led to the formation of relatively uniform nanofibres here. Previously Seoul et al. [122] indicated that these increases in viscosity were a result of nanotube entanglement. However, it was concluded in Chapter 2 that this was not the case as indicated by differences in viscosity of MWNT/PVC and MWNT/PAN solutions showing that the MWNT caused the entanglement and/or interaction of the polymer chains within the solution.

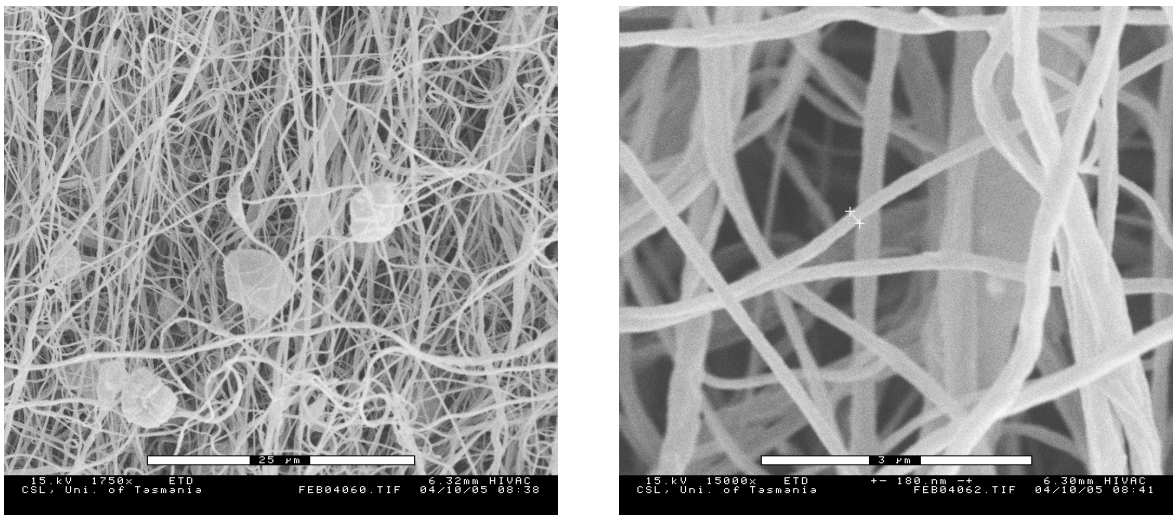

(a) (b)

Figure 3.34 SEM micrographs of fibres electrospun from MWNT 0.5% PVC 10% in THF/DMF (a) Mag: 1,750X, (b) Mag: 15,000X

The addition of 1% dodecylbenzenesulfonic acid (DBSA) to assist in dispersion, and subsequently electrospinning of the MWNT/polymer blends, altered the structure of these MWNT/PVC fibres further in comparison to those of neat PVC [Figures 3.35 (a) and (b)].

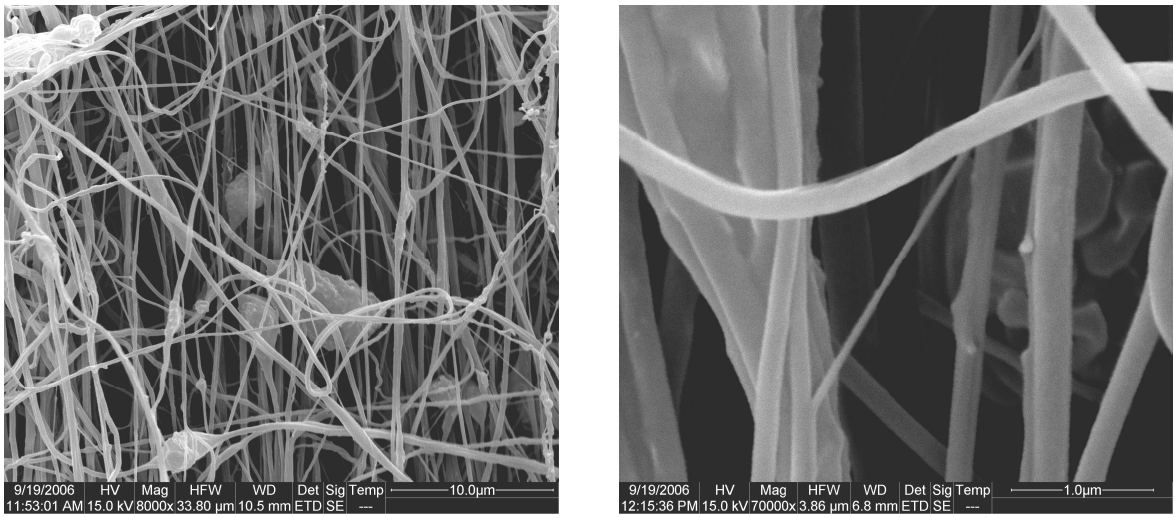

(a) (b)

Figure 3.35 SEM micrographs of fibres electrospun from MWNT 0.5% PVC 10% DBSA 1% in THF/DMF (a) Mag: 8,000X, (b) Mag: 70,000X

The fibres have lost their uniformity, instead exhibiting a variety of different structures and textures. Furthermore the beads and globules increased slightly in number compared with MWNT 0.5% PVC 10% fibres. The presence of DBSA may have assisted in the dispersion of MWNT, but produced fibres of lower quality and diverse morphologies.

3.3.14 MWNT/PAN Electrospun Fibres

The addition of MWNT to PAN produced significantly different fibres compared to PAN 3% and also PAni 1% PAN 3% fibres. These fibres can be observed in Figures 3.36 (a) and (b).

Whilst the fibres of PAN 3% were relatively smooth [Figures 3.5 (a) and (b)] those in Figure 3.36 are extremely rough. There are some similarities to PAni 1% PAN 3% electrospun fibres [Figures 3.13 (a) and (b)] particularly in the location and number of bead-type structures along the fibres. Closer inspection in Figure 3.36 (b) reveals that these fibres appear somewhat porous and possess a significant number of small protrusions on the surface, possibly aggregates of MWNT. It was noted in Section 2.4.1 that the viscosity of the MWNT/PAN solutions were slightly higher than straight PAN solutions, however this small increase would not be expected to induce these significant morphological changes. As also noted in Chapter 2, measurements of surface tension and conductivity of MWNT/PAN blends were not undertaken. Thus assuming comparable affects on PAN solution surface tension and conductivity as reported for PVC, it appears that the morphology is directly a result of the MWNT aggregations, and not changes in overall solution characteristics.

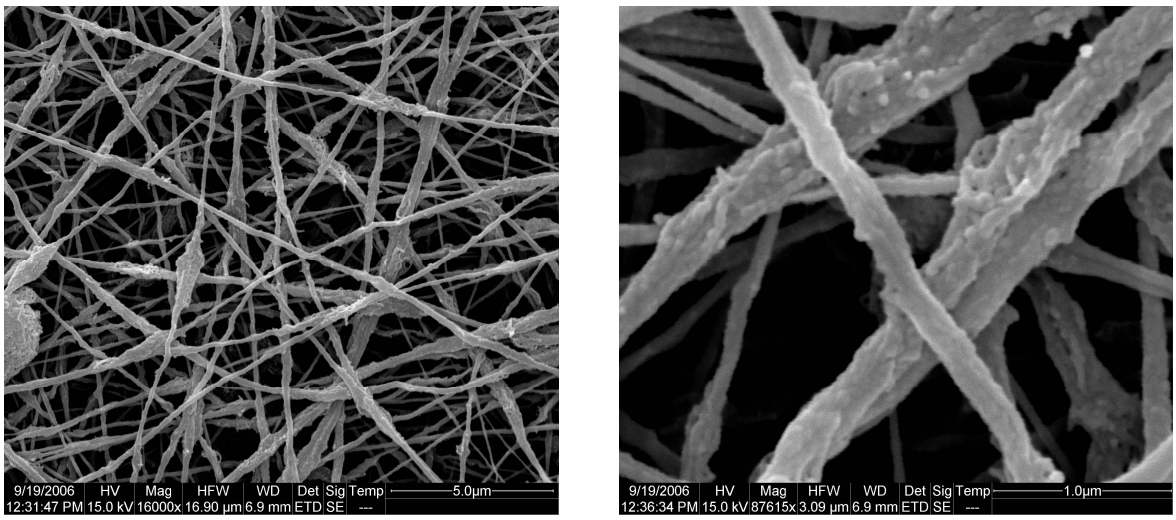

(a) (b)

Figure 3.36 SEM micrographs of fibres electrospun from MWNT 0.5% PAN 3% in DMSO/DMF (a) Mag: 16,000X, (b) Mag: 87,615X

The presence of DBSA, again to assist in dispersion and electrospinning, radically changed the fibre mat, increasing the number of globules and beads, similar to observations for MWNT 0.5% PVC 10%. SEMs of these fibres are given in Figures 3.37 (a) and (b).

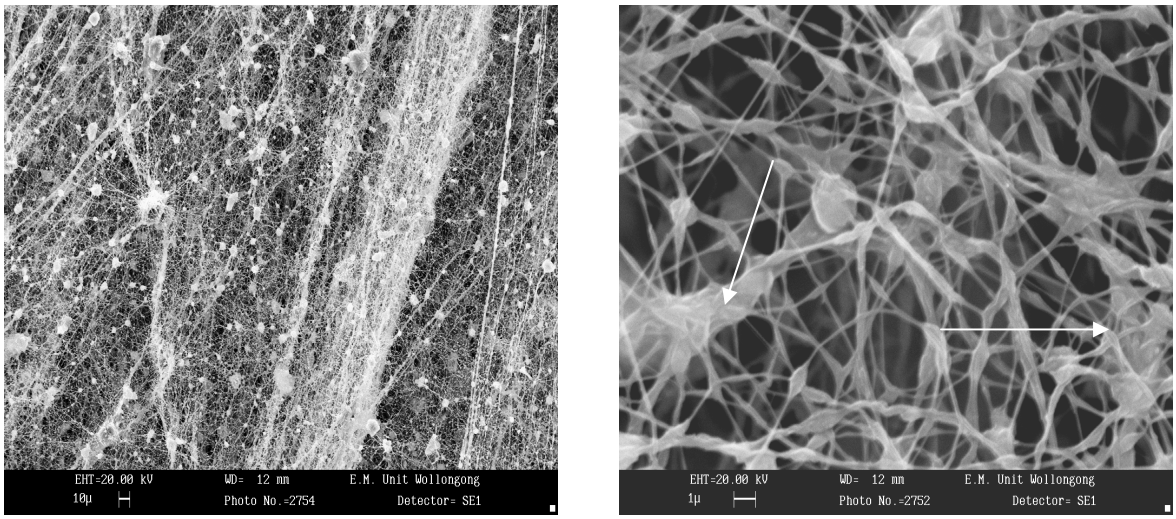

(a) (b)

Figure 3.37 SEM micrographs of fibres electrospun from MWNT 0.5% PAN 3% in DMSO/DMF (a) and (b)

Whilst the DBSA may have assisted in dispersion of the MWNT, the overall fibre structure and morphology has deteriorated significantly. The arrows in Figure 3.37 (b) indicate areas where the fibre structure has completely collapsed and started to form a film-like surface. Thus, the presence of DBSA has a detrimental affect on the formation of electrospun fibres from blends of MWNT/PVC and MWNT/PAN.

3.4 Results and Discussion – Fibre Diameter Determination

3.4.1 PVC Electrospun Fibres

Whilst the electrospinning of PVC 5% from THF/DMF did not produce any fibres, increasing the concentration by 5% increments up to 20% led to the formation of fibres, with increasing diameter (Table 3.1).

PVC 5%		PVC 10%		PVC 15%		PVC 20%	
	Diameter (nm)		Diameter (nm)		Diameter (nm)		Diameter (nm)
Mean	No Fibres	Mean	206	Mean	477	Mean	1020
Std. Dev.	No Fibres	Std. Dev.	94	Std. Dev.	196	Std. Dev.	650

Table 3.1 Fibre diameters for fibres electrospun from PVC in THF/DMF

This increase in fibre diameter with increasing PVC concentration in the electrospinning solution supports the statement that an increase in viscosity is related to an increase in the chain entanglement and cohesive forces within the polymer, and in turn leads to an increase in the fibre diameter [98, 119, 209]. It is also possible that these increases in diameter were a result of inhibition of electrospinning with increasing viscosity, leading to less whipping of the polymer jet. Overall, the increase in fibre diameters exhibited a direct relationship to increases in the viscosity of the solution.

From the standard deviation values, approximately half that of the fibre diameters for all concentrations of PVC, it is clear that there was significant variation in the diameters of the fibres.

3.4.2 PAN Electrospun Fibres

The PAN fibres exhibited diameters significantly lower than the PVC electrospun fibres for all concentrations of PAN, presented in Table 3.2.

This is interesting considering the viscosity of the PAN solutions were not too dissimilar to those of PVC, as detailed in Section 2.4. This was most likely a result of the conductivity of the PAN solutions, detailed in Section 2.6.1. The high solution conductivity has increased the whipping of the polymer jet or limited other forms of electrospinning instabilities, leading to a decrease in overall fibre diameter, similar to observations by Tan et al. [190] for poly(L-lactid-co-caprolactone) (PLLA-CL) dissolved in dichloromethane (DCM), DCM/DMF and DCM/pyridine.

PAN 1%		PAN 3%		PAN 5%		PAN 7%	
	Diameter (nm)		Diameter (nm)		Diameter (nm)		Diameter (nm)
Mean	No Fibres	Mean	112	Mean	215	Mean	266
Std. Dev.	No Fibres	Std. Dev.	23	Std. Dev.	30	Std. Dev.	27

Table 3.2 Fibre diameters for fibres electrospun from PAN in DMSO/DMF

The diameters of the electrospun fibres were quite uniform across the concentration range. Whilst the deviation as a percentage of the mean decreased with increasing polymer concentration, the standard deviation was relatively constant over all three compositions. This indicates that the increase in viscosity did not significantly increase variation in the fibre diameter unlike the PVC solutions.

3.4.3 PAni/PVC Electrospun Fibres

The addition of PAni led to a considerable reduction in the fibre diameter compared with the PVC-only solutions, as can be observed in Table 3.3.

PAni 1% PVC 5%		PAni 1% PVC 10%		PAni 1% PVC 15%		PAni 1% PVC 20%	
	Diameter (nm)		Diameter (nm)		Diameter (nm)		Diameter (nm)
Mean	63	Mean	129	Mean	214	Mean	452
Std. Dev.	18	Std. Dev.	58	Std. Dev.	85	Std. Dev.	246

Table 3.3 Fibre diameters of fibres electrospun from PAni/PVC in THF/DMF

The addition of PAni to PVC 5% produced true nanofibres i.e. fibres with a diameter below 100nm, however the morphology was not uniform, as reported in Section 3.3.3. Further increases in the PVC concentration increased the fibre diameter, however these were well below the values observed for the fibres electrospun from the PVC-only solutions. These decreases may have been a result of the increase in conductivity observed in the presence of PAni (Section 2.6.4), leading to an increase in the whipping of the jet, and hence lower fibre diameters. This is quite plausible as the viscosity of the polymer solution increased with the addition of PAni and the surface tension did not change significantly, as detailed in Chapter 2.

Similar to the PVC-only fibres the diameters varied widely with respect to the average fibre diameter. Again the standard deviation was approximately half that of the average fibre diameter, except for the PAni 1% PVC 5% fibrous mat. As this was consistent across both PAni and non-PAni PVC solutions, it appears that the result was due to the combination of viscosity, solution surface tension and solution conductivity of the PVC solution. These properties, in conjunction with variability in the electrospinning process such as ‘pulsation’ of the whipping jet, may have produced varied fibre diameters. This pulsation has been reported previously by Hayati [85], and is a cycle of jet formation

followed by relaxation of the solution, up until a suitable electric field is reached to overcome this. The pulsation, observed only in the PVC solutions, developed on the solution cone. The jet would form, spin for a brief period and then dissipate as the volume of the droplet at the end of the pipette decreased. Increasing the potential of the power supply resolved this issue, but it is possible that some form of pulsation may have remained at higher potentials. Thus, in this context, the viscosity and surface tension of the PVC solution may have limited a constant single jet forming, whilst the conductivity of the solution, in tandem with the applied voltage, would assist in producing a stable jet.

3.4.4 PAni/PAN Electrospun Fibres

The PAni/PAN fibres electrospun from DMSO/DMF showed both differences and similarities to the PAN fibres analysed previously. The average fibres diameters are given in Table 3.4.

PAni 1% PAN 1%		PAni 1% PAN 3%		PAni 1% PAN 5%		PAni 1% PAN 7%	
	Diameter (nm)		Diameter (nm)		Diameter (nm)		Diameter (nm)
Mean	68	Mean	69	Mean	317	Mean	349
Std. Dev.	15	Std. Dev.	15	Std. Dev.	75	Std. Dev.	108

Table 3.4 Fibre diameters of fibres electrospun from PAni/PAN in DMSO/DMF

Similar to the PAni/PVC fibres the introduction of PAni to PAN 1% allowed the formation of true nanofibres. PAni 1% PAN 3% electrospun fibres decreased in diameter significantly compared with PAN 3%. The mean diameters for the PAni 1% PAN 5% and PAni 1% PAN 7% fibres were larger than those for the corresponding neat PAN solutions, unlike the PAN 3% case where the addition of 1% PAni decreased the average fibre diameter. This was related to the increase in viscosity of the electrospun

solutions (Section 2.4.1), and possibly the decrease in the bead presence (Section 3.3.4). A more viscous solution would resist thinning during the electrospinning process, and the failure of beads to form may have resulted in a greater polymer volume within the fibres. The increase in conductivity, detailed in Section 2.6.3 for these blends, was insufficient to produce fibre diameters as low as those from the corresponding straight PAN solutions for PAni 1% PAN 5% and PAni 1% PAN 7% blends. In addition, the standard deviation of the fibre diameters also increased, but remained proportional across the different PAN concentrations. Considering the standard deviation did not change significantly for the neat PAN mats, it appears the PAni not only increased the fibre diameter, it also increased the variability of the diameters.

3.4.5 PAni/PVC/NPOE and PAni/PVC/TOAB Electrospun Fibres

Due to the failure to electrospin fibres from PAni/PVC and PAni/PAN solutions with higher concentrations of 2-NPOE, this ionophore will be grouped with TOAB for fibre size analysis (Table 3.5).

The addition of 2-NPOE 5% to PAni 1% PVC 10% solution almost doubled the average diameter of the electrospun fibres compared with the PAni 1% PVC 10% fibres. This increase in fibre diameter could be based in the viscosity of the solution, assuming that the addition of 2-NPOE increased the viscosity of the solutions, similar to other additives such as PAni and TDAB.

On the other hand, the diameter of fibres spun from PAni 1% PVC 10% TOAB 5% solution increased only slightly relative to the PAni/PVC fibres, whilst the PAni 1% PVC 10% TOAB 20% fibre mat had a significantly higher average diameter.

PAni 1% PVC 10% 2-NPOE 5%		PAni 1% PVC 10% TOAB 5%		PAni 1% PVC 10% TOAB 20%	
	Diameter (nm)		Diameter (nm)		Diameter (nm)
Mean	201	Mean	140	Mean	268
Std. Dev.	71	Std. Dev.	61	Std. Dev.	140

Table 3.5 Fibre diameters for fibres electrospun from PAni/PVC/2-NPOE and PAni/PVC/TOAB in THF/DMF

According to Section 3.3.7, the fibre orientation of the PAni/PVC/TOAB 5% fibres [Figure 3.20 (a)] was significantly different to those observed for PAni/PVC/2-NPOE 5% [Figure 3.16 (a)], indicating that the different ionophores had imparted different properties on the electrospinning of the solutions. It appears that this difference also resulted in changes in the fibre diameters. The increased looping of the PAni/PVC/TOAB 5% fibres may indicate that the jet was whipping to a larger extent, possibly as a result of an increase in the conductivity due to the presence of TOAB. A further increase in TOAB concentration to 20% would have possibly increased the viscosity of the solution, which in turn, would have negated an increase in conductivity, leading to the significant, but not exceptional increase in fibre diameter. This is based on the viscosity of the PAni 1% PVC 10% TDAB 20% solution increasing by over 400% compared with the PAni 1% PVC 10% solution.

3.4.6 PAni/PAN/2-NPOE and PAni/PAN/TOAB Electrospun Fibres

The addition of 2-NPOE and TOAB to PAni/PAN increased the average fibre diameter significantly, as can be observed in Table 3.6.

PAni 1% PAN 3% 2-NPOE 5%		PAni 1% PAN 3% TOAB 5%		PAni 1% PAN 3% TOAB 20%	
	Diameter (nm)		Diameter (nm)		Diameter (nm)
Mean	468	Mean	351	Mean	443
Std. Dev.	99	Std. Dev.	90	Std. Dev.	118

Table 3.6 Fibre diameters for fibres electrospun from PAni/PAN/2-NPOE and PAni/PAN TOAB in DMSO/DMF

The diameter of fibres electrospun from PAni 1% PAN 3% 2-NPOE 5% were almost seven times the diameter of PAni 1% PAN 3% fibres. The addition of TOAB also increased the fibre diameter substantially, in comparison to PAni/PAN. These increases were far greater than those observed for additions to PVC blends. This indicates that whilst viscosity may have played some role in the higher fibre diameters of the PAni/PAN/2-NPOE and PAni/PAN/TOAB blends, the actual interaction of the ionophores with the polymer solution appears to have contributed significantly more to these changes. This is further supported by the significant morphological changes of PAni/PAN/2-NPOE and PAni/PAN/TOAB fibres observed in Sections 3.3.6 and 3.3.8 compared with the PAni/PAN fibres in Section 3.3.4, where changes in the bead structures and fibre network were observed.

Thus the presence of these two additives produced poor fibre properties due to the influence of these groups on the overall solution properties, including viscosity, solution surface tension and solution conductivity. Combined, these parameters may have been the cause of such large fibre diameters, but together with the significant morphological changes it appears the introduction of 2-NPOE or TOAB disrupts the polymer/polymer and polymer/solvent chemical interactions.

3.4.7 PAni/PVC/TDAB Electrospun Fibres

The addition of TDAB did not change the average fibre diameter significantly, and the values for all three concentrations of TDAB are well within the error for the average diameter observed for the PAni 1% PVC 10% fibrous mat (Table 3.7).

In comparison with observations from Section 3.3.9, the morphological properties of these fibres only changed slightly with the addition of TDAB, however the properties of

the PAni/PVC/TDAB solutions changed substantially with significant increases in the conductivity, viscosity and surface tension. Thus it appears a balance of these variables was retained after the addition of TDAB, such that the viscosity was sufficiently high to counter the increased surface tension, and the higher conductivity overcame the higher viscoelastic properties to ensure polymer jet elongation.

PAni 1% PVC 10% TDAB 0.5%		PAni 1% PVC 10% TDAB 5%		PAni 1% PVC 10% TDAB 10%	
	Diameter (nm)		Diameter (nm)		Diameter (nm)
Mean	116	Mean	169	Mean	125
Std. Dev.	44	Std. Dev.	75	Std. Dev.	52

Table 3.7 Fibre diameters of fibres electrospun from PAni/PVC/TDAB in THF/DMF

3.4.8 PAni/PAN/TDAB Electrospun Fibres

The PAni/PAN/TDAB fibres recorded a larger diameter after the addition of TDAB in comparison to PAni 1% PAN 3% electrospun fibres. The average fibre diameters are given in Table 3.8.

PAni 1% PAN 3% TDAB 0.5%		PAni 1% PAN 3% TDAB 5%		PAni 1% PAN 3% TDAB 10%	
	Diameter (nm)		Diameter (nm)		Diameter (nm)
Mean	105	Mean	127	Mean	155
Std. Dev.	28	Std. Dev.	29	Std. Dev.	43

Table 3.8 Fibre diameters of fibres electrospun from PAni/PAN/TDAB in DMSO/DMF/THF

With respect to the standard deviation, the diameters of the electrospun fibres remained constant with increasing concentration of TDAB. This would indicate that TDAB had little influence on the solution interactions, however from Section 3.3.10 it is clear this is not the case with the overall fibre morphology changing notably with increasing TDAB concentration. Thus, whilst fibre morphology altered, a consequence of changes

in the solution properties, such as viscosity, surface tension and conductivity, the net affect was no change in the average fibre diameter.

3.4.9 PAni/PVC/TAEAB Electrospun Fibres

It was noted previously that higher concentrations of TAEAB were unable to be adequately dissolved and electrospun from solution due to incompatibilities with the solvent blend. Only the PAni 1% PVC 10% TAEAB 0.5% solution was successfully electrospun. These fibres exhibited a mean fibre diameter of 99 nm ± 30, lower than that observed for PAni 1% PVC 10%. However, the standard deviation was well within the limits, indicating that TAEAB had very little effect on the fibre diameter at this concentration. This is supported by the fibre morphology observed in Section 3.3.11.

3.4.10 PAni/PAN/TAEAB Electrospun Fibres

The addition of TAEAB to PAni/PAN produced mean fibre diameters similar to those observed for the PAni/PAN/TDAB apart from TAEAB 10%. These diameters are recorded in Table 3.9.

PAni 1% PAN 3% TAEAB 0.5%		PAni 1% PAN 3% TAEAB 5%		PAni 1% PAN 3% TAEAB 10%	
	Diameter (nm)		Diameter (nm)		Diameter (nm)
Mean	109	Mean	132	Mean	379
Std. Dev.	32	Std. Dev.	31	Std. Dev.	92

Table 3.9 Fibre diameters of fibres electrospun from PAni/PAN/TAEAB in DMSO/DMF

From SEM analysis in Section 3.3.12 the bead structure and texture remained relatively uniform for PAni 1% PAN 3% TAEAB 0.5% and 5% fibres, but not PAni 1% PAN 3% TAEAB 10%. In addition, there was a change in the overall fibre morphology, including a change in the orientation of the fibres and the presence of globules. From Table 3.9, a

disproportionate increase in the average fibre diameter with the increase in TDAB from 5% to 10% can also be observed. These differences imply that viscosity was responsible for increases in the mean fibre diameter. That is, the increase in TAEAB concentration increased the viscosity of the polymer solution, especially at high concentrations, in turn increasing the fibre diameter whilst the increase in conductivity had no major effect.

3.4.11 MWNT/PVC and MWNT/PAN Electrospun Fibres

The introduction of MWNT to PVC and PAN solutions produced very similar fibre diameters (Table 3.10). This was unexpected considering the differences in the viscosities detailed in Section 2.4. The viscosity of the MWNT/PVC blend was approximately ten times that of PVC alone, changing from 22 mPa.s to 202 mPa.s for the addition of 0.5% MWNT to PVC 10% in THF/DMF, whilst the addition of 0.5% MWNT to PAN 3% in DMSO/DMF resulted in a doubling of viscosity to 98 mPa.s.

MWNT 0.5% PVC 10%		MWNT 0.5% PVC 10% DBSA 1%	
	Diameter (nm)		Diameter (nm)
Mean	226	Mean	260
Std. Dev.	51	Std. Dev.	83
MWNT 0.5% PAN 3%		MWNT 0.5% PAN 3% DBSA 1%	
	Diameter (nm)		Diameter (nm)
Mean	252	Mean	163
Std. Dev.	77	Std. Dev.	48

Table 3.10 Fibre diameters of fibres electrospun from MWNT/PVC in THF/DMF and MWNT/PAN in DMSO/DMF

The MWNT/PAN mean fibre diameter was twice that of the PAN solution, as was the viscosity, while the MWNT/PVC mean fibre diameter remained relatively constant. Thus, it was possible that in this case viscosity alone was responsible for the increase in fibre diameter.

If this is the case there must be some other variable that influenced the fibre diameter to account for the observations of MWNT/PVC. Possibly the interaction between the MWNT, polymer and solvent blends was much higher than compared with MWNT/PAN and previous PAni/PVC blends. This would account for the extremely large viscosity, but not the fibre diameter. Thus, the MWNT has imparted some property to the blend that ensured the increased viscosity had no bearing on the fibre diameter, either by chemical interaction or through some physical contribution, although it is unclear as what this may be.

The addition of DBSA to ensure dispersion of MWNT appeared to have had little influence on the electrospun MWNT/PVC fibres with the mean diameters comparable to that of MWNT/PVC. However, in the case of MWNT/PAN, the fibre diameter decreased by nearly 40% with the addition of DBSA. This is despite MWNT/PVC/DBSA and MWNT/PAN/DBSA fibres having comparable morphology, though MWNT 0.5% PAN 3% DBSA 1% did posses a greater number of beads throughout the sample. It was surmised in Section 3.4.4 that bead formation may have led to a decrease in the diameter of the fibres. Thus, DBSA impacted only on the diameters of MWNT/PAN fibres, indicating changes to PAN, either through interactions between PAN and DBSA, or through PAN and the solvents in the presence of DBSA.

3.5 Conclusions

Both PVC and PAN solutions produced electrospun fibres from concentrations above a certain minimum level of 10% for PVC and 3% for PAN, becoming smoother and more uniform with increasing concentration of the relevant polymer. In addition the PAN fibres were consistently smaller in diameter compared with PVC electrospun fibres, and were not as variable, indicative of the higher conductivity of PAN solutions.

The addition of 1% PAni to the lower concentrations of PVC and PAN (5% and 1%/ respectively) allowed the electrospinning of polymer blends. Furthermore, the addition of PAni led to marked improvement in fibre quality for PAni 1% PVC 10% and PAni 1% PAN 3% compared to PVC and PAN fibres. Unfortunately, the quality declined with higher support polymer concentrations. Thus the addition of PAni led to an increase in the viscoelastic properties of the solutions that was sufficient to both produce electrospun fibres, and to alter the solution properties of viscosity, solution surface tension and solution conductivity, to make these uniform. This is also supported by the fibre diameter analysis which showed marked decreases in the fibre diameters after the addition of PAni for all solutions, apart from PAni 1% PAN 5% and PAni 1% PAN 7%, as well as a decrease in the standard deviation of these diameters.

The addition of the plasticiser 2-NPOE to PAni/polymer solutions led to the production of ‘point-bonded’ fibres at low 2-NPOE concentrations, and porous films at higher concentrations. As plasticisers are often employed in polymer solutions for their ability to assist processability, this creates a problem for the technique of electrospinning. Specifically ISEs often use high concentrations of plasticiser, but in this case, combining 2-NPOE with electrospinning led to a collapse in the fibre structure, and an

increase in fibre diameter, negating the process of electrospinning and rendering the resultant electrodes as useless.

The addition of quaternary ammonium salt ionophores in the spinning solutions led to fibres exhibiting similar morphologies to the PAni/polymer/2-NPOE samples, indicating that these components can have a detrimental affect on the quality of the electrospun fibres. It was found that the quality of the fibre mat was related to the concentration of the QAS added, such that higher concentrations of QAS produced fibres with a greater amount of point-bonding throughout the mat. This is not necessarily detrimental to the overall electrode operation as this morphology would most likely lead to a greater conducting PAni network. However, this point-bonding also coincided with the formation of film-like characteristics, such as broadening and irregularity in the fibre structure, at high concentrations for PAni/PVC solutions, which would lead to a decrease in surface area.

In the PAni/PAN blends these additives also produced a great increase in the number of beads and globules in most blends with QAS. The morphologies in the cases of TOAB, TDAB and 10% TAEAB PAni/PAN samples were not uniform, and the beads were found to actively bond with individual fibres. Thus, the interaction of QAS with the solution components, and affect on the solution properties of viscosity, surface tension and conductivity have, in many cases, produced fibres lower in quality in comparison to PAni/polymer and polymer-only electrospun fibres. The fibre diameters of PAni/PVC/ionophore were comparable to PAni/PVC samples, however one trend that appeared was that the fibre diameter would increase with increasing QAS concentration for the majority of samples. This was also the case for PAni/PAN/ionophore, except for samples of PAni/PAN/2-NPOE and PAni/PAN/TOAB which exhibited significant

increases in mean fibre diameter. It was postulated that this was a result of the direct influence of 2-NPOE and TDAB on the polymer-polymer and polymer-solvent interactions.

The replacement of PAni with MWNT in the PVC solution led to fibres that exhibited little difference to PAni/PVC electrospun fibres. This signifies that MWNT interact with PVC in a similar manner to PAni, leading to an increase in viscosity, an increase in the diameter of the fibres, and an improvement in the quality of the fibres compared with PVC 10%. This was not the case for MWNT/PAN fibres which were far rougher compared with both PAni/PAN and PAN electrospun fibres, indicating that aggregations of MWNT persisted in this solution. However, the fibre diameter with the addition of MWNT to PAN also increased, whilst the mean fibre diameter for MWNT/PVC decreased. This indicates that the MWNT imparted some property to reduce the influence of viscosity for MWNT/PVC, but not MWNT/PAN. The addition of DBSA to assist MWNT dispersion led to a severe decline in the quality of the electrospun fibres, leading to a high number of beads and globules throughout both MWNT/polymer blends, as well as an overall change in morphology. Whilst DBSA may have assisted dispersion, and in the case of MWNT/PAN, decreased the average fibre diameter, it had a detrimental impact on the fibrous structure, and would be classified as an unsuitable additive to the solution.

Chapter 4 - Fibre Properties

"Sir, you have seen the Raman effect on alcohol; please do not try to see the alcohol effect on Raman."

Chandrasekhara Venkata Raman (1888 – 1970)

after being offered a toast for his Nobel Prize in Physics in 1930

4.1 Introduction

A number of groups have utilised Raman spectroscopy for characterisation of polyaniline (PAni) in reactions, solutions and powders. Specifically Raman can be used to determine the chemical form of PAni i.e. leucoemeraldine, emeraldine or pernigraniline, and whether it is in the base state or protonated [222-231] . The spectra obtained from Raman is dependent on both the oxidation state and the degree of protonation of the PAni, and also the laser excitation wavelength [223, 224]. This chapter will provide an analysis of the degree of protonation of the electrospun fibres, differences in the chemical properties between the blends of PAni/PVC and PAni/PAN, the dispersion of PAni within these fibre mats, and the affect of the ionophores on the chemical properties of PAni.

According to Lee et al. [84], electrospun fibre mats have poor mechanical properties, however this is dependent on fibre structure, make up of the blend and the interaction of the components in the blend. In addition, the mechanical strength is also dependent on the fibre size and the adherence of fibres to each other, as well as the geometrical lie of the fibres [142]. This chapter will also provide a measure of the physical strength these properties have, and show the variability in strenght inherent between the samples.

4.1.1 Raman Analysis of Polyaniline

According to Liu et al. [224] Raman intensity bands below 1000 cm^{-1} are lower for a 633 nm laser compared with a 735 nm laser. This can be correlated with UV/Vis absorption. Strong UV/Vis absorption occurs for the quinoid structure in undoped PAni at a wavelength of 630nm. Conversely the polarons in doped PAni present significant, broad UV/Vis absorption in the region of 950 nm. Thus the Raman intensity can be

controlled by exciting the PAni sample using a suitable wavelength to allow a uniform response of these doped and undoped components.

Raman spectroscopy has also been used to study changes in the doping of PAni. Pereira de Silva et al. [232] presented changes in the spectra of PAni after secondary doping. They observed a decrease in bands corresponding to quinoid units after PAni was exposed to m-cresol. They also observed merging of the two radical cation bands and evolution of a shoulder at ~1370 cm^{-1} which corresponded to an increase in the free-charge carriers along the polymer backbone. Further to this, Lindfors and Ivaska [233] studied PAni using laser excitation wavelengths of 514, 633 and 780 nm whilst increasing and decreasing the pH between 2 and 9. They were able to measure the pH of buffer solutions by observing changes in the Raman band corresponding to C=N stretch at 1439 cm^{-1}. In addition Crochet et al. [228] observed decreases in the intensity of C=N stretch at 1480 cm^{-1} and C-N stretch at 1220 cm^{-1}. They also reported the appearance of a band at 1332 cm^{-1} corresponding to the presence of the radical cation species during doping of emeraldine base.

Job et al. [225] observed chemical interaction between PAni and latex whereby the latex was assisting the doping of PAni films. This doping was reported to be both primary and secondary. The primary doping was evident by the presence of the radical cation band at 1332 cm^{-1}, whilst the intensity of the band at 1602 cm^{-1} increased significantly, similar to the observations of Pereira de Silva et al. [232]. No hypothesis was offered as to why the latex assists the primary and secondary doping of the PAni due to a lack of detail of the structure of the latex [225].

4.1.2 Tensile Testing

Tensile testing provides a measure of the resistance of a material to applied stress [234], and this can provide information on the ability of that material to withstand breakage or deformation. The application of stress leads to the elongation or compression of the material, and the deformation per unit length is termed strain [234, 235].

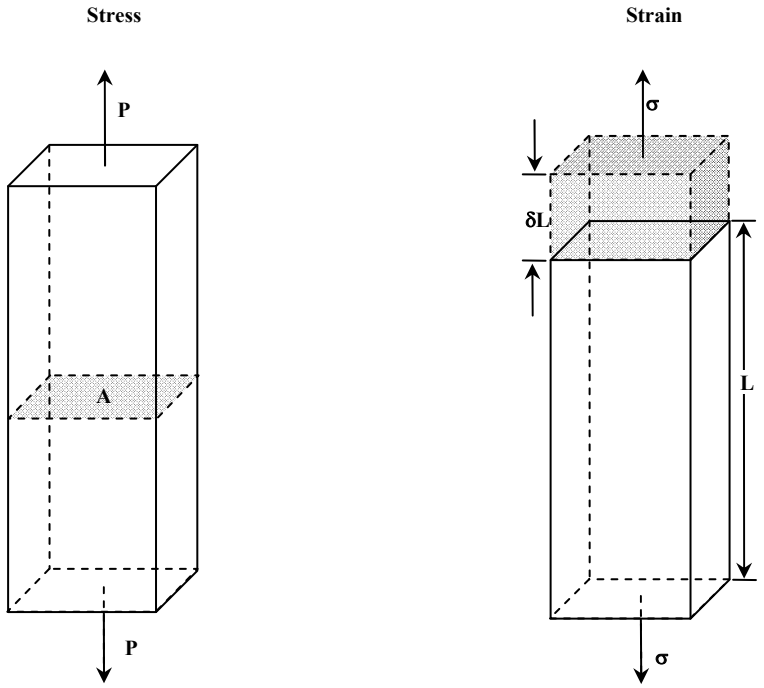

Figure 4.1 Stress and strain in tensile testing [235]

According to Gordon [235], Augustin Cauchy defined stress as 'the load per unit area of the cross section at a particular point in a material'. That is, stress is the applied load distributed over an area within a segment of a sample, at any cross-sectional area within that sample. This provides a direct measure of stress provided that the load distributed through this cross-sectional area is uniform [236]. This is presented in Figure 4.1. Stress (σ) here is the load (P) on a cross-sectional area (A) where stress can be tensile or compressive, and is defined as.

$$\sigma = P/A$$

Equation 4.1 Stress of a material [235, 236]

This assumes that the force applied is uniform over the sample and the sample itself is uniform in its cross-sectional area. If this is not the case then a stress concentration factor can be used to determine the maximum stress [237].

The strain (ε), often expressed as a percentage, is the ratio between the change in the length of a sample when exposed to stress, compared with the original length.

$$\varepsilon = \delta L/L$$

Equation 4.2 Strain of a material [235]

From Figure 4.1 the original length (L) alters with the application of stress (σ), leading to the change in length (δL). As the stress can be tensile or compressive, strain can increase with elongation or decrease with contraction. In addition the strain of an object can change with temperature, and is referred to as thermal stress [235-237].

Under elastic deformation, stress is proportional to strain with the constant of proportionality known as the elastic modulus (E), also referred to as Young's modulus or the tensile modulus [236, 237]. This relationship is presented in Figure 4.2.

The limit of proportionality is the limit of the elastic response, and leads on to a plastic response where the material remains deformed and does not revert to its original state. After this is a small yield point section where the strain increases without any increase in load, followed by increases in strain with applied stress until the maximum tensile

strength is reached. Once the maximum tensile strength has been determined the material begins to fail and eventually fractures at the breaking point [237].

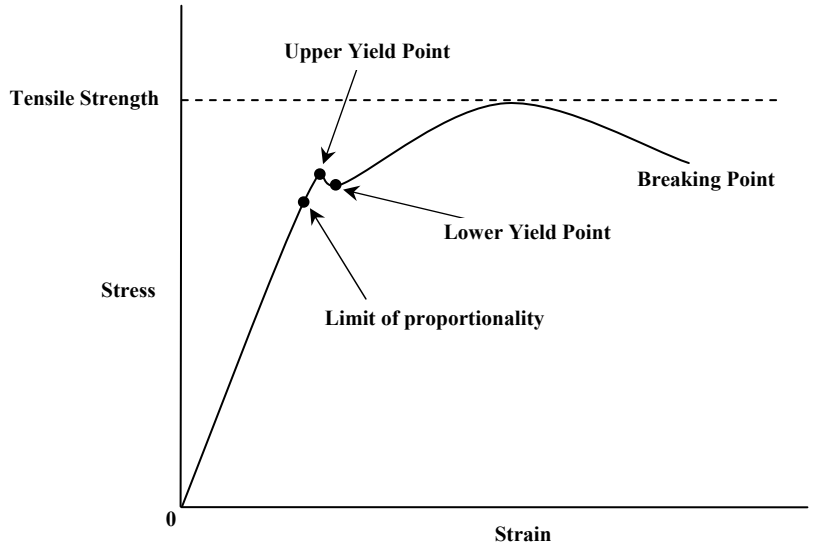

Figure 4.2 Stress-strain graph of mild steel[237]

$$E = \sigma/\varepsilon$$

Equation 4.3 Young's Modulus [235-237]

From a stress/strain diagram Young's Modulus is directly determined by the slope of the linear segment of the graph. This modulus provides an indication of the stiffness, or rigidity, of the material. The greater the value of E the stiffer the material, whilst a lower value of E indicates a flexible material [235]. It is important to note that the strength of a material is the force required to fracture that material [236], and depends on the bonding of the atoms [238]. Covalent bonding of diamond leads to an elastic modulus of 1200 GPa. whilst metallic materials have a modulus between 80-250 GPa. Steel for example has a modulus of 207 GPa. Polymers possess covalent bonding and van der Waals attractions, with the modulus dependent on both the original material and their treatment [236]. Processing of materials to form different structures can yield

increases in the strength of the material. For example, the tensile strength of bulk glass is roughly 170 MPa; however glass in fibrous formation is as much as 17 times that of the bulk form and this can be increased further with additional processing [236].

Thermoplastics often exhibit relatively low tensile strength, however the observed breaking strain can be quite high, whilst thermosetting plastics are relatively strong but brittle [236]. Again these properties depend on the method of manufacture and also the reinforcement of the material, along with the properties of the polymer itself. For example, many polymers exhibit changes when exposed to extreme temperatures. Low temperatures may lead to the glass transition where the material becomes brittle. Alternatively, higher temperatures may lead to the deformation of the polymer to become a viscous liquid [234].

The crystallinity of polymers also plays a role in their mechanical properties. Polymers may possess crystalline structures, termed crystallites, where the polymer chains may be organised into highly regular geometric forms. However, this depends on the structure of the polymer chains and the interaction of these chains with one another. For example polyethylene (PE) possesses linear polymer chains that can organise to form a lattice type structure and achieve up to 80% crystallinity. PVC possesses less crystallinity as the chain has large Cl groups along its length, whilst polymethylmethacrylate (PMMA) consists of lumpy side chains that inhibit crystallisation. In general, the more complex the chain structure of the polymer, the less chance that it will possess crystalline areas. These crystalline areas reduce the viscoelastic effects in the polymer, thus producing a more brittle material with higher strength [234].

In addition to the crystallinity of polymers, amorphous regions of polymer contribute to their mechanical properties. Felbeck and Atkins [234] offered an analogy for mechanical behaviour for long chain polymers based on tangled 'string' and 'spaghetti' with no specific orientation. For the string analogy, the mechanical behaviour of the polymer depends on the viscoelastic behaviour where the polymer may be stretched until the material becomes stiff. After this point it is necessary to break some string to continue extension of the sample. The spaghetti analogy accounts for the friction between the entangled polymer chains which leads to an increase in the mechanical strength. The longer the polymer chain length, the greater the friction. In the presence of cross-linking of the polymer chains the spaghetti reverts to the string analogy [234].

This is not too dissimilar to the theories reviewed by Nissan and Battern [239]. They reviewed the molecular and structural theories as they apply to paper. In terms of the molecular theory, Young's modulus is derived from the number density and hydrogen bond characteristics of the paper, while the structural theory suggest Young's modulus is derived from both the modulus of the fibres, and their spatial distribution. Nissan and Battern suggest that the two theories converge on an 'ideal' value for paper; however, both theories have their limitation under different conditions.

4.1.3 Tensile Testing of Electrospun Fibres

Kim and Reneker [113] studied the use of polybenzimidazole (PBI) electrospun fibres as a support network in both an epoxy matrix and in a styrene-butadiene rubber (SBR) matrix. Sheets of electrospun PBI fibres were prepared and placed into a compression mould to which epoxy resin was added and the film cured. In the case of the SBR film the fibres were added as chopped segments and then mixed throughout the matrix followed by curing. The fracture toughness and fracture energy of the PBI and epoxy

films increased significantly with increasing fibre content. For 3% w/w fibre content the modulus increased from 4.25 GPa to 5.27 GPa in comparison with the epoxy compound without fibres, while the SBR composite produced a ten-fold increase in Young's Modulus from 1.8 MPa to 19.6 MPa with the addition of the fibres.

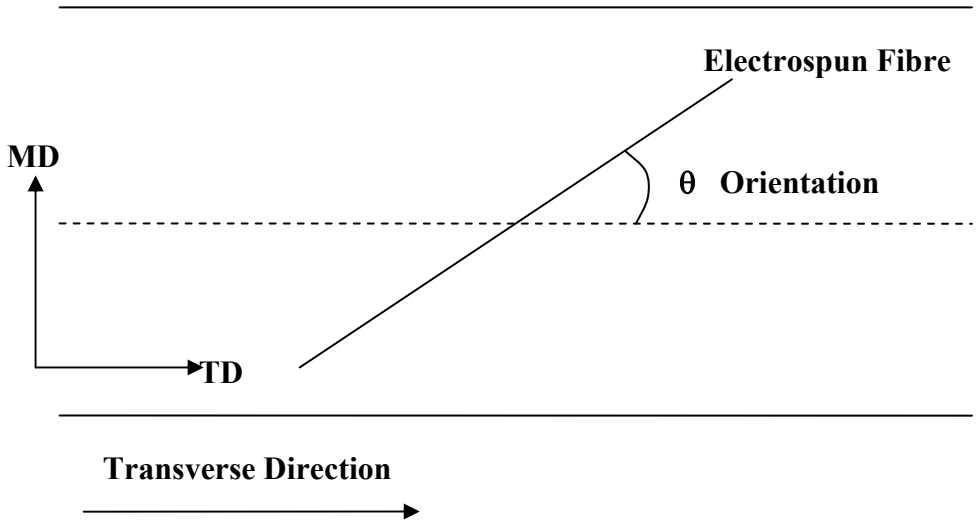

Figure 4.3 Definition of the fibre orientation angle [142]

Lee et al. [142] observed changes in the stress-strain characteristics with changes in the electrospinning procedure. They electrospun samples of PVC using a rotating collector, but also with a collector that moved left and right relative to the fibre jet. This allowed the tensile strength to be determined for different fibre orientations based on the transverse direction (TD) and mechanical direction (MD). The fibre orientation angle was determined with respect to the TD, and is presented in Figure 4.3. They observed a slight increase in the tensile strength of the fibres orientated towards the TD with increasing movement of the target left to right compared with rotation. The opposite was observed with an increase in the rotation of the collection target with the fibres exhibiting a higher tensile strength for the machine direction. The strain of the fibres also differed for the two fibre directions and alterations to the fibre collection. The

strain for the MD was marginally higher than the TD with increased left-right movement, however again this was reversed when the rotation of the collection target was increased. Thus simple changes in the collection of a sample can yield increases in the mechanical strength of the fibre samples which may be useful to specific applications [142].

In a later study, Lee et al. [84] analysed tensile strength with changes in the composition of the fibres. Polyurethane (PU) fibres exhibited significant elongation during testing, up to 1,210% whilst PVC fibres gave only 153%. The combination of PVC and PU on the other hand produced fibres with greater strength but less elongation. Young's modulus of electrospun PVC fibres recorded a value of 3.75 MPa, compared to the PVC (25%) / PU (75%) modulus of 8.94 MPa and the PVC (50%) / PU (50%) modulus of 11.80 MPa. Further increases in PU composition led to a significant decrease in strength of the fibres.

This initial increase in strength was a result of the connections between the fibres. PU had a larger degree of point-bonded fibre connections compared with PVC. These connections increase the elasticity of the mat as a whole up to breaking point. As PVC does not have these inter-fibre connections the strength came from friction and entanglement of the fibres. By combing the two polymers the properties combined whereby the PU offered elasticity and structural integrity through the point-bonded connections and the PVC utilised these connections as physical support structures to increase the entanglement of PVC [84].

4.2 Preparation of Samples

4.2.1 Polymer Solution Preparation

The appropriate amount of PVC or PAN was dissolved in THF/DMF or DMSO/DMF, respectively, and magnetically stirred overnight to prepare a homogeneous polymer solution.

4.2.2 PAni/Polymer Solution Preparation

All PAni/polymer solutions utilised 1% PAni due to previously recognised limitations in its solubility [52, 58, 78, 129, 145]. Camphorsulfonic acid (CSA) was weighed into a scintillation vial, and suitable volumes of solvent were added. After CSA had dissolved, PAni was added slowly and stirred on a magnetic stirrer until dissolved. Following this the commodity plastic was added and mechanically stirred until dissolved.

4.2.3 Other Polymer Solutions

If other additives were required, such as quaternary ammonium salts (QAS), this material was weighed and added to the solutions prior to the addition of PAni. It is important to note that a small amount of THF was added to assist in the dissolution of the TDAB in PAni/PAN blends prior to the addition of PAni due to insolubility of TDAB in DMSO/DMF.

In the case of MWNT solutions, MWNT (0.5%) was weighed and added to a scintillation vial, followed by the addition of the solvents. The MWNT were dispersed by sonification, after which the support polymers were added to the solution and left to dissolve by magnetic stirring.

Further details of solution preparation can be found in Section 2.3 Preparation of Samples.

4.2.4 Electrospun Fibres

Electrospun fibres were manufactured by withdrawing 100 uL of the pre-prepared polymer solutions by Eppendorf® pipette, and placing the pipette tip on a length of platinum wire attached to a coaxial cable. High potential was applied, leading to the fabrication of electrospun fibres that were collected on rotating gold-coated Mylar® targets. This process was repeated twice more for a total volume of 300 uL of polymer solution.

Further details of electrospinning can be found in Section 3.2 Preparation of Samples

4.2.5 Analysis of Samples – Raman Spectroscopy

Electrospun fibre samples were analysed by a Jobin Yvon Horiba HR800 Raman spectrometer with an integrated microscope using a 785 nm laser utilising a 300-line/mm grating, 1100 μm hole, 400 μm slit, a laser focus point of ~2μm in diameter and calibrated with SiO_2 prior to sample analysis. Analysis time was 10 seconds repeated 10 times at 50X magnification. Raman mapping of select samples was also carried out by analysing a segment of electrospun mat at 2 μm x 2 μm steps over the electrospun samples utilising the same settings.

All assignments are based on Raman spectroscopy results from literature unless otherwise state. In the case that IR assignments are employed, the notation of (IR) in the assignment tables will be present.

4.2.6 Analysis of Samples – Tensile Testing

Electrospun fibres were prepared as noted above, carefully removed from the Au/Mylar backing and were analysed on a Q800 Dynamic Mechanical Analysis (DMA, TA Instruments) utilising the film tension clamp. It is important to note that the samples were not fashioned into dumbbell shapes due to their size and fragility, and that they were roughly rectangular with dimensions of ~8 mm x ~5 mm. The thicknesses of the samples were measured using a digital micrometer calliper.

4.3 Results and Discussion – Raman Spectroscopy

4.3.1 PVC Powder

The Raman spectrum of untreated PVC powder (M_W = 63 000, Sigma-Aldrich) is presented in Figure 4.4 with peak assignments given in Table 4.1. The two peaks obtained at 640 cm^{-1} and 699 cm^{-1} were characteristic of C-Cl stretch associated with PVC, but according to Voyiatzis et al. [240], these two peaks, in total, consist of eight to ten Lorentzian peaks in the range of 600-700 cm^{-1}, corresponding to different conformations of the PVC molecule.

Wavenumber (cm^{-1})	Assignments	References
640	C-Cl Stretch	[240-246]
699	C-Cl Stretch	[240-246]
1111	C-C Stretch	[240, 243, 244, 247-250]
1184	Unassigned	[243, 244]
1265	Unassigned	[243]
1328	CH_2 twist –CH_2 wag	[240, 243]
1386	Unassigned	[251]
1434	C-H Bend	[240, 243]
1659	Possible Plasticiser	[249]
1701	Possible Plasticiser	[249]
1765	Possible Plasticiser	[249]

Table 4.1 Peak assignments for PVC powder

Peaks at 1184 cm^{-1}, 1265 cm^{-1} and 1386 cm^{-1} are all unassigned, but the first two bands were observed in spectra from Ellahi and Hester [243], and the second band was also observed in Liebman et al. [244], whilst the 1386 cm^{-1} peak was noted by Koenig and Druesedow [251].

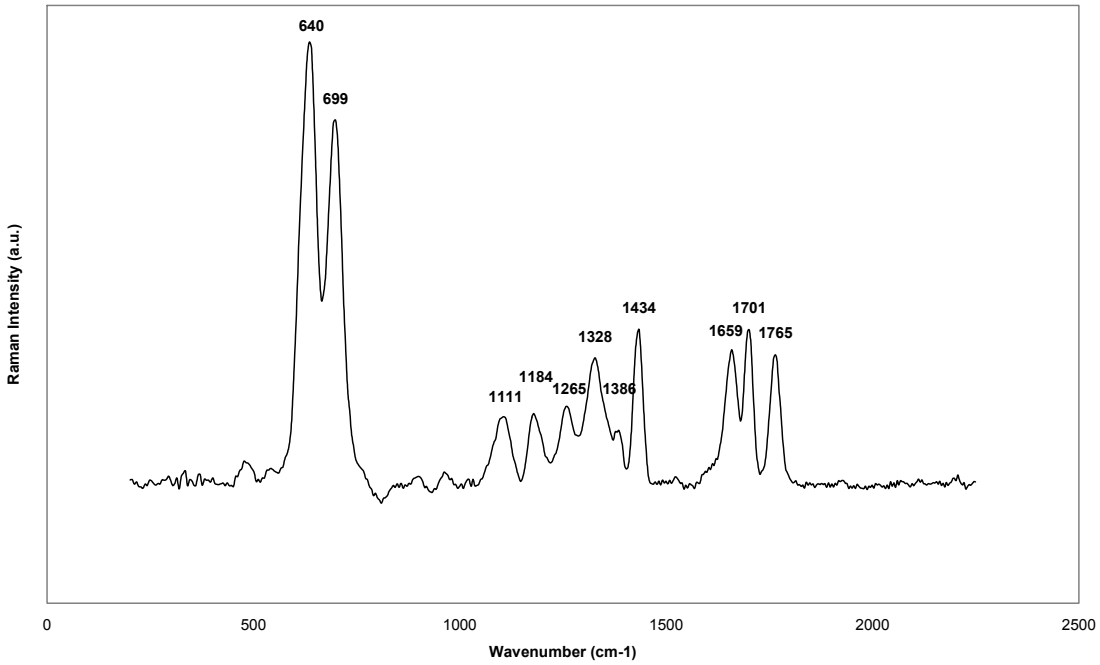

Figure 4.4 Raman spectrum of untreated PVC powder

The peak observed at 1434 cm^{-1} is a result of C-H bend [240, 243], whilst ambiguity exists for the three bands at 1659 cm^{-1}, 1701 cm^{-1} and 1765 cm^{-1}. These last three peaks have not been identified, but may correspond to C=C vibrations, depending on the structure of the alkyl groups [252]. Williams and Gerrard [249] indicate that these peaks may be a result of plasticiser in the sample. They analysed a reference sample not exhibiting these peaks, whilst a PVC resin did exhibit peaks in the 1500 cm^{-1} to 1700 cm^{-1} range. As the certificate of analysis from Sigma-Aldrich for the PVC used in the current work did not indicate any plasticiser in the sample, and an IR spectrum from

Sigma-Aldrich did contain these peaks, it is unlikely that these bands correspond to plasticiser.

4.3.2 PAN Powder

The Raman spectrum of PAN is shown in Figure 4.5 and peak assignments presented in Table 4.2. As few Raman spectroscopy studies have been reported, some assignments are based on IR studies whilst some bands are not assigned.

Wavenumber (cm^{-1})	Assignments	References
431	C=N Bend (IR)	[253]
709	C-CN Wag + C=N Bend (IR)	[253]
834	CH_2 Rock (IR)	[254, 255]
1088	Possible C-CN Bend (IR) or CH_2 Twist (IR)	[253, 256]
1106	CH_3 Rock (IR)	[256]
1124	CH_3 Rock (IR)	[256]
1261	C-H Wag (IR) or C-H Rock + CH_2 Wag (IR)	[253, 256]
1324	CH_2 Wag + CH Rock	[256]
1386	CH_2 Wag or CH Bend (IR)	[256, 257]
1456	CH_3 + CH_2 Bend	[255, 256]
1663	C=N (IR)	[258, 259]
1702	C=O From Polymerisation (IR) or C=N	[258, 259]
1765	Possible Impurities	[253]

Table 4.2 Peak assignments for PAN powder

Whilst the band observed at 709 cm^{-1} has been as assigned to C-CN wag plus C=N bend, Mathieu et al. [256] stated that peaks between 1050 – 650 cm^{-1} may correspond to C-C stretch. The band observed at 1088 cm^{-1} may be a product of CH_2 twist in line with the observations of Mathieu et al. [256], however Liang and Kimm [253] indicates that this is a result of C-CN bend . The band observed at 1261 cm^{-1} is assigned to CH_2 wag and C-H rock, but may possibly be C-H wag [253, 256].

The peaks observed at 1663 cm^{-1} and 1702 cm^{-1} respectively are reported to correspond to C=N [259] and C=O absorption. This C=O presence has been reported as the result of the polymerisation of PAN, specifically the polymerisation initiator [258]. The last peak at 1765 cm^{-1} is not identified in literature and can not be assigned; however, Beevers [255] states the all polyacrylonitriles have several IR absorption peaks within the 1500-1800cm^{-1} range that vary in intensity depending on the initial polymerisation and thermal treatment.

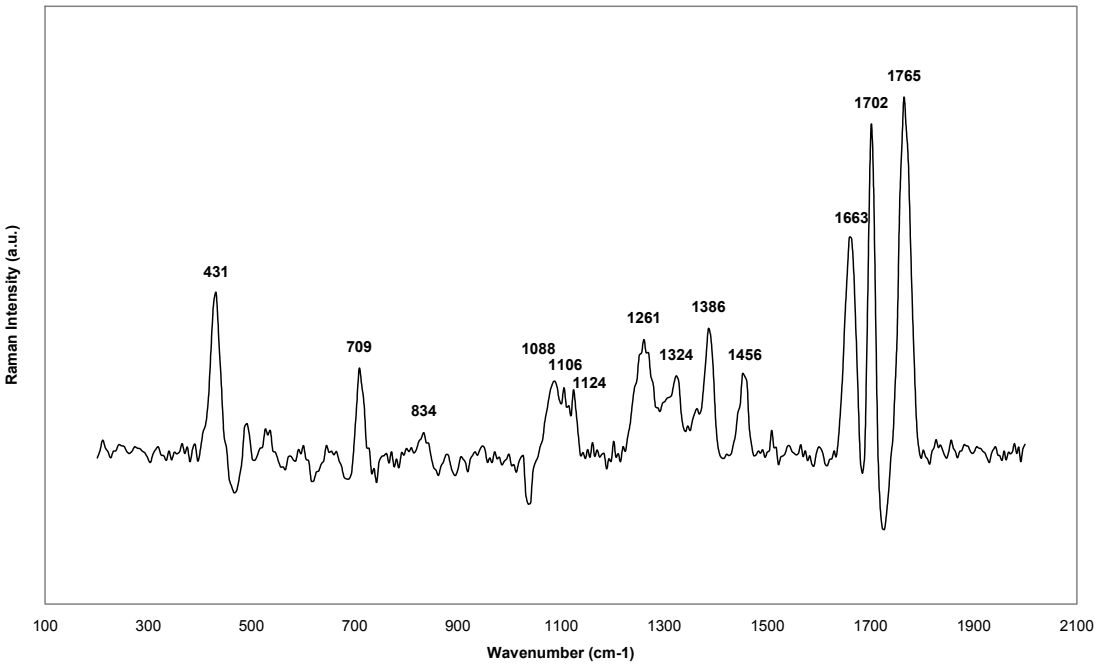

Figure 4.5 Raman spectrum of untreated PAN powder

4.3.3 Un-doped PAni Powder

It is necessary to confirm the synthesis of emeraldine base for use in preparation of electrospun fibres containing PAni. Thus Raman spectroscopy of PAni powder in the form of emeraldine base is presented in Figure 4.6 and assignments given in Table 4.3.

According to Cochet et al. [227] and Liu et al. [224] the first band observed at 416 cm^{-1} corresponds to an out-of-plane deformation for the benzenoid and quinoid rings. However Job et al. [225] adds that this may be also due to C-H wag.

The band at 1220 cm^{-1} corresponds to C-N stretch vibrations of the benzenoid groups, but it is also possible that there is some contribution from $C\text{-}N^{+\bullet}$ semi-quinone radicals as the shift lies between those observed by Lindfors and Ivaska for C-N and $C\text{-}N^{+\bullet}$ bands [233]. Thus it is possible the PAni has not been fully de-doped after synthesis and may consist of some doped components.

Wavenumber (cm^{-1})	Assignments	References
416	Ring Deformation or C-H Wag (Q)	[224, 225, 227]
532	Ring Deformation (Q)	[225, 227]
752	Ring Deformation (Q)	[223-225, 227, 233]
781	Ring Deformation (Q)	[223, 225, 227, 233, 260]
844	C-H Wag	[227]
1166	C-H Bend (Q)	[223-225, 233, 260]
1220	C-N Stretch (B)	[223, 225, 228, 233, 260]
1482	C=N Stretch (Q) and C=C Stretch (Q)	[223-225, 228, 233, 260]
1591	C=C Stretch	[223-225, 233]

Table 4.3 Peak assignments of undoped PAni powder; (B) - Benzenoid; (Q) - Quinoid

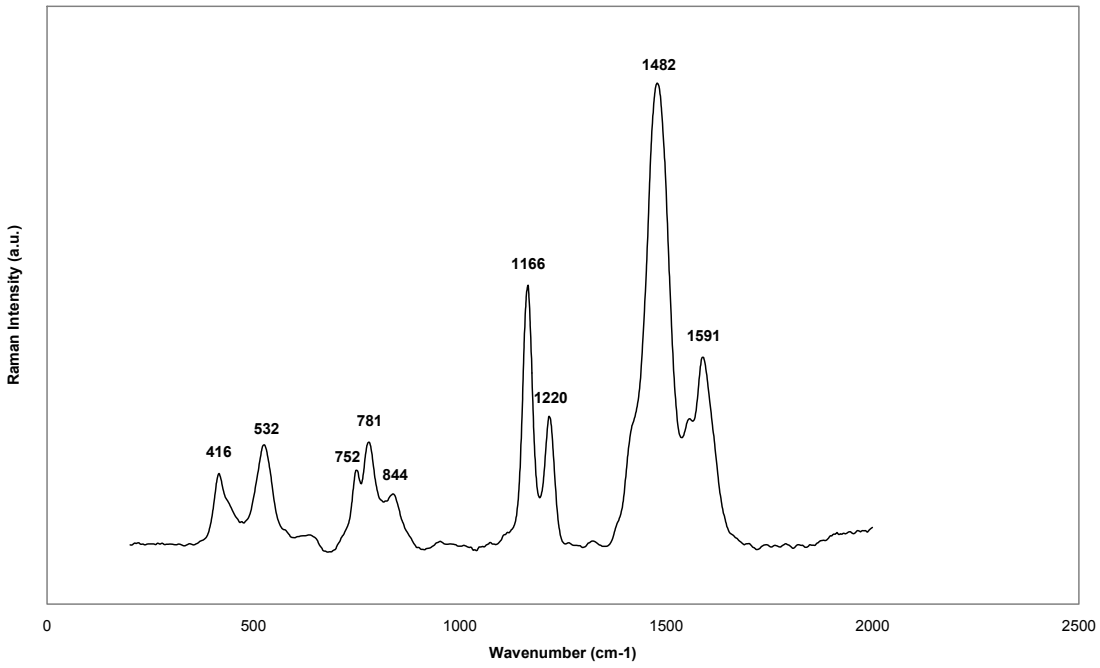

Figure 4.6 Raman spectrum of undoped PAni powder

4.3.4 PAni/PVC Electrospun Fibres

It is necessary to identify and characterise the components of doped PAni to ensure that doping of the emeraldine base has occurred and that electrospinning has no noticeable effect on the doped state of the fibres.

An overlay of Raman spectra of electrospun PAni 1% PVC 10% is given in Figure 4.7 with assignments provided in Table 4.4. It was expected that combining both PAni and PVC would lead to a superimposition of the spectra with characteristics of both compounds evident. However, the intensity of the unprocessed PVC powder was significantly lower than PAni, and PAni exhibited some degree of fluorescence during analysis. This lower intensity can be seen more clearly in Figure 4.8 which is the overlay of undoped, unprocessed PAni, and unprocessed PVC from Figures 4.6 and 4.4 respectively.

Wavenumber (cm^{-1})	Assignments	References
400	Ring Deformation (B) or C-H Wag (Q)	[224, 225, 228]
517	C-N-C Torsion	[224, 228]
586	Amine Deformation (B)	[224, 228]
659	Ring Deformation (B)	[224, 225, 228]
710	C-C Ring Deformation (B)	[224, 225, 228, 260]
812	C-H Deformation (Q)	[224, 225, 228]
876	Ring Deformation (B)	[224, 225, 228, 233, 260]
1171	C-H Bend (B)	[224, 225, 228, 260, 261]
1252	C-N Stretch (B) or C-H Bend (B)	[224, 228, 260, 261]
1320	$C\text{-}N^{+\bullet}$ Stretch	[225, 232, 233, 260-262]
1342	$C\text{-}N^{+\bullet}$ Stretch	[224, 228, 232, 260, 261]
1488	C=C Stretch (Q) + C=N Stretch (Q)	[224, 225, 232, 233]
1512	N-H Bend	[224, 225]
1582	C=C Stretch (Q)	[224, 228, 232, 233, 260]

Table 4.4 Peak assignments for fibres electrospun from PAni 1% PVC 10% in THF/DMF; (B) - Benzenoid; (Q) - Quinoid

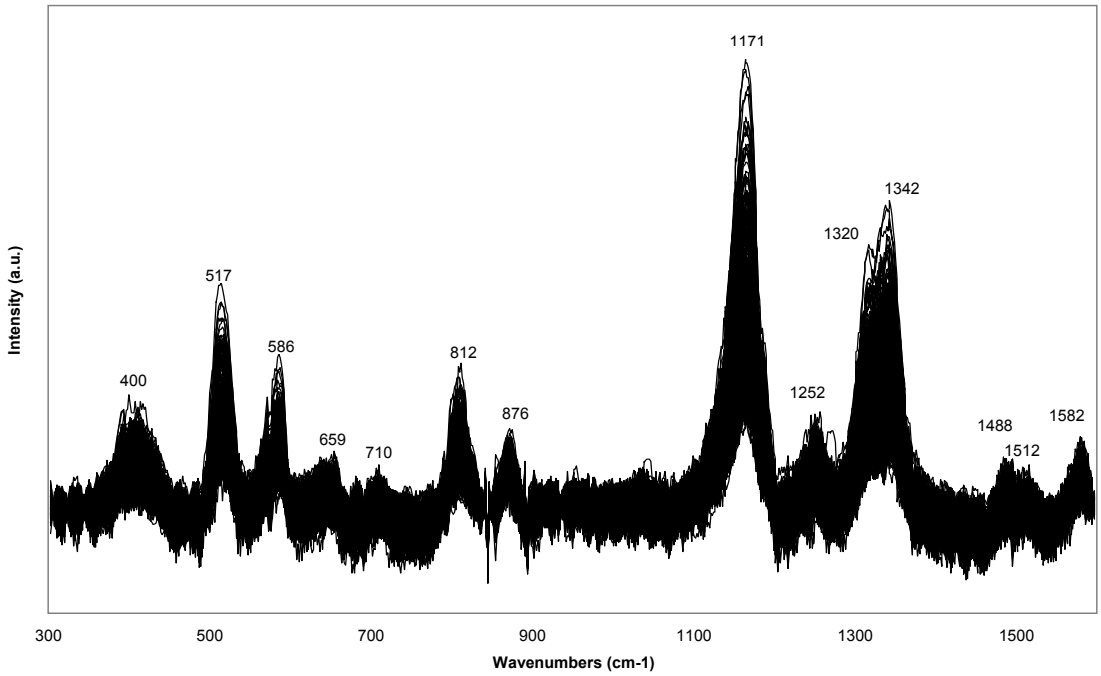

Figure 4.7 Overlay of 456 Raman spectra of a 48 µm x 38 µm segment of fibres electrospun from PAni 1% PVC 10% in THF/DMF

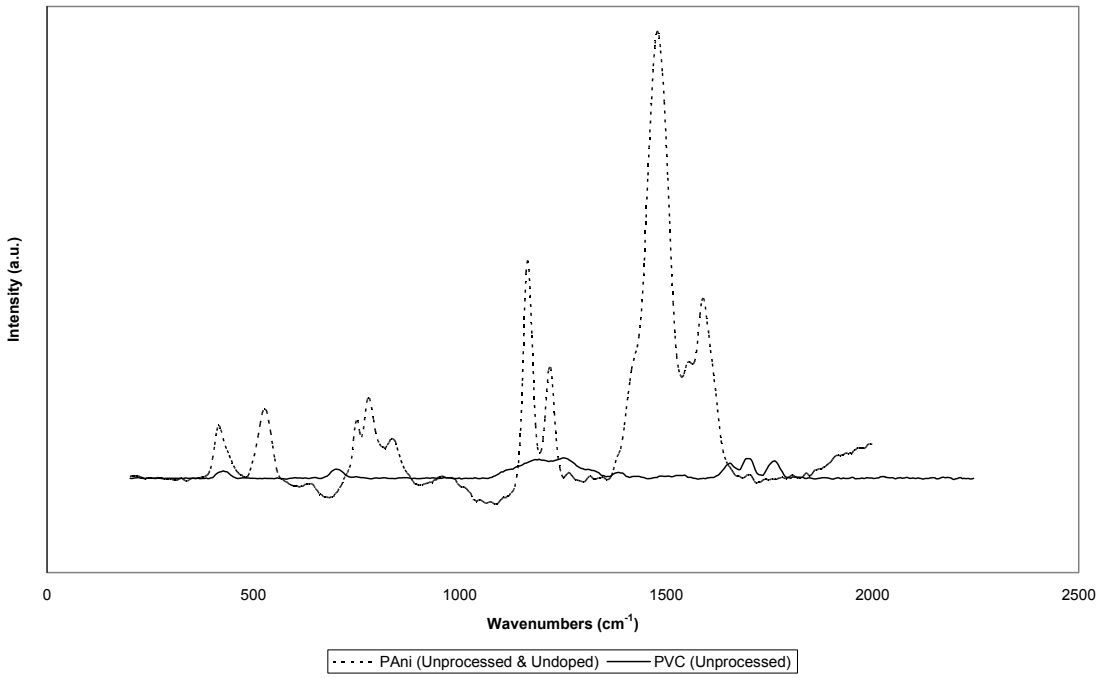

Figure 4.8 Overlay of undoped/unprocessed PAni and unprocessed PVC

The most significant peak observed in the spectra occurs at 1171 cm^{-1} and is a product of in-plane C-H bend on the benzenoid units [261]. Undoped PAni also exhibited this peak, however it was assigned to C-H bend of the quinoid units. Pereira da Silva et al. [261] associates this shift with the secondary doping of PAni. As mentioned in Section 4.1.2, secondary doping is associated with a change in conformation of PAni, and in turn an increase in free-charge carriers, leading to a significant increase in PAni conductivity.

In-plane stretch of C-N on the benzenoid group is responsible for the small, broad band observed at 1252 cm^{-1}, however there may be an overlap with the peak assigned by Baibarac et al. [260] at ~1260 cm^{-1} assigned to C-H bend in the benzenoid group.
The two peaks observed at 1320 cm^{-1} and 1342 cm^{-1} both correspond to characteristic stretch of the nitrogen radical cation associated with primary doped PAni [232]. In the

case of secondary doping of PAni these two separate peaks would be expected to unite into a single band and for a shoulder to evolve at ~1380 cm^{-1} [232]. It follows from this that it is likely that PAni was only primary doped in these fibres.

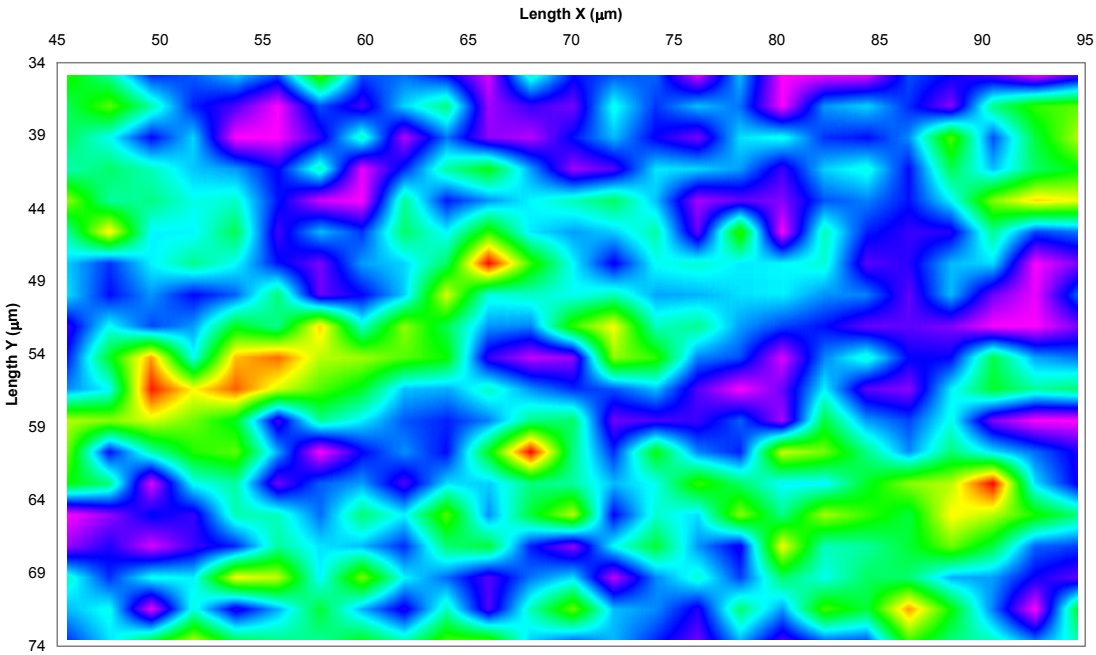

Figure 4.9 PAni dispersion map of fibres electrospun from PAni 1% PVC 10% in THF/DM; bands 1100-1400 cm^{-1}

Based on Lindfors and Ivaska [233] the peak at 1488 cm^{-1} has been assigned to C=C and C=N stretch, and this peak should decrease with doping [228], as has been the case compared to the Raman spectrum of emeraldine base in Figure 4.6. The last peak observed at 1582 cm^{-1} was also assigned to C=C stretch of the quinoid group [233]. It has shifted to a lower wavenumber noticeably compared with the undoped PAni and has also decreased in intensity relative to other peaks, similar to the 1488 cm^{-1} band.

By overlaying Raman spectra a segment of electrospun fibre samples, the uniformity of the chemical composition can be estimated. From Figure 4.7 the overlay of spectra shows that doped PAni is consistently present in the sample with good agreement in the

peaks. Using these spectra a dispersion map can be created to provide a more accurate measure of the dispersion of PAni throughout the fibre mat, this is given in Figure 4.9. The areas of high PAni concentration correspond to areas where there are large green-yellow patches while low concentrations are denoted by blue-purple areas.

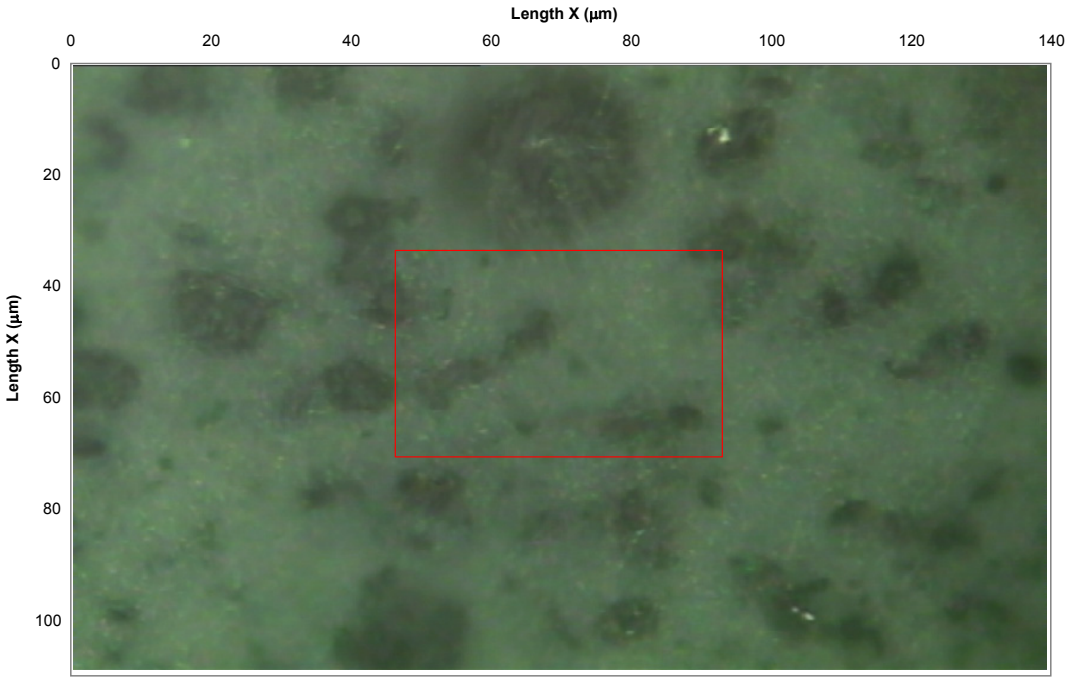

Figure 4.10 Optical micrograph of fibres electrospun from PAni1% PVC 10% in THF/DMF

The variation in colour in Figure 4.9 corresponds to electrospraying of large PAni particles onto the target substrate, also evident in Figure 4.10, and thus producing concentration discrepancies within the sampled area. This is supported from the particle analysis of PAni solutions in Section 2.7.2 where large particles were observed within the spinning solution. SEM analysis presented in Section 3.3.3 also indicated that electrospraying of the polymer solution occurred. However, these globules were smaller in size compared with the areas affected in the micrograph of PAni 1% PVC 10% fibres (Figure 4.10). As the samples used in SEM analysis and Raman sampling were

different, it indicates that the actual electrospinning process differed, either due to changes in the solution properties such as viscosity, surface tension and conductivity, or the process itself. If the solution composition did change it would be expected that this would have been slight and not have produced significantly different samples, based on the evidence from SEM analysis. Thus it appears that the electrospinning process itself has inconsistencies that could lead to significant variability in sample morphology, and hence chemistry.

Whilst there were particles of PAni present, the areas possessing only PAni/PVC fibres were relatively uniform in terms of PAni concentration. For example, the top of Figure 4.10 presents an area consisting of predominantly of electrospun PAni/PVC fibres. The corresponding Raman map in Figure 4.9 indicates that whilst there were areas of differing concentration of PAni, these were small. Thus, even though there were large particles PAni on the target, the PAni within the electrospun fibres was relatively evenly dispersed.

4.3.5 PAni/PAN Electrospun Fibres

The spectra of PAni 1% PAN 3% electrospun fibres were similar to PAni 1% PVC 10%, though it contained some obvious differences. Firstly it is important to note that a Raman map of PAni 1% PAN 3% electrospun fibres was not undertaken, however a spot analysis was carried out on two visibly different regions of the electrospun mat. The Raman spectra for these two spots are provided in Figure 4.11 with corresponding assignments in Table 4.5. The assignments in general were similar to those for the PAni 1% PVC 10% analysis. This was to be expected due to the significant influence of PAni and the small contribution of PAN to the Raman spectrum, similar to observations for

PAni and PVC. However, there were some notable differences, particularly wavenumber shifts for the majority of bands.

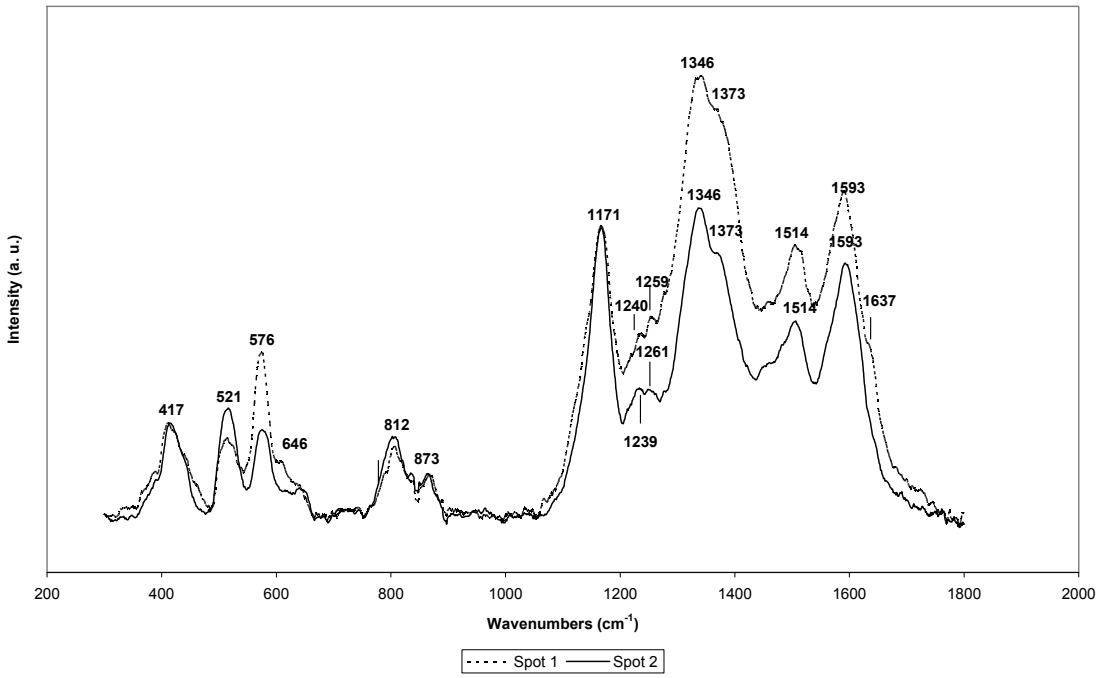

Figure 4.11 Overlayed Raman spectra of fibres electrospun from PAni 1% PAN 3% in DMSO/DMF

There is some ambiguity as to the assignments for the peaks at ~1240 cm^{-1} and ~1260 cm^{-1}. Baibarac et al. [260] assigns the 1240 cm^{-1} peak to C-N stretch whilst the 1260 cm^{-1} peak is assigned to C-H bend. However, other literature assigns the 1260 cm^{-1} peak as C-N stretch [223, 228].

A shoulder appears at 1373 cm^{-1} whilst the peaks associated with the radical cation between 1300 and 1350 cm^{-1} have coalesced into a single band at 1346 cm^{-1}. This shoulder was noted by Pereira da Silva et al. [232, 261] as being associated with the vibration of free charge carriers in the conducting form of PAni and conformational changes in PAni, that is, secondary doped PAni. This may be a result of the interaction

of PAni with the PAN backbone, due to the polarity of the nitrogen group located on the PAN chain as discussed in Section 2.4.1. These interactions may have altered the orientation of the PAni chain with respect to the support polymer, changed the PAni conformation, or possibly influenced the nitrogen cation. The CSA dopant would not be sufficient to secondary dope the PAni as other literature indicates that further treatment is required to induce secondary doping [225, 232, 261].

Wavenumber (cm^{-1})	Assignments	References
417	Ring Deformation or C-H Wag (Q)	[224, 225, 228]
521	C-N-C Torsion	[224, 228]
576	Amine Deformation (B)	[224, 228]
646	Ring Deformation (B)	[224, 225, 228]
812	C-H Deformation (Q)	[224, 225, 228]
873	Ring Deformation (B)	[224, 225, 228, 233, 260]
1171	C-H Bend (B)	[224, 225, 228, 260, 261]
1240 (S1) /1239 (S2)	C-N Stretch (B)	[222, 225, 233, 260, 263]
1260 (S1) /1259 (S2)	C-N Stretch (B) or C-H Bend (B)	[228, 260]
1346	$C\text{-}N^{+\bullet}$ Stretch	[224, 228, 232, 260, 261]
1373	Conformational Change	[225, 232, 261]
1514	N-H Bend	[224, 225]
1593	C=C Stretch (Q)	[224, 228, 232, 233, 260]
1637 (S2)	C-C Stretch (Q)	[228, 261]

Table 4.5 Peak assignments for fibres electrospun from PAni 1% PAN 3% in DMSO/DMF; (B) - Benzenoid; (Q) - Quinoid; (S1) - Spot 1; (S2) - Spot 2

The band observed at 1514 cm^{-1}, not observed in PAni/PVC, was assigned to N-H bend based on observations by Liu et al. [224], and is indicative of deprotonated quinoid units. The peak observed at 1593 cm^{-1}, and the shoulder at 1637 cm^{-1} for Spot 1 appears to correspond to C=C and C-C stretch respectively. According to Cochet et al. [228] there are two bands associated with C-C stretch between 1550-1650 cm^{-1} for primary doped PAni, but these becomes a single broad band after secondary doping. Once again there is a noticeable shift in the peak wavenumbers, most likely due to the effects of

PAN. This shoulder was also noted by Pereira da Silva et al. [261] and decreases in magnitude with the conversion of quinoid species to benzenoid species during secondary doping. Thus, this shoulder is evidence of primary doping in the electrospun fibres, but there was also evidence to suggest that there was some conformational change or secondary doping of PAni in the presence of PAN. It is quite possible as the area analysed by Raman is quite large (the laser is ~2um in diameter), and could contain a mixture of primary doped and secondary doped PAni.

4.3.6 PAni/PVC/TDAB Electrospun Fibres

The Raman spectra obtained for PAni 1% PVC 10% TDAB 0.5% (tetradodecylammonium bromide, a commercial nitrate ionophore) fibres were different to those obtained from PAni 1% PVC 10% sample. Although there are some significant similarities the peak assignments, the present of other peaks and shoulders, and shifts in peak show that they are different. Figure 4.12 presents the spot analysis of electrospun fibres of the former, with the assignments for the analysis given in Table 4.6.

As the spectra from the original PAni 1 % PVC 10% electrospun fibres were limited to 1600cm^{-1}, a band at 1622 cm^{-1} appears for the first time in PAni 1% PVC 10% TDAB 0.5% fibres, corresponding to C-C stretch of the quinoid units that was also reported for PAni 1% PAN 3% fibres at 1637 cm^{-1}. Otherwise the assignments compare well with those observed in the spectra of PAni 1% PAN 3% electrospun fibres.

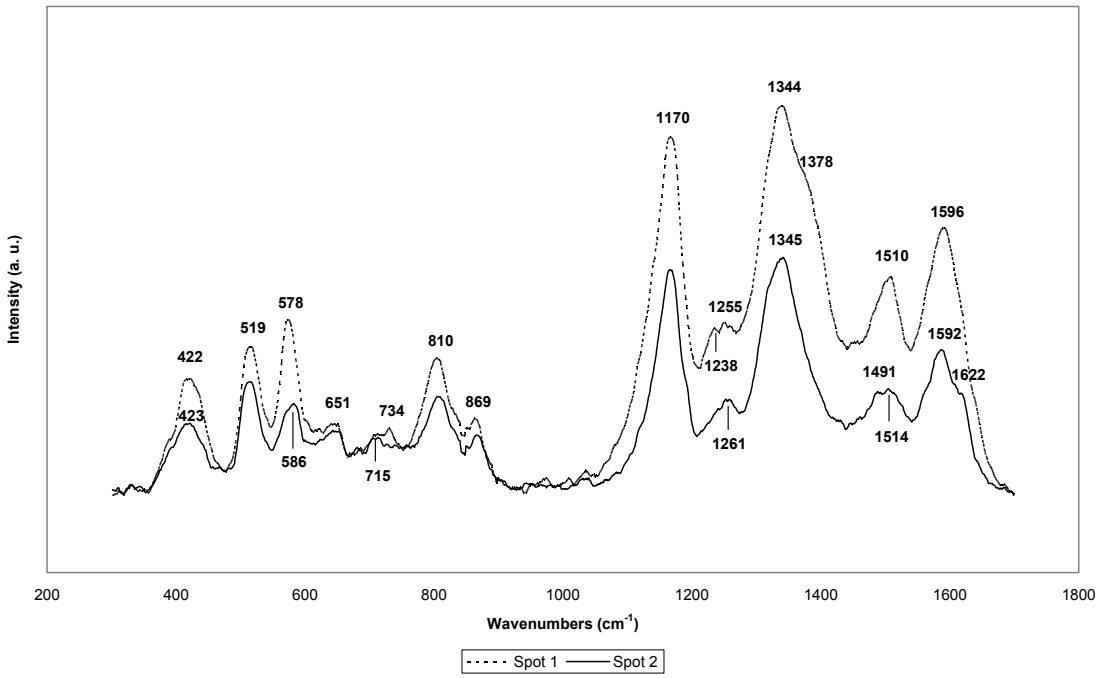

Figure 4.12 Overlayed Raman spectra of fibres electrospun from PAni 1% PVC 10% TDAB 0.5% in THF/DMF

Wavenumber (cm^{-1})	Assignments	References
422 / 423	Ring Deformation or C-H Wag (Q)	[224, 225, 228]
519	C-N-C Torsion	[224, 228]
578 / 586	Amine Deformation (B)	[224, 228]
651	Ring Deformation (B)	[224, 225, 228]
734 / 715	Ring Deformation (B)	[224, 225, 228]
810	C-H Deformation (Q)	[224, 225, 228]
869	Ring Deformation (B)	[224, 225, 228, 233, 260]
1170	C-H Bend (B)	[224, 225, 228, 260, 261]
1238 (S1) / 1241 (S2)	C-N Stretch (B)	[222, 225, 233, 260, 263]
1255 (S1) / 1261 (S2)	C-N Stretch (B) or C-H Bend	[228, 260]
1344 (S1) / 1345 (S2)	$C\text{-}N^{+\bullet}$ Stretch	[224, 228, 232, 260, 261]
1378 (S1)	Conformational Change	[225, 232, 261]
1491 (S2)	C=C Stretch (Q) + C=N Stretch (Q)	[224, 225, 232, 233]
1510 (S1) / 1514 (S2)	N-H Bend	[224, 225]
1596 (S1) / 1592 (S2)	C=C Stretch (Q)	[224, 228, 232, 233, 260]
1622 (S2)	C-C Stretch (Q)	[228, 261]

Table 4.6 Peak assignments for fibres electrospun from PAni 1% PVC 10% TDAB 0.5% in THF/DMF; (B) - Benzenoid; (Q) - Quinoid; (S1) - Spot 1; (S2) - Spot 2

An optical micrograph of the sample surface and the location of the sample points used for analysis are given in Figure 4.13. Whilst there was the electrospray of PAni, the resultant Raman spectra indicated relatively high concentrations of PAni within the fibrous mat, and not just in the particulate matter, indicating the PAni was dispersed through the electrospun fibres.

The relative difference between the two spots is small with both exhibiting the same bands and similar peak sizes apart from the 1378 cm^{-1} and 1510 cm^{-1} peaks and the evolution of a shoulder at 1622 cm^{-1} for Spot 2. It is possible that the filtering of the Raman response reduced the definition of these peaks, leading to the coalescence of these peaks, or that the large bands at 1345 cm^{-1} and 1510 cm^{-1} overlapped the bands associated with conformational change and C=N stretch of the quinoid groups, respectively. However, increasing the ionophore concentration shows this to be unlikely.

Changes in the ionophore concentration produced some similarities and differences in comparison with spectra and peak assignments for the PAni 1% PVC 10% TDAB 0.5% analysis. The spectra for PAni 1% PVC 10% TDAB 5% and PAni 1% PVC 10% TDAB 10% electrospun fibres are presented in Figure 4.14 and Figure 4.15, respectively.

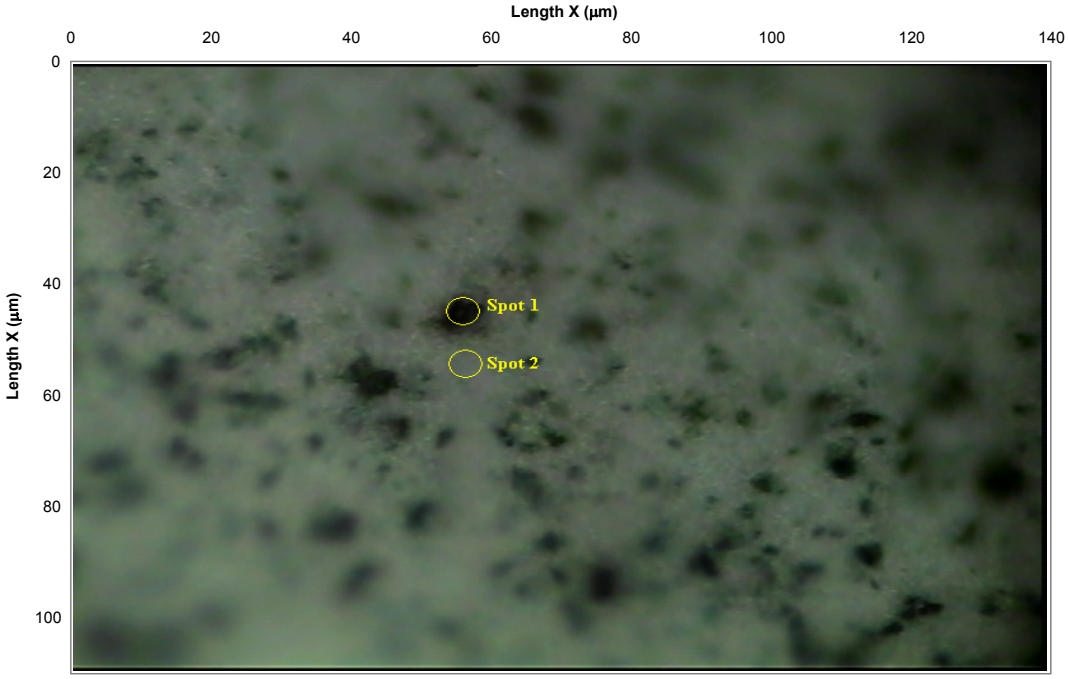

Figure 4.13 Optical micrograph of fibres electrospun from PAni 1% PVC 10% TDAB 0.5% in THF/DMF

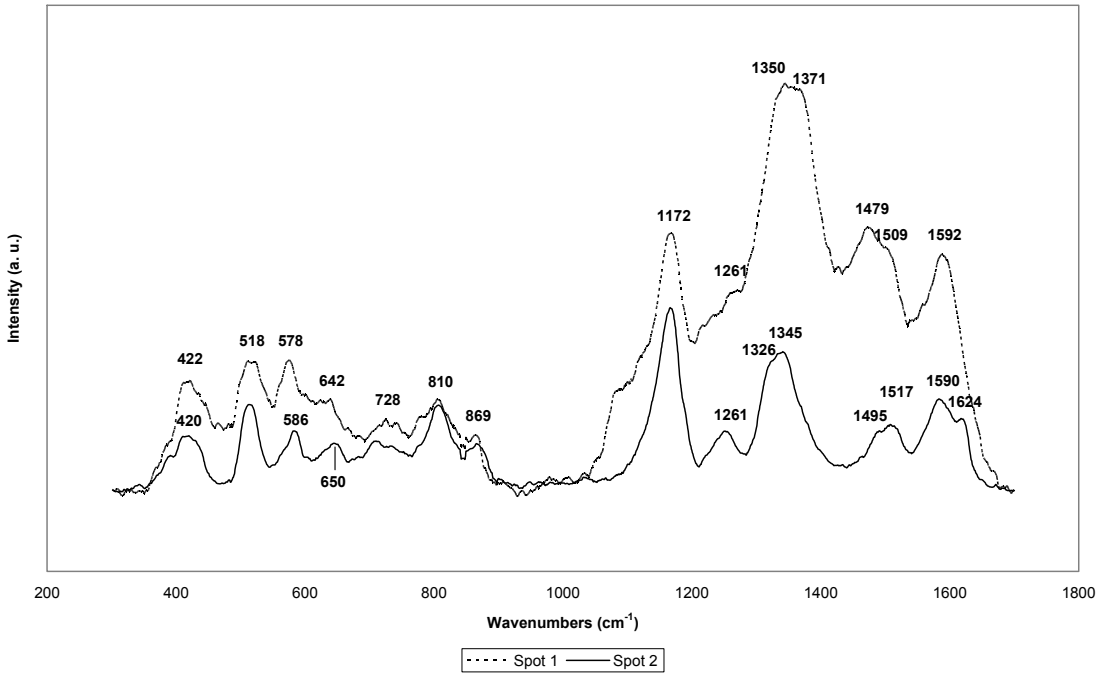

Figure 4.14 Overlayed Raman spectra of fibres electrospun from PAni 1% PVC 10% TDAB 5% in THF/DMF

The analysis of Spot 2 in Figure 4.14 indicated changes between 1300 cm^{-1} and 1380 cm^{-1} where the two peaks corresponding to the nitrogen radical cation could be clearly observed at 1326 and 1345 cm^{-1}. The peak associated with conformational changes and secondary doping of PAni at ~1370 cm^{-1}, observed in the PAni/PAN electrospun fibres, was not present in the PAni 1% PVC 10% TDAB 5% spectra of Spot 2. However, in Figure 4.15 there was some indication of a shoulder at 1372 cm^{-1}, and both PAni/PVC/TDAB 5% and 10% Raman spectra displayed a peak at ~1622 cm^{-1}, consistent with primary doped samples, but again the Spot 1 analyses for both samples did not.

It is unlikely electrospinning was responsible for the evolution of these bands. Fong and Reneker [65] stated that polymer chains are expected to be elongated and orientated axially during electrospinning as a change from random coil structure to uncoiled state occurs due to the strain from the electrospinning process, which may affect the PAni orientation. However, if the process of electrospinning were responsible for these new peaks it would be expected that the original PAni/PVC fibres would have exhibited similarities to this PAni/PVC/TDAB sample, and that the spectra would be consistent for all concentrations of TDAB.

It is, in fact, more likely that the ionophore interacted with, and had a direct influence on, individual properties of groups along the PAni chain, leading to the appearance of secondary doping, and that this influence increased with increasing TDAB concentration in the PAni/PVC fibres. If this is true it would indicate that the actual QAS was not dispersed through the electrospin fibres for it would be expected that both regions would exhibit the shoulder at ~1370 cm^{-1}.

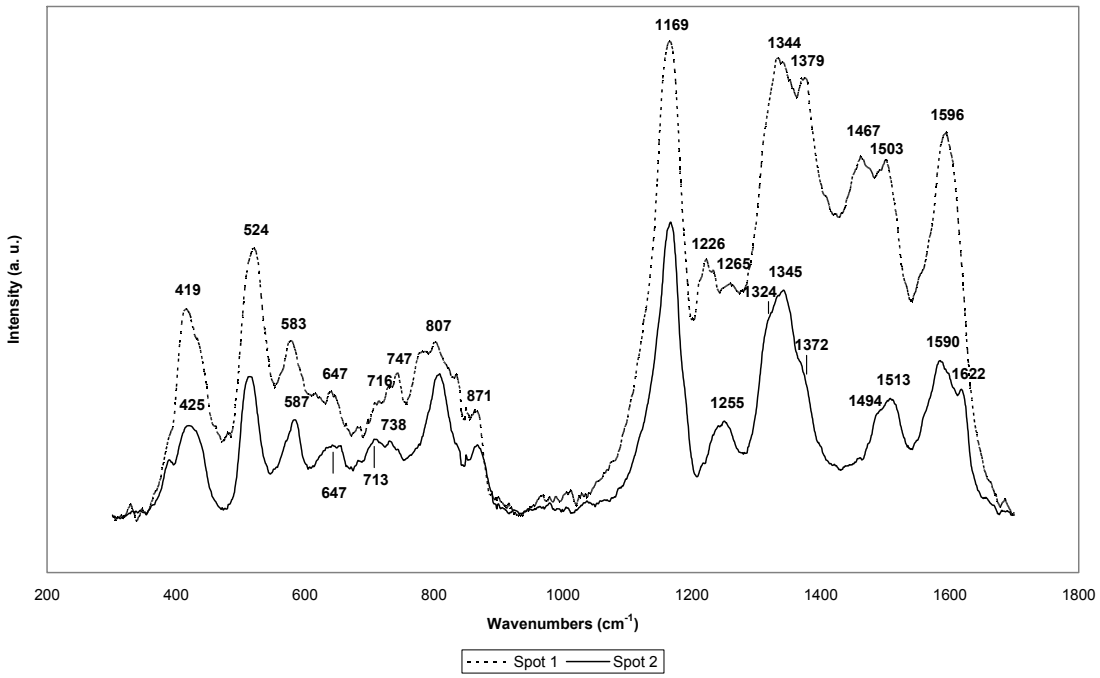

Figure 4.15 Overlayed Raman spectra of fibres electrospun from PAni 1% PVC 10% TDAB 10% in THF/DMF

As noted in Section 2.4.2, the viscosity of the PAni/PVC solutions increased significantly after the addition of TDAB. It was proposed that TDAB interacted with one or more of the components of the solution, leading to a change in the conformation of the polymer components. Thus it appears this was the case with TDAB uncoiling the PAni chain within the electrosprayed droplets, leading to the presence of the peak at ~1375 cm^{-1} associated with secondary doping, but not for the electrospun fibres. Instead the fibres exhibited characteristics of primary doping, indicating the electrospinning, whilst not assisting doping, instead restricted the degree of doping of PAni and its conformation within the electrospun fibres.

The morphology of the fibres appeared to change only slightly when compared to the PAni/PVC micrograph, producing a fibrous mat that exhibited less particulate PAni on the mat. This was supported by SEM observations in Section 3.3.9. This may indicate

that the TDAB actively assisted the dispersion of PAni throughout the solution and limited the electrospraying of the blend, possibly a result of the cationic charges influencing the surface tension and conductivity of the solution outlined in Chapter 2.

4.3.7 PAni/PAN/TDAB Electrospun Fibres

PAni/PAN/TDAB 0.5%, 5% and 10% electrospun fibres were analysed by Raman spectroscopy with the fibrous mat PAni 1% PAN 3% TDAB 10% mapped to observe the dispersion of PAni. Figure 4.16 is the Raman spectra of two distinct spots on the electrospun fibres of PAni 1% PAN 3% TDAB 0.5%, with the corresponding band assignments noted in Table 4.7.

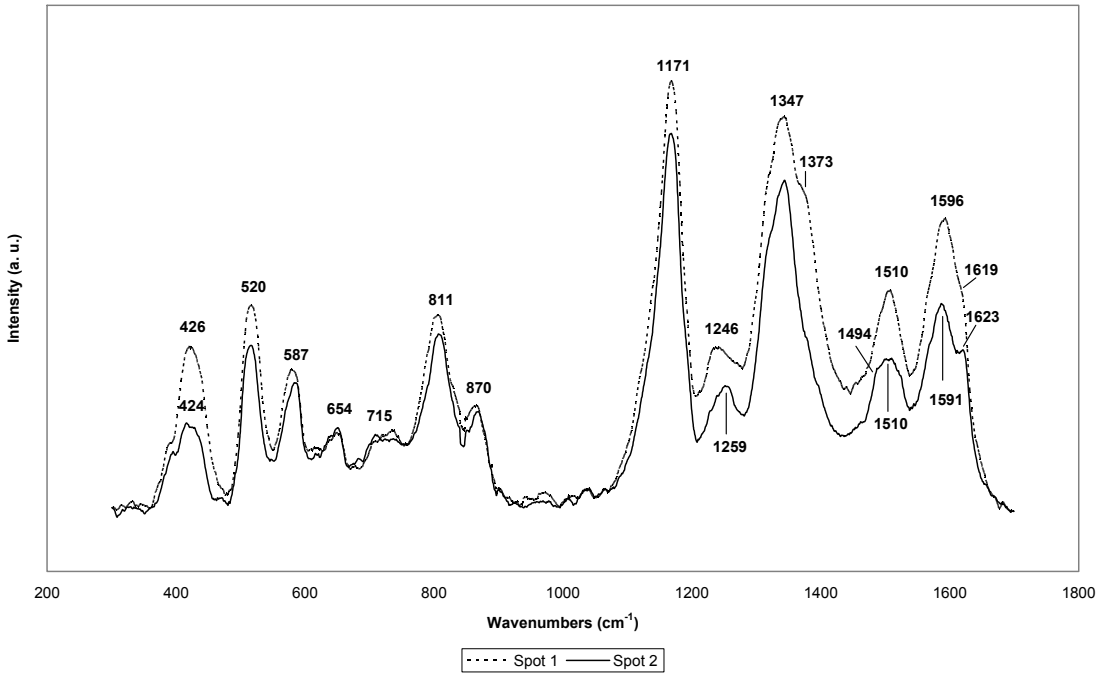

Figure 4.16 Overlayed Raman spectra of fibres electrospun from PAni 1% PAN 3% TDAB 0.5% in DMSO/DMF/THF

The spectra of PAni 1% PAN 3% TDAB 0.5% were quite similar to the PAni 1% PAN 3%, however one noticeable change was the absence of the shoulder at ~1370 cm^{-1} for

the Spot 2 analysis in this sample. This may have been due to this band coalescing with the 1347 cm^{-1} peak. However, this response was similar those for PAni/PVC/TDAB 0.5% and 5% samples, in that the particulate PAni exhibited this peak whilst the underlying fibres did not. Again, it is unlikely that the electrospinning limited the ability of PAni to alter its conformation in the fibre as the shoulder at ~1370 cm^{-1} was observed in the original PAni/PAN Raman spectra for both particulate matter and electrospun fibres. Thus, it would appear that the ionophore contributed to this conformational change. Furthermore, the small band at 1494 cm^{-1} associated with C=C and C=N stretch of quinoid units, and the small shoulder at 1623 cm^{-1} associated with C-C stretch of the quinoid group was far more prominent in the Spot 2 sample, evidence that the electrospun fibres exhibited both primary doped and secondary doped characteristics, possibly due to the influence and poor dispersion of TDAB.

Wavenumber (cm^{-1})	**Assignments**	**References**
426 / 424	Ring Deformation or C-H Wag (Q)	[224, 225, 228]
520	C-N-C Torsion	[224, 228]
587	Amine Deformation (B)	[224, 228]
654	Ring Deformation (B)	[224, 225, 228]
715	Ring Deformation (B)	[224, 225, 228]
811	C-H Deformation (Q)	[224, 225, 228, 233, 260]
870	Ring Deformation (B)	[224, 225, 228, 260, 261]
1171	C-H Bend (B)	[222, 225, 233, 260, 263]
~1246	C-N Stretch (B) or C-H Bend (B)	[228, 260]
1347	$C\text{-}N^{+\bullet}$ Stretch	[224, 228, 232, 260, 261]
1373	Conformational Change	[225, 232, 261]
1494	C=C Stretch (Q) + C=N Stretch (Q)	[224, 225, 232, 233]
1510 (S1) / 1510 (S2)	N-H Bend	[224, 225]
1596 (S1) / 1591(S2)	C=C Stretch (Q)	[224, 228, 232, 233, 260]
1623 (S2)	C-C Stretch (Q)	[228, 261]

Table 4.7 Peak assignments for fibres electrospun from PAni 1% PAN 3% TDAB 0.5% in DMSO/DMF/THF; (B) - Benzenoid; (Q) - Quinoid; (S1) - Spot 1; (S2) - Spot 2

Another difference between the TDAB blend and the original PAni/PAN blend is the appearance of the peak at ~715 cm^{-1}. It is likely that the presence of this band was due to the baseline correction of the original PAni/PAN as this peak was present in the original PAni/PVC fibres (Figure 4.7) corresponding to PAni benzenoid ring deformation, or alternatively, due to some minor interaction between the PAni and the ionophore.

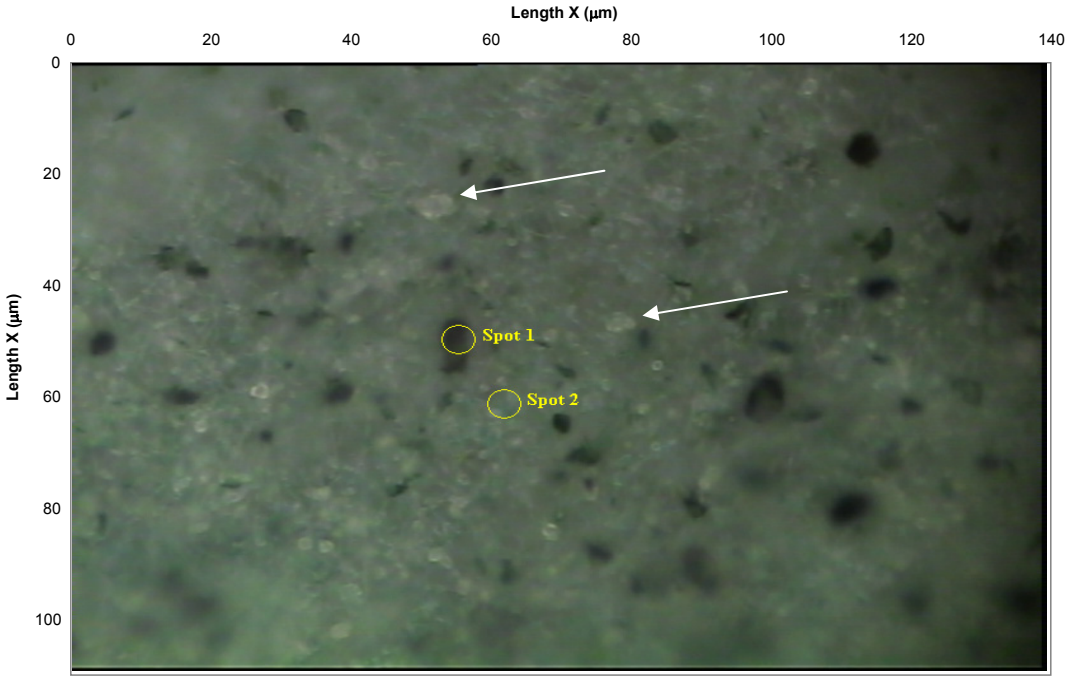

Figure 4.17 Optical micrograph of fibres electrospun from PAni 1% PAN 3% TDAB 0.5% in DMSO/DMF/THF

From visual inspection of the micrograph in Figure 4.17, the fibrous mat contained a large number of PAni particles, however there was also evidence of individual particles not consistent with PAni, present as white speckles on the electrode surface indicated by the arrows. SEM morphology in Section 3.3.10 also showed electrosprayed particulate matter was present, indicating that these particles were other components of the spinning solution, such as PAN or TDAB. It was noted in Section 4.2.3 that

PAni/PAN/TDAB solutions required the addition of THF to assist the dissolution of TDAB, thus perhaps the TDAB was not fully dissolved and crystallised out during electrospinning.

Changes in the concentration of the TDAB appear to have had some effect on the Raman spectra. Figure 4.18 gives a spot analysis of PAni 1% PAN 3% TDAB 5% electrospun fibres. From these spectra it can be seen that the shoulder at 1370 cm^{-1}, associated with conformational change of PAni, previously evident in the PAni particle (Spot 1, Figure 4.17) is now present and more pronounced in both the particle and the background fibres (Spots 1 and 2, respectively, Figure 4.18).

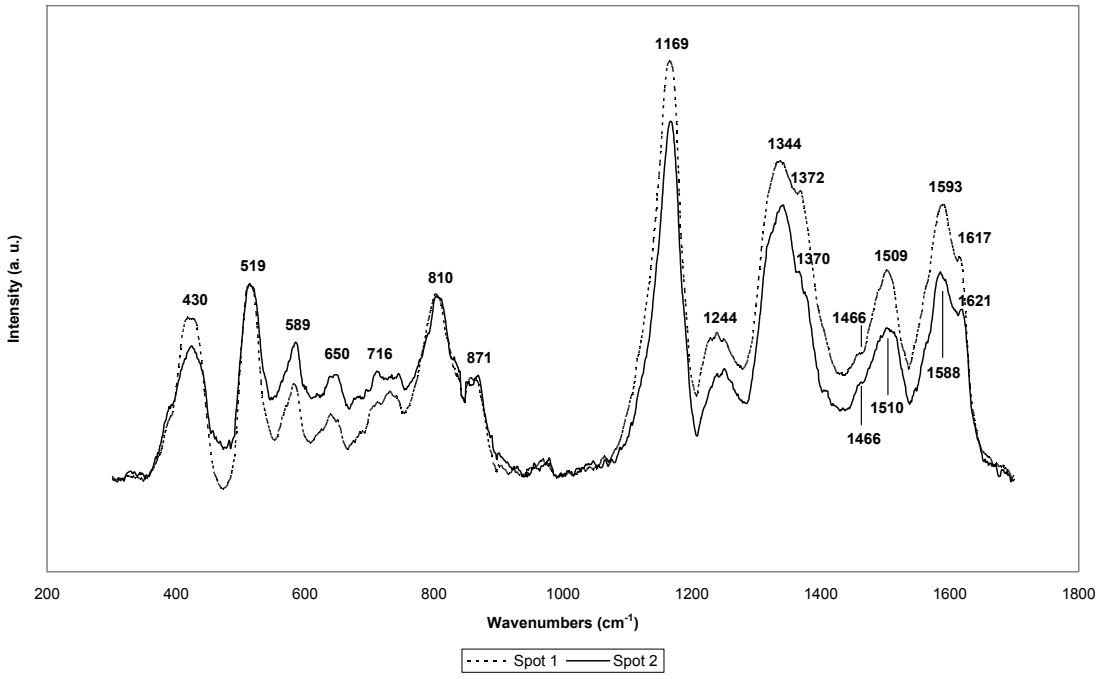

Figure 4.18 Overlayed Raman spectra of fibres electrospun from PAni 1% PAN 3% TDAB 5% DMSO/DMF/THF

In Section 4.3.5 it was noted that the shoulder at ~ 1620 cm^{-1} was observed for original PAni/PAN electrospun fibres, and that at 0.5% TDAB, this peak was present for the electrospun fibres, but not prominent in the particulate PAni. This may indicate that at

low concentrations TDAB significantly disrupts the doping of PAni. However, as the concentration increased to 5% TDAB, it would appear that TDAB influenced the blend, with both shoulders (~1370 cm^{-1} and ~1620 cm^{-1}) more prominent as a result. Considering that the shoulder at ~1370 cm^{-1} is indicative of secondary doping, and hence conformational change, and the shoulder at ~1620 cm^{-1} is characteristic of primary doped PAni may indicate that TDAB was insufficiently dispersed throughout the sample. This is consistent with the appearance of possible TDAB particles in the micrograph (Figure 4.17), resulting in different degrees of doping of PAni throughout the fibres

Visual inspection from the optical micrograph of PAni 1% PAN 3% TDAB 10% electrospun fibres (Figure 4.19) indicated that the dispersion of PAni was again poor. A segment of this sample was mapped by Raman to provide a detailed PAni concentration analysis. The overlay of the Raman spectra is presented in Figure 4.20.

The spectra overlay each other quite well, indicating that PAni was consistently present throughout the sample, however the concentration does vary as evident by the differing layers in the Raman spectra. The bands are also in relatively good agreement with the previous spectra (Figure 4.16 and 4.18), though there were some differences such as shifts to a lower wavenumber for the peaks at 1157 cm^{-1} and 1215 cm^{-1}. There was a significant increase in the peak at ~1465 cm^{-1} corresponding to C=C stretch and C=N stretch, and also at ~1501 cm^{-1} corresponding to N-H bend for some regions of the fibre sample. This indicates the doping of the sample in these regions was lower compared to other areas of the sample.

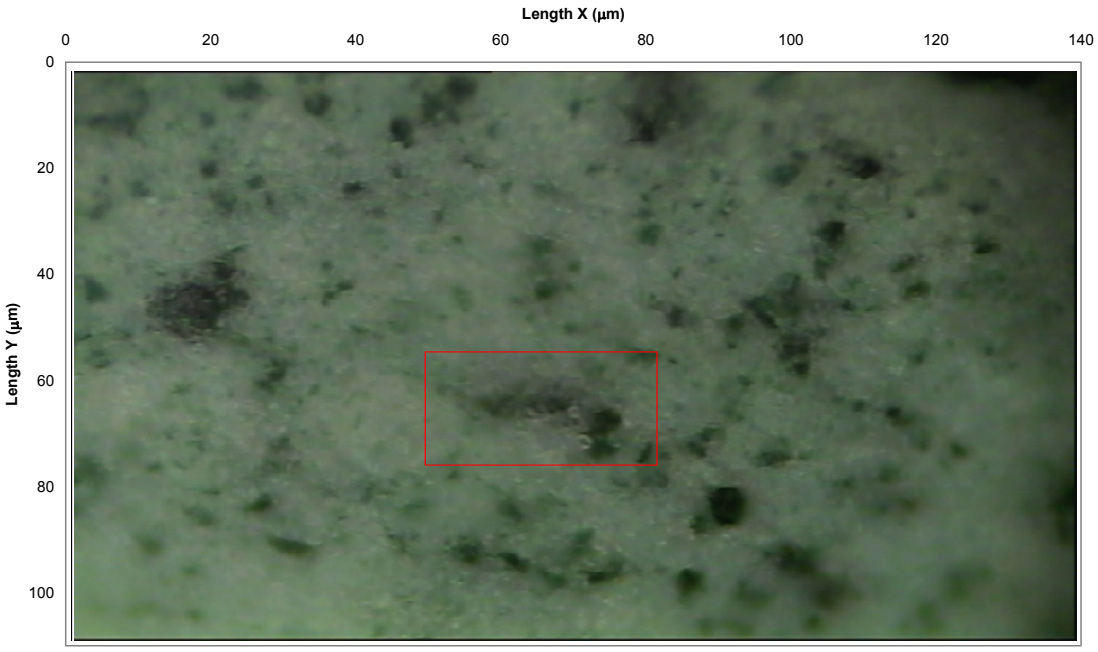

Figure 4.19 Optical micrograph of fibres electrospun from PAni 1% PAN 3% TDAB 10% in DMSO/DMF/THF

It is unclear as to why these peaks were so intense, especially considering they were far less significant in the PAni/PAN, PAni/PAN/TDAB 0.5% and PAni/PAN/TDAB 5% samples. It is possible the higher concentration of TDAB de-doped the PAni to some extent, or reduced the ability of PAni to dope prior to electrospinning. However, the presence of the peak at 1339 cm^{-1} and at 1379 cm^{-1} corresponding to the radical cation indicate that the PAni was doped to some degree. This 'peak' at 1379 cm^{-1}, previously noted as corresponding to conformational change, usually appears as a shoulder on the band at ~1340 cm^{-1}. If TDAB were de-doping the PAni, it would be anticipated this 'peak' at 1379 cm^{-1} would have decreased significantly due to the relatively high concentration of TDAB, however this was not the case. The layering of fibres with areas indicative of both primary doped, secondary doped and low-doped PAni suggests that if the TDAB was actively doping or de-doping the PAni, then it was not dispersed throughout the blend, leading to this variability in degree of doping.

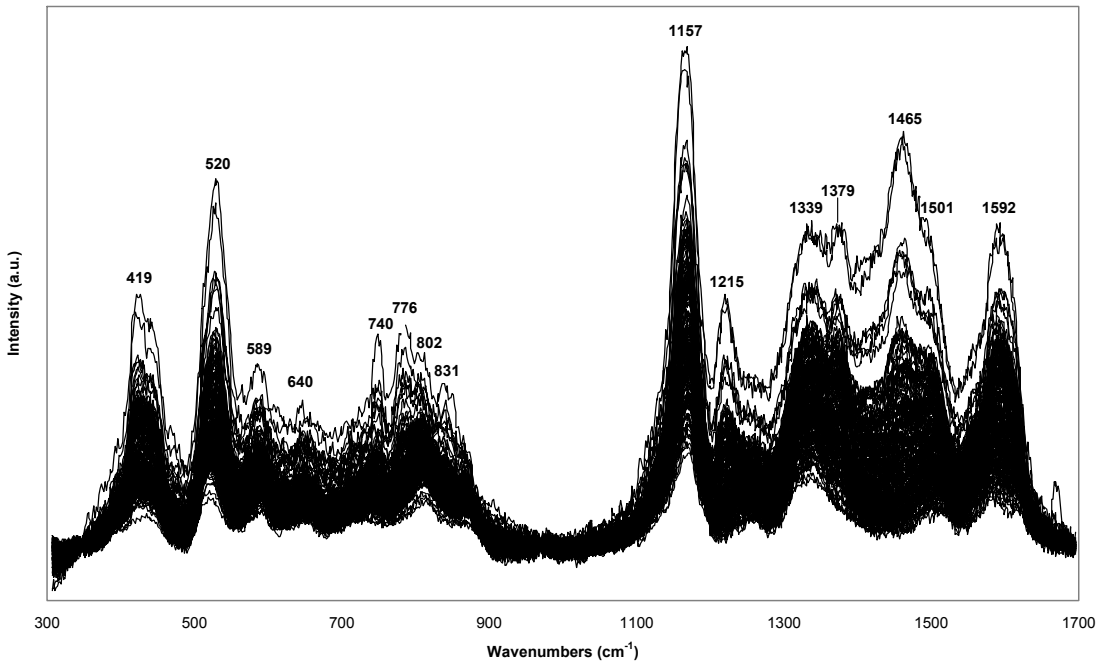

Figure 4.20 Overlay of 300 Raman spectra of a 40 µm x 30 µm segment of fibres electrospun from PAni 1% PAN 3% TDAB 10% in DMSO/DMF/THF

The dispersion map is given in Figure 4.21, taken from the fibre sample identified in Figure 4.19. Clearly there were areas of high PAni concentration within the sample, evident by the light green features in Figure 4.21, however these areas correspond with electrosprayed matter rather than electrospun fibres, based on visual inspection of Figure 4.19. Furthermore, the presence of PAni in the underlying electrospun fibres represented by the darker blue areas was relatively consistent, although there were areas of high PAni concentration. The small purple areas correspond to the low doped PAni.

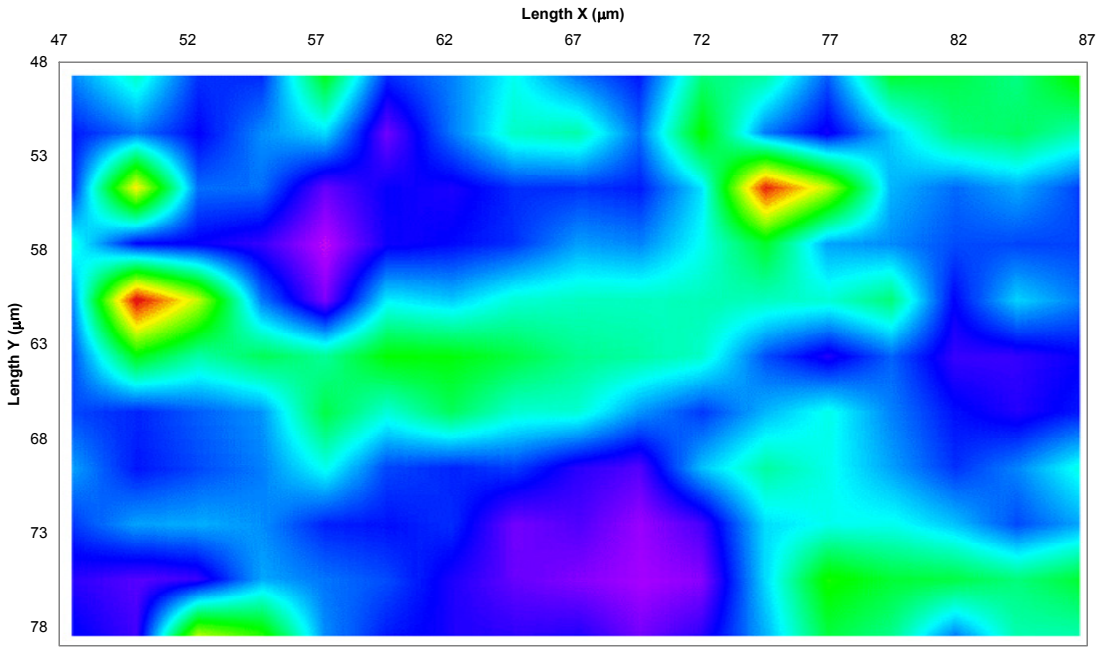

Figure 4.21 PAni dispersion map of fibres electrospun from PAni 1% PAN 3% TDAB 10% in DMSO/DMF/THF; bands 1100-1400 cm^{-1}

4.3.8 PAni/PVC/TAEAB Electrospun Fibres

As stated previously it appears the introduction of the QAS led to a change in the interaction between PAni and PVC, in turn leading to a change in the conformational properties of the PAni within the fibres. This is repeated for Raman spot spectra of PAni 1% PVC 10% TAEAB 0.5% (triallylethylammonium bromide, a documented nitrate ionophore) electrospun fibres, presented in Figure 4.22 with the assignments given in Table 4.8.

The assignments are consistent with the literature and generally agree with the bands observed in PAni 1% PVC 10% electrospun fibres. However, there were some discrepancies, notably small shifts in the bands observed at ~1300 – 1400 cm^{-1}, and the presence of bands at 1495 cm^{-1} and 1625 cm^{-1} for Spot 2 compared to Spot 1.

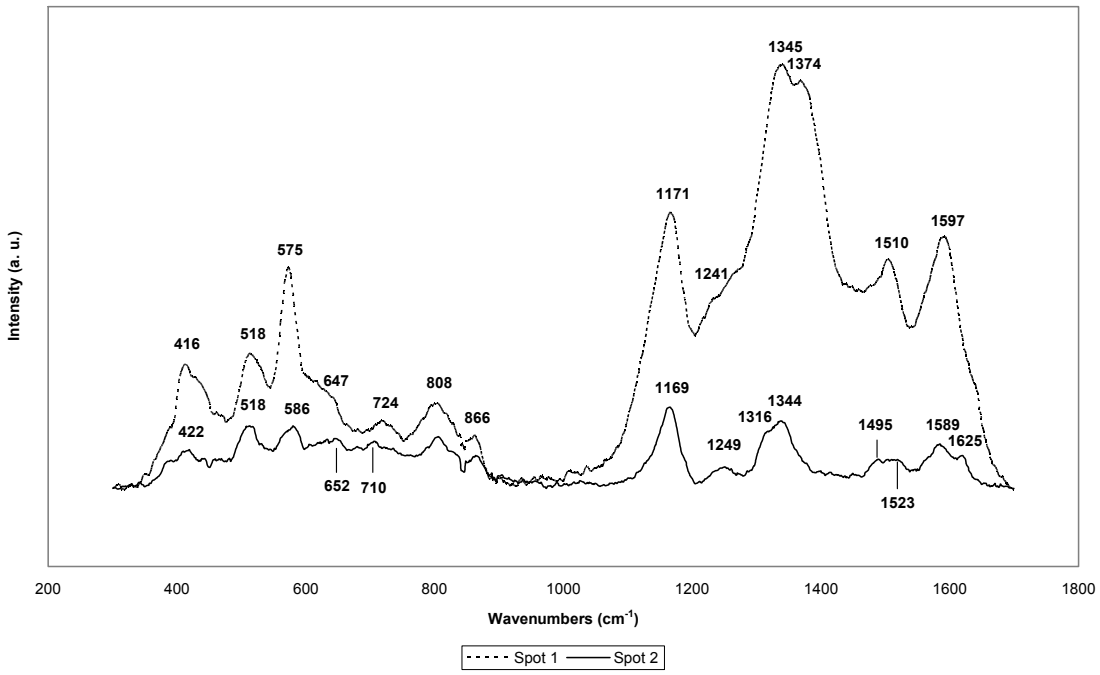

Figure 4.22 Overlayed Raman spectra of fibres electrospun from PAni 1% PVC 10% TAEAB 0.5% in THF/DMF

Wavenumber (cm^{-1})	Assignments	References
416 (S1) / 422 (S2)	Ring Deformation or C-H Wag (Q)	[224, 225, 228]
518	C-N-C Torsion	[224, 228]
575(S1) / 586(S2)	Amine Deformation (B)	[224, 228]
647(S1) / 652(S2)	Ring Deformation (B)	[224, 225, 228]
724(S1) / 710(S2)	Ring Deformation (B)	[224, 225, 228]
808	C-H Deformation (Q)	[224, 225, 228, 233, 260]
866	Ring Deformation (B)	[224, 225, 228, 260, 261]
1171(S1) /1169 (S2)	C-H Bend (B)	[222, 225, 233, 260, 263]
1241/1249	C-N Stretch (B) or C-H Bend (B)	[228, 260]
1345 (S1) /1316 + 1344 (S2)	$C\text{-}N^{+\bullet}$ Stretch	[224, 228, 232, 260, 261]
1374(S1)	Conformational Change	[225, 232, 261]
1495	C=C Stretch (Q) + C=N Stretch (Q)	[224, 225, 232, 233]
1510(S1) / 1523(S2)	N-H Bend	[224, 225]
1597(S1) / 1589(S2)	C=C Stretch (Q)	[224, 228, 232, 233, 260]
1625	C-C Stretch (Q)	[228, 261]

Table 4.8 Peak assignments for fibres electrospun from PAni 1% PVC 10% TAEAB 0.5% in THF/DMF; (B) - Benzenoid; (Q) - Quinoid; (S1) - Spot 1; (S2) - Spot 2

The addition of this ionophore produced characteristic peaks observed in the PAni/PVC/TDAB spectra, such as the peak associated with conformation change and free charge carriers at 1374 cm^{-1}, but only for Spot 1, the particulate PAni, for this sample. This was similar to observations reported for PAni/PVC/TDAB 0.5% (Figure 4.12) where Spot 1 and Spot 2 differed, both chemically and physically. Observation of the micrograph in Figure 4.23 showed that these conformational changes associated with Spot 1 were in electrosprayed particles of PAni/PVC/TAEAB and not within the actual electrospun fibres. Thus the PAni appears to have variable conformation depending on its morphology.

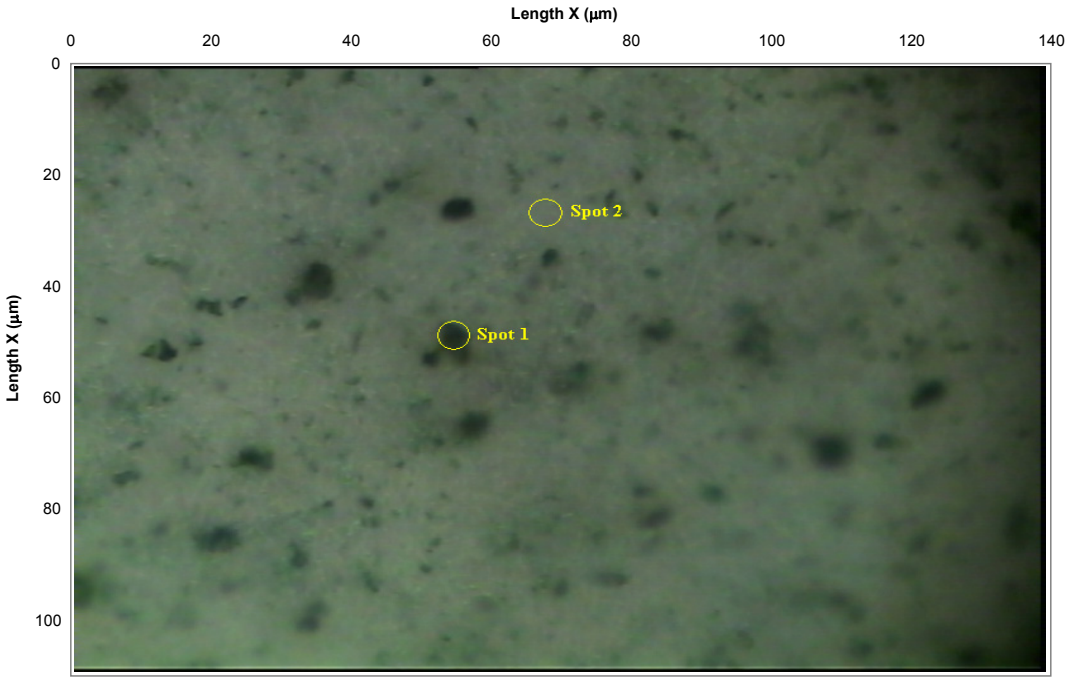

Figure 4.23 Optical micrograph of fibres electrospun from PAni 1% PVC 10% TAEAB 0.5% in THF/DMF

Spot 2 however, did not exhibit this shoulder at 1374 cm^{-1}, but instead retained the two peaks at 1316 cm^{-1} and 1344 cm^{-1} indicative of the radical cation for primary doped PAni, and a peak at 1625 cm^{-1} associated with C-C stretch in primary doped PAni. As

postulated for the PAni/PVC/TDAB and PAni/PAN/TDAB samples, the QAS may not be adequately dispersed throughout the sample, or the electrospinning of PAni/polymer solutions limits the extent of PAni to alter its conformation within the fibres. If the PVC was directing the conformation of PAni within the electrospun fibres, or electrically screening PAni and leading to a coiled PAni conformation, it would be expected that this response would differ between the samples sites, if the particulate matter were PAni or PAni/QAS only. Thus, it is possible that both a lack of TDAB and the presence of PVC resulted in inconsistencies between the two sample sites. This is pertinent considering 10% TDAB in PAni/PVC produced Raman spectra exhibiting this shoulder at ~1370cm^{-1} for both spot analyses. This may also hold for TAEAB where a higher concentration may alter the conformation of PAni in PVC.

It is apparent in Figure 4.23 that there were again two discrete regions associated with PAni, specifically lighter green regions associated with electrospun fibres, and darker green spatter that would appear was electrosprayed PAni. In conjunction with the high intensity of the Raman spectra of Spot 1 compared with Spot 2 in Figure 4.22, it was evident there was a lack of PAni dispersion through the sample due to the larger particles of PAni. Overall the actual micrograph indicated a uniform mat of PAni/PVC/TAEAB electrospun fibres. Thus whilst there was some electrospraying and possibly some undispersed particles of PAni, there is evidence that the underlying fibrous mat offers electrospun fibres containing dispersed and protonated PAni, albeit primary doped.

No spectra were recorded for blends of PAni1% PVC 10% TAEAB 5% and 10% as TAEAB failed to dissolve adequately in these blends.

4.3.9 PAni/PAN/TAEAB Electrospun Fibres

The Raman spectra of PAni 1% PAN 3% TAEAB 0.5% electrospun fibres were consistent with both the spectra observed for PAni 1% PAN 3% and for PAni 1% PVC 10% TAEAB 0.5% electrospun fibres. The Raman spot analysis is presented in Figure 4.24 with the assignments provided in Table 4.9.

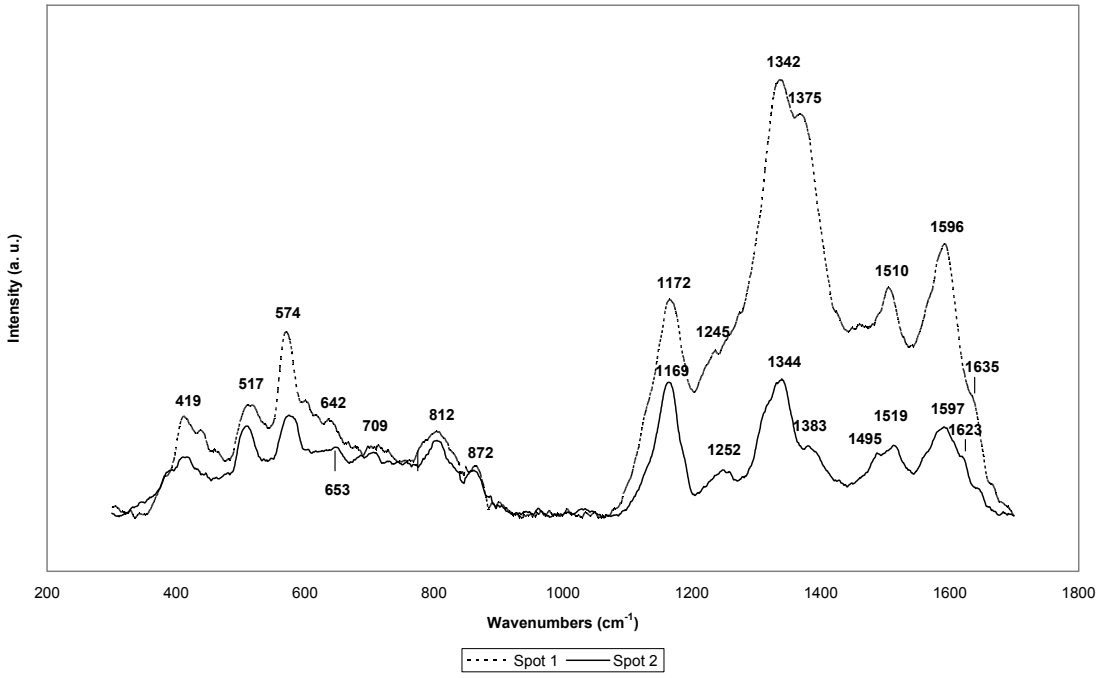

Figure 4.24 Overlayed Raman spectra of fibres electrospun from PAni 1% PAN 3% TAEAB 0.5% in DMSO/DMF

The spectra are similar to the Raman spectra of PAni 1% PAN 3% electrospun fibres except for the presence of a band at 709 cm^{-1}, a lower intensity of the shoulder at 1383 cm^{-1}, the presence of a small peak for Spot 2 at 1495 cm^{-1}, and the presence of a shoulder at 1623 cm^{-1} for Spot 2. The peak at 709 cm^{-1}, due to ring deformation, was not observed in the original PAni 1% PAN 3% fibres, but was present in the PAni/PAN/TDAB fibres, and it was surmised that an error in the baseline correction of

the original PAni/PAN blend was responsible for this observation, as this peak was previously observed in spectra of PAni/PVC electrospun fibres.

Wavenumber (cm^{-1})	Assignments	References
419	Ring Deformation or C-H Wag (Q)	[224, 225, 228]
517	C-N-C Torsion	[224, 228]
574	Amine Deformation (B)	[224, 228]
646	Ring Deformation (B)	[224, 225, 228]
709	Ring Deformation (B)	[224, 225, 228]
812	C-H Deformation (Q) / Ring Deformation (Q)	[224, 225, 228, 260]
872	Ring Deformation (B)	[224, 225, 228, 260]
1172(S1) / 1169(S2)	C-H Bend (B)	[224, 225, 228, 260]
1245(S1) / 1252(S2)	C-N Stretch (B) / C-C Stretch / C-H Bend (B)	[225, 228, 260, 262]
1342(S1) / 1344(S1)	$C\text{-}N^{+\bullet}$ Stretch	[225, 232, 233, 260, 262]
1375(S1) / 1389(S2)	Free Charge Carriers	[225, 232, 261]
1495	C-C Stretch / C-H Deformation / C=N	[224, 228, 262]
1510(S1) / ~1519(S2)	N-H Bend / C=N Stretch	[228, 262]
1596(S1) / 1597(S2)	C-C Stretch (B)/ C=C Stretch (Q)	[224, 228, 232, 233, 260, 262]
1635(S1) / 1623(S2)	C-C Stretch (Q)	[228, 261]

Table 4.9 Peak assignments for fibres electrospun from PAni 1% PAN 3% TAEAB 0.5% in DMSO/DMF; (B) - Benzenoid; (Q) - Quinoid; (S1) - Spot 1; (S2) - Spot 2

The peak at ~1343 cm^{-1} for both spot analyses is evidence that the PAni within the fibres was protonated, even though the peak associated with deprotonated quinoid units at ~1514 cm^{-1} was present. There was evidence of some degree of secondary doping/conformation change as evident by the shoulder at ~1380cm^{-1} for both spectra, which combined would indicate that PAni was doped, although this shoulder at 1380 cm^{-1} was smaller for the background electrospun fibres. Similar to the spectra for PAni 1% PVC 10% TDAB 0.5% fibres (Figure 4.16), there was the presence of a weak band at 1495 cm^{-1} for Spot 2, and in conjunction with the assignments above, it is again likely that this the PAni in the fibres exhibited both doped and secondary doped characteristics.

As the introduction of the ionophore produced only a slight change in the Raman bands compared with the spectra of PAni 1% PAN 3% fibrous mat (Figure 4.11), it is evident the properties of the electrospun PAni/PAN fibres were much more dependent on the relationship between PAni and PAN rather than the presence of QAS. This is supported by evidence of conformational changes in the PAni due to the presence of the shoulder at ~1380 cm^{-1} for both spots, as was found in the original PAni/PAN sample, only small changes in the Raman spectra of PAni/PAN/TDAB samples with increasing TDAB (Figures 4.16, 4.18 and 4.20), and by the fact that PAni/PVC fibres exhibited significant differences compared with PAni/PVC/ionophore fibres. From this, it could be inferred that the properties of PAni/PVC fibres were less dependent on their PAni-PVC interaction compared to PAni/PAN fibres. If this is true it could be generalised that the interaction between PAni and a support polymer determines the degree of doping and the affect from electrospinning and the presence of QAS.

The electrospun sample of PAni 1% PAN 3% TAEAB 0.5% (Figure 4.25) exhibited almost identical morphologically in comparison to PAni 1% PVC 10% TAEAB 0.5% fibres from the optical micrograph in Figure 4.23. It is important to note that it was observed in Section 3.3.10 and Section 3.3.12 these morphological characteristics were much more significant at a higher magnification. Again there were indications that electrospraying occurred with the presence of large green particles consistent with PAni, spread throughout the fibre mat.

As with other spot analyses the Raman spectra indicated that whilst present as large particles on the fibres, PAni was also present within the fibrous mat. This indicates that whilst there may have been some suspended particles, there was also dispersion of PAni throughout the original solution to produce composite PAni/PAN electrospun mats.

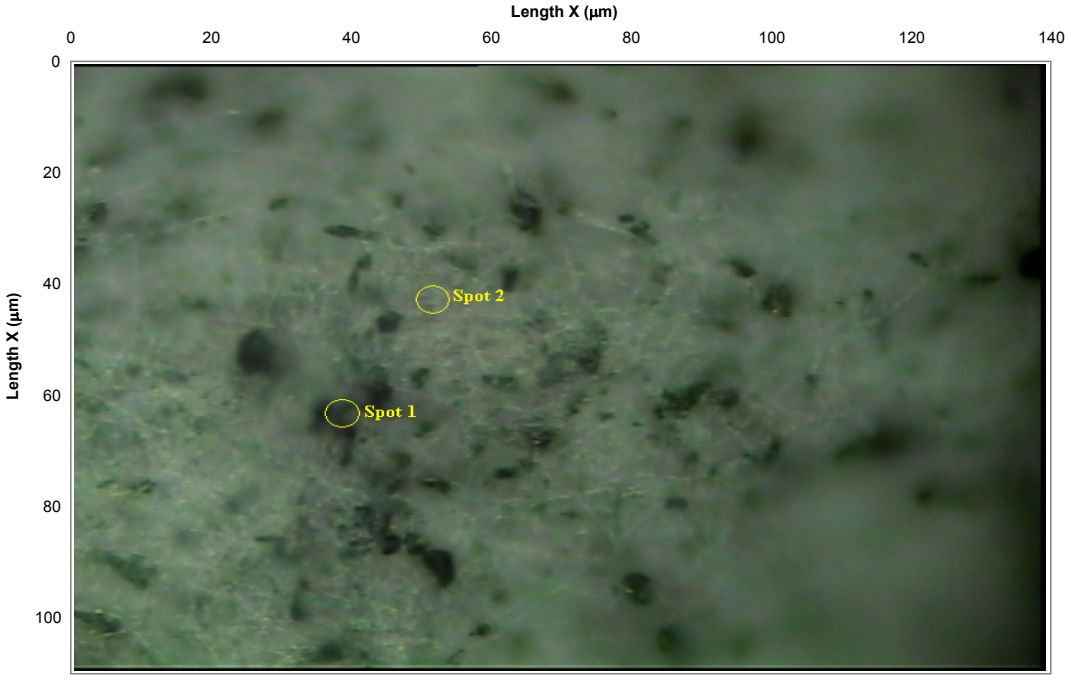

Figure 4.25 Optical micrograph of fibres electrospun from PAni 1% PAN 3% TAEAB 0.5% in DMSO/DMF

Increasing the concentration of the ionophore produced only slight changes in the Raman spectra of the PAni/PAN/TAEAB samples. Figure 4.26 is the Raman spot analyses of a sample of electrospun PAni 1% PAN 3% TAEAB 5% fibres whilst Figure 4.27 is the Raman spot analyses of a sample of electrospun PAni 1% PAN 3% TAEAB 10% fibres.

Both spectra are consistent with the previous PAni 1% PAN 3% TAEAB 0.5% spectra and assignments. The differences observed between the three different samples are the presence of a shoulder at 1489 cm^{-1} in Spot 1 for the PAni/PAN/TAEAB 10% spectrum, the presence of a shoulder at 1621 and 1623 cm^{-1} for both analyses of this sample, indicative of primary doped PAni, and another shoulder at 1643 cm^{-1} corresponding to a cyclised structure containing nitrogen [224, 225]. The spectra of PAni/PAN/TAEAB

5% are practically identical to the PAni/PAN/TDAB spectra, apart from some minor shifts in the shoulders at ~1620 cm^{-1} for both Spot analyses.

The peak at ~1380 cm^{-1} for the Spot 2 analysis of PAni/PAN/TAEAB 10% was quite small, implying similar observations to the PAni 1% PAN 3% TDAB 0.5% spectra where one spot possessed the ~1380 cm^{-1} band whilst the other did not. Again, this may have been a result of the influence of the ionophore on the properties of PAni within the fibre. There was also a noticeable increase in the area for the band located at ~411 cm^{-1} due to baseline correction of the spectra.

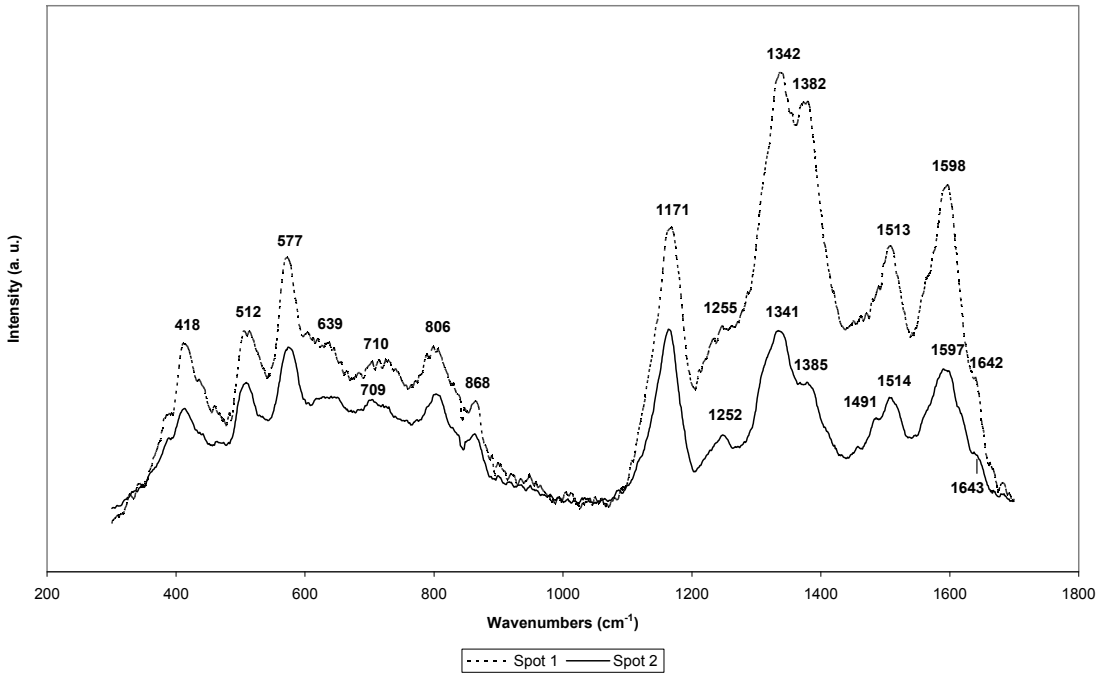

Figure 4.26 Overlayed Raman spectra of fibres electrospun from PAni 1% PAN 3% TAEAB 5% in DMSO/DMF

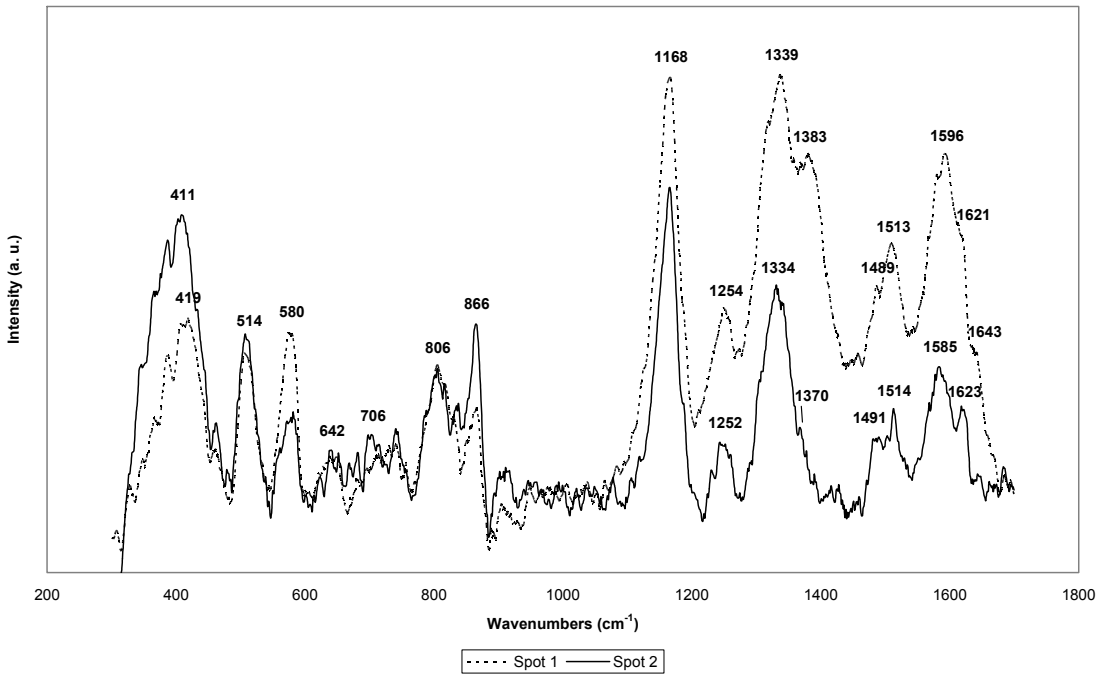

Figure 4.27 Overlayed Raman spectra of fibres electrospun from PAni 1% PAN 3% TAEAB 10% in DMSO/DMF

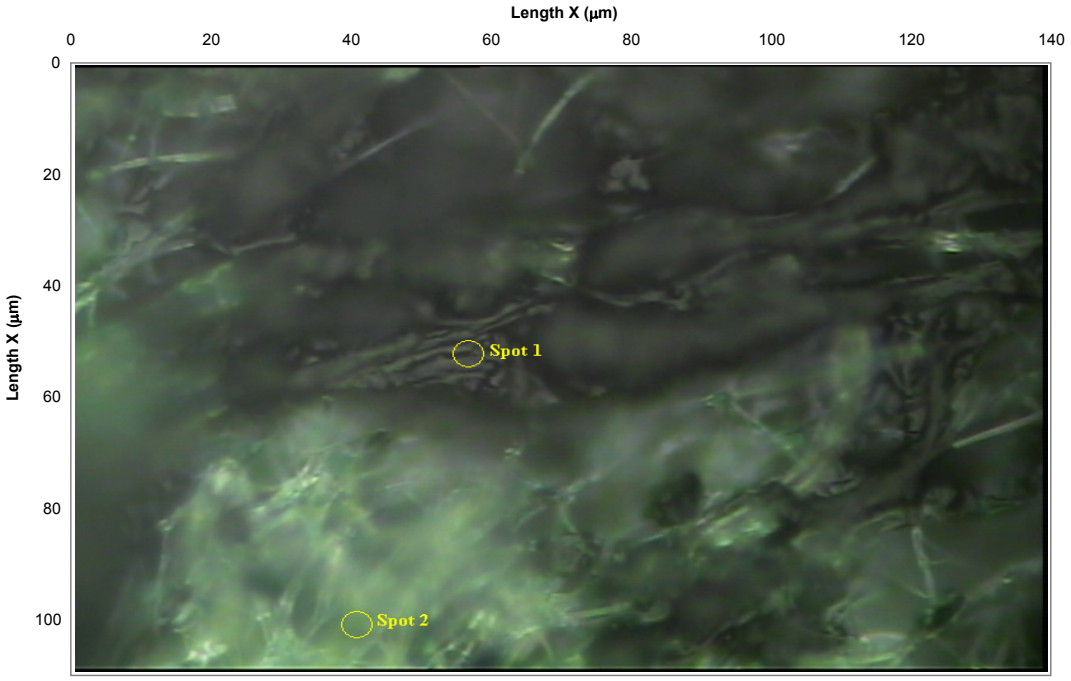

Figure 4.28 Optical micrograph of fibres electrospun from PAni 1% PAN 3% TAEAB 10% in DMSO/DMF

The high concentration of TAEAB in the sample may have influenced the solution properties, such as viscosity, solution conductivity and surface tension, in PAni/PAN solutions as the optical micrograph in Figure 4.28 presents significant morphological changes compared to other electrospun samples. There were no longer large particles or droplets through the mat, but rather film-like areas of PAni were present, along with areas that appear to have no, or much lower concentrations of PAni. This was partially supported by evidence in Section 3.3.12 where areas of film were also observed, although the majority of the sample was fibrous. Regardless of this change in morphology there still appears to be the presence of doped PAni within the non-woven mat, although this should be treated with caution at this high concentration of TAEAB due to the significant morphological change observed in Figure 4.28.

4.3.10 MWNT

Raman analysis of raw MWNT and MWNT/polymer electrospun fibres were also performed to determine the distribution of MWNT, and also to determine the quality of MWNT employed.

The Raman spectra of raw MWNT powder consisted of two dominant peaks corresponding to two different properties of nanotubes (Figure 4.29).

The D-band at ~1350 cm^{-1}, also referred to as the disorder-induced peak, occurs due to the double-resonance effect in the sp^2 carbons [264]. Double resonance occurs when the energy of the incoming scattered photon from the laser source matches the transition energy of an allowed electronic transition and leads not to a virtual transition, but a real and observed one [265].

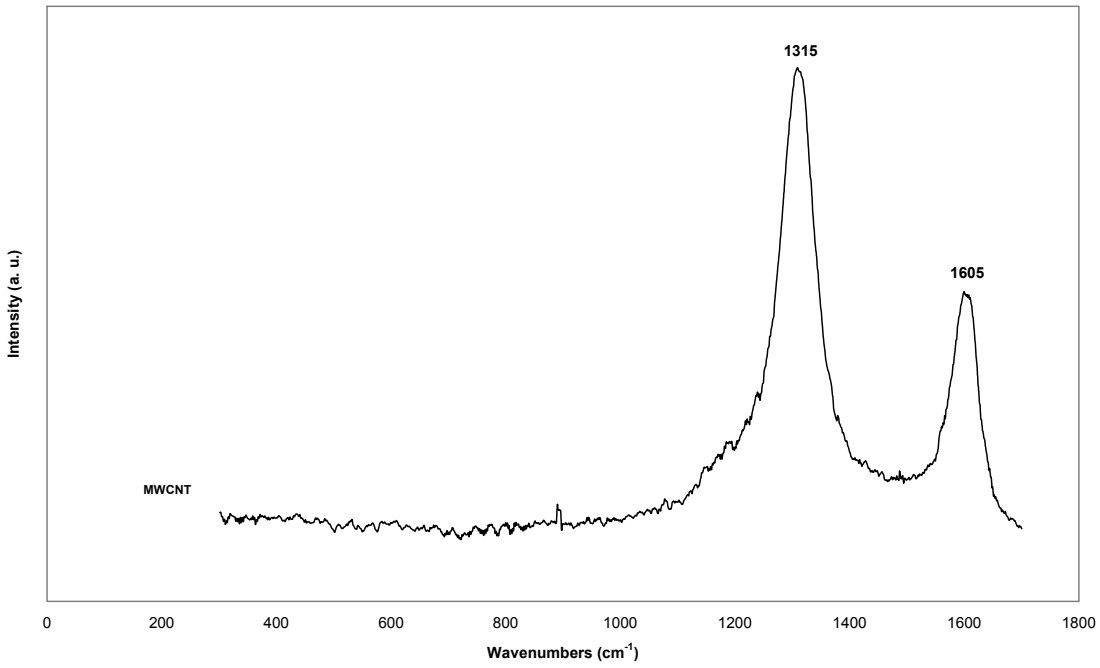

Figure 4.29 Raman spectra of raw MWNT powder

It is also suggested that this peak is a product of defects in the nanotube structure and decreases in purified samples [264, 266, 267]. As the sample utilised here was used 'as received' it may well be relatively impure, which would contribute to the large D-band, most likely as a result of amorphous carbon by-products and defects in the nanotubes.

The G-band at 1605 cm^{-1} is named due to the relationship of nanotubes with graphite. Raman spectra of graphite produce a peak at 1582 cm^{-1} due to tangential vibrations of the carbon atoms. These vibrations are also observed in carbon nanotubes but the Raman band may shift due to the curvature of the nanotubes in comparison to graphite sheets [266, 268]. These vibrations in nanotubes are presented diagrammatically in Figure 4.30.

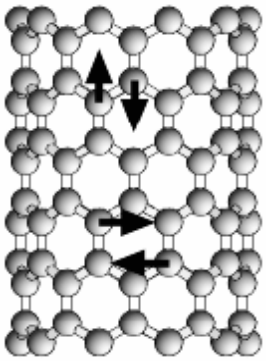

Figure 4.30 Tangential vibrations of carbon atoms in carbon nanotubes [268]

4.3.11 MWNT/PEO Electrospun Fibres

Figure 4.31 is the Raman spectrum of MWNT 0.5% PEO 3% electrospun fibres. There were two major peaks observed in both spectra and assigned in Table 4.10. Two peaks should be prominent in Raman spectra of MWNT, specifically the D-band observed in the range of 1320-1400 cm^{-1} and the G-band between 1530 – 1640 cm^{-1} [267-270].

There are three other notable peaks in the spectra (See Table 4.10) and these were assigned to the CH_3 rocking and bend from PEO [271]. However, the areas of these bands indicate that the contribution from the MWNT is far more intense than that from PEO.

Wavenumber (cm^{-1})	Assignments	References
805	CH_3 Rocking	[271]
840	CH_3 Rocking	[271]
1333	D-band	[267-270]
1466	CH_3 Bend	[271]
1603	G-band	[267-270]

Table 4.10 Peak assignments for fibres electrospun from MWNT 0.5% PEO 3% in $CHCl_3$

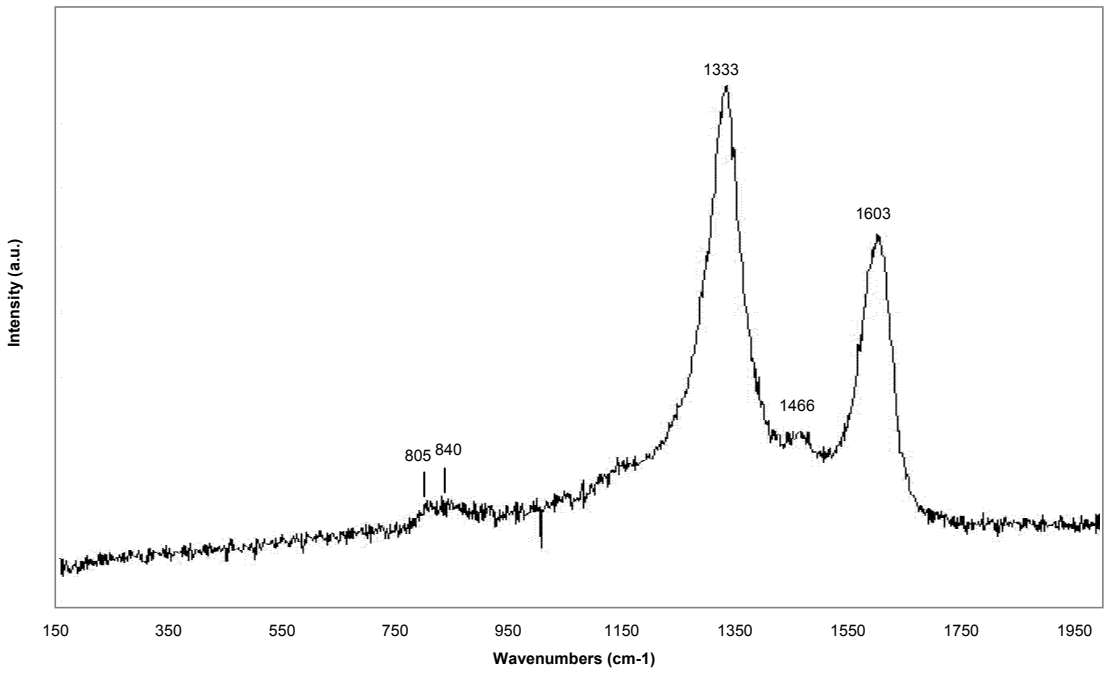

Figure 4.31 Raman spectrum of fibres electrospun from MWNT 0.5% PEO 3% in $CHCl_3$

4.3.12 MWNT/PVC Electrospun Fibres

By mapping a sample of MWNT 0.5% PVC 10% fibres the relative dispersion of MWNT throughout the fibres can be determined. Figure 4.32 provides an overlay of a sample of MWNT 0.5% PVC 10% that was mapped.

Again there are two major peaks that occur in the overlay of MWNT 0.5% PVC 10% corresponding to the D-band and G-band. The assignments for these peaks are provided in Table 4.11. Similar to the MWNT 0.5% PEO 3% fibres, there was no significant contribution from PVC and it is difficult to confirm the presence of PVC in these samples.

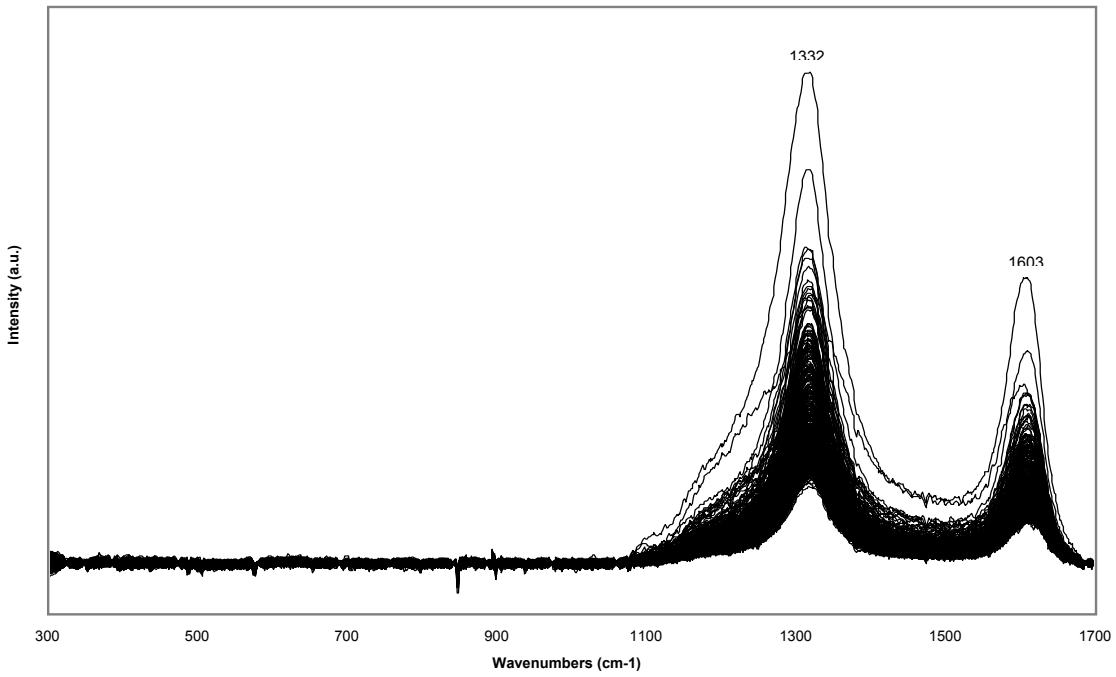

Figure 4.32 Overlay of 552 Raman spectra of a 48 µm x 46 µm segment of fibres electrospun from MWNT 0.5% PVC 10% in THF/DMF

Wavenumber (cm^{-1})	Assignments	References
1332/1337	D-Band	[267-270]
1603	G-Band	[267-270]

Table 4.11 Peak assignments for fibres electrospun from MWNT 0.5% PVC 10% in THF/DMF

The dispersion map in Figure 4.33 was prepared by selecting only the D-band and G-band MWNT peaks in the overlay of MWNT/PVC electrospun fibres.

By selecting only these peaks the changes in the concentration of MWNT can be observed as indicated by changes in the colour. As there are no extreme colour changes in the map there was little change in the concentration of the MWNT present throughout the sample.

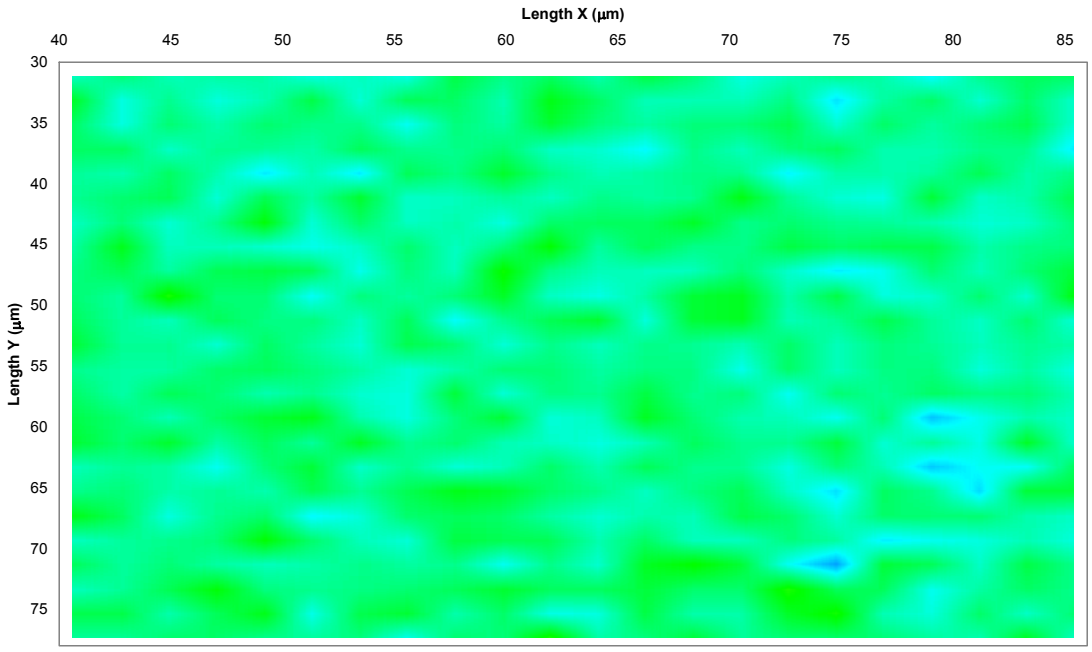

Figure 4.33 MWNT dispersion map of fibres electrospun from MWNT 0.5% PVC 10% in THF/DMF

4.3.13 MWNT/PAN Electrospun Fibres

MWNT/PAN blends give similar results to MWNT/PVC and MWNT/PEO spectra, with the presence of the two significant MWNT peaks (1312 and 1604 cm^{-1}) in good agreement with observations made by Li et al. [269]. The Raman spot spectra are given in Figure 4.34, the assignments provided in Table 4.12, and the optical micrograph of the analysis region given in Figure 4.35.

The individual spot spectra are in agreement, presenting similar intensity characteristics indicating that the MWNT were dispersed throughout the electrospun fibres. Again, the Raman response for the MWNT is significantly more intense than the PAN, and again the two major peaks present are assigned to the MWNT D-band and G-band.

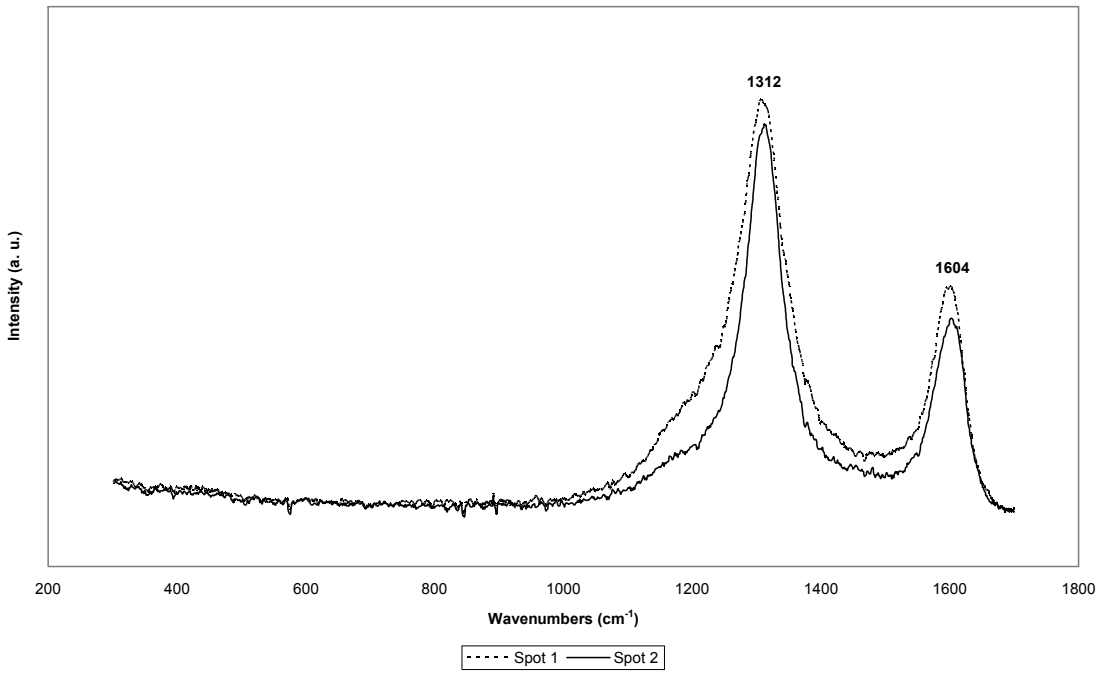

Figure 4.34 Overlayed Raman spectra of fibres electrospun from MWNT 0.5% PAN 3% in DMSO/DMF

Wavenumber (cm^{-1})	Assignments	References
1312	D-Band	[267-270]
1604	G-Band	[267-270]

Table 4.12 Peak assignments for fibres electrospun from MWNT 0.5% PAN 3% in DMSO/DMF

The surface of the sample indicates that there has been the electrospraying of droplets or that agglomeration of MWNT occurred, indicative of inadequate dispersion of nanotubes. However, the Raman overlay indicates that MWNT has been dispersed through the sample with both spots offering similar spectra. This is pertinent due to the different appearance of the analyses regions in Figure 4.35, with Spot 1 appearing to be high in MWNT concentration and Spot 2 appearing to be relatively low.

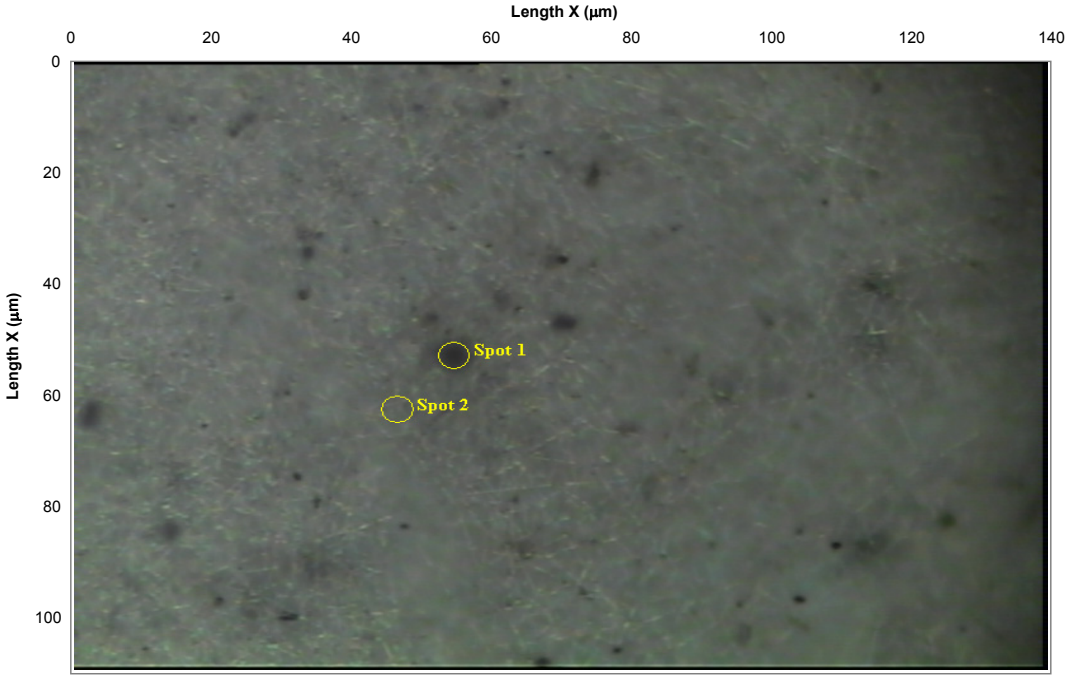

Figure 4.35 Optical micrograph of fibres electrospun from MWNT 0.5% PAN 3% in DMSO/DMF

4.4 Results and Discussion – Tensile Testing

4.4.1 PVC Electrospun Fibres

The electrospun samples of PVC were not particularly rigid, requiring very little force to extend the samples. According to Hannah and Hillier [236] un-reinforced plastics have a Young's modulus in the area of 1.4 GPa, depending on the processing and the properties of the polymer. Lee et al. [84] reported a modulus of 3.75 MPa for a pure PVC fibre mat electrospun from THF/DMF. In addition they also observed elongations of the electrospun PVC fibre mat up to 153 % at maximum yield.

In this the present work, two PVC samples electrospun from THF/DMF gave values of 144 kPa and 119 kPa for Young's modulus, given in Figure 4.36 and Table 4.13. It is

obvious that these values were much lower than those suggested by Hannah and Hillier [236], and also significantly lower than those by Lee et al. [84].

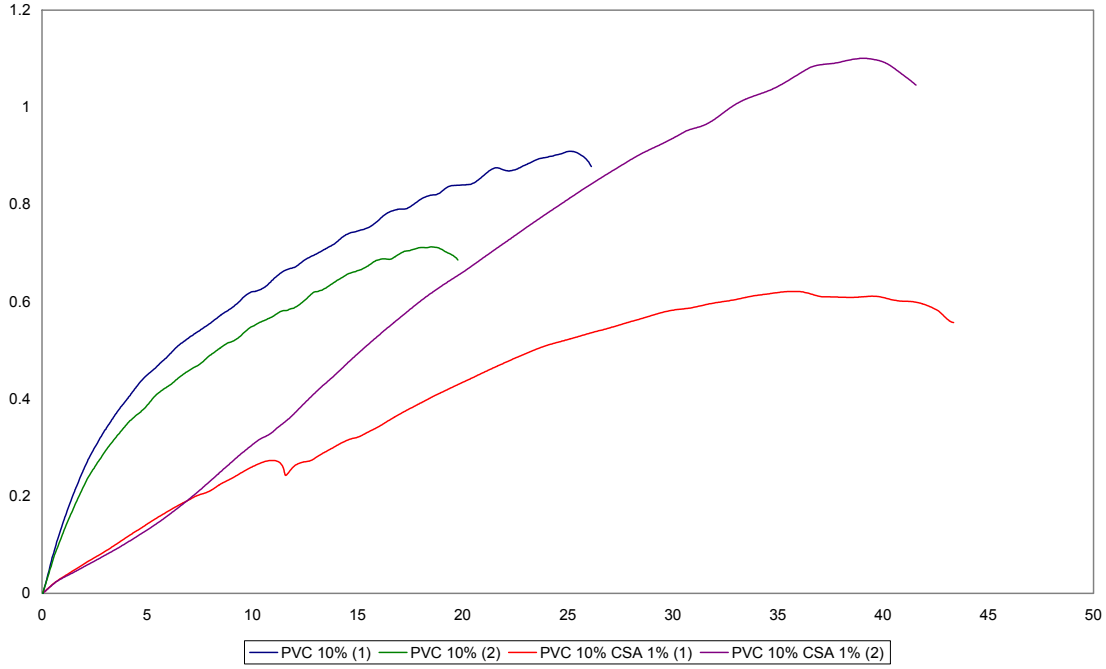

Figure 4.36 Stress-strain graph of fibres electrospun from PVC 10% and PVC 10% CSA 1% in THF/DMF

Sample	Young's Modulus (kPa)	Yield Strength (kPa)	Elongation at Yield (%)	Sample Thickness (mm)
PVC 10 % (1)	144	910	25.48	0.037
PVC 10 % (2)	119	713	18.79	0.037
Average	132	811	22.14	
St. Dev	17	139	4.73	
Sample	**Young's Modulus (kPa)**	**Yield Strength (kPa)**	**Elongation at Yield (%)**	**Sample Thickness (mm)**
PVC 10% CSA 1% (1)	25	611	35.95	0.100
PVC 10% CSA 1% (2)	37	1101	39.38	0.100
Average	31	856	37.67	
St. Dev	8	346	2.43	

Table 4.13 Young's modulus, yield strength and elongation of fibres electrospun from PVC 10% and PVC 10% CSA 1% in THF/DMF

The PVC 10% replicates in the current work also gave different moduli and yield strengths, though the actual stress/strain characteristics were similar. These may be a product of the preparation of the samples for testing, whereby segments of sample had to be cut from a larger component, resulting in some fibre linkages being removed, and possibly decreasing the structural stability of the fibres. It is also likely that these differences were derived from some variability in the electrospinning process, resulting in slight differences in the electrospun fibre mats. It was previously stated that the PVC fibres electrospun by Lee et al. [84] did not possess many point-bonded connections, and that the rigidity of the sample came from friction and entanglement of the fibres [84]. This is a significant issue as it would indicate the elastic modulus would change with changes in density of fibres.

As stated in Section 4.2.4 the electrospun fibre mats in the current work were prepared by electrospinning approximately 300 μL of solution. If the thickness of the mats electrospun from this volume were relatively low it could be assumed that the sample possessed a high fibre density and that the electrospun fibres were tightly packed. Conversely, a thicker sample may imply that the fibre density was relatively low as the electrospun fibres were not packed as closely. However, this assumes that the portion of the 300μL electrospun onto the Mylar® was consistent for all polymer blends. This may or may not have been the case, and it was not determined if the 'efficiency' of electrospinning differs.

A mat possessing a high fibre density would possess relatively high levels of hydrogen bonding and van der Waals forces between fibres, in turn increasing the modulus of elasticity during stretching, similar to suggestions by Nissan and Battern [239]. A greater fibre density would also imply a greater degree of physical entanglement

between the fibres, leading to an increase in the modulus. Whilst the physical dimensions of the sample were taken into account, the entanglement of the electrospun fibres would be difficult to determine, as would the mechanical contribution this entanglement would produce.

The contribution of point-bonding throughout the mat would also be difficult to quantify. It would be expected that a fibre mat with a greater density, and possessing a point-bonded configuration, would have a greater modulus than one with low density and little point-bonding, similar to observations from Lee et al. [84]. Similarly, a mat that exhibits long, straight fibres, devoid of curls, kinks and crimps would also be expected to have a larger modulus compared with a mat possessing these properties [239]. Again, these parameters would be difficult to measure in these mats, and also difficult to accurately quantify.

Furthermore, the overlap of individual polymer chains at any point within an electrospun fibre may vary. That is, in any one cross-sectional area of an electrospun fibre the number of polymer chains may vary, thus leading to a difference in the strength of the individual fibre. Overall these properties make it difficult to analyse the mechanical strength of bundled electrospun fibres using this method and that there is inherent difficulty in comparing these results and those by other researchers.

As Lee et al. [84] pointed out, polyurethane (PU) and PVC exhibit different rigidities due to differences in the point-bonded structure of the fibres as PVC is less tangled than PU. Both of these points are supported by Felbeck and Atkins [234] with respect to the string-spaghetti analogy. Furthermore, at room temperature PU is above its glass

transition temperature (T_g) [272] whilst PVC is below its T_g [238]. Thus it would be expected that PU would exhibit flexibility, while PVC would be stiffer, but more brittle.

Though they did not directly give the M_W of the PVC used in their study, Lee et al. [84] gave the degree of polymerisation as being 800. The degree of polymerisation is a measure of the molecular weight of the polymer, with respect to the number of repeat units in an average chain [238]. Assuming this is the weight-average degree of polymerisation then the M_w of the PVC in Lee et al. [84] study was 50,000. This is slightly less than the PVC employed in this work and indicates that minor differences in molecular weight were not enough to significantly alter the tensile properties of the electrospun fibres, especially considering the M_W of the PVC used in this study was above the entanglement molecular weight of PVC. (The entanglement molecular weight is the minimum molecular weight required for interaction with neighbouring polymer chains. In the case of PVC this value is 5,560 g mol^{-1} [238]).

The presence of 1% CSA in PVC 10% fibres led to some interesting results, noted previously in Table 4.13 and Figure 4.36. Young's modulus decreased by an average factor of 4.5 from 144 and 119 kPa to 25 and 37 kPa respectively, while the strain of the samples almost doubled in comparison to the PVC 10% electrospun fibres. As noted previously, there appears to be some variability in the electrospinning, and hence the results, however it appears the CSA imparts some property that reduces stiffness, but consistently allows the stretching of the nanofibres. It may be that the CSA was plasticising the PVC, reducing the friction between the polymer chains and in turn, the fibres. This is similar to the observations made by Shah and Shertukde [273] who observed a decrease in the tensile strength and increase in the elongation of PVC sheets with the addition of butyl benzyl phthalate. It is important to note that butyl benzyl

phthalate is a recognised plasticiser for PVC, softening the polymer and reducing the mechanical strength. CSA has been noted before as a plasticiser for nitrocellulose by Matsubara & Wakabayashi [274], however there is no literature indicating its effects on the mechanical strength of PVC. From the data here it appears that CSA had an affect on the properties of the electrospun PVC fibres, possibly as a plasticiser, or in the capacity as a lubricant by allowing the electrospun fibres to be pulled out from entangled mat with greater ease.

The thickness of the PVC/CSA electrospun fibrous mat for both samples was 0.100 mm, and for electrospun PVC it was 0.037 mm. As expected, this increased mat thickness, and hence decreased fibre density, did not translate into an increase in the elastic modulus. Overall, it would appear that CSA decreased fibre density, decreased fibre entanglement, reduced the chemical interaction between the fibres and/or actively lubricated the fibres and decreased the friction between them.

4.4.2 PAni/PVC Electrospun Fibres

Young's moduli of PAni 1% PVC 10% electrospun fibres were notably higher than the PVC fibres; however they were still lower than the values observed by Lee et al. [84]. The two samples recorded moduli of 216 kPa and 368 kPa for PAni 1% PVC 10% (1) and PAni 1% PVC 10% (2) respectively. These values plus the elongation at yield are given in Table 4.14, along with the stress-strain graph in Figure 4.37.

The slope in Figure 4.37 was similar for both samples after the yield points, indicating the samples were relatively uniform and the testing regime was not appreciably different between the two tests during this secondary increase in strength. This also indicates that the possibility of physical faults in the samples is unlikely. As the samples were prepared from the same solution and during the same process, it is likely that any

chemical faults in the fibres would be present in both samples, and would be present in both stress/strain plots. Thus, it is likely that variability in electrospinning process itself was responsible for these differences.

Sample	Young's Modulus (kPa)	Yield Strength (kPa)	Elongation at Yield (%)	Sample Thickness (mm)
PAni 1% PVC 10% (1)	216	2608	31.24	0.030
PAni 1% PVC 10% (2)	368	2964	36.11	0.030
Average	292	2786	33.68	
St. Dev	108	252	3.44	

Table 4.14 Young's modulus, yield strength and elongation of fibres electrospun from PAni 1% PVC 10% in THF/DMF

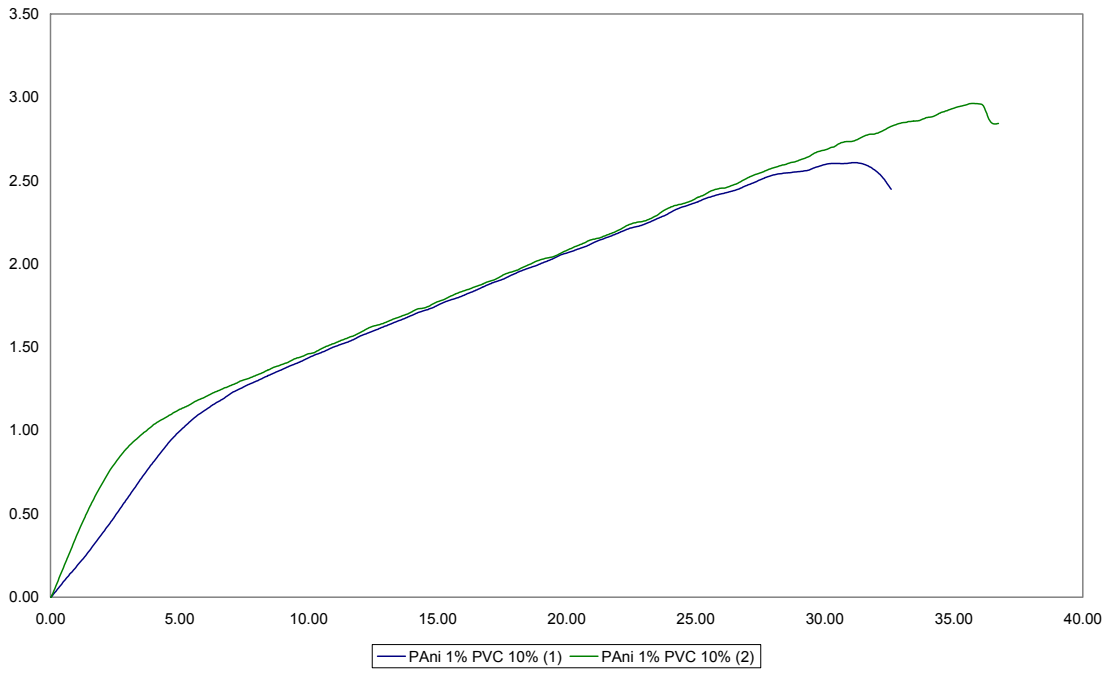

Figure 4.37 Stress-strain graph of fibres electrospun from PAni 1% PVC 10% in THF/DMF

Comparison of PVC and PVC/CSA fibres with the electrospun fibres PAni/PVC in Table 4.13 and 4.14, respectively, indicated the inclusion of PAni increased both the strength and stiffness of the fibres substantially. Young's moduli of PAni/PVC electrospun fibres, 216 kPa and 368 kPa respectively, were approximately twice that for

PVC (144 kPa and 119 kPa), and up to ten times that of PVC/CSA electrospun fibres (25 kPa and 37 kPa). This provides further evidence that PAni interacted with PVC to some extent, increasing the rigidity of the fibrous mat, perhaps a result of the PAni imparting structural strength. The PAni 1% PVC 10% fibre mats were also thinner, and hence had a higher fibre density than PVC electrospun fibres, leading to an increase in Young's modulus. Taking into account the decreased fibre density and elastic modulus for the PVC/CSA fibres, evident by the larger sample thickness for these samples, PAni actively contributed to the mechanical strength of the fibre mat of PAni/PVC.

Pron et al. [275] observed decreases in the elastic modulus of PAni films with increasing plasticiser. They produced pressed films of PAni containing dialky ester bis(2-ethylhexyl) hydrogen phosphate (DiOHP) with elastic moduli of 0.23 GPa and 0.14 GPa for PAni:DiOPH molar ratios of 0.33 and 0.36, respectively. Thus a small change in percentage of the dopant led to a significant decrease in the elastic modulus of the film. This may have occurred in the PAni/PVC fibres containing CSA. Whilst CSA is not noted as an effective plasticiser, there was evidence that it was either acting as a plasticiser or a lubricant in the PVC/CSA fibres. If this affect can be carried to the PAni/PVC fibres, then it is likely that CSA was also reducing the stiffness or lubricating the PAni/PVC fibres. However, from the mechanical testing of the PAni/PVC fibres it appears that PAni contributed more to the increased rigidity of the fibres than the negative effect of CSA. It is also important to note that the doping of PAni by exposure to CSA may have led to this increase, and that un-doped PAni/PVC fibres may exhibit a lower mechanical strength due to differences in the chemical nature of PAni in the doped and un-doped states.

4.4.3 PAni/PVC/TOAB Electrospun Fibres

The inclusion of the ionophore tetraoctylammonium bromide (TOAB) into the blend led to significant changes in the mechanical properties of the electrospun fibres. These results are presented in Table 4.15 and Figure 4.38.

Sample	Young's Modulus (kPa)	Yield Strength (kPa)	Elongation at Yield (%)	Sample Thickness (mm)
PAni 1% PVC 10% TOAB 5% (1)	81	1221	20.91	0.100
PAni 1% PVC 10% TOAB 5% (2)	34	1103	28.26	0.100
PAni 1% PVC 10% TOAB 5% (3)	76	716	16.21	0.100
Average	64	1014	21.79	
St. Dev	26	264	6.07	

Table 4.15 Young's modulus, yield strength and elongation of fibres electrospun from PAni 1% PVC 10% TOAB 5% in THF/DMF

Young's moduli were notably lower than the PAni/PVC (292 kPa) and PVC fibres (132 kPa), with PAni/PVC/TOAB 5% recording values of 81, 34 and 76 kPa for the three replicates. However, Young's moduli for these TOAB samples were higher than the PVC/CSA fibres, which recorded an average modulus of 31 kPa. The maximum yield strength, where maximum stress was achieved, was on average higher for PAni/PVC/TOAB than the PVC and PVC/CSA fibres, but significantly lower than the PAni/PVC electrospun fibres. This indicates the inclusion of TOAB had a detrimental effect on the mechanical properties of the electrospun fibres of PAni/PVC.

There was appreciable variation between the tensile strength of the three replicate electrodes of PAni 1% PVC 10% TOAB 5% (Table 4.15 and Figure 4.38). Though samples (1) and (3) exhibited similar moduli, the maximum yield strength was slightly lower for sample (3), and the strain compared well between samples (1) and (2). This may indicate that some breakage of fibres within the mat occurred for sample (2), reducing the physical properties of entanglement, and in turn reducing the rigidity but

retaining the ability to stretch. If this is the case then it is likely the ionophore affected the chemical properties of the electrospun fibres for samples (1) and (3).

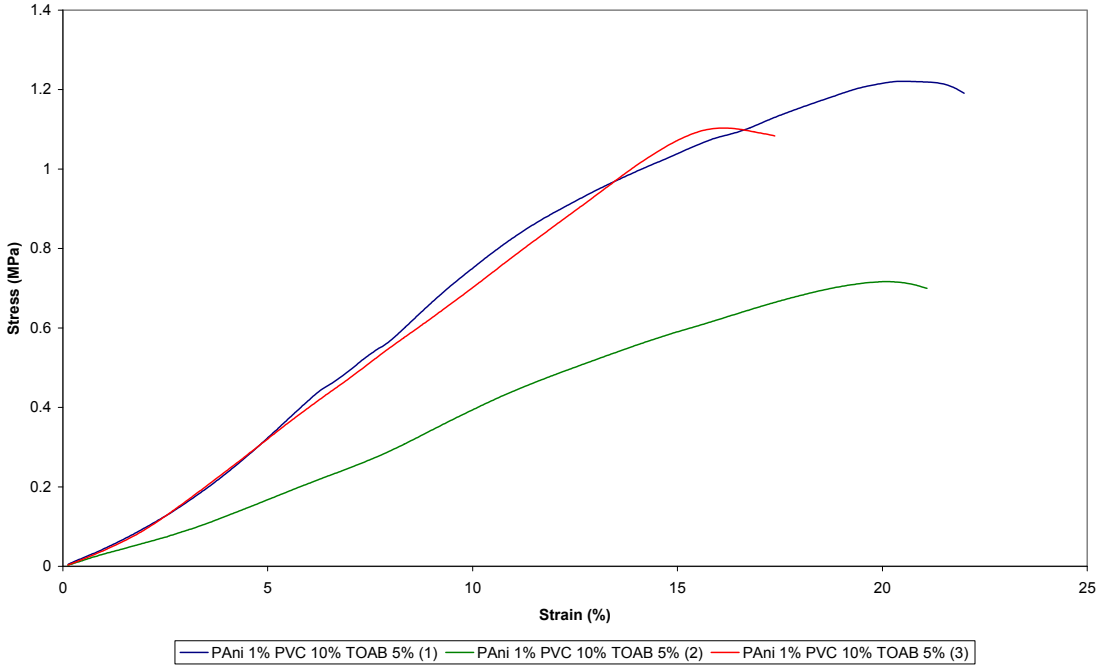

Figure 4.38 Stress-strain graph of fibres electrospun from PAni 1% PVC 10% TOAB 5% in THF/DMF

Whilst quaternary ammonium salts (QAS) are recognised for their ion-selectivity properties, there is also an indication that they extend a plasticisation effect on other materials [276, 277]. Thus TOAB in this case may have been plasticising the PAni/PVC fibres, leading to a decrease in Young's modulus whilst the maximum tensile yield remained comparable to PVC and PVC/CSA fibres. However, Jacobsen and Fritz [278] observed the maximum tensile strength of polylactide (PLA) film decreased with increasing concentration of plasticiser. Matuana et al. [279] and Pita et al. [280] both observed decreases in Young's modulus and the maximum tensile yield of the PVC films when blended with plasticisers. Shah and Shertukde [273] also observed a

decrease in Young's modulus, but an increase in the maximum tensile yield of a PVC film; however they indicated that this was due to the polar nature of the plasticiser. TOAB is a relatively polar molecule due to the large charge discrepancy brought about by the positive nitrogen and the negative bromide, and by the surfactant nature of QAS [184]. It is probable that the ionophore disrupted the interaction between the PAni and PVC, leading to a decrease in the rigidity of the fibres, but not altering the PVC support structure, and thus the maximum yield strength of the fibrous mat. This is supported with previous results (Chapter 2 and Chapter 3) where the presence of ionophores altered the properties of the spinning solution and also produced changes in the morphology of the electrospun fibres.

Another factor that may have influenced the mechanical properties is the fibre density of the samples. The thickness of the all PAni 1% PVC 10% TOAB 5% samples was 0.10 mm. The fibre density is significantly lower than the PAni 1% PVC 10% fibrous mats, indicating that the presence of the ionophore reduced the physical and chemical interaction of the electrospun fibres., or altered the electrospinning efficiency.

4.4.4 PAni/PVC/TDAB Electrospun Fibres

The addition of 5% TDAB produced the strongest fibrous mat of those containing PAni. From Table 4.16 and Figure 4.39, replicate samples produced elastic moduli of 382 kPa and 509 kPa, and a maximum yield strength 3790 kPa and 4492 kPa, respectively. Not only is the modulus comparable with PAni 1% PVC 10% fibres, but the yield strength is noticeably higher. It appears that TDAB imparts far more benefits to the mechanical properties of a PAni/PVC fibre mat than TOAB. It is unknown as to why the stiffness of the PAni/PVC fibres has increased in the presence of this ionophore and not TOAB. The point-bonding of electrospun fibres, reported in Section 3.3.7 and 3.3.9, was

significantly greater for TOAB samples than TDAB samples, and this was not the cause for improvement. However, the longer alkyl chains on TDAB may enhance the interaction between the PVC and PAni, as well as the interaction between the fibres.

Sample	Young's Modulus (kPa)	Yield Strength (kPa)	Elongation at Yield (%)	Sample Thickness (mm)
PAni 1% PVC 10% TDAB 5% (1)	382	3790	20.48	0.051
PAni 1% PVC 10% TDAB 5% (2)	509	4492	29.38	0.051
Average	446	4141	24.93	
St. Dev	90	496	6.29	

Table 4.16 Young's modulus, yield strength and elongation of fibres electrospun from PAni 1% PVC 10% TDAB 5% in THF/DMF

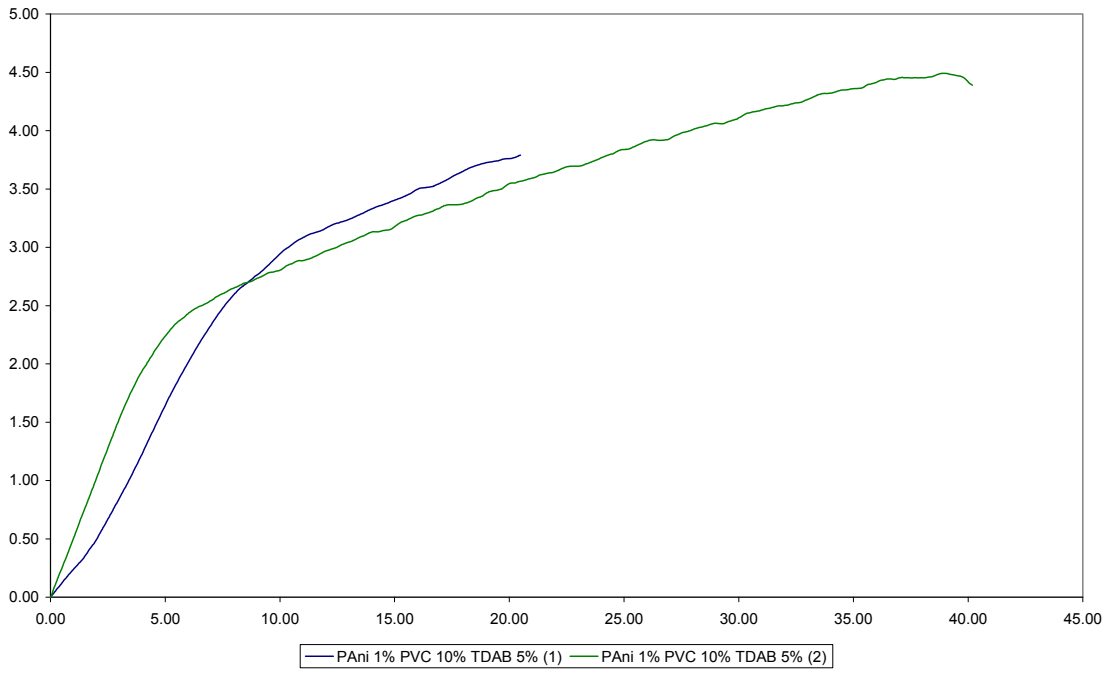

Figure 4.39 Stress-strain graph of fibres electrospun from PAni 1% PVC 10% TDAB 5% in THF/DMF

If TOAB was plasticising the PAni/PVC fibres as previously hypothesised, than TDAB had the opposite effect, altering the conformation of PVC or PAni, increasing the interactions between PAni and PVC, or both. It was noted in Section 4.3.6 that PAni exhibited a change in conformation in the presence of TDAB, leading to a Raman

response that differed to PAni/PVC. It is also possible this effect was a result of anti-plasticisation of the fibrous mat instead of plasticisation.

Anti-plasticisation is the phenomenon whereby a polymer mixed with a small amount of plasticiser will exhibit an increase in the elastic modulus and maximum tensile yield, in conjunction with a decrease in the elongation and disappearance of the secondary transition point [281-283].

Lourdin et al. [282] stated that two hypotheses account for these changes in the polymer properties. In the first hypothesis the plasticiser increases the mobility of the polymer chains, allowing the chains to orientate and reorganize to produce a highly crystalline structure. This increases the polymer strength but reduces its yield at break due to a physical cross-linking effect. According to Guerrero [281] this process occurs in PVC, though there is uncertainty in the role of the solvent, and its influence on the mechanical properties of PVC has not been determined.

Lourdin's second hypothesis is that, instead of mobility, strong interactions occur between the plasticiser and the polymer, also leading to a cross-linking effect as well as crystallisation [282]. In addition Tiemblo et al. [283] state that a decrease in the free volume between the polymer chains leads to a decrease in chain motion, thus increasing the strength.

The increase in the elastic modulus and maximum yield strength indicated that anti-plasticisation may have occurred in the PAni 1% PVC 10% TDAB 5% fibres; however only one sample recorded a reduced elongation. This is problematic especially given the fact that the elongation of sample (2) was comparable to the PAni 1% PVC 10% fibres and Guerrero [281] reports that the anti-plasticisation of PVC leads to a reduction in the

stretching of the sample. In addition, the modulus between the two samples was quite different again with sample (1) having a lower stiffness. Thus it is difficult to conclude whether TDAB produced an anti-plasticisation effect or not, however it is clear that the introduction of TDAB altered the properties of the PAni/PVC blend significantly.

The electrospun fibres observed in Section 3.3.7 for PAni/PVC/TOAB and Section 3.3.9 for PAni/PVC/TDAB showed a comparable morphology with no significant differences. Furthermore the fibre diameters of these two samples in Chapter 3 were effectively identical. The only major difference between the two samples was the thickness of the material used for tensile testing. The PAni/PVC/TOAB sample was twice as thick as the PAni/PVC/TDAB sample, indicating the TDAB fibres were much denser than the TOAB fibres.

Based on the assumption that less dense samples are weaker, it is likely that the density was responsible for the differences in the mechanical strength of the electrospun fibres. Thus it appears the ionophore has significantly altered the solution properties (i.e. viscosity, conductivity and surface tension) of the spinning solution, leading to an increase in fibre density by altering the electrospinning process.

4.4.5 MWNT/PVC Electrospun Fibres

Though it was expected that the introduction of MWNT into a PVC blend would increase the structural integrity, leading to an increase in both Young's modulus and the maximum yield strength, this was not observed. Table 4.17 and Figure 4.40 present the tensile test results of three replicate MWNT 0.5% PVC 10% electrospun mats.

The uniformity in the mechanical aspects of the samples compared with previous PVC blends is quite good. Young's modulus for the three samples were 102 kPa, 105 kPa and 103 kPa, and the maximum tensile yields were 1303 kPa, 1473 kPa and 1356 kPa, respectively. These values were not dissimilar to those for PVC 10% electrospun fibres. This indicates that the addition of MWNT did not significantly alter the structural strength of the fibrous mat.

Sample	Young's Modulus (kPa)	Yield Strength (kPa)	Elongation at Yield (%)	Sample Thickness (mm)
MWNT 0.5% PVC 10% (1)	102	1303	31.46	0.080
MWNT 0.5% PVC 10% (2)	105	1437	29.85	0.080
MWNT 0.5% PVC 10% (3)	103	1356	31.70	0.080
Average	103	1365	31.00	
St. Dev	1	67	1.01	

Table 4.17 Young's modulus, yield strength and elongation of fibres electrospun from MWNT 0.5% PVC 10% in THF/DMF

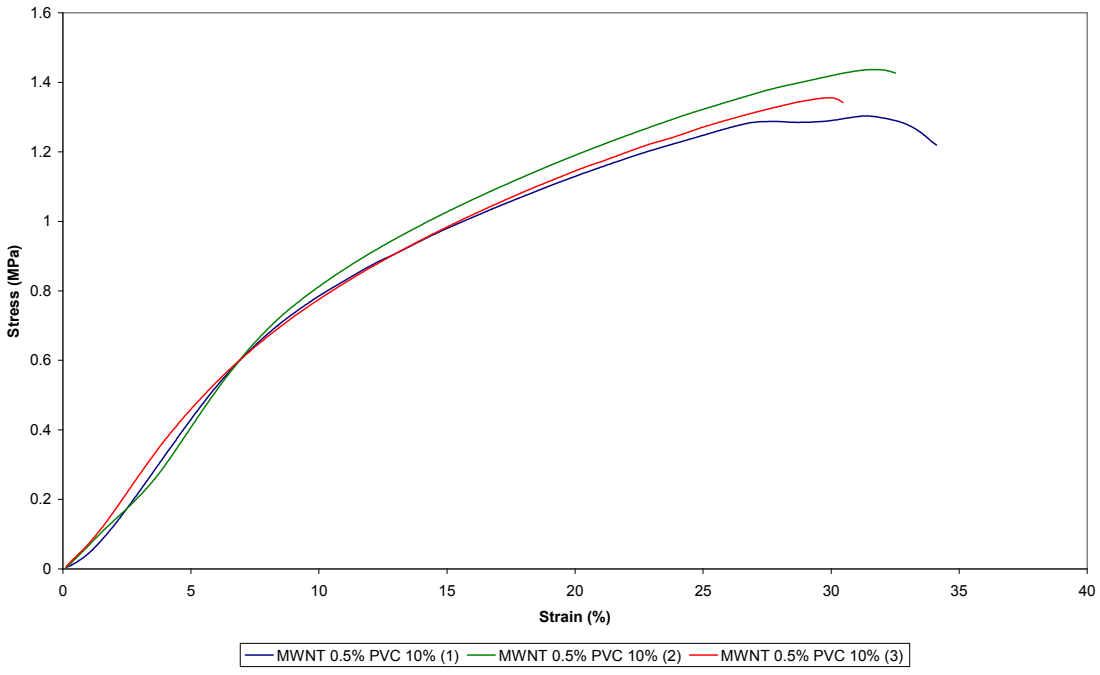

Figure 4.40 Stress-strain graph of fibres electrospun from MWNT 0.5% PVC 10% in THF/DMF

The increased thickness of the electrospun MWNT/PVC fibrous mats compared with both PVC 10% and PAni 1% PVC 10% electrospun mats indicated that the presence of MWNT altered the electrospinning process, and in turn decreased the fibre density. Previous data and discussion suggests that if the fibre density is high an increase in the mechanical strength occurs. Thus the presence of MWNTs are actually detrimental to the morphological and mechanical properties of the MWNT/PVC fibre mats, and do not provide any structural support.

Literature has reported the introduction of MWNT can lead to an increase in the strength of polymer composites [214, 284-288]. This increase may be the result of different properties imparted by the MWNT. Ruan et al. [287] observed MWNT acting as nucleating centres allowing secondary polyethylene (PE) crystallites to form, leading to an increase in the ductility of the material. In addition an increase in the strength of the composite material was also observed due to the load-bearing effect of the MWNT, whereby the MWNT would embed and intertwine with polymer chains. Jung et al. [284] chemically bonded the carbon nanotubes to polyurethane (PU), cross-linking the PU to MWNT which in turn led to an increase in both the tensile strength and the elastic modulus. Gong et al. [286] reports that the addition of MWNT to epoxy increased the elastic modulus by more than 30% in the presence of a surfactant, even though the MWNT were not homogenously dispersed through the sample. They indicated that the surfactant may interact with both the MWNT and the epoxy resin through hydrophobic and hydrophilic interaction. They also note the blend of MWNT and epoxy without the surfactant produced only moderate gains in the mechanical properties of the blend.

According to Breuer and Sundararaj [285] there are two variables that control the strength of nanotube (NT) composites. Firstly, the interfacial interaction between the nanotubes and the matrix must be strong. Weak interaction leads to the nanotubes

behaving as defects or gaps within the composite rather than contributing to the mechanical strength. Secondly, the dispersion of the nanotubes also influences the mechanical strength of polymer composites. If the nanotubes are not dispersed they possess less interaction with the composite material and the applied force will instead pull the aggregates apart rather than individual nanotubes, leading to significantly reduced strength. In addition Andrews and Weisenberger [214] state the degradation of nanotubes due to processing will also lead to decreased strength.

It is unlikely that the dispersion of MWNT in PVC electrospun fibres contributed to the poor mechanical strength. It was detailed in Section 4.3.12 that the MWNT appear to be dispersed throughout the PVC fibres when examined using Raman spectroscopy. However, it is possible that the quality of the MWNT may have had a significant bearing on the tensile strength of the electrospun fibres. As noted by Andrews and Weisenberger [214] the degradation of nanotubes due to processing can lead to a decrease in their mechanical properties. The MWNT quality was previously noted to be relatively low by Raman analysis in Section 4.3.10. Thus, if there were amorphous carbon or poor quality nanotubes then the strength of these components would have compromised the strength of the electrospun fibres. The interaction between the MWNT and the PVC may also have contributed to the weakness in these fibres. Taking into account the low fibre density for MWNT/PVC, comparison of the elastic moduli between PVC fibres and the MWNT/PVC fibres indicate the MWNT contributed to the overall rigidity and strength of the mat, albeit to a small extent. As these nanotubes were approximately 1-2μm in length, the interaction would have been only over a very short length.

The addition of the anionic surfactant dodecylbenzenesulfonic acid (DBSA) to a MWNT/PVC blend in THF/DMF did not increase the mechanical properties of the mat,

but instead produced wide variation in both Young's modulus and the maximum tensile yield. These values for the five replicate samples are reported in Table 4.18, and the stress-strain graphs are given in Figure 4.41.

Sample	Young's Modulus (kPa)	Yield Strength (MPa)	Elongation at Yield (%)	Sample Thickness (mm)
MWNT 0.5% PVC 10% DBSA 1% (1)	23	554	40.87	0.040
MWNT 0.5% PVC 10% DBSA 1% (2)	25	503	44.40	0.040
MWNT 0.5% PVC 10% DBSA 1% (3)	65	914	23.43	0.040
MWNT 0.5% PVC 10% DBSA 1% (4)	108	2070	32.79	0.040
MWNT 0.5% PVC 10% DBSA 1% (5)	168	1024	12.92	0.040
Average	78	1013	30.88	
St. Dev	61	632	12.89	

Table 4.18 Young's modulus, yield strength and elongation of fibres electrospun from MWNT 0.5% PVC 10% DBSA 1% THF/DMF

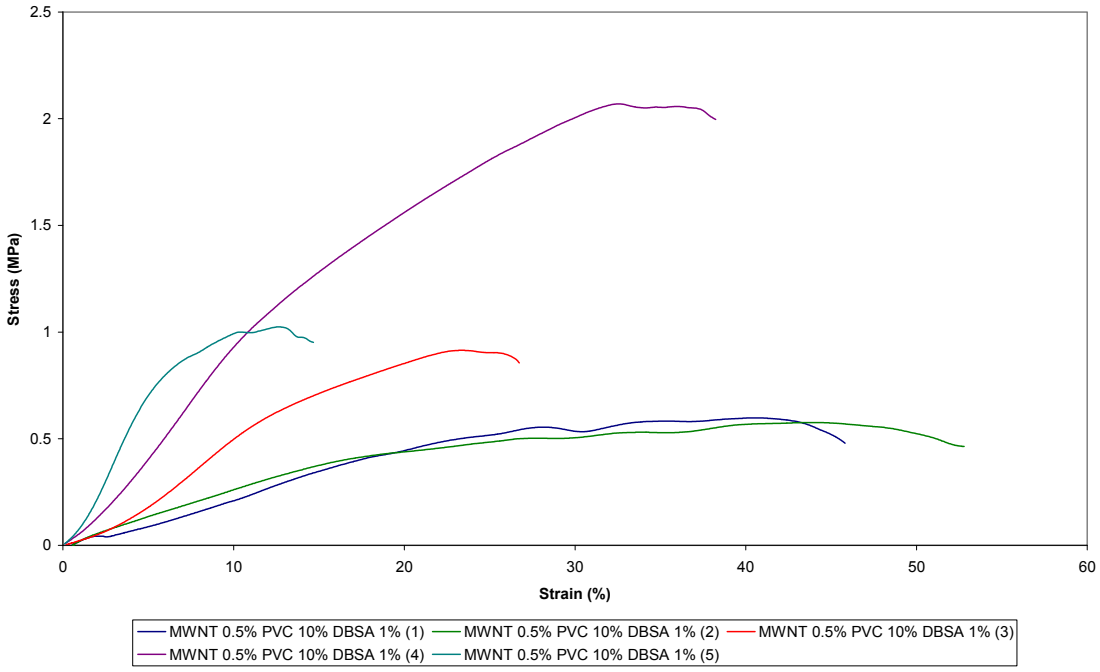

Figure 4.41 Stress-strain graph of fibres electrospun from MWNT 0.5% PVC 10% DBSA 1% in THF/DMF

Samples (1)-(3) had significantly low values for Young's modulus, and also lower values for the maximum tensile yield compared with MWNT/PVC fibres. Only samples (4) and (5) recorded values comparable to the previous MWNT/PVC analyses, with sample (4) recording a modulus value of 108 kPa and a maximum tensile yield of 2070 kPa, whilst sample (5) recorded 169 kPa and 1024 kPa, respectively. These two samples presented quite different values to all other samples of MWNT/PVC/DBSA and MWNT/PVC with sample (5) recording a modulus 60% higher than sample (4).

On the other hand the maximum tensile yield of sample (4) was over twice that of sample (5). These variations are extremely large and may be a result of the introduction of DBSA. Previously it was observed that PVC solution containing CSA produced electrospun fibres that varied greatly in their properties. As postulated earlier with regards to CSA, the DBSA may have been acting as a plasticiser, thus altering the nature of the electrospun fibres. It is important to note that the thicknesses of the analysed samples were notably higher than the MWNT/PVC without DBSA, indicating the presence of DBSA does alter the electrospinning process. It is also possible that in all five samples the preparation resulted in some fibre linkages being removed, and possibly decreasing the structural stability of the fibres, or the DBSA produced defects in the electrospun fibres.

4.5 Conclusions

Raman spectroscopy of PVC and PAN powder were consistent with literature, but more importantly the intensity of these polymers compared with PAni was significantly lower. This excluded assignments corresponding to either PVC or PAN in fibrous mats containing PAni. This was also the case for quaternary ammonium salts, and was a result of fluorescence of the PAni within the samples.

The Raman spectroscopy of electrospun fibres provided strong evidence that PAni was significantly affected by other constituents of the spinning solution. It was observed that electrospun PAni/PVC fibres exhibited characteristics of primary doping, whilst electrospun PAni/PAN fibres exhibited evidence of secondary doping and conformational change of the PAni chain. It was postulated that the greater polarity of the PAN chain, due to the significant dipole on the cyano-groups, was responsible for this change in conformation, providing a support structure for the PAni chains. However, there was also evidence that the PAni was not completely doped, which indicated that the degree of doping differed throughout the electrospun fibres.

The addition of TDAB and TAEAB to PAni/PVC samples led to further evolution of a Raman band corresponding to secondary doping/conformation change of PAni, previously observed in the PAni/PAN electrospun fibres. However, this shoulder was present only in electrosprayed particles for all PAni/PVC/ionophore samples, and within the electrospun fibres of PAni 1% PVC 10% TDAB 10%. This shoulder was not present in the spectra of electrospun PAni/PVC fibres for lower concentrations of TDAB or TAEAB. Thus from this it was concluded that TDAB and TAEAB actively assisted the uncoiling of PAni within the PAni/PVC spinning solution.

These characteristics were also observed for PAni 1% PAN 3% TDAB 0.5%, in that the Raman spectra for electrospun fibres did not exhibit the band at ~1370 cm^{-1} corresponding to changes in conformation of PAni, though the particulate PAni did. However, this shoulder did evolve for higher concentrations of TDAB in the spectra of electrospun fibres, further evidence that QAS alter the degree of doping of PAni within the electrospun fibres.

Additionally, these differences for PAni/PAN and PAni/PVC samples in the presence or absence of an ionophore indicated that the properties of the electrospun PAni/PAN fibres were greatly dependent on the relationship between PAni and PAN, but this was less so for PAni/PVC fibres. Thus the interaction between PAni and the support polymer ultimately dictates the chemical properties of the electrospun fibres in the presence of an ionophore.

Spot analyses and dispersion maps of PAni/polymer indicated that whilst particulate PAni was electrosprayed onto the fibre mat, the underlying fibres possessed relatively uniform PAni dispersion for all samples. This was also the case for MWNT/polymer samples with good dispersion observed in the electrospun fibres, but it was also noted that the MWNT employed in these samples were relatively impure, and contained other carbonaceous material besides MWNT.

Tensile testing of electrospun fibres indicated that the introduction of PAni to PVC increased the mechanical strength of these fibres, possibly due to PAni imparting its own mechanical properties, and due to an increase in fibre density in the electrospun samples, leading to greater fibre entanglement. The tensile testing of samples of PVC/CSA indicated CSA acts a plasticiser or lubricant, reducing the mechanical

stiffness of the electrospun fibres or allowing individual fibres to pull-out from the entangled mat, unlike PVC samples. The properties of PAni overcame these negative affects of CSA.

The addition of TOAB led to a significant decrease in the mechanical strength of PAni/PVC electrospun fibres, by possibly disrupting the PAni/PVC interaction and hence individual fibre strength. This result may also have been due to the lower fibre density of the electrospun samples leading to a decrease in fibre entanglement, and in turn the physical interaction of the fibres.

Fibre samples of PAni 1% PVC 10% TDAB 5% were not affected in the same manner as PAni/PVC/TOAB samples. Instead Young's modulus increased, as did the maximum yield strength. It was postulated that this may have been a result of anti-plasticisation, where crystallisation takes place within the polymer structure, leading to an increase in the strength of individual fibres, or that there was some cross-linking between the polymer chains. It was also suggested that this response was due to an increase in the fibre density of the samples, however it was clear that TDAB contributed positively to the strength of the electrospun fibres.

The mechanical strength of MWNT/PVC and MWNT/PVC/DBSA fibre samples was less than expected. It was anticipated that presence of MWNT would have imparted the structural properties associated with this material, and would have led to an increase in the mechanical strength of the electrospun fibres. Instead Young's moduli and the maximum yield strength were much lower than the corresponding PVC electrospun fibres. It was suggested that the low quality of the MWNT, observed in Raman

spectroscopy, or a lack of interaction with PVC may have resulted in fibres with poor mechanical properties.

Chapter 5 - Electrochemical Characterisation

"For a smart material to be able to send out a more complex signal it needs to be nonlinear. If you hit a tuning fork twice as hard it will ring twice as loud but still at the same frequency. That's a linear response. If you hit a person twice as hard they're unlikely just to shout twice as loud. That property lets you learn more about the person than the tuning fork."

Neil Gershenfeld, from *When Things Start to Think* (1999)

5.1 Introduction

For any conducting polymer to act as a useful component of an electrospun fibre, it must be either electroactive and/or conductive. Cyclic voltammetry is a useful way of studying the redox mechanism of PAni, in combination with changes in the cycling solution composition [46, 263, 289]. This section will present an electrochemical analysis of electrospun PAni/PVC and PAni/PAN fibre electrodes, both with and without ionophores, and evaluate these electrodes for use as sensor for NO_3^- in aqueous solutions.

5.1.1 Cyclic Voltammetry of Polyaniline

PAni can be both synthesised, as noted in Section 1.1.2, and characterised by cyclic voltammetry to produce a characteristic oxidation/reduction response. A typical voltammogram of PAni is presented in Figure 5.1 with the peaks correlating to the transformation of PAni to different oxidation states, as indicated in the voltammogram.

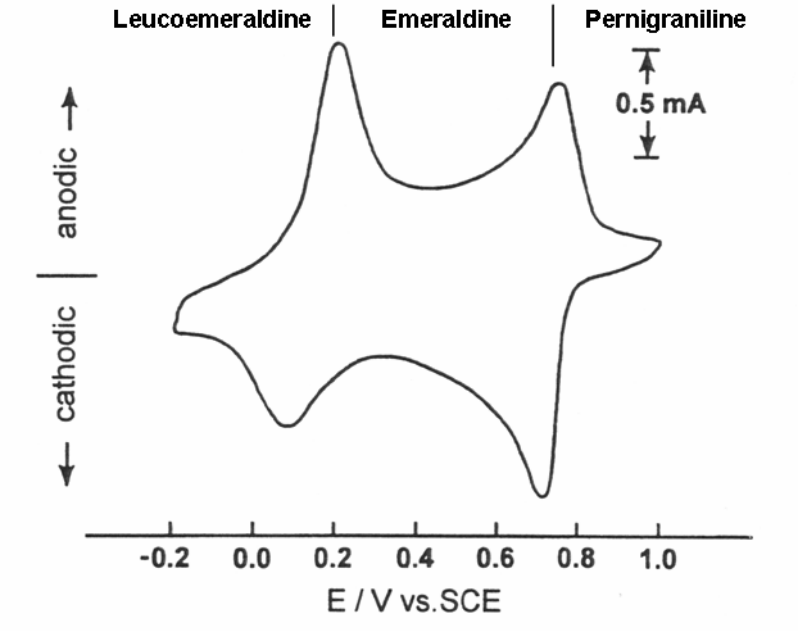

Figure 5.1 Cyclic voltammogram of PAni in 1.0M $HCl_{(aq)}$ [27]

According to Huang et al. [28] PAni synthesised chemically or electrochemically is identical in electrochemical response, however the shape of PAni voltammograms can alter according to film thickness [5], scan rate [290], degradation of PAni [290], the dopant acid [291-294], the counter-ion in solution [22, 289, 295, 296], the concentration of PAni within a composite [297] and the type of composite [298], and the pH of the electrolyte solution [28, 46].

During electrochemical polymerisation of aniline, the oxidation and reduction peak currents will increase, indicating growth of the polymer and increasing thickness of PAni, and the peak potentials may shift. In addition, a higher scan rate will lead to a proportional increase in the redox currents which is dependent on the electroactivity of the PAni [297], and the kinetic electron-limited transfer between the underlying electrode and the attached PAni [5, 299, 300]. Evidence of this electron dependent transfer was reported by Andrieux et al. [299] using an PAni ultra-microelectrode that showed the initial oxidation peak associated with the oxidation of leucoemeraldine to emeraldine did not shift in potential with an increasing scan rate up to 10,000 V/s.

The degradation of PAni can lead to the production of other peaks within its cyclic voltammogram. Genies et al. [301] reported the evolution of a third peak between the redox peak corresponding to emeraldine formation and that corresponding to pernigraniline formation. It was suggested that this peak is associated with the cross-linking of PAni chains, however Pruneanu et al. [292] note that this peak was the result of degradation products of benzoquinone and hydroquinone. Genies et al. [301] reported that washing a PAni film with acetone or dimethylsulfoxide did not change the electrochemical characteristics of the film, indicating that the product was not soluble

oligomers. In contrast Trivedi [302] also reported a third peak between the emeraldine and pernigraniline peaks related to the adsorption of quinone and hydroquinone created during electrochemical deposition of PAni. Trevedi also states the intensity of this peak increases with a spike of quinone and hydroquinone added to the supporting electrolyte. This third peak was also reported by Motheo et al. [293] as a degradation peak, and they noted that the type of dopant acid employed during growth can alter the presence of this peak. Specifically dopant acids with a high-molecular weight had a smaller degradation peak compared to HCl, and this may have been due to a decrease in the polymerisation rate of PAni for these high molecular weight dopants.

Additionally, Pruneanu et al. [292] reported a change in the electrochemistry of PAni during electrochemical synthesis in the presence of different dopant acids. Specifically PAni films were prepared in either 1 M perchloric acid ($HClO_4$), trichloroacetic acid (CCl_3COOH) or chloroacetic acid ($CClH_2COOH$). The peak potential for the first redox pair (leucoemeraldine to emeraldine) for the PAni film prepared in the presence of $HClO_4$ did not shift with increasing scan rate, but both peaks of the second redox pair (emeraldine to pernigraniline) did shift towards negative potentials. The PAni film grown in the presence of CCl_3COOH exhibited positive potential shifts for the first redox pair whilst the oxidation peak for the second redox pair became broader. Pruneanu et al. state that this was the result of a more difficult charge-transfer step. The last film of PAni synthesised in the presence of $CClH_2COOH$ produced a single broad redox pair, with a positive potential shift for the oxidation process and a negative potential shift for the reduction process. They surmised that the changes in the shapes of the voltammograms were a result of differences in the electrostatic interaction of the dopant acid with the ‘chemically flexible -NH- groups’ of PAni, and that these are due to the different structure and molecular weight of the anions [292].

Grzeszczuk and Szostak [303] also reported a change in the electrochemical response of an electrochemically grown PAni film after replacing HCl with tribromoacetate (CBr_3COOH) as the supporting electrolyte. Both the oxidation and the reduction peaks altered in response to the change in the solution electrolyte. This can be clearly seen in Figure 5.2.

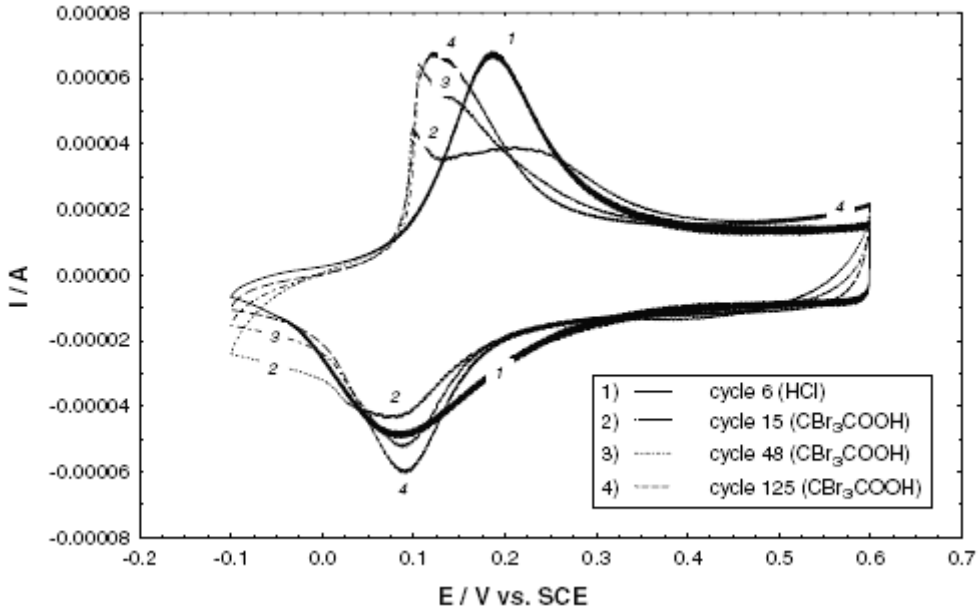

Figure 5.2 The response of a PAni-HCl electrodeposited film with a change in the supporting electrolyte anion [303].

The voltammogram shows two oxidation peaks corresponding to Cl^- (voltammogram 1) and CBr_3COO^- (voltammograms 2 to 4). The peak current associated with Cl^- at ~0.20 V decreases with an increasing number of scans in the presence of CBr_3COO^-, until eventually it disappears. The second peak associated with CBr_3COO^- appears at ~0.10 V in voltammogram 2 and subsequently increases in current and shifts slight to ~0.15 V in voltammogram 4, indicating ion exchange of the CBr_3COO^- for Cl^-. Grzeszczuk and Szostak also reported the redox hysteresis of the redox peaks of PAni. Hysteresis is the 'delay' in a response behind its cause and, in this context, refers to the delay in charge-

transfer of PAni. The separation of the redox peak potentials between the oxidation peak and the reduction peak of the cyclic voltammogram of PAni is a measure of this. According to Grzeszczuk and Szostak, the hysteresis of a PAni electrode is dependent on the thickness of the film, the concentration of the supporting electrolyte and the electrolyte temperature. In an earlier study [304] they suggested that the hysteresis of PAni differed with different counter-ions, and this was a result of molecular interactions with the ions and different redox forms of PAni. In this later study [303] incorporating trihalogenoacetate counter-ions (i.e. trifluroacetate, trichloracetate and tribromoacetate) they concluded the type of counter-ion employed significantly affected the hysteresis of the PAni electrode, and the degree of hysteresis decreased with decreasing size of the trihalogenoacetate ion.

The composition of a PAni/polymer blend has also been reported to affect the electrochemical characteristics of PAni. Namazi et al. [297] reported an electroactive PAni/PVC blend with a percolation threshold of 0.007% w/w PAni. The electroactivity of this blend was low compared with PAni/PVC blends containing a higher PAni content, as the voltammogram exhibited two oxidation peaks and only a single, broad reduction peak. Hosseini and Entezami [298] also observed changes in the electrochemical response of PAni in three different composites. Voltammograms of PAni/PVC, PAni/polystyrene (PS) and PAni/poly(vinyl acetate) (PVAc) were all markedly different. PAni/PVC produced two redox pairs characteristic of PAni, however both PAni/PS and PAni/PVAc exhibited only one redox couple. Hosseini and Entezami state that this was a result of the composites quickly transferring ions, and low levels of doping. Yang et al. [305] reported the electrochemical properties of blends of PAni/poly(vinyl phenylmethylamine) (PVBMA) and PAni/poly(vinyl benzylmethylamine) during growth of the films. These composites exhibited different

electroactivity when electrochemically grown in DMF/water solutions containing 0.1 M aniline and 0.1 M H_2SO_4, and it was suggested that these differences were a result of bulky groups on PVBMA decreasing the interaction between PVBMA chains. This decreased interaction allowed PAni to create a conducting network.

The pH of the supporting electrolyte solution has been identified as a significant factor in the electrochemical response of PAni. According to Ping et al. [41] PAni will undergo oxidation from leucoemeraldine to pernigraniline when cycled at any pH greater than 4. They conclude in a pH range of 4-6 the non-protonated leucoemeraldine oxidises to a partially protonated pernigraniline state via a partially protonated emeraldine state. Above pH 6 PAni oxidises from a non-protonated leucoemeraldine state to a non-protonated pernigraniline state via a non-protonated emeraldine state [41]. The oxidation of leucoemeraldine to emeraldine is pH independent above pH 1; however, this is not the case for the emeraldine to pernigraniline oxidation, which is pH dependent in the pH range of 1-3. As a result the peak potential of the second redox couple decreases with increasing pH, until eventually the two redox couples overlap at ~pH 5 [28, 46]. This new single redox couple is also pH dependent, and according to Lukachova et al. [43], the sum of the area of the individual redox peaks at low pH are equal to the area of the single peak at high pH, assuming no loss of electroactivity. Ye and Baldwin [22] reported increases in the current response of PAni films in an acetate buffer with the addition of anions at pH 5.45. They postulate that the PAni response at this pH may be a result of employing the correct electrolyte anion, and that the anion offsets the build-up of positive charges within the oxidised film. The influence of the counter-ion has also been implicated in the response in terms of pKa [295], such that the presence of different counter-ions could lead to different pKa values for the protonation of PAni in acetate solutions.

5.1.2 Cyclic Voltammetry & Sensors

Cyclic voltammetry has been used as a signal generator in conjunction with a number of specific working electrodes. Aussawasathien et al. [16] utilised cyclic voltammetry in the detection of glucose and hydrogen peroxide where redox currents from PAni/PS electrodes were found to be proportional to glucose and hydrogen peroxide concentrations. These currents were plotted, with respect to the weight of the deposited polymeric material to account for differences between the electrospun fibre electrode and the polymer film electrode, to produce a linear electrochemical response with increasing concentration of these species.

Nguyen et al. [306] studied different PPy electrodes using cyclic voltammetry with different counter-ions to produce a polymer sensor array. This array was used to evaluate detection and discrimination between potassium and methylamine electrolyte solutions using the pattern recognition method of principal component analysis (PCA).

Thompson et al. [307] produced a PPy electrode that detected the hybridisation process of DNA. DNA oligomer molecules were immobilised on the surface of the PPy by forming a bidentate complex between Mg^{2+} and an alky phosphonic acid group on the PPy, and the phosphate group on the DNA. The hybridisation produced a decrease in the current response in PPy. This current decrease was the result of the negatively charged complementary 27-unit oligonucleotide preventing the passage of chloride at the PPy/solution interface. Non-complementary oligonucleotides did not lead to a change in current as the oligonucleotide did not hybridise with the immobilized DNA oligomer and thus allowed the exchange of chloride.

5.1.3 Electrospun Sensors

There are a limited number of studies on electrospun fibres for sensor applications, although these ultrafine fibres have been touted as possibly useful in such applications as optical, gas and biomaterial sensing [16, 59, 60, 62, 64, 74-76, 308-310].

Wang et al. [60, 76] developed an electrospun membrane based on the synthesis of a fluorescent polymer from pyrene methanol and poly(methyl methacrylate) (PMMA). This membrane utilised fluorescence as a detector for 2,4-dinitrotoluene (DNT) in which the DNT would quench the fluorescing pyrene chromophores in proportion to its concentration. They observed that the electrospun membrane was far more sensitive to DNT than a continuous film, and that this was a direct result of the higher surface area of the electrospun fibres. They also prepared electrospun electrodes for metallic ions and DNT detection using poly(acrylic acid) (PAA) and poly(pyrene methanol) and again observed increased sensitivity compared to continuous thin films [310].

Wang et al. [64] also prepared an electrospun biochemical sensor for the detection of the herbicide methyl viologen. This sensor also utilised fluorescence whereby methyl viologen would quench the fluorescence of hydrolysed poly[2-3(3-thienyl)ethanol butoxy carbonyl-methyl urethane] (H-PURET). The sensor itself was produced by electrospinning cellulose acetate (CA) onto a target and then H-PURET was electrostatically assembled onto the surface of the CA fibres. This sensor was sensitive to methyl viologen at levels as low as 10^{-8} mol L^{-1}. They attributed this sensitivity to the high surface area to volume ratio of the electrospun fibres in addition to the localisation of the quenching group on the surface of the electrospun CA fibre.

An ammonia sensor was prepared by Ding et al. [309] by the electrospinning of a poly(vinyl alcohol) (PVA) and poly(acrylic acid) (PAA) solution onto a quartz crystal microbalance (QCM). The PAA could not be electrospun from water due to strong hydrogen bonds between the water and carboxyl groups of PAA. Thus PVA was used as a support polymer for the electrospinning. These electrospun samples were compared to continuous film samples coated onto QCMs. They reported that the PAA interacts with basic gases such as NH_3, and that the nanofibres produced faster response times for the detection of NH_3 with better sensitivity. Further work by Ding et al. [62] led to the production of an electrospun sensor for NH_3 based only on PAA and not a composite blend. This sensor also employed QCM for detection and they observed a notable increase in the sensitivity towards NH_3 in the order of ppb, as well as a higher sensitivity compared with continuous films of PAA.

Aussawasathien et al. [311] studied the use of electrospun $LiClO_4$ doped PEO for use as a humidity sensor. They observed a decrease in the resistance of electrospun fibrous mats with increasing humidity. However, the electrospun fibres would deform and collapse in the presence of moisture. They also observed that the initial resistance of the electrospun fibre mat was far more than that of a film. They suggested that this was a result of the porous nature of the electrospun sample and also the testing regime where the analysis was based on volume resistivity rather than the individual fibres.

One of the first conducting polymer electrospun sensors was prepared by Wannatong et al. [140] for the determination of gaseous acetone. They blended chemically synthesised polypyrrole (PPy) and polystyrene (PS) in NMP and electrospun the resultant solution. They observed an increased sensitivity to acetone vapour for the electrospun mat compared with a continuous film of the PPy/PS. They also observed that the electrospun

samples required a greater time to equilibrate compared to the film. They suggested that this was a result of the high surface area of the electrospun samples, as the PPy in the electrospun samples has a greater number of exposed active sites. They hypothesised that the response time of the electrode would be improved if the fibrous mat were more porous.

Possibly the first electrospun polymer sensor containing the conducting polymer polyaniline (PAni) was constructed by Liu et al. [312]. In this work they electrospun single nanofibres of PAni/PEO across four-terminal gold electrodes to study the detection of NH_3 by changes in the conductivity of PAni. This produced a sensor that was sensitive to NH_3 gas down to 0.5 ppm. They also observed that the diameter of the individual fibres contributed to the response times of the sensors where a smaller diameter fibre would produce a faster response time.

Aussawasathien et al. [16] also produced a hydrogen peroxide sensor by electrospinning solutions of PAni/PS, and a glucose sensor by immobilising glucose oxidase (GOX) onto the surface on the electrospun PAni/PS. The electrospun devices produced a higher sensitivity to the H_2O_2 compared with a continuous film of PAni/PS, and also produced linear redox current responses to H_2O_2. The GOX-immobilised electrospun fibres also exhibited a greater sensitivity to glucose compared with a continuous film. Again this was due to the higher surface area of the fibres which allowed a greater amount of GOX to be immobilised on the surface of the fibres compared with the surface of a continuous film.

5.2 Preparation of Samples

5.2.1 PAni/Polymer Solution Preparation

PAni (1%) was weighed and added slowly to a scintillation vial containing suitable volumes of solvent and the appropriate amount of dissolved CSA to dope the polymer to emeraldine salt, and allowed to dissolve. The commodity plastic was then added and the mixture was stirred overnight prior to electrospinning. If required, other additives such as quaternary ammonium salts (QAS) were added to the CSA/solvent solution prior to the addition of PAni and allowed to dissolve. Further details of solution preparation can be found in Section 2.3 Preparation of Samples.

5.2.2 Electrospun Fibres

Electrospun fibres were manufactured by withdrawing 100 μL of the pre-prepared polymer solutions by Eppendorf® pipette, and placing the pipette on a length of platinum wire attached to a coaxial cable. A high potential was applied, leading to the fabrication of electrospun fibres that were collected on grounded rotating gold-coated Mylar® targets. Further details of electrospinning can be found in Section 3.2 Preparation of Samples.

5.2.3 Analysis of Samples

Cyclic voltammetry was carried out in a three electrode cell controlled by a MacLab potentiostat connected to a PowerLab interface (Model 400, ADInstruments). The three electrode system was comprised of an Ag/AgCl reference electrode, stainless steel mesh auxillary electrode and a working electrode consisting of polymer samples electrospun on gold-coated Mylar®. All cyclic voltammetry data was managed by EChem software

(Version 1.5.2).The instrument was calibrated monthly using a solution of 0.006 M $K_2Fe(CN)_6$ in 1.0 M KNO_3.

A stock buffer solution of 0.1M CH_3COOH and 0.1M CH_3COONa (pH 4.62) was prepared. A HCl/KCl solution of 0.1M HCl and 0.1M KCl was also prepared. Changes in solution concentration and concentrations of anion species are noted in the individual voltammograms. Samples were analysed under different voltammetric conditions outlined in Table 5.1 below.

Initial Potential (V, vs. Ag/AgCl)	-0.30	Upper Potential (V, vs. Ag/AgCl)*	0.60 and 0.75
Lower Potential (V, vs. Ag/AgCl)	-0.30	Rate (mV/s)	50
Step Width (ms)	40	Cycles Per Run	10
Current Range (mA)*	1		

Table 5.1 Experimental conditions for cyclic voltammetric analysis

*Note the upper potential limit was increased to 0.75 V after the first 10 cycles of testing all electrodes. This lower limit was to initially test the response of the electrode without risk of overoxidation. The remaining analysis was carried out to an upper limit of 0.75 V. The current range was also altered after the first 10 cycles depending on the maximum peak currents from the voltammograms.

**A single electrode was used for the concentration range (0, 10^{-4}, 10^{-3}, 10^{-2} and 10^{-1} M) of analyte anion (NO_3^-, Cl^- or BF_4^-) in a constant ionic strength acetate buffer.

5.3 Results and Discussion

5.3.1 PAni/PVC Electrospun Fibres

Figure 5.3 is a cyclic voltammogram of fibres electrospun from a solution of PAni 1% PVC 10% in THF/DMF. The voltammogram clearly shows the two oxidation and two reduction peaks normally associated with PAni. These appear at 0.16 V and 0.64 V for the oxidation peaks with the corresponding reduction peaks at 0.02 V and 0.57 V, respectively.

This voltammogram compared well with those observed by Wallace et al. [1], Fock et al. [46], and Genies and Lapkowski [313] for PAni films, as well as Figure 5.1. The overlay indicated that the PAni in the fibres was electroactive, quite stable and that a steady-state response was achieved quickly, with only slight alteration to the first oxidation peak after the initial scan.

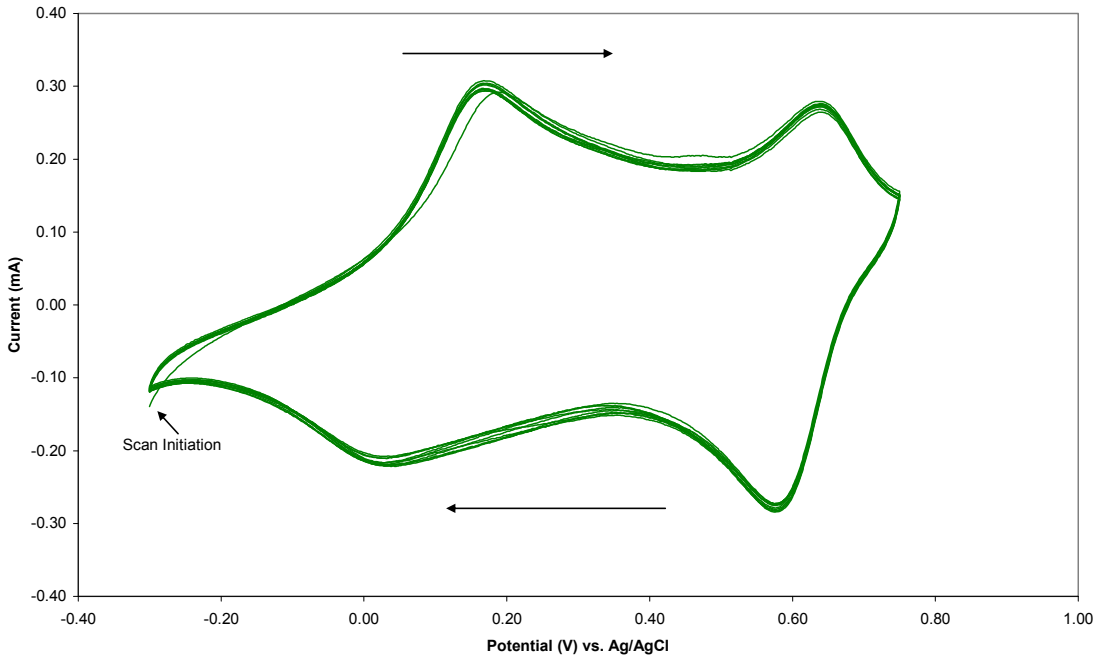

Figure 5.3 Cyclic voltammogram (10 cycles) of an electrode electrospun from PAni 1% PVC 10% in THF/DMF and scanned at 50 mV/s in 0.1 M HCl/KCl.

The redox properties of PAni were described in Section 1.1.3 where PAni undergoes oxidation or reduction, depending on the applied potential, to produce different conducting and non-conducting forms. The initial state observed prior to the first oxidation peak corresponded to the leucoemeraldine form of PAni where all the aniline repeat units are reduced. The PAni was oxidised to the emeraldine form during the first oxidation peak at 0.16 V. The second oxidation peak at 0.64 V was consistent with further oxidation to the pernigraniline form [1, 30, 46]. The scan direction was reversed at 0.75 V and reduction of pernigraniline to emeraldine occurred at 0.57 V followed by the reduction of emeraldine to leucoemeraldine at 0.02 V. Thus, though the solid electrospun fibres were only ~8% PAni, these fibres exhibited the full electroactivity of PAni in the range -0.30 V to 0.75V.

5.3.2 PAni/PAN Electrospun Fibres

The cyclic voltammogram of fibres electrospun from PAni 1% PAN 3% in DMSO/DMF in Figure 5.4 was somewhat different in shape to the voltammogram of the PAni/PVC fibres, though it still exhibited characteristic oxidation and reduction peaks, with slight shifts in the peak potentials.

The first oxidation peak, corresponding to the oxidation of leucoemeraldine to emeraldine occurred at 0.14V, and the second peak, the oxidation of emeraldine to pernigraniline appeared at 0.67 V. The corresponding reduction peak of pernigraniline to emeraldine occurred at 0.59 V whilst the emeraldine to leucoemeraldine reduction appeared at 0.00 V. Estimates of the oxidation and reduction peak potentials for both PAni/PVC and PAni/PAN electrodes are given in Table 5.2.

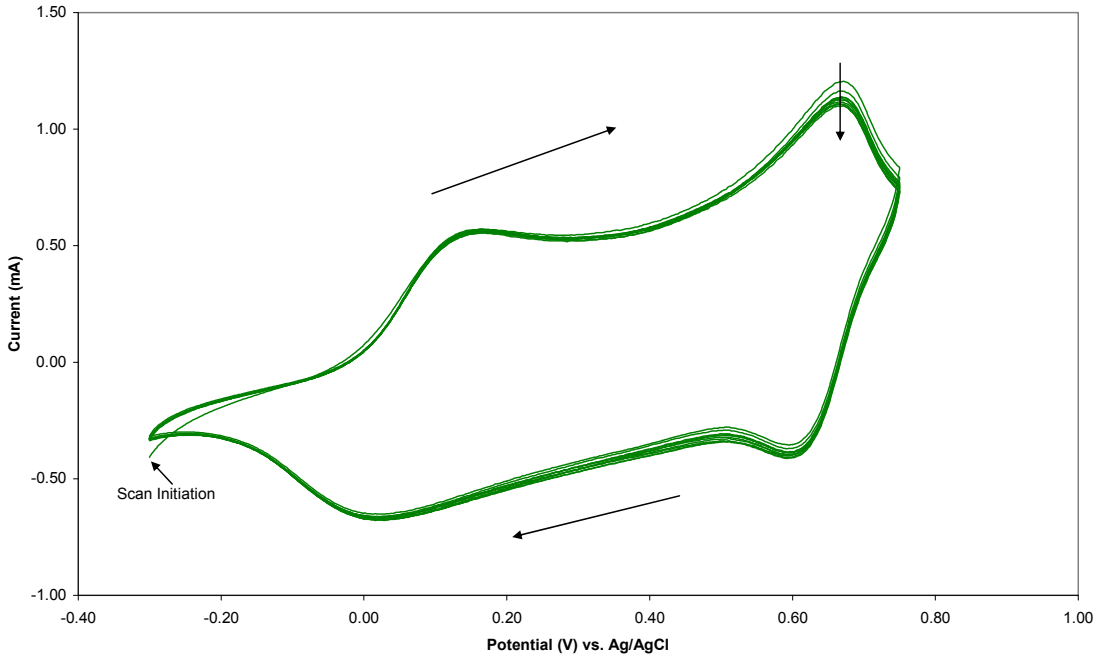

Figure 5.4 Cyclic voltammogram (10 cycles) of an electrode electrospun from PAni 1% PAN 3% in DMSO/DMF and scanned at 50 mV/s in 0.1 M HCl/KCl.

	Oxidation Peak 1		Reduction Peak 1		Oxidation Peak 2		Reduction Peak 2	
	V, vs. Ag/AgCl	Current (mA)	V, vs. Ag/AgCl	Current (mA)	V, vs. Ag/AgCl	Current (mA)	V, vs. Ag/AgCl	Current (mA)
(a)	0.16	0.30	0.02	-0.20	0.64	0.27	0.57	-0.28
(b)	0.14	0.55	0.00	-0.67	0.67	1.10	0.59	-0.39

Table 5.2 Redox peak potentials and currents for (a) PAni 1% PVC 10%; (b) PAni 1% PAN 3% electrospun electrodes cycled in 0.1 M HCl/KCl.

The peak currents for PAni/PAN fibres were notably higher compared with PAni/PVC, however this is most likely the result of the relatively higher content of PAni within the PAni/PAN fibres compared with PAni/PVC. Assuming complete evaporation of the solvent and taking into account the contribution of camphorsulfonic acid (CSA) and the support polymer, the PAni/PAN fibres would contain ~20% PAni whilst the PAni/PVC fibres would contain only ~8%. In addition the voltammogram from PAni/PAN initially appears tilted, but this declines with an increasing number of scans. This may indicate a

greater degree of difficulty for ion exchange through these fibres compared to the PAni/PVC electrodes, requiring more time to achieve a steady-state response.

Hosseini and Entezami [298] prepared and characterised films of PAni blended with PVC, PS and polyvinylacetate (PVAc). They observed three different voltammograms from each of the three different blends. These differences included the presence or absence of the oxidation and reduction peaks, the oxidation and reduction potentials, as well as the redox peak currents. They stated that the presence of the oxidation peaks was a result of the transfer of ions through the PAni as well as the degree of doping.

Park and Yang [314] observed higher currents for the cyclic voltammetry of films of PAni/poly(vinyl methylaniline) (PVMA) compared to a PAni/PVC composite indicating that the PAni/PVMA blend was more electrochemically active than the PAni/PVC composite. In addition they also observed shifts in the redox peak potentials of PAni with increasing cycle number. Yang and Go [305] also reported changes in the electrochemical properties of composites of PAni/poly(vinyl phenylmethylamine (PVPMA) and PAni/poly(vinyl benzyl methylamine) (PVBMA). However, these changes were most significant when the composition of the water/DMF solution for the electropolymerisation of PAni was altered. In addition different voltammograms were produced from both composites.

Jones and Kalaji [315] observed different electrochemical characteristics for a PAni film array depending on the contact area between the PAni film and the substrate electrode. They noted that the contact area was responsible for changes in the oxidation peak potential, concluding that the contact area influences the percolation threshold

potential by delaying the onset of oxidation of PAni until a higher potential was reached, which in turn increased the extent of oxidation and the peak current.

Thus, there may be a number of factors affecting the electrochemical properties of the PAni/PVC fibres and the PAni/PAN fibres, including morphology (fibre thickness, density and homogeneity) and the influence of the blend composition (permeability, hydrophobicity/hydrophilicity and homogeneity), but the individual contributions of these could not be determine.

5.3.3 PAni/PVC/2-NPOE Electrospun Fibres

Cyclic voltammograms of PAni 1% PVC 10% 2-NPOE 5% (2-nitrophenoloctylether, a commercial plasticiser and solvent mediator) in THF/DMF electrospun fibres with increasing [NO_3^-] is given in Figure 5.5. This voltammogram is indicative of the electrochemical response of both these fibres and fibres electrospun with a higher 2-NPOE loading from PAni 1% PVC 10% 2-NPOE 20% THF/DMF. As a result data for voltammograms based on PAni/PVC/2-NPOE have been tabulated and are presented in Table 5.3. The comments column provides a comparison with Figure 5.5 of the visual aspects of the voltammograms.

The electrospun fibres for all samples exhibited electroactivity as indicated by the presence of a single oxidation peak and single reduction peak. Compared to the previous electrospun PAni/PVC blend there was an absence of a second oxidation and reduction peak corresponding to the emeraldine/pernigraniline couple, however this most likely resulted from the pH (4.62) of the acetate buffer [1, 22, 41]. According to Ping et al. [41] this single redox couple is attributed to the oxidation of leucoemeraldine directly to pernigraniline, however it is important to note Ye and Baldwin [22] previously reported

a PAni based chemically modified electrode (CME) that detected anions in an acetate buffer that also exhibited only a single couple peak during cyclic voltammetry.

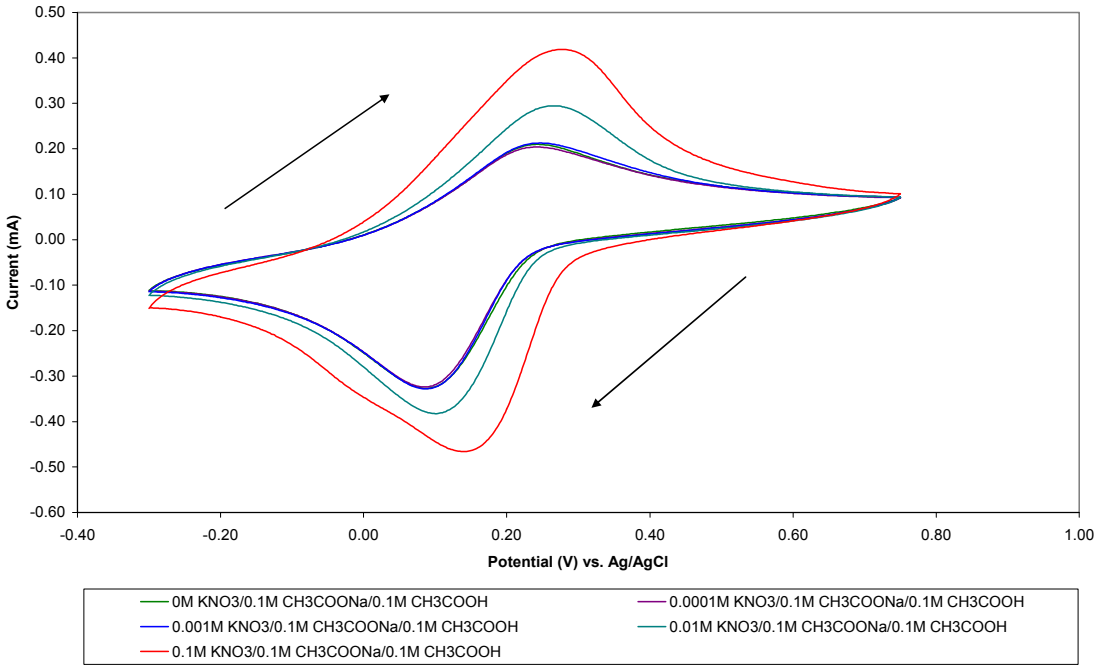

Figure 5.5 Cyclic voltammograms (10th cycle) of an electrode electrospun from PAni 1% PVC 10% 2-NPOE 5% in THF/DMF and scanned at 50 mV/s in NO_3^-/acetate buffer.

To test this electrode for use as a nitrate sensor, the sample was cycled in increasing concentrations of NO_3^- in acetate buffer as indicated in Figure 5.5 and noted in Table 5.3. Though the oxidation response appeared to increase with increasing NO_3^- concentration, further investigation revealed that this was not the case. The PAni 1% PVC 10% 2-NPOE 5% sample in 10^{-4} M NO_3^- in acetate buffer gave oxidation/reduction peak currents of 0.20/-0.32 mA, smaller than the oxidation/reduction peak currents from the neat acetate buffer with values of 0.24/-0.33 mA. Increasing the [NO_3^-] to 10^{-3} M produced peak currents equal to those for the acetate buffer, with further increases in the concentration leading to further increases in

the peak currents. This was also the case for the PAni 1% PVC 10% 2-NPOE 20% electrode cycled in acetate/NO_3^- in acetate buffer where the peak current decreased initially after cycling in 10^{-4} M NO_3^- compared with the acetate buffer, followed by increases in the peak currents with increasing nitrate concentration. However, the peak current values, when cycled in 10^{-3} M NO_3^-, were lower than the peak currents in acetate buffer cycle. Subsequent increases in concentration of NO_3^- in acetate buffer to 10^{-2} M and 10^{-1} M increased the peak currents, though these changes in peak currents for all solutions were small for this electrode.

[2-NPOE] (%)	[NO_3] (M)	Oxidation Peak 1		Reduction Peak 1		Comparison of Voltammograms
		Potential (V) (vs. Ag/AgCl)	Current (mA)	Potential (V) (vs. Ag/AgCl)	Current (mA)	
5	0	0.24	0.21	0.09	-0.33	Voltammogram in Figure 5.5
	0.0001	0.25	0.20	0.09	-0.32	
	0.001	0.25	0.21	0.09	-0.33	
	0.01	0.27	0.30	0.10	-0.38	
	0.1	0.28	0.42	0.14	-0.47	
20	0	0.32	0.09	0.02	-0.10	Similar peak current response, albeit with a smaller overall response.
	0.0001	0.30	0.07	0.00	-0.09	
	0.001	0.33	0.08	0.00	-0.09	
	0.01	0.36	0.10	0.01	-0.11	
	0.1	0.36	0.11	0.03	-0.11	
2-NPOE (%)	**[Cl^-] (M)**	**Oxidation Peak 1**		**Reduction Peak 1**		**Comparison of Voltammograms**
		Potential (V) (vs. Ag/AgCl)	**Current (mA)**	**Potential (V) (vs. Ag/AgCl)**	**Current (mA)**	
5	0	0.27	0.20	0.04	-0.30	Slightly broader redox peaks Reduction tail also broader, indicating some capacitance
	0.0001	0.28	0.20	0.06	-0.31	
	0.001	0.25	0.20	0.06	-0.32	
	0.01	0.27	0.26	0.05	-0.37	
	0.1	0.30	0.37	0.08	-0.44	
	0.001 NO_3^-	0.30	0.33	0.09	-0.39	
20	0	0.28	0.04	0.10	-0.05	Decrease in overall response to addition of Cl^- Appearance of reduction tail
	0.0001	0.30	0.04	0.09	-0.05	
	0.001	0.31	0.04	0.09	-0.04	
	0.01	0.30	0.05	0.08	-0.05	
	0.1	0.30	0.06	0.11	-0.06	

Table 5.3 Redox potentials of PAni/PVC/2-NPOE electrospun fibres cycled in acetate buffer/NO_3^- and acetate buffer/Cl^-.

It is unclear why the response of the electrospun electrodes initially decreased slightly with the initial addition of NO_3^- for both the 5% and 20% 2-NPOE samples. This was

not the case for fresh electrodes of PAni/PVC/2-NPOE 5% and 20% cycled in [Cl^-] and acetate buffer, and used to determine the selectivity of the electrodes towards NO_3^-. From Table 5.3 it can be seen the PAni/PVC/2-NPOE 5% electrospun fibres cycled in 10^{-4} M Cl^- in acetate buffer did not exhibit a decrease in the peak currents. Instead the oxidation and reduction peak currents increased uniformly when this electrode was cycled in increasing concentrations of Cl^- in acetate buffer. As was the case with increasing [NO_3^-], the PAni/PVC/2-NPOE 20% electrode showed little response to change in [Cl^-].

For the PAni/PVC/2-NPOE 5% electrode, cycled in Cl^-/acetate buffer, the last cycle was generated after spiking the solution to 10^{-3} M NO_3^-. If the electrode were selective towards NO_3^- it would be anticipated that the current would increased significantly after this addition. However, the peak current decreased after this spike, indicating that electrode did not respond preferentially to NO_3^-, or that the presence of Cl^- may have substantially inhibited the response of PAni/PVC/2-NPOE 5%.

Both the lack of specifity towards NO_3^- and the peak current trend is presented more clearly in Figure 5.6. This plot shows the increase in oxidation peak current with increasing NO_3^- and Cl^- concentration for both PAni/PVC/2-NPOE electrodes. The PAni/PVC/2-NPOE 5% electrodes exhibit some measure of proportionality in oxidation peak current with increasing NO_3^- and Cl^- concentration at anion concentrations higher than 10^{-3} M. However, this was not the case for 20% 2-NPOE in PAni/PVC, possibly due to the morphology of the electrodes at this 2-NPOE concentration. From Section 3.3.5 the morphology of these electrodes were film-like rather than fibrous, which would have altered the diffusion characteristics of the electrode, leading to a decreased response. In addition, the basis of employing acetate was so the larger CH_3COO^- ions

would have been limited in their ability to exchange with the PAni during oxidation/reduction whilst the smaller NO_3^- ions would be expected to interact with PAni to a greater degree. Thus these varied responses to NO_3^- and Cl^- indicate non-specific interaction with the PAni.

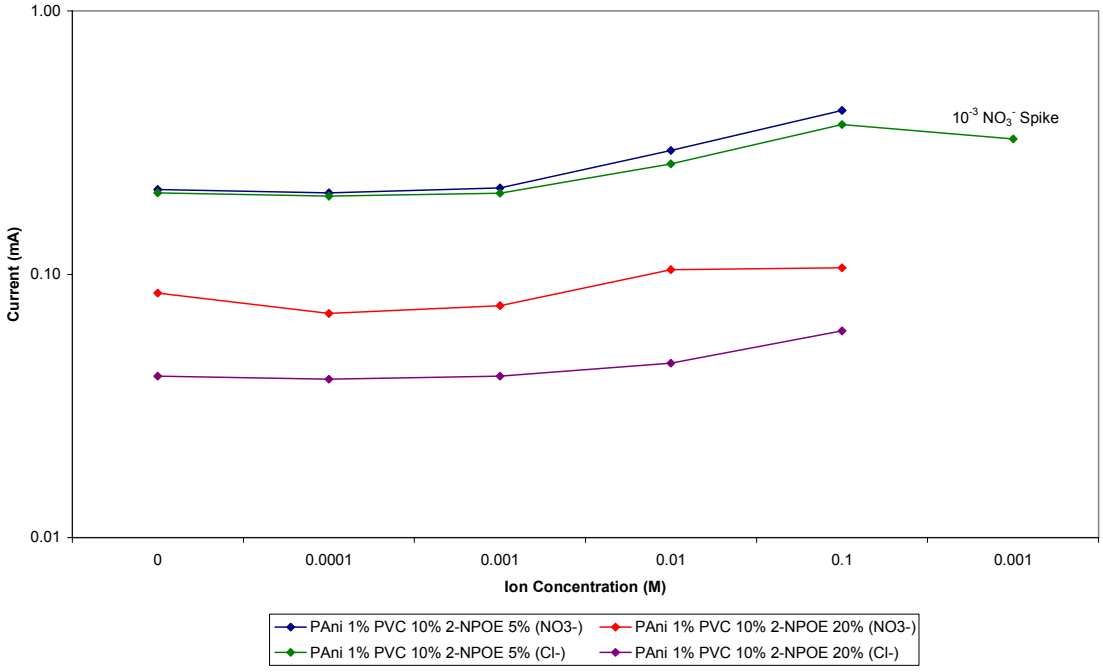

Figure 5.6 Oxidation peak currents for PAni 1% PVC 10% 2-NPOE 5% and PAni 1% PVC 10% 2-NPOE 20% for NO_3^- and Cl^- analyses.

Similar to the peak current response with increasing anion concentration, the hysteresis of the electrode appeared to vary depending on both the fibre composition and supporting electrolyte. From Table 5.3 the separation between the oxidation and reduction peaks for the PAni/PVC/2-NPOE 5% samples cycled in 10^{-1} M NO_3^- in acetate buffer was ~0.14 V, whilst there was a peak separation of ~0.33 V in 10^{-1} M Cl^- /acetate buffer. When these two electrodes were cycled in straight acetate buffer these differences were 0.15 V and 0.30 V respectively, indicating that the redox peak separation was electrode and not anion dependent. This implies significant variations in

morphology or properties of individual electrodes, such as fibre density and the dispersion of PAni and/or 2-NPOE. Similar results were also recorded for the PAni/PVC/2-NPOE 20% electrodes, again indicating appreciable variation between individual electrodes electrospun from the same solution.

5.3.4 PAni/PAN/2-NPOE Electrospun Fibres

Cyclic voltammetry of fibres electrospun from PAni 1% PAN 3% 2-NPOE 0.5% in DMSO/DMF with increasing [NO_3^-] in acetate buffer is presented in Figure 5.7. This voltammogram is indicative of the typical response for PAni/PAN/2-NPOE samples and similar to PAni/PVC/2-NPOE peak currents and potentials. Comments on the structure of the voltammograms have been tabulated and are given in Table 5.4.

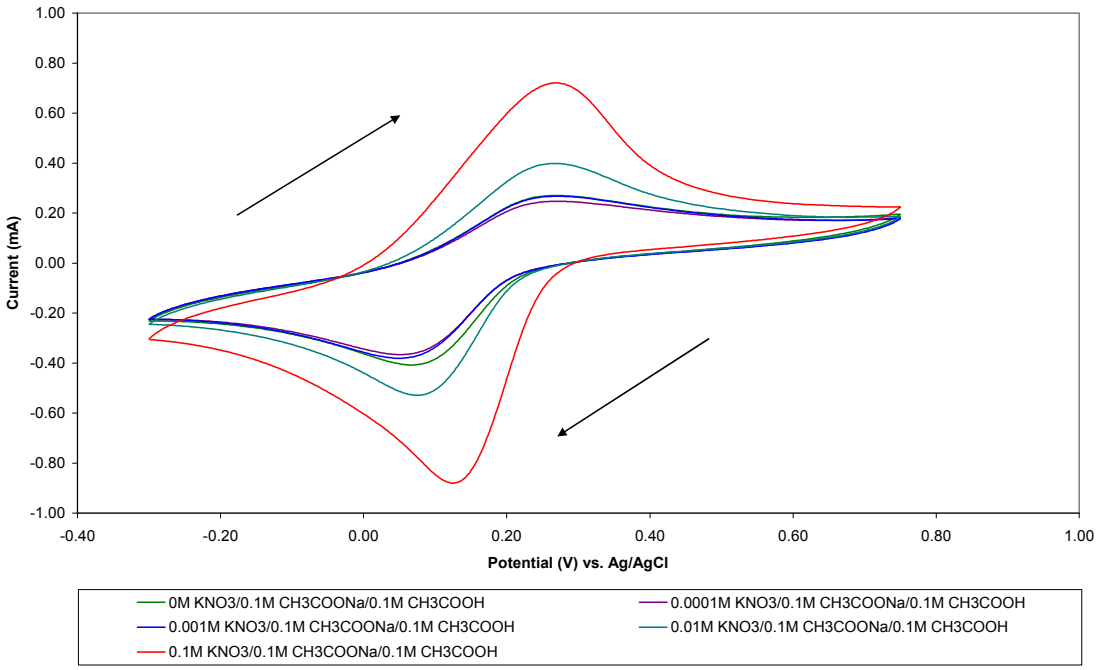

Figure 5.7 Cyclic voltammograms (10^{th} cycle) of an electrode electrospun from PAni 1% PAN 3% 2-NPOE 5% in DMSO/DMF and scanned at 50 mV/s in NO_3^-/acetate buffer.

Similar characteristics were observed for the PAni/PAN/2-NPOE electrodes compared with those of PAni/PVC/2-NPOE. Electroactivity was indicated by a single oxidation peak at approximately 0.27 V and reduction peak within the range of 0.5 V and 0.12 V, depending on the solution composition. Again there was no indication of a second oxidation and reduction couple due to the pH (~4.62) of the solution [41].

[2-NPOE] (%)	$[NO_3]$ (M)	Oxidation Peak 1		Reduction Peak 1		Comparisons of Voltammograms
		Potential (V) (vs. Ag/AgCl)	Current (mA)	Potential (V) (vs. Ag/AgCl)	Current (mA)	
5	0	0.27	0.27	0.07	-0.41	Voltammogram in Figure 5.7
	0.0001	0.27	0.25	0.05	-0.37	
	0.001	0.27	0.27	0.05	-0.38	
	0.01	0.27	0.40	0.08	-0.53	
	0.1	0.27	0.72	0.13	-0.88	
20	0	0.25	0.83	0.06	-0.96	Broadening of redox peaks Increase in the redox currents at upper & lower limits
	0.0001	0.25	0.75	0.04	-0.89	
	0.001	0.26	0.75	0.04	-0.87	
	0.01	0.27	1.44	0.04	-1.54	
	0.1	0.30	2.50	0.02	-2.51	
2-NPOE (%)	**$[Cl^-]$ (M)**	**Oxidation Peak 1**		**Reduction Peak 1**		**Comparison of Voltammograms**
		Potential (V) (vs. Ag/AgCl)	**Current (mA)**	**Potential (V) (vs. Ag/AgCl)**	**Current (mA)**	
5	0	0.23	0.37	0.10	-0.53	Very similar structure to Figure 5.7, but a decrease in the hysteresis between the redox peaks
	0.0001	0.23	0.33	0.09	-0.48	
	0.001	0.23	0.31	0.08	-0.44	
	0.01	0.24	0.45	0.09	-0.62	
	0.1	0.26	0.75	0.10	-0.88	
	0.001 NO_3^-	0.26	0.78	0.10	-0.90	
20	0	0.26	1.18	0.04	-1.41	Slightly broader redox peaks and increases in the redox currents at upper & lower limits
	0.0001	0.26	1.02	0.03	-1.22	
	0.001	0.26	0.98	0.03	-1.16	
	0.01	0.28	1.52	0.02	-1.78	
	0.1	0.31	3.16	0.02	-3.61	

Table 5.4 Redox potentials of PAni/PAN/2-NPOE electrospun fibres cycled in acetate buffer/NO_3^- and acetate buffer/Cl^-.

The oxidation/reduction peak currents of PAni/PAN/2-NPOE 5% decreased slightly after the addition of 10^{-4} M NO_3^- to the acetate buffer, from 0.27/-0.41 mA to 0.25/-0.37 mA. An increase in $[NO_3^-]$ to 10^{-3} M increased the oxidation peak current to 0.27 mA and the reduction peak to -0.38 mA. Further increases in nitrate concentration led to further increases in the peak currents. These increases in the peak currents did appear to

be proportional to nitrate concentration at concentrations of 10^{-3} M and higher (Figure 5.8).

For Cl^- this was also the case where the oxidation/reduction peak currents decreased initially after the addition of 10^{-4} M Cl^- from 0.37/-0.53 mA to 0.33/-0.48 mA. However, the peak currents decreased further after cycling in the 10^{-3} M Cl^- in acetate buffer to 0.31/-0.44 mA, followed by current increases with further increases in $[Cl^-]$. This analysis also exhibited a proportional response at concentrations of 10^{-3} M Cl^- and greater. These observations are detailed in Figure 5.8.

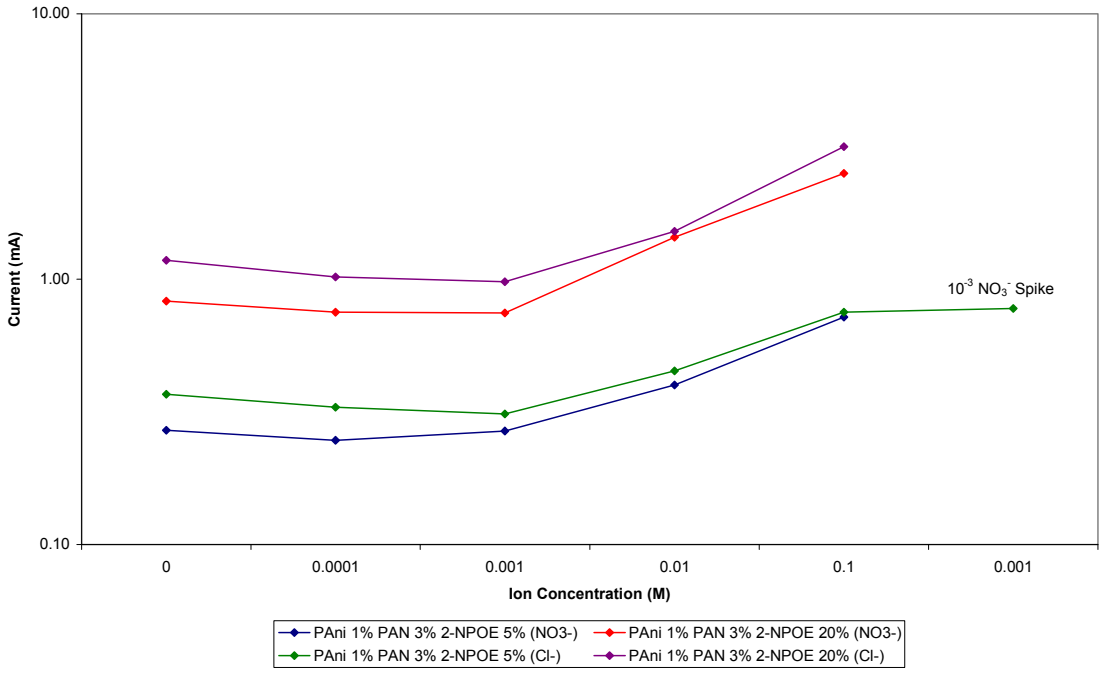

Figure 5.8 Oxidation peak currents for PAni 1% PAN 3% 2-NPOE 5% and PAni 1% PAN 3% 2-NPOE 20% for NO_3^- and Cl^- analyses.

This peak current trend (decrease with the addition of 10^{-4} M NO_3^- to the acetate buffer followed by increasing currents for higher concentration) was also observed for PAni 1% PAN 3% 2-NPOE 20% cycled in increasing nitrate concentration, as well as for

chloride. For these analyses the peak currents after the addition of the either NO_3^- or Cl^- were lower than the corresponding peak currents for the samples cycled in the acetate buffer solution, until the concentration of the ionic species reached 10^{-3} M. Again at concentrations greater than 10^{-3} M there was some proportionality between peak current response and anion concentration (see Figure 5.8).

As this decrease-increase trend was noted for PAni/PVC/2-NPOE and PAni/PAN/2-NPOE electrodes, it was also apparent that the support polymer (PVC or PAN) did not contribute to this effect. Previously in Chapters 2 and Chapter 4 it was suggested that PVC and PAN interact with PAni to different degrees, leading to differences in the physical and chemical properties of the spinning solutions and resultant fibres. Thus these decreases in peak current after the addition of 10^{-4} M NO_3^- or Cl^- to the acetate buffer may have been due to the presence of 2-NPOE. It is possible that 2-NPOE initially inhibits the interaction of these ions with PAni as it is oxidised or reduced, leading to an observed decrease in its electrochemical response when these ions are present at very low concentration. Higher concentrations of NO_3^- or Cl^- will overcome this inhibition and the response will increase with concentration. In essence, the PAni appears to have been 'de-doped', or decreased in electroactivity to some extent after these anions are added to solution, indicating an intrinsic change in the chemical properties of PAni, however it appears to be're-doped', or increased in electroactivity at higher concentrations.

Spiking the 10^{-1} M Cl^- in acetate buffer solution to 10^{-3} M NO_3^- for the PAni 1% PAN 3% 2-NPOE 5% electrode did lead to a slight increase in the oxidation peak current from 0.75 mA to 0.78 mA, and that of the reduction peak from -0.88 mA to -0.99 mA. As stated previously for the PAni/PVC/2-NPOE 5%, if the electrode were selective to

NO_3^- it would be expected that the current would have significantly increased. Conversely, if these fibres were selective to Cl^- it would be expected that no increase in the peak current would have occurred. Thus this small increase in peak current appears to be a direct result of the small increase in the overall ionic strength of the solution, and not any specificity towards NO_3^- nor Cl^-.

In comparing the structures of the cyclic voltammograms, the peaks for the PAni/PAN/2-NPOE 5% electrode were relatively sharp, while the peaks for PAni/PAN/2-NPOE 20% were much broader, indicating the fibrous electrodes offered a faster response than the film-like electrodes of 20% 2-NPOE (see Section 3.3.6). Furthermore the hysteresis of the voltammogram of Cl^- analysis for the PAni/PAN/2-NPOE 5% electrode was noticeably less than that observed for the NO_3^- analysis. Again, this is likely due to the original electrochemical properties of the fibre electrodes as the hysteresis was quite different for these electrodes when cycled in neat acetate buffer. It is doubtful that the variation in the shape of the cyclic voltammograms was due to the affects of ion size on ion-exchange processes (reported by Grzeszczuk and Szostak [303] as affecting the electrochemical response of PAni) as the radii of hydrated Cl^- ion (0.340 nm) is not too dissimilar to that of NO_3^- (0.332 nm) [316].

In comparison with the PAni/PVC/2-NPOE samples, the peak currents were significantly higher overall, indicating the higher content of PAni within the electrospun fibres produced a higher electrochemical response, similar to observations in Section 5.3.1 and 5.3.2 for PAni/PVC and PAni/PAN electrospun fibres, respectively. It is also important to reiterate that these differences in the structure of the voltammograms could also be a product of the overall fibre morphology or the affect from the support polymers, including electrospun fibre density, the permeability and hydrophobicity of

the electrodes, and contact with the underlying substrate, derived from the different composition of the samples, specifically the different support polymers.

5.3.5 PAni/PVC/TOAB Electrospun Fibres

Typical cyclic voltammograms of PAni 1% PVC 10% TOAB 5% (tetraoctylammonium bromide, a commercial ionophore) electrospun fibres with increasing [NO_3^-] in acetate buffer is given in Figure 5.9, with peak potentials, peak currents and comments on the voltammograms given in Table 5.5.

The cyclic voltammograms are similar to those observed for the PAni/PVC/2-NPOE electrodes, with a single redox pair associated with PAni at high pH (~4.62 for the acetate buffer) and the continuing trend of decreased redox peak currents after the addition of low concentrations of NO_3^- and Cl^-.

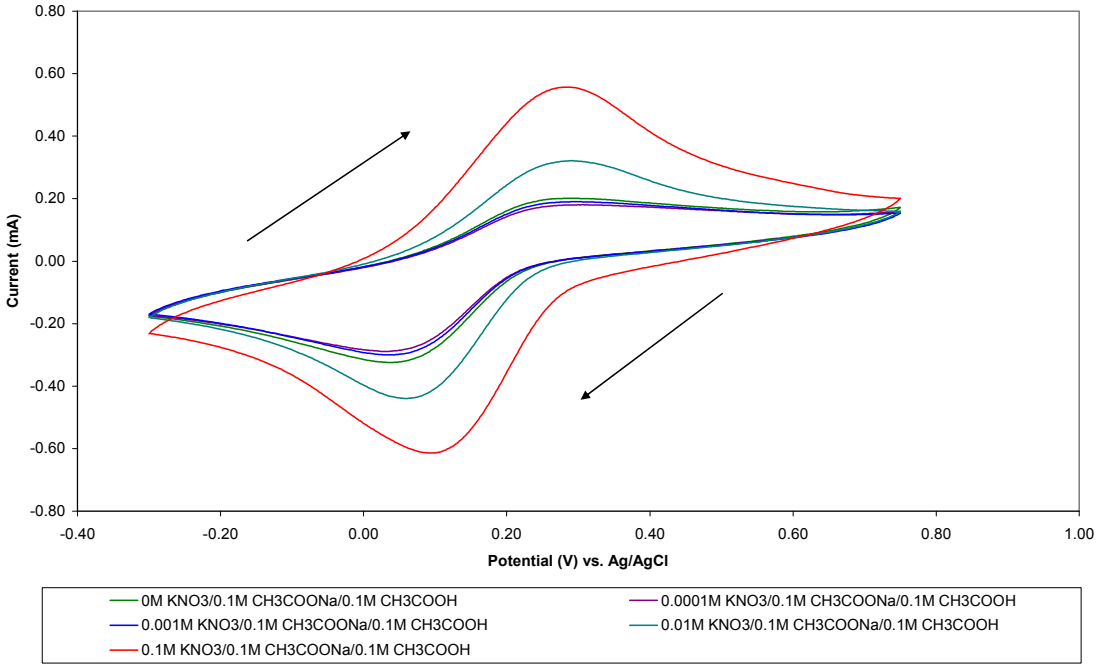

Figure 5.9 Cyclic voltammograms (10^{th} cycle) of an electrode electrospun from PAni 1% PVC 10% TOAB 5% in THF/DMF and scanned at 50mV/s in NO_3^-/acetate buffer.

In the presence of NO_3^-, the peak currents for cyclic voltammograms of both PAni/PVC/TOAB 5% and 20% initially decreased with the addition of 10^{-4} M NO_3^- to the acetate buffer: from 0.20/-0.32 mA to 0.18/-0.29 mA for the oxidation/reduction peaks of PAni/PVC/TOAB 5%, and from 0.08/-0.12 mA to 0.06/-0.10 mA for PAni/PVC/TOAB 20%. The peak currents then slightly increased when [NO_3^-] was increased to 10^{-3} M, but still remained below the values obtained when cycled in the straight acetate buffer. The current response further increased for 10^{-2} M NO_3^- in a manner similar to PAni/PVC/2-NPOE electrospun fibres.

[TOAB] (%)	[NO_3] (M)	Oxidation Peak 1		Reduction Peak 1		Comparison of Voltammograms
		Potential (V) (vs. Ag/AgCl)	Current (mA)	Potential (V) (vs. Ag/AgCl)	Current (mA)	
5	0	0.29	0.20	0.04	-0.32	Voltammogram in Figure 5.9
	0.0001	0.31	0.18	0.03	-0.29	
	0.001	0.30	0.18	0.03	-0.30	
	0.01	0.30	0.32	0.06	-0.44	
	0.1	0.28	0.56	0.09	-0.61	
20	0	0.27	0.08	0.10	-0.12	Evolution of reduction tail at lower potential limit
	0.0001	0.27	0.06	0.09	-0.10	
	0.001	0.29	0.07	0.08	-0.11	
	0.01	0.31	0.12	0.09	-0.15	
	0.1	0.29	0.14	0.13	-0.16	
[TOAB] (%)	**[Cl^-] (M)**	**Oxidation Peak 1**		**Reduction Peak 1**		**Comparison of Voltammograms**
		Potential (V) (vs. Ag/AgCl)	**Current (mA)**	**Potential (V) (vs. Ag/AgCl)**	**Current (mA)**	
5	0	0.35	0.20	-0.01	-0.28	Broadening of redox peaks at high Cl^- concentrations Increase in hysteresis
	0.0001	0.38	0.17	-0.01	-0.22	
	0.001	0.40	0.15	-0.07	-0.20	
	0.01	0.39	0.18	-0.04	-0.24	
	0.1	0.38	0.29	0.05	-0.32	
	0.001 NO_3^-	0.38	0.30	0.05	-0.32	
20	0	0.35	0.08	0.04	-0.10	Broadening of redox peaks at high Cl^- concentrations Hysteresis
	0.0001	0.37	0.07	0.05	-0.09	
	0.001	0.37	0.08	0.04	-0.10	
	0.01	0.38	0.09	0.02	-0.11	
	0.1	0.34	0.14	0.06	-0.15	

Table 5.5 Redox potentials of PAni/PVC/TOAB electrospun electrodes cycled in acetate buffer/NO_3^- and acetate buffer/Cl^-.

This decrease-increase response was mirrored for both PAni/PVC/TOAB electrodes cycled in increasing [Cl^-], and again peak currents remained below those of neat acetate

buffer until 10^{-2} M Cl^- for PAni/PVC/TOAB 5% and 10^{-3} M for PAni/PVC/TOAB 20%. Spiking the PAni /PVC/TOAB 5% sample cycled in Cl^-/acetate buffer to 10^{-3} M NO_3^- in acetate buffer led to only a slight increase in the oxidation current, but no significant increase in the reduction current (see Figure 5.10 and Table 5.5). From this it appears that the inclusion of TOAB in the PAni/PVC blend failed to induce selectivity towards NO_3^-.

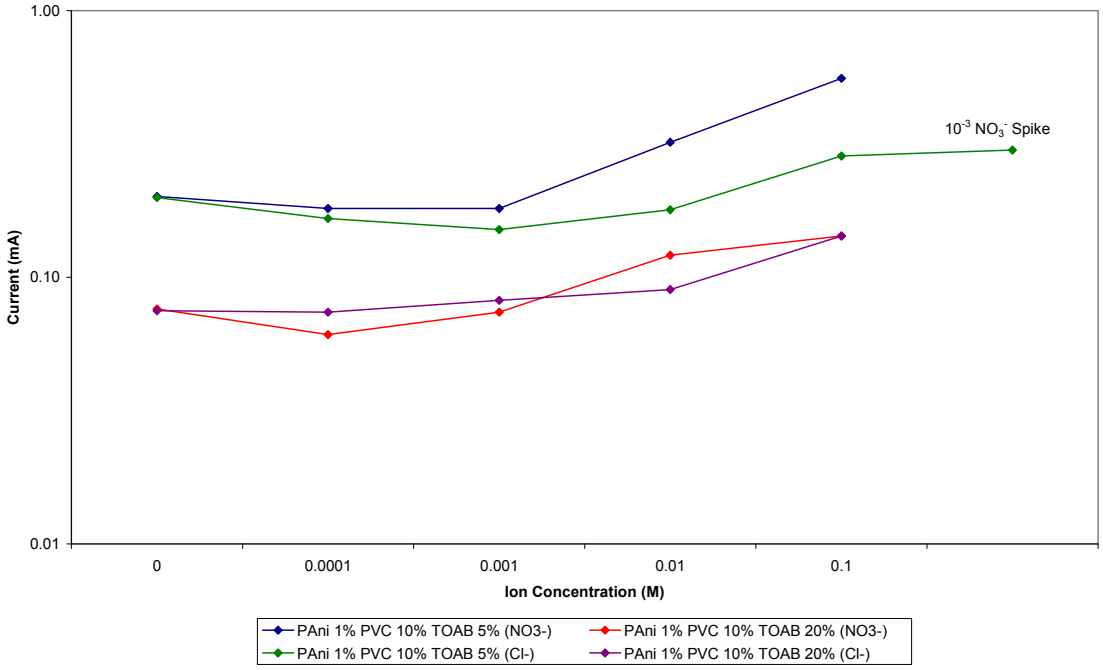

Figure 5.10 Oxidation peak currents for PAni 1% PVC 10% TOAB 5% and PAni 1% PVC 10% TOAB 20% for NO_3^- and Cl^- analyses.

In addition to the lack of specificity towards nitrate, the relationship between oxidation peak currents and ion concentration for all PAni/PVC/TOAB electrodes varied significantly. Figure 5.10 displays this relationship, and it can be seen that PAni/PVC/TOAB 5% cycled in NO_3^- exhibits a degree of linearity at nitrate concentrations of 10^{-3} M and greater, whilst an electrode of the same composition cycled in [Cl^-] exhibited a less linear increase with concentration.

As expected, a degree of variability was seen between the electrodes even when they were cycled in acetate buffer. Figure 5.11 is the cyclic voltammograms of two PAni/PVC/TOAB 5% electrodes cycled in acetate buffer, whilst Figure 5.12 is that of two PAni/PVC/TOAB 20% electrodes cycled under the same conditions (prior to NO_3^- or Cl^- analysis in all cases).

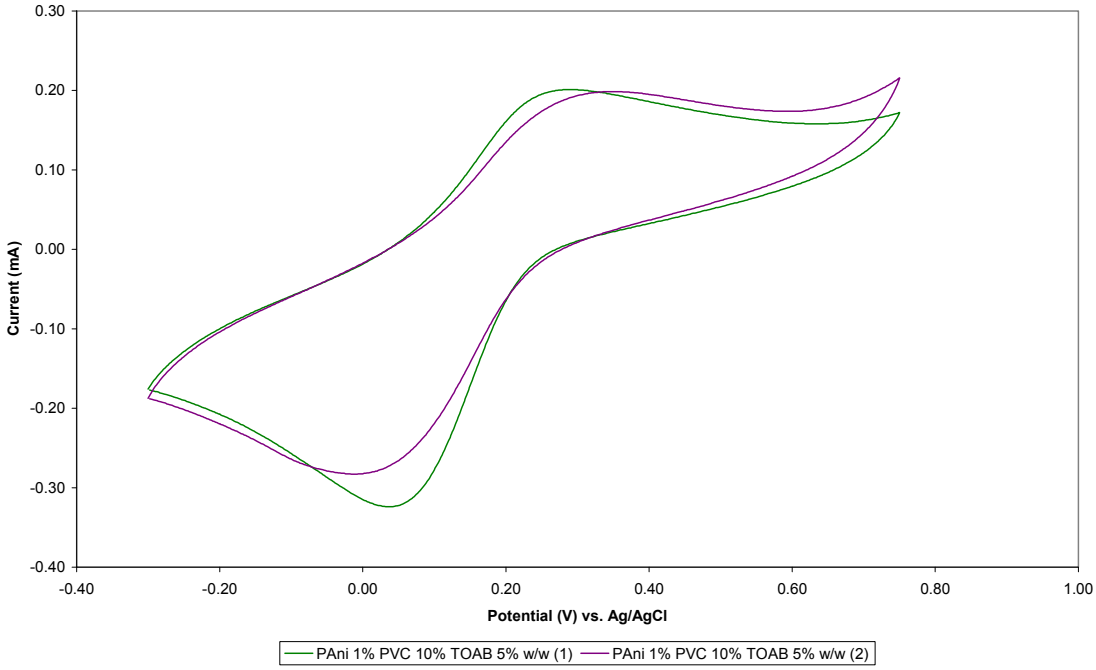

Figure 5.11 Cyclic voltammograms (10^{th} cycle) of replicate electrodes electrospun from PAni 1% PVC 10% TOAB 5% in THF/DMF and scanned at 50 mV/s in acetate buffer.

Both PAni/PVC/TOAB (1) electrodes from Figures 5.11 and 5.12 exhibit similarities, such as similar hysteresis, as do PAni/PVC/TOAB (2) electrodes. However, the redox peaks of the replicates of the same blend are notably different, occurring at different potentials, whilst the reduction peak currents also differ, but less so for the oxidation peak currents. These results indicate that the electrochemical response varies between individual electrodes, most likely caused by variability in the electrospinning process and a lack of uniformity in the electrospun electrodes. Clearly a 'baseline'

voltammogram would be required, or the electrode would require calibration, for each individual electrode before use due to this inherent variability. Furthermore, the cyclic voltammograms also differ significantly in terms of their maximum currents with PAni/PVC/TOAB 5% exhibiting an overall greater cycle current. However, this was expected as the relative composition of PAni in the electrospun fibres decreased with increasing ionophore content.

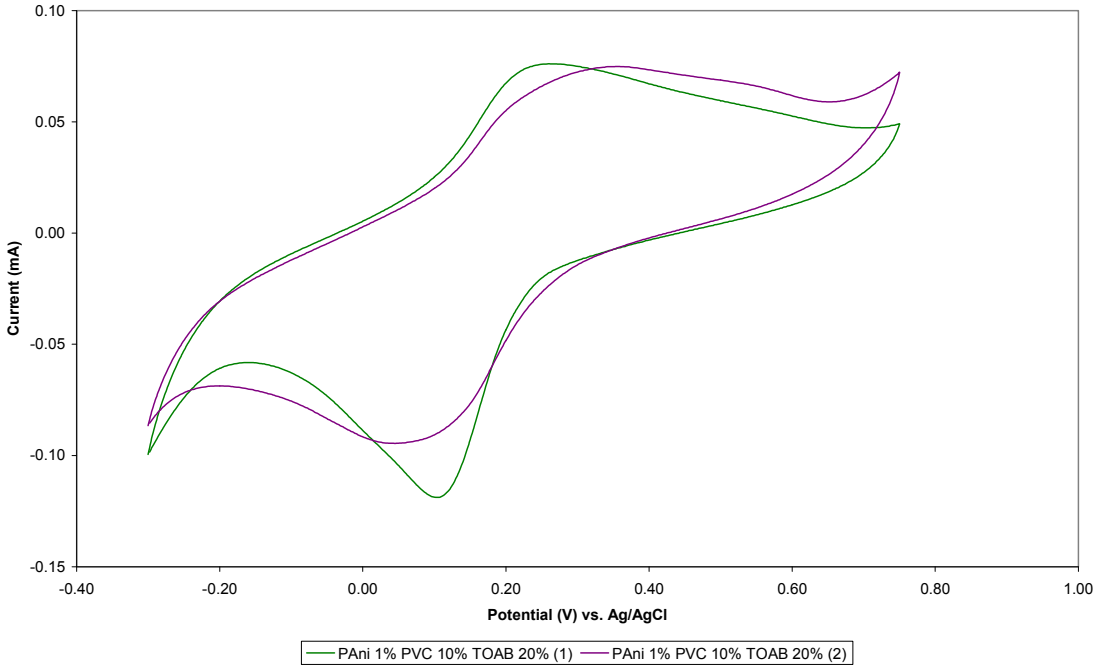

Figure 5.12 Cyclic voltammograms (10th cycle) of replicate electrodes electrospun from PAni 1% PVC 10% TOAB 20% in THF/DMF and scanned at 50 mV/s in acetate buffer.

Lastly, the onset of a reduction 'tail' from -0.20 V was observed for the PAni/PVC/TOAB 20% electrodes. Other electrodes had not exhibited the onset of a reduction tail for the previous analyses. Whilst the tail was observed for this sample when cycled in the acetate buffer, it became more pronounced with increasing [NO_3^-], indicating that water was being reduced at a more positive potential. It is unlikely that these tails were a product of overoxidation of the sample as both PAni/PVC/TOAB 5%

and TOAB 20% electrodes for Cl^- analysis exhibited a slight decline in electroactivity, surmised to be overoxidation, yet only the PAni/PVC/TOAB 20% electrode exhibited this tail. As these tails were not previously observed for other electrodes it appears that these discrepancies may have possibly been derived from the ionophore altering the hydrophobicity of the electrode.

5.3.6 PAni/PAN/TOAB Electrospun Fibres

Typical cyclic voltammograms of fibre electrodes electrospun from PAni 1% PAN 3% TOAB 5% in DMSO/DMF and PAni 1% PAN 3% TOAB 20% in DMSO/DMF, and cycled in increasing [NO_3^-] in acetate buffer are presented in Figures 5.13 and 5.14. Tabulated redox potentials and currents, as well as comments on the voltammograms are given in Table 5.6 (NO_3^- analyses) and Table 5.7 (Cl^- analyses).

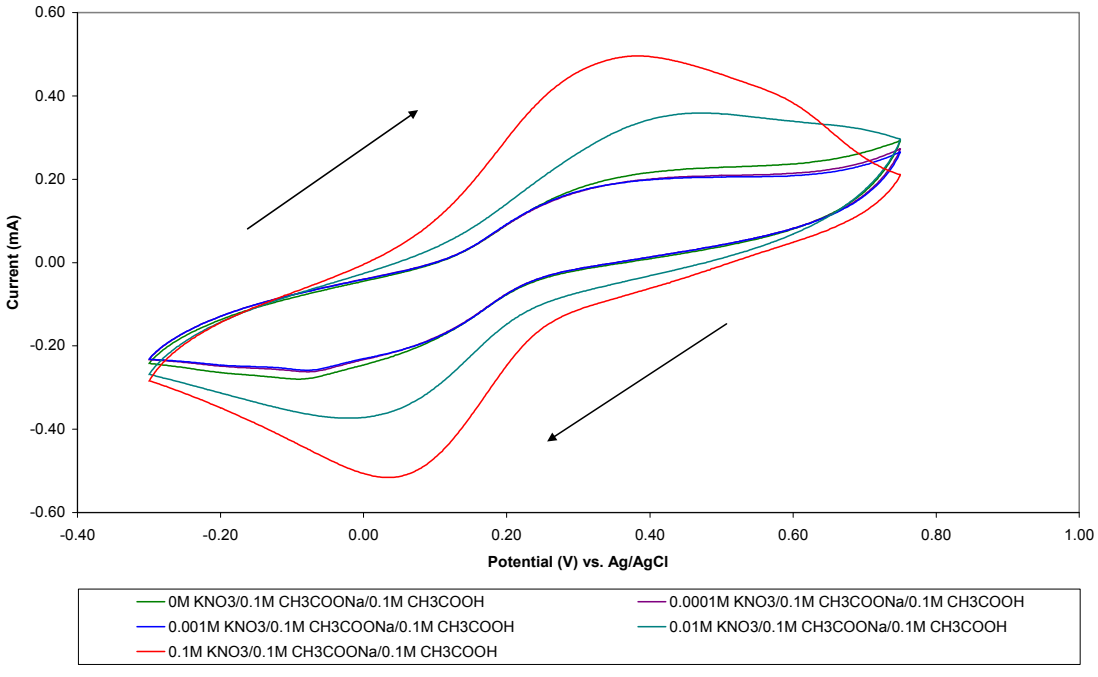

Figure 5.13 Cyclic voltammograms (10^{th} cycle) of an electrode electrospun from PAni 1% PAN 3% TOAB 5% in THF/DMF and scanned at 50 mV/s in NO_3^-/acetate buffer.

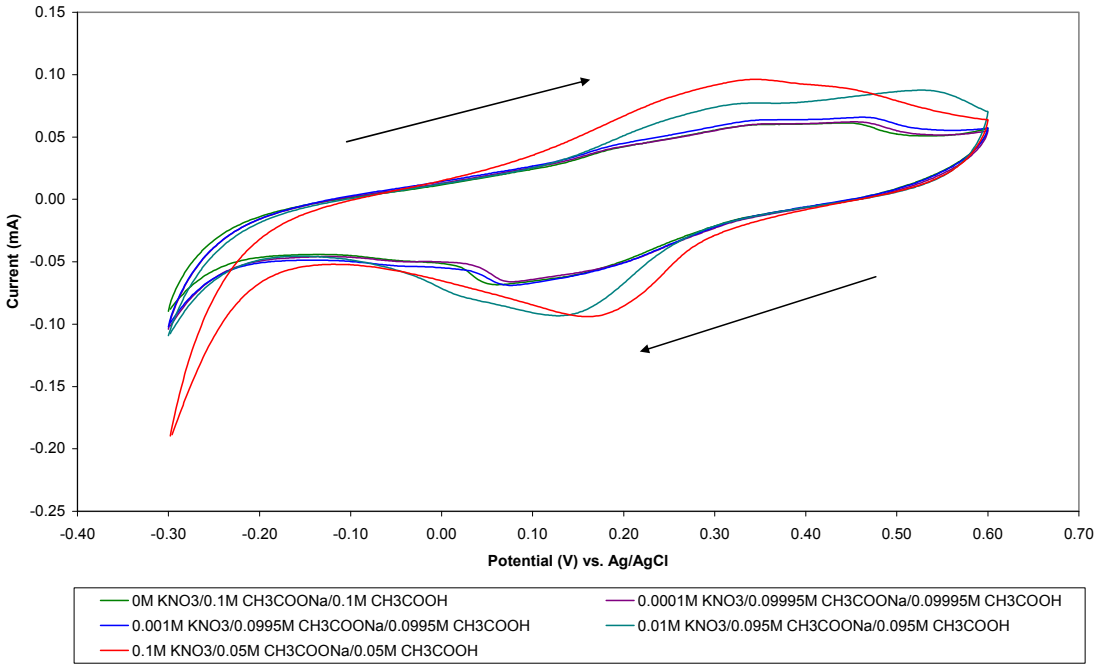

Figure 5.14 Cyclic voltammograms (10th cycle) of an electrode electrospun from PAni 1% PAN 3% TOAB 20% in THF/DMF and scanned at 50 mV/s in NO_3^-/acetate buffer.

[TOAB] (%)	[NO_3] (M)	Oxidation Peak 1		Reduction Peak 1		Comparison of Voltammograms
		Potential (V) (vs. Ag/AgCl)	Current (mA)	Potential (V) (vs. Ag/AgCl)	Current (mA)	
5	0	0.45	0.23	-0.09	-0.28	Voltammogram in Figure 5.13
	0.0001	0.45	0.21	-0.08	-0.26	
	0.001	0.45	0.20	-0.08	-0.26	
	0.01	0.48	0.36	-0.02	-0.37	
	0.1	0.39	0.50	0.03	-0.52	
20	0	0.40	0.06	0.06	-0.07	Sharper redox peaks at 10^{-1} M [Cl^-] Small oxidation tails at upper potential limit
	0.0001	0.40	0.06	0.08	-0.07	
	0.001	0.40	0.06	0.07	-0.07	
	0.01	0.35	0.08	0.13	-0.09	
	0.1	0.34	0.10	0.16	-0.09	

Table 5.6 Redox potentials of PAni/PAN/TOAB electrospun electrodes cycled in acetate buffer/NO_3^-.

Similar to observations for PAni/PVC/TOAB electrodes, peak currents again decreased after the addition of 10^{-4} M NO_3^- to the acetate buffer, from 0.23/-0.28 mA to 0.21/-0.26 mA for the oxidation/reduction peaks, for the PAni/PAN/TOAB 5% electrode Though, in this case the oxidation peak current decreased further when cycled in 10^{-3} M NO_3^-

/acetate buffer to 0.20 mA, however the reduction peak remained stable. Further increases in the concentration then led to approximately linear increases in the peak currents with [NO_3^-] greater than 10^{-3} M.

[TOAB] (%)	[Cl^-] (M)	Oxidation Peak 1		Reduction Peak 1	
		Potential (V) (vs. Ag/AgCl)	Current (mA)	Potential (V) (vs. Ag/AgCl)	Current (mA)
5	0	0.35	0.10	-0.05	-0.15
	0.0001	0.35	0.09	-0.05	-0.13
	0.001	0.35	0.10	-0.04	-0.14
	0.01	0.34	0.12	-0.05	-0.14
	0.1	0.32	0.32	-0.03	-0.29
	0.001 NO_3^-	0.32	0.34	0.00	-0.32
20	0	0.35	0.07	0.04	-0.10
	0.0001	0.35	0.07	0.06	-0.09
	0.001	0.35	0.08	0.15	-0.09
	0.01	0.34	0.08	0.13	-0.10
	0.1	0.30	0.12	0.13	-0.14
[TOAB] (%)	Oxidation Peak 2		Reduction Peak 2		Comparison of Voltammograms
	Potential (V) (vs. Ag/AgCl)	Current (mA)	Potential (V) (vs. Ag/AgCl)	Current (mA)	
5	No Peak	No Peak	No Peak	No Peak	Voltammogram in Figure 5.14
	No Peak	No Peak	No Peak	No Peak	
	No Peak	No Peak	No Peak	No Peak	
	No Peak	No Peak	No Peak	No Peak	
	No Peak	No Peak	No Peak	No Peak	
	No Peak	No Peak	No Peak	No Peak	
20	0.55	0.06	0.12	-0.09	Evolution of two redox couples Larger reduction tails at lower potential limit
	0.55	0.07	0.14	-0.09	
	0.54	0.07	0.14	-0.09	
	0.54	0.08	0.14	-0.10	
	-	-	0.13	-0.14	

Table 5.7 Redox potentials of PAni/PAN/TOAB electrospun electrodes cycled in acetate buffer/Cl^-.

Cycling the PAni/PAN/TOAB 5% electrode in increasing chloride concentration produced relatively constant peak currents with some decrease-increase response for the redox peaks. However, cycling in 10^{-1} M Cl^- increased the peak currents significantly compared with the previous cycles in Cl^-/acetate buffer, from an average of 0.10/-0.14 mA for the oxidation/reduction peaks of the previous cycles, to 0.32/-0.29 mA for 10^{-1}

M Cl^-/acetate buffer. Spiking this solution to 10^{-3} M NO_3^- led to only a slight increase in the cycle current to 0.34/-0.32 mA, indicating little selectivity for NO_3^-.

Decreases in peak currents after the initial addition of NO_3^- or Cl^- were not observed for the PAni/PAN/TOAB 20% electrodes, though the peak currents were relatively small, as were any changes in peak currents with analyte concentration. Overall responses for both NO_3^- and Cl^- analyses for PAni/PAN/TOAB 20% were similar, indicating a higher concentration of TOAB had little affect on the specificity of the electrode towards NO_3^-.

It was stated previously that this decrease-increase response with the initial addition of NO_3^- or Cl^- to the acetate buffer was similar to a de-dope/dope process for PAni, in that the sample was de-doping with the addition of low anion concentrations, leading to a decreased electrochemical response followed by an increased response indicative of greater doping at higher NO_3^- or Cl^- concentrations. The differences in Figures 5.13 and 5.14 indicate that the extent of the actual doping of PAni may have been significantly affected by this process. From Figure 5.13 there is the presence of a single redox pair indicative of the oxidation of PAni at high pH (~4.62). However, in Figure 5.14 there may be two redox pairs similar to the electrochemical response of PAni at lower pH, such as that shown in Figure 5.1. It is difficult to determine if two oxidation/reduction peaks are real, or whether only a single broad redox pair is present, however PAni/PAN/TOAB 20% cycled in Cl^- did exhibit two separate redox peaks indicative of PAni at lower pH (Figure 5.15).

This may indicate the presence of this ionophore, at concentrations of 20% in PAni/PAN spinning solution, has resulted in an increase in the protonation of PAni. Considering that the PAni/PVC/TOAB 20% samples did not exhibit these observations,

it is possible the combination of PAN and TOAB had a direct influence on the redox properties of PAni within the electrospun fibres. It was previously discussed in Chapter 4 that the presence of these quaternary ammonium salts influenced the chemical nature of the PAni within the electrospun fibres, thus this has possibly carried over into the electrochemical response.

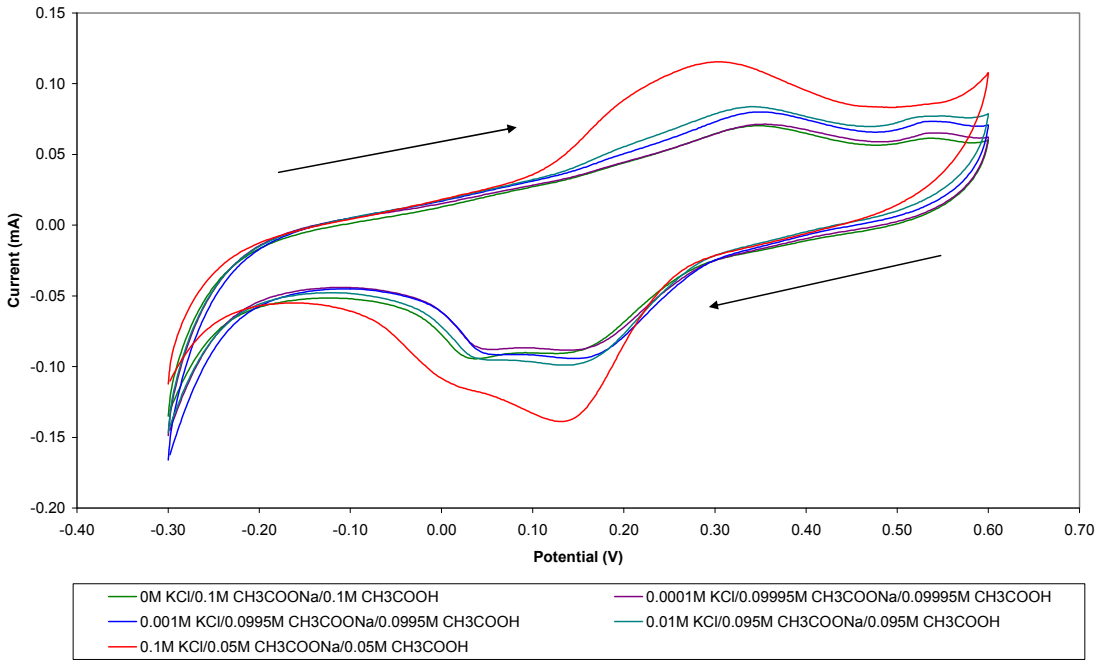

Figure 5.15 Cyclic voltammograms (10th cycle) of an electrode electrospun from PAni 1% PAN 3% TOAB 20% in THF/DMF and scanned at 50 mV/s in Cl$^-$/acetate buffer.

This affect of TOAB, in conjunction with the blend composition, also appears to have influenced the shape of the cyclic voltammograms. Compared with the PAni/PVC/TOAB electrodes the redox peaks for these samples were far broader, and the peak potentials were generally higher. In addition the hysteresis was also much larger. Compared with the 2-NPOE electrodes, and considering that 2-NPOE has previously been used as a solvent mediator [168-170], it is likely that TOAB in the PAni/PAN fibres limited the diffusion of ions and interaction of ions and fibres by

altering the permeability or hydrophobicity of the electrospun fibres. It is possible the physical morphological properties of the electrospun fibres contributed to these differences, as these fibres were slightly different to PAni/PAN/2-NPOE fibres as noted in Section 3.3.6. Furthermore, the intrinsic properties of the fibres, specifically the degree of dispersion of PAni or TOAB within the electrospun fibre, may have also contributed to these responses.

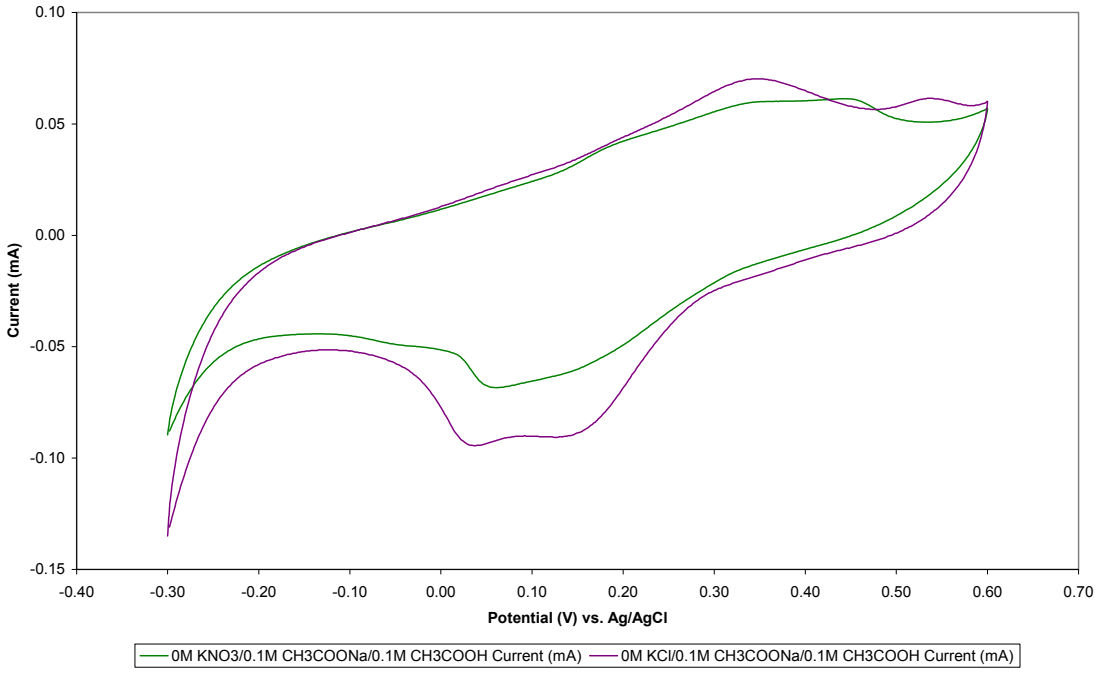

Figure 5.16 Cyclic voltammograms (10th cycle) of replicate electrodes electrospun from PAni 1% PAN 3% TOAB 20% in THF/DMF and scanned at 50 mV/s in acetate buffer.

5.3.7 PAni/PVC/TDAB Electrospun Fibres

Cyclic voltammograms of fibres electrospun from PAni 1% PVC 10% TDAB 0.5% (tetradodecylammonium bromide, a commercial nitrate ionophore) in THF/DMF, in increasing [NO_3^-] in acetate buffer are provided in Figure 5.17. These cyclic voltammograms were representative of the electrochemical response for this electrode composition. The electrochemical response for PAni 1% PVC 10% TDAB 0.5%

exhibited similar characteristics to both the PAni/PVC/TDAB 5% electrode, and the PAni 1% PVC 10% TDAB 20% electrode. Figure 5.18 is a characteristic response for a PAni/PVC/TDAB 20% electrospun electrode. Tabulated data of redox peak potentials and peak currents are also given in Table 5.8 (NO_3^- analyses), 5.9 (Cl^- analyses) and 5.10 (BF_4^- analyses). The tetrafluoroborate ion (BF_4^-) was included in tests as it was felt that the ionophore may respond to Cl^- (a known interferent for many commercial ionophore based nitrate electrodes), as well as NO_3^-. It was assumed that any responses with BF_4^- would be due to non-specific interactions, probably with PAni.

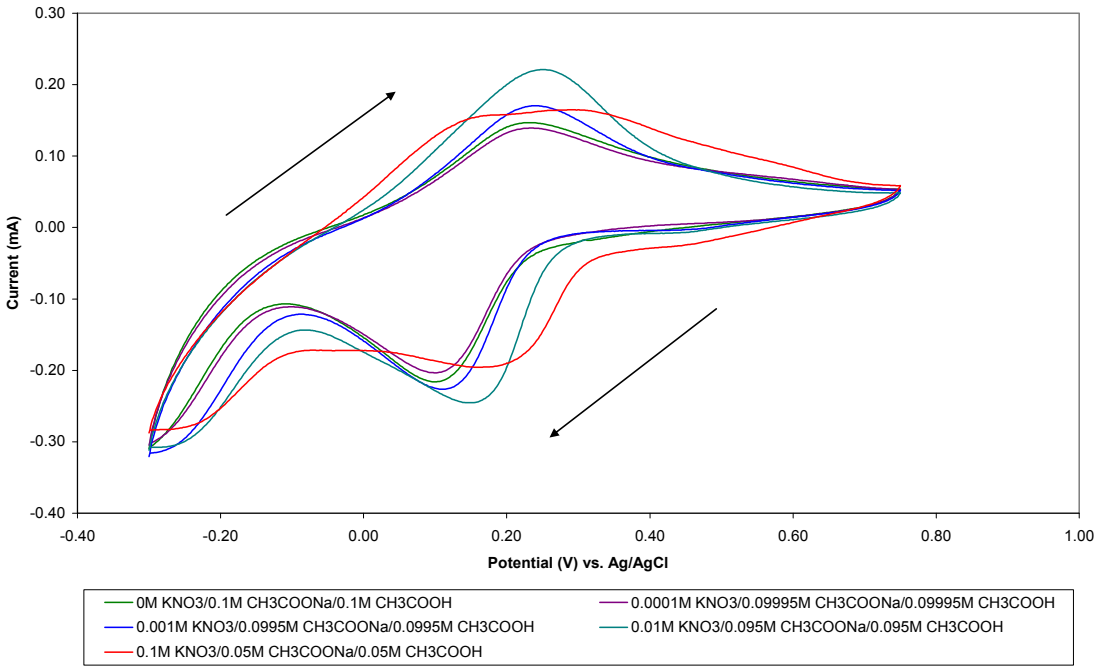

Figure 5.17 Cyclic voltammograms (10^{th} cycle) of an electrode electrospun from PAni 1% PVC 10% TDAB 0.5% in THF/DMF and scanned at 50 mV/s in NO_3^-/acetate buffer.

In what was a consistent trend for the majority of the electrodes analysed, the peak current of the electrospun fibres decreased when cycled in 10^{-4} M NO_3^-/acetate buffer compared with the acetate buffer alone. In the case of PAni/PVC/TDAB 0.5% the peak current initially decreased from 0.15/-0.22 mA to 0.14/-0.20 mA for the

oxidation/reduction peaks. This was followed by an increase in the peak currents to values greater than those of the acetate buffer after the addition of NO_3^- to 10^{-3} M. This trend was the same for PAni/PVC/TDAB 5% with an initial decrease in oxidation /reduction peak currents from 0.22/-0.30 mA to 0.20/-0.28 mA after the addition of 10^{-4} M NO_3^-. Again this was followed by a subsequent increase in peak current with increasing [NO_3^-]. However, the peak currents for PAni/PVC/TDAB 10% electrode consistently increased with increasing [NO_3^-], albeit by only small values.

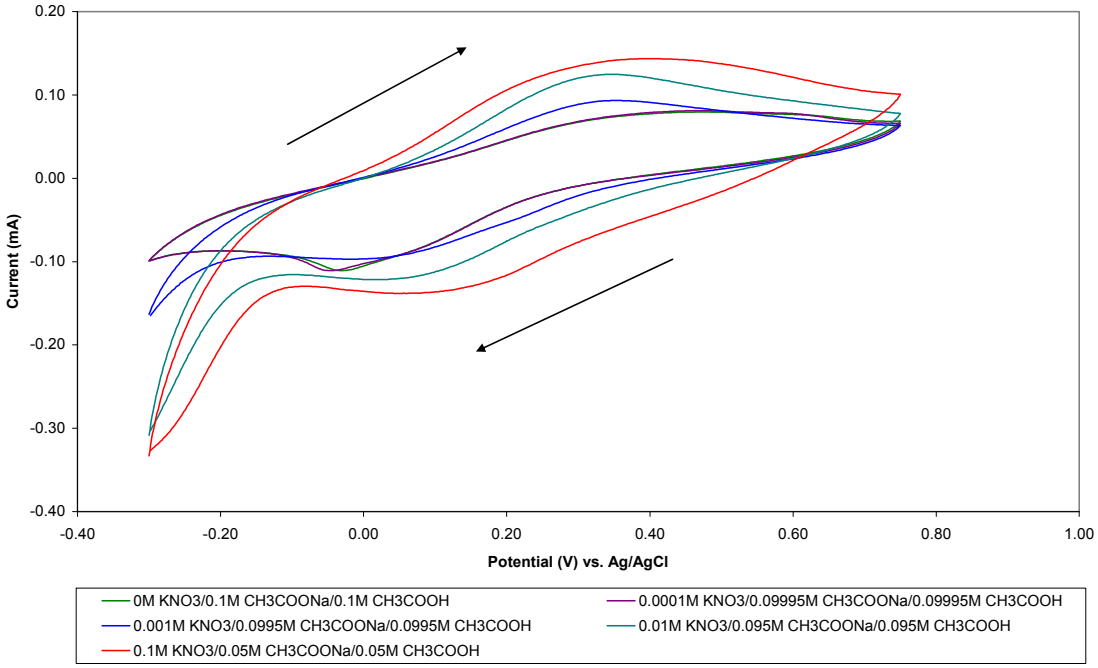

Figure 5.18 Cyclic voltammograms (10^{th} cycle) of an electrode electrospun from PAni 1% PVC 10% TDAB 10% in THF/DMF and scanned at 50mV/s in NO_3^-/acetate buffer.

At 10^{-1} M NO_3^- the PAni redox pairs broadened, their peak currents decreased, and a second redox pair appeared for both PAni/PVC/TDAB 0.5% (Figure 5.17) and PAni/PVC/TDAB 5% electrodes. This did not appear to be a result of pH changes. The pH of the acetate buffer was 4.62, whilst for the acetate buffer/10^{-1} M NO_3^- it was 4.56. It would be expected that a pH change of only 0.06 would not have been sufficient to

affect the electrochemical response of PAni to such an extent that the evolution of two oxidation and reduction peaks would occur.

[TDAB] (%)	[NO_3] (M)	Oxidation Peak 1		Reduction Peak 1	
		V, vs. Ag/AgCl	Current (mA)	V, vs. Ag/AgCl	Current (mA)
0.5	0	0.24	0.15	0.09	-0.22
	0.0001	0.24	0.14	0.10	-0.20
	0.001	0.24	0.17	0.11	-0.23
	0.01	0.26	0.22	0.15	-0.25
	0.1	0.17	0.16	0.16	-0.20
5	0	0.30	0.22	0.02	-0.30
	0.0001	0.30	0.20	0.02	-0.28
	0.001	0.31	0.25	0.04	-0.31
	0.01	0.32	0.36	0.07	-0.42
	0.1	0.36	0.39	0.10	-0.41
10	0	0.47	0.08	-0.03	-0.11
	0.0001	0.47	0.08	-0.05	-0.11
	0.001	0.36	0.09	-0.02	-0.10
	0.01	0.35	0.13	0.01	-0.12
	0.1	0.40	0.14	0.04	-0.14
[TDAB] (%)	Oxidation Peak 2		Reduction Peak 2		Comparison of Voltammograms
	V, vs. Ag/AgCl	Current (mA)	V, vs. Ag/AgCl	Current (mA)	
0.5	No Peak	No Peak	No Peak	No Peak	Voltammogram in Figure 5.17
	No Peak	No Peak	No Peak	No Peak	
	No Peak	No Peak	No Peak	No Peak	
	No Peak	No Peak	No Peak	No Peak	
	0.30	0.17	-0.05	-0.17	
5	No Peak	No Peak	No Peak	No Peak	Broadening of redox peaks at 10^{-1} M NO_3^- Significantly smaller reduction tail than Figure 5.13, comparable to 5.18
	No Peak	No Peak	No Peak	No Peak	
	No Peak	No Peak	No Peak	No Peak	
	No Peak	No Peak	No Peak	No Peak	
	0.52	0.39	0.52	-0.03	
10	No Peak	No Peak	No Peak	No Peak	Voltammogram in Figure 5.18
	No Peak	No Peak	No Peak	No Peak	
	No Peak	No Peak	No Peak	No Peak	
	No Peak	No Peak	No Peak	No Peak	
	No Peak	No Peak	No Peak	No Peak	

Table 5.8 Redox potentials of PAni/PVC/TDAB electrospun electrodes cycled in acetate buffer/NO_3^-.

It was previously suggested for PAni/PAN/TOAB that the ionophore may have had some bearing on the electrochemical response, particularly as a second redox pair was observed in the presence of Cl^- at higher concentrations of TOAB. This may also be the

case here, in that the TDAB and PAni interact to increase the protonation of PAni at high concentrations of nitrate. Additionally, this would imply that at low concentrations of analyte, the PAni would be deprotonated to some extent. This may be responsible for the decrease-increase response in peak current, such that the presence of low concentrations of test analyte deprotonates the PAni, initially leading to a decrease in the peak current response, followed by an increase at increasing analyte concentration.

[TDAB] (%)	[Cl⁻] (M)	Oxidation Peak 1		Reduction Peak 1	
		V, vs. Ag/AgCl	Current (mA)	V, vs. Ag/AgCl	Current (mA)
0.5	0	0.24	0.07	0.14	-0.11
	0.0001	0.25	0.06	0.12	-0.11
	0.001	0.24	0.07	0.13	-0.12
	0.01	0.25	0.10	0.20	-0.14
	0.1	0.26	0.10	0.16	-0.13
5	0	0.29	0.05	0.08	-0.08
	0.0001	0.29	0.05	0.08	-0.08
	0.001	0.29	0.07	0.09	-0.09
	0.01	0.30	0.09	0.11	-0.10
	0.1	0.33	0.10	0.13	-0.11
10	0	0.50	0.08	-0.03	-0.08
	0.0001	0.50	0.04	-0.02	-0.05
	0.001	0.49	0.04	-0.02	-0.05
	0.01	0.44	0.04	-0.04	-0.06
	0.1	0.23	0.04	0.06	-0.06
[TDAB] (%)	**Oxidation Peak 2**		**Reduction Peak 2**		**Comparison of Voltammograms**
	V, vs. Ag/AgCl	**Current (mA)**	**V, vs. Ag/AgCl**	**Current (mA)**	
0.5	No Peak	No Peak	No Peak	No Peak	Increase in magnitude of the reduction tail compared with Figure 5.17
	No Peak	No Peak	No Peak	No Peak	
	No Peak	No Peak	No Peak	No Peak	
	No Peak	No Peak	No Peak	No Peak	
	No Peak	No Peak	No Peak	No Peak	
5	No Peak	No Peak	No Peak	No Peak	Broadening of peaks and larger reduction tail compared with Figure 5.17
	No Peak	No Peak	No Peak	No Peak	
	No Peak	No Peak	No Peak	No Peak	
	No Peak	No Peak	No Peak	No Peak	
	No Peak	No Peak	No Peak	No Peak	
10	No Peak	No Peak	No Peak	No Peak	Very broad peaks, similar to Figure 5.14, smaller reduction tail than Figure 5.18, plus more capacitive
	No Peak	No Peak	No Peak	No Peak	
	No Peak	No Peak	No Peak	No Peak	
	No Peak	No Peak	No Peak	No Peak	
	0.37	0.05	-0.08	-0.06	

Table 5.9 Redox potentials of PAni/PVC/TDAB electrospun electrodes cycled in acetate buffer/Cl⁻.

[TDAB] (%)	[BF_4^-] (M)	Oxidation Peak 1		Reduction Peak 1	
		V, vs. Ag/AgCl	Current (mA)	V, vs. Ag/AgCl	Current (mA)
0.5	0	0.22	0.05	0.13	-0.08
	0.0001	0.21	0.05	0.13	-0.08
	0.001	0.21	0.05	0.13	-0.08
	0.01	0.24	0.06	0.18	-0.09
	0.1	0.17	0.04	-	-
5	0	0.49	0.04	0.00	-0.07
	0.0001	0.39	0.04	0.08	-0.06
	0.001	0.30	0.05	0.08	-0.06
	0.01	0.34	0.06	0.09	-0.07
	0.1	0.65	0.06	0.05	-0.06
10	0	0.48	0.04	0.00	-0.07
	0.0001	0.32	0.04	0.06	-0.05
	0.001	0.31	0.04	0.06	-0.05
	0.01	0.32	0.05	0.12	-0.06
	0.1	0.37	0.06	0.23	-0.06
[TDAB] (%)	**Oxidation Peak 2**		**Reduction Peak 2**		**Comparison of Voltammograms**
	V, vs. Ag/AgCl	**Current (mA)**	**V, vs. Ag/AgCl**	**Current (mA)**	
0.5	No Peak	No Peak	No Peak	No Peak	Increase in magnitude of the reduction tail compared with Figure 5.17 Shift in peak potentials
	No Peak	No Peak	No Peak	No Peak	
	No Peak	No Peak	No Peak	No Peak	
	No Peak	No Peak	No Peak	No Peak	
	0.35	0.05	0.28	-0.07	
5	No Peak	No Peak	No Peak	No Peak	Characteristics of reduction tails from both Figure 5.17 and 5.18, specifically grows then decreases
	No Peak	No Peak	No Peak	No Peak	
	No Peak	No Peak	No Peak	No Peak	
	No Peak	No Peak	No Peak	No Peak	
	No Peak	No Peak	No Peak	No Peak	
10	No Peak	No Peak	No Peak	No Peak	Broad redox peaks increased reduction tail
	No Peak	No Peak	No Peak	No Peak	
	No Peak	No Peak	No Peak	No Peak	
	No Peak	No Peak	No Peak	No Peak	
	No Peak	No Peak	No Peak	No Peak	

Table 5.10 Redox potentials of PAni/PVC/TDAB electrospun electrodes cycled in acetate buffer/BF_4^-.

Alternatively, at a concentration of 10^{-2} M, it is possible that the active sites within the ionophore or electrospun fibres were saturated with nitrate. It is possible that at low concentrations the ionophore may have irreversibly 'bound' the analyte, limiting its release. Assuming the ionophore has no selectivity towards acetate buffer in the absence of NO_3^-, any current is due to PAni/acetate response. With the introduction of NO_3^-, which interacts with the ionophore, this response is decrease. At 10^{-1} M NO_3^- the

ionophore is saturated, in turn limiting any subsequent increase in the peak current with increased [NO_3^-]. This would lead to shifts in peak potentials in the cyclic voltammogram indicative of ion exchange between PAni and the analyte rather than TDAB and the analyte. This is particularly relevant considering these decrease-increase characteristics were observed for nitrate at low TDAB concentrations for this polymer composition, possibly indicating higher ionophore concentrations provide more sites for exchange.

There was a slight decrease in the oxidation peak current with the addition of 10^{-4} M [Cl^-] to acetate buffer for PAni/PVC/TDAB 0.5%, but no change was seen for the reduction peak. This was followed by increases in the peak currents with increasing [Cl^-], up to 10^{-2} M Cl^-. The oxidation/reduction currents for PAni/PVC/TDAB 5% were initially stable at 0.05/-0.08 mA after the addition of 10^{-4} M Cl^-, followed by small increases up to a maximum of 0.10/-0.11 mA for 10^{-1} M Cl^-.

The PAni/PVC/TDAB 10% voltammogram had relatively high oxidation/reduction peak currents for the acetate buffer (0.08/-0.08 mA), compared with 0.5% and 5% TDAB electrodes, taking into account the relative decrease in PAni concentration with increased ionophore. This was followed by a significant decrease to 0.04/-0.05 mA for 10^{-4} M Cl^- and the currents remained relatively stable thereafter, in addition to indications of a second redox process. This indicates that TDAB was not particularly sensitive to Cl^- in solution as these current responses were much lower than those reported for NO_3^-, though this may also have been a result of the electroactivity of the electrodes, and the change in the electrochemistry of PAni for 10^{-1} M Cl^- indicates the evolution of the secondary redox pair is independent of the analyte employed.

To check electrode stability and reversibility of the process the PAni 1% PVC 10% TDAB 10% electrode was then cycled in decreasing chloride concentration, with the peak currents and potentials presented in Table 5.11.

[TDAB] (%)	[Cl⁻] (M)	Oxidation Peak 1		Reduction Peak 1	
		Potential (V) (vs. Ag/AgCl)	Current (mA)	Potential (V) (vs. Ag/AgCl)	Current (mA)
10	0.1	0.23	0.04	0.06	-0.06
	0.01	0.37	0.05	-0.05	-0.06
	0.001	0.50	0.05	-0.01	-0.06
	0.0001	0.38	0.05	-0.01	-0.06
	0	0.38	0.05	-0.01	-0.06

Table 5.11 Redox potentials of PAni/PVC/TDAB 10% electrospun electrode cycled in acetate buffer/Cl^- with decreasing [Cl^-]

Decreasing [Cl^-] from 10^{-1} M through 10^{-2}, 10^{-3} and 10^{-4} M to 0 M led to no significant change in the peak currents for this electrode. However, the electroactivity of the PAni appeared to decrease as indicated by the broadening of the redox peaks, resulting in a change in peak potentials, loss of the second redox pair observed for the 10^{-1} M solution, and tilting of the voltammograms. This indicates the electrode was becoming more resistive, and was most likely degrading through overoxidation. This also possibly indicates a lack of reversibility in the response of the electrode due to binding of ions within the electrode, in turn reducing movement and diffusion of ions between the fibres and the external solution, or potential affects of the ionophore on the electrochemical properties of PAni over time.

Cycling electrospun fibres of PAni/PVC/TDAB in BF_4^- led to relatively stable electrochemical responses. From Table 5.10 the peak currents increased by a maximum of only 0.02 mA for any electrode analysed, indicating little sensitivity for BF_4^-. In the case of PAni/PVC/TDAB 0.5% the oxidation/reduction peak currents increased only from 0.05/-0.08 mA in acetate buffer to 0.06/-0.09 mA in 10^{-2} M BF_4^-/acetate buffer.

This was followed by what appeared to be the evolution of two oxidation peaks at 10^{-1} M BF_4^-, but only a single reduction peak. This may have possibly indicated some degradation of the electrode, but it is likely the major reduction peak overlapped the second reduction peak as the reduction peak potentials shifted to more positive values with increasing concentration. The oxidation peak that evolved at 0.17 V appeared to be new, and as such was assigned as oxidation peak 1, whilst the oxidation peak previously observed at 0.24 V for the 10^{-2} M solution shifted to 0.35V for 10^{-1} M. The corresponding reduction peak also shifted from 0.18 V for 10^{-2} M to 0.28 V for 10^{-1} M. Thus it appears, similar to observations for PAni/PVC/TDAB 0.5% cycled in NO_3^-, the response of PAni changed leading to two redox couples in BF_4^-/acetate buffer.

There was also some indication that two redox couples existed for PAni/PVC/TDAB 5%, however the redox peaks associated with cycling this electrode in 10^{-1} M BF_4^- were extremely broad and the voltammogram was largely capacitive. The peak currents for both PAni/PVC/TDAB 5% and PAni/PVC/TDAB 10% only increased slightly for the entire range of [BF_4^-], initially with oxidation/reduction peak currents of 0.04/-0.07 mA in the neat acetate buffer, and culminating in 0.06/-0.06 mA for the 10^{-1} M BF_4^-/acetate buffer. There may again have been some indication of a second redox process at this concentration due to the significant shift in redox peaks, similar to PAni/PVC/TDAB 0.5%. Again this was difficult to quantify and may instead have been a lack of specificity for BF_4^-, or slow diffusion and interaction of BF_4^- with the electrospun fibres.

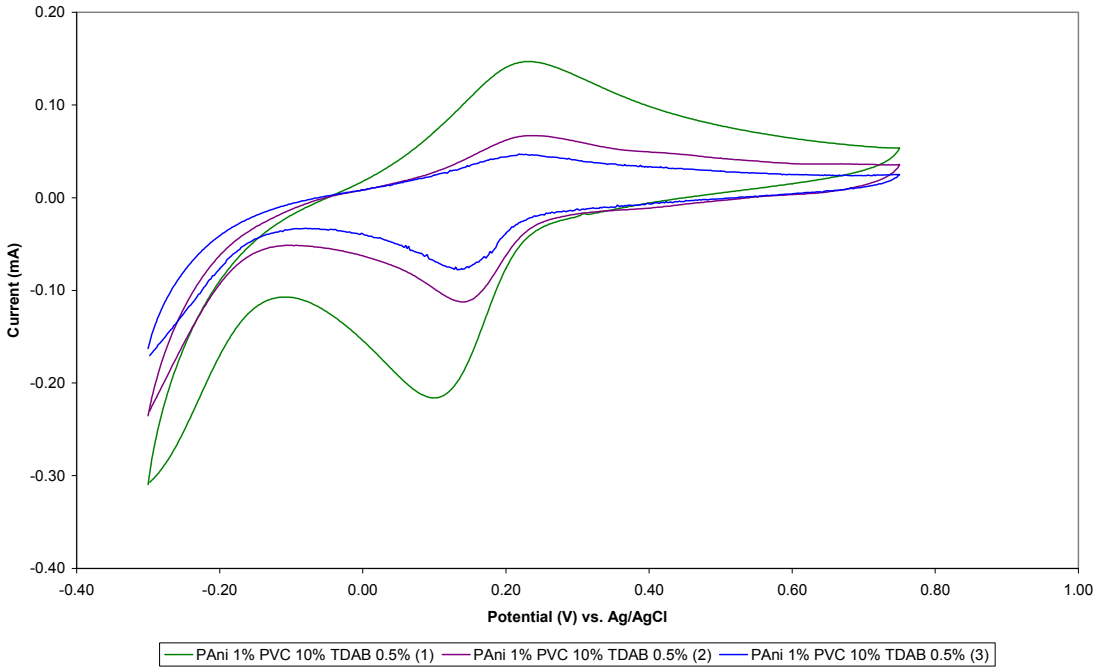

Figure 5.19 Cyclic voltammograms (10th cycle) of replicate electrodes electrospun from PAni 1% PVC 10% TDAB 0.5% in THF/DMF and scanned at 50mV/s in acetate buffer.

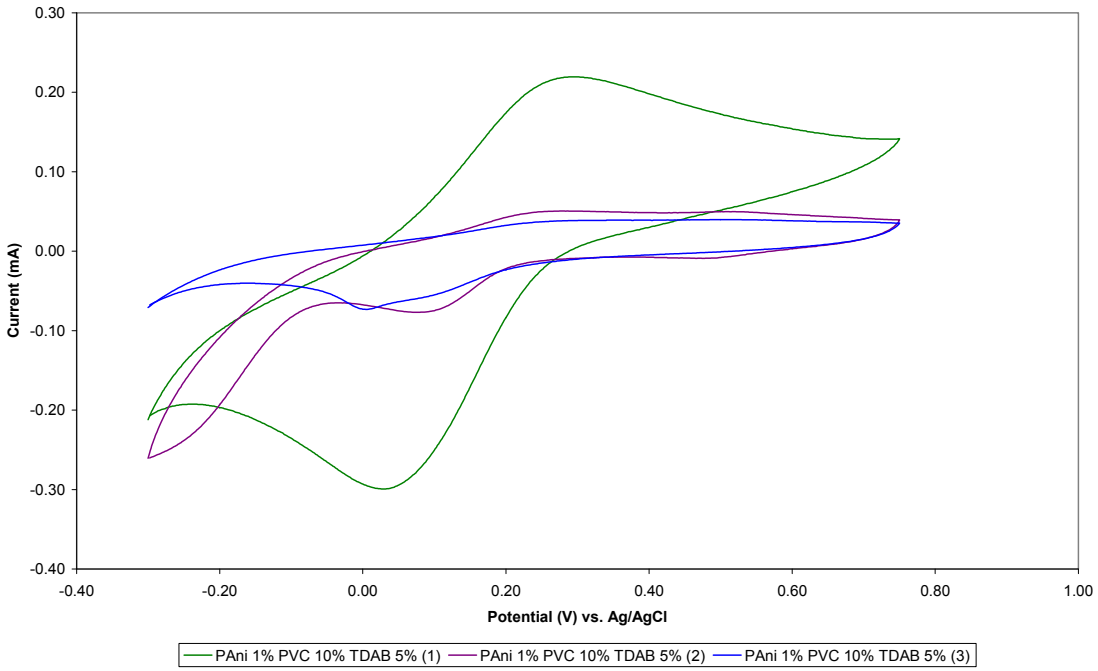

Figure 5.20 Cyclic voltammograms (10th cycle) of replicate electrodes electrospun from PAni 1% PVC 10% TDAB 5% in THF/DMF and scanned at 50mV/s in acetate buffer.

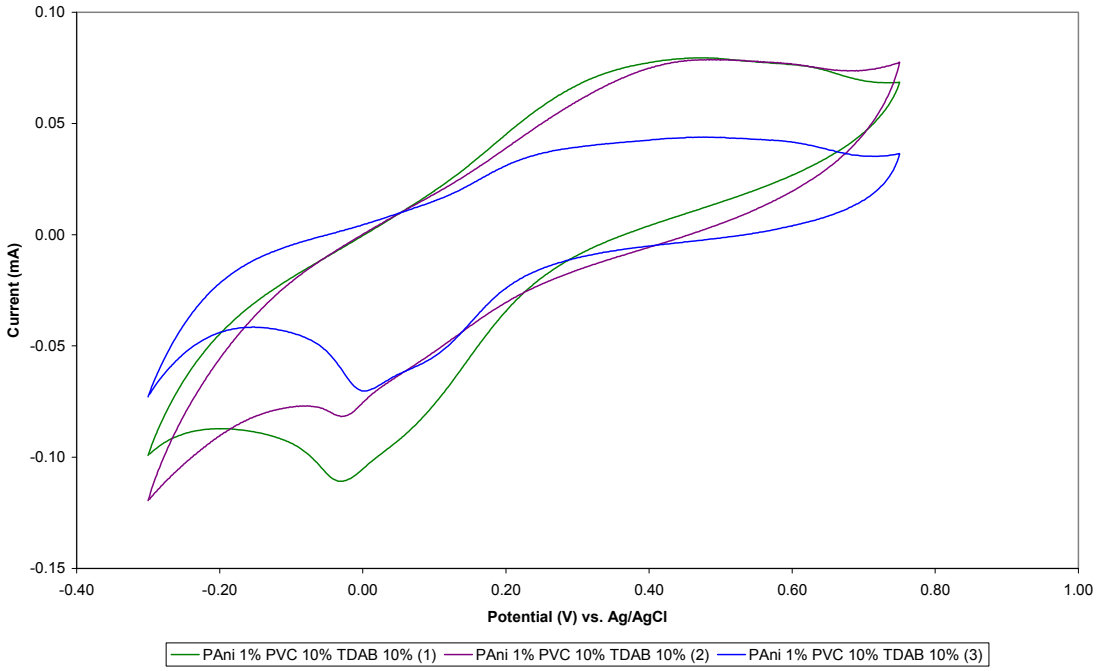

Figure 5.21 Cyclic voltammograms (10^{th} cycle) of replicate electrodes electrospun from PAni 1% PVC 10% TDAB 10% in THF/DMF and scanned at 50mV/s in acetate buffer.

Figure 5.19 presents cyclic voltammograms of replicate PAni/PVC/TDAB 0.5% electrodes cycled in acetate buffer, whilst Figures 5.20 and 5.21 are replicates of PAni/PVC/TDAB 5% and 10% electrodes, respectively, under the same conditions. The first observation from these three figures is that there is considerable variation between, and within, the electrospun electrodes. This is particularly so for electrode (2) electrospun from PAni 1% PVC 10% TDAB 5% in THF/DMF, but all three replicates exhibit variability.

In addition, the hysteresis also changed significantly with increasing TDAB concentration. The separation between the oxidation and reduction peak potentials increased significantly across the three different electrode sets with increasing TDAB concentration. This indicates that TDAB was participating in the interaction of ions with PAni and altering the overall electrochemical response of the electrospun fibres.

Fibre morphology from Section 3.3.9 indicated increasing point-bonding at fibre cross-over junctions with increasing TDAB concentration, but no other major differences in the morphology of the fibres. It would be expected that this point-bonding would have resulted in a more interconnected PAni network, though this did not lead to an increase in electroactivity. Instead the fibre electrodes became less electroactive with increasing TDAB concentration. This decrease in electroactivity may have been arisen from an overall decrease in the relative amount of PAni within the blends, or possibly by changes in the hydrophobicity brought about by the presence of TDAB.

Regardless, this data indicates that TDAB possessed little selectivity towards NO_3^- in this PAni/PVC blend, with the larger increases in peak current during cycling in NO_3^- from the significantly greater electroactivity of this individual electrode compared with the electrodes used for the Cl^- and BF_4^- analyses. However, at higher concentrations of NO_3^- and BF_4^- for PAni/PVC/TDAB 0.5%, NO_3^- and Cl^- for PAni/PVC/TDAB 5%, and BF_4^- for PAni/PVC/TDAB 10% the electrochemical response of PAni changed significantly, indicating changes in its degree of doping. Increasing the concentration of TDAB in the samples led to a reduction in the electroactivity of PAni, in turn affecting the response of the electrodes with the addition of specific anions in solution.

5.3.8 PAni/PAN/TDAB Electrospun Fibres

Figures 5.22 and 5.23 are the cyclic voltammograms of electrodes electrospun from PAni 1% PAN 3% TDAB 0.5% and PAni 1% PAN 3% TDAB 10% in DMSO/DMF/THF, respectively, both cycled in NO_3^- in acetate buffer. Tables 5.12 (NO_3^- analyses), 5.13 (Cl^- analyses) and 5.14 (BF_4^- analyses) give the peak currents and potentials for the various PAni/PAN/TDAB electrodes.

It is important to note that a small amount of THF was added to DMSO/DMF solvents to assist in the dissolution of the ionophore prior to the addition of PAni. This was carried out in a trial-and-error approach to determine the minimum volume of THF required to dissolve the ionophore. This accounted for 0.8 mL per 2 mL of total solvent volume for subsequent blends of TDAB.

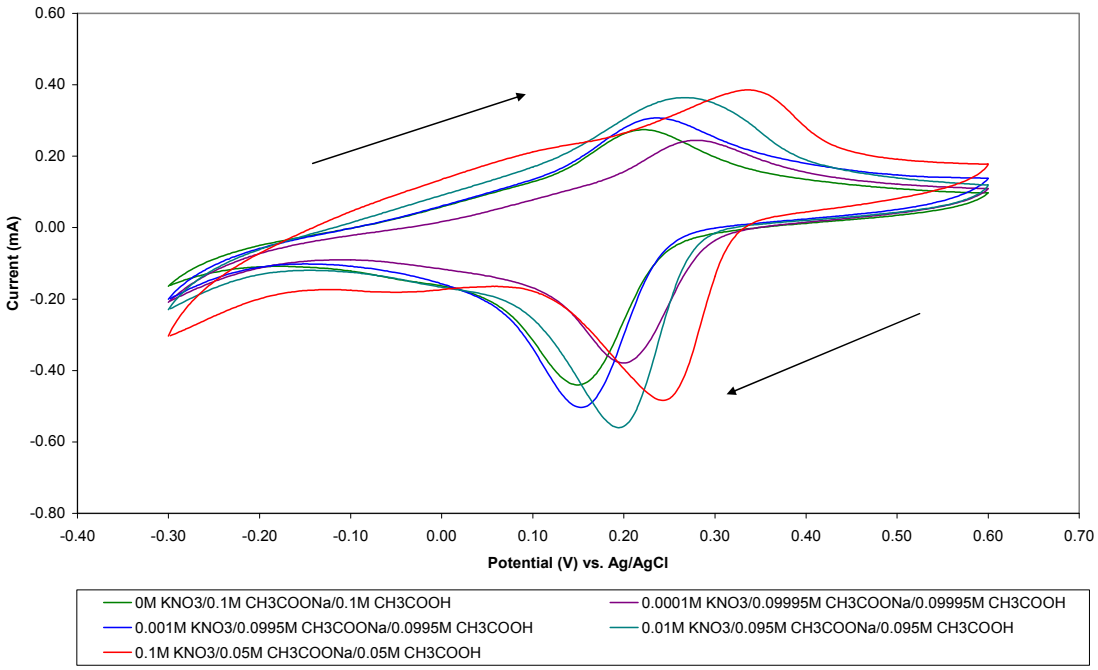

Figure 5.22 Cyclic voltammograms (10th cycle) of an electrode electrospun from PAni 1% PAN 3% TDAB 0.5% in DMSO/DMF/THF and scanned at 50 mV/s in NO_3^-/acetate buffer.

From Figure 5.22, the oxidation/reduction peak currents for the PAni/PAN/TDAB 0.5% electrode decreased from 0.27/-0.44 mA when cycled in the acetate buffer to 0.25/-0.38 mA for the 10^{-4} M [NO_3^-] in acetate buffer. This was followed by increasing peak currents with further additions of nitrate, though these were not proportional to concentration, as well as significant shifts in the peak potentials. This may indicate

some difficulty in the diffusion and interaction of NO_3^- ions with this blend, in turn delaying the oxidation of PAni.

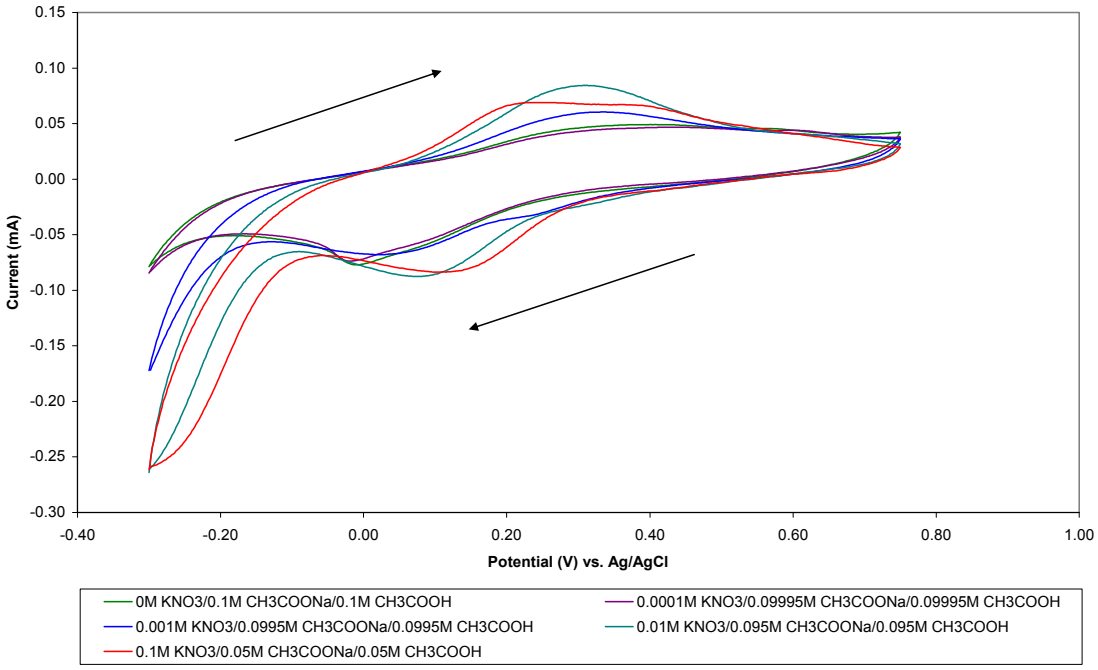

Figure 5.23 Cyclic voltammograms (10th cycle) of an electrode electrospun from PAni 1% PAN 3% TDAB 10% in DMSO/DMF/THF and scanned at 50 mV/s in NO_3^-/acetate buffer.

PAni/PAN/TDAB 5% and PAni/PAN/TDAB 10% electrodes did not exhibit the peak current decrease-increase phenomenon, and instead the peak currents increased with all additions of nitrate. Again these increases were not proportional to $[NO_3^-]$. Thus the ionophore displayed little selectivity towards NO_3^-, or this anion may have been limited in its diffusion to, and interaction, with the ionophore and/or PAni. At 10^{-1} M NO_3^- the PAni/PAN/TDAB 10% electrode began to evolve a second redox process similar to observations for PAni/PVC/TDAB, however this only occurred for the oxidation process. This observed 'split' in the major oxidation peak to form two separate oxidation processes corresponded to a decrease in the peak current, indicating that two

separate processes were occurring. It is likely that the reduction peak corresponding to the new oxidation peak had not fully evolved and still remained coalesced with the major reduction peak.

[TDAB] (%)	[NO_3] (M)	Oxidation Peak 1		Reduction Peak 1	
		V, vs. Ag/AgCl	Current (mA)	V, vs. Ag/AgCl	Current (mA)
0.5	0	0.22	0.27	0.15	-0.44
	0.0001	0.28	0.25	0.20	-0.38
	0.001	0.24	0.31	0.15	-0.50
	0.01	0.29	0.36	0.19	-0.56
	0.1	0.34	0.39	0.24	-0.48
5	0	0.23	0.05	0.09	-0.09
	0.0001	0.23	0.05	0.13	-0.10
	0.001	0.26	0.07	0.14	-0.10
	0.01	0.25	0.08	0.17	-0.14
	0.1	0.28	0.10	0.21	-0.16
10	0	0.40	0.05	-0.01	-0.08
	0.0001	0.43	0.05	-0.02	-0.07
	0.001	0.33	0.06	0.02	-0.07
	0.01	0.31	0.08	0.08	-0.09
	0.1	0.25	0.07	0.11	-0.08
[TDAB] (%)	Oxidation Peak 2		Reduction Peak 2		Comparison of Voltammograms
	V, vs. Ag/AgCl	Current (mA)	V, vs. Ag/AgCl	Current (mA)	
0.5	No Peak	No Peak	No Peak	No Peak	Voltammogram in Figure 5.22
	No Peak	No Peak	No Peak	No Peak	
	No Peak	No Peak	No Peak	No Peak	
	No Peak	No Peak	No Peak	No Peak	
	No Peak	No Peak	No Peak	No Peak	
5	No Peak	No Peak	No Peak	No Peak	Broader redox peaks Growth of reduction tail with increasing [NO_3^-] and change in structure
	No Peak	No Peak	No Peak	No Peak	
	No Peak	No Peak	No Peak	No Peak	
	No Peak	No Peak	No Peak	No Peak	
	No Peak	No Peak	No Peak	No Peak	
10	No Peak	No Peak	No Peak	No Peak	Voltammogram in Figure 5.23
	No Peak	No Peak	No Peak	No Peak	
	No Peak	No Peak	No Peak	No Peak	
	No Peak	No Peak	No Peak	No Peak	
	0.40	0.07	No Peak	No Peak	

Table 5.12 Redox potentials of PAni/PAN/TDAB electrospun electrodes cycled in acetate buffer/NO_3^-

[TDAB] (%)	[Cl⁻] (M)	Oxidation Peak 1		Reduction Peak 1	
		V, vs. Ag/AgCl	Current (mA)	V, vs. Ag/AgCl	Current (mA)
0.5	0	0.30	0.04	-0.01	-0.06
	0.0001	0.30	0.04	0.00	-0.05
	0.001	0.44	0.07	-0.01	-0.08
	0.01	0.28	0.05	-0.03	-0.06
	0.1	0.18	0.05	-0.10	-0.07
5	0	0.34	0.09	-0.02	-0.13
	0.0001	0.35	0.09	-0.02	-0.14
	0.001	0.40	0.07	-0.01	-0.11
	0.01	0.34	0.14	-0.03	-0.17
	0.1	0.34	0.18	0.09	-0.23
10	0	0.38	0.09	-0.01	-0.14
	0.0001	0.41	0.08	0.00	-0.14
	0.001	0.39	0.09	-0.01	-0.15
	0.01	0.34	0.18	-0.03	-0.21
	0.1	0.33	0.20	0.09	-0.26
[TDAB] (%)	**Oxidation Peak 2**		**Reduction Peak 2**		**Comparison of Voltammograms**
	V, vs. Ag/AgCl	**Current (mA)**	**V, vs. Ag/AgCl**	**Current (mA)**	
0.5	0.57	0.04	0.14	-0.05	Broad redox peaks
	0.57	0.04	0.14	-0.04	Tilting of voltammogram
	No Peak	No Peak	0.16	-0.05	Presence of
	0.44	0.05	0.10	-0.05	second redox pair
	0.37	0.07	0.15	-0.08	Smaller reduction tail
5	No Peak	No Peak	No Peak	No Peak	Broad redox peaks that sharpened with increasing [Cl⁻]
	No Peak	No Peak	No Peak	No Peak	
	No Peak	No Peak	No Peak	No Peak	
	No Peak	No Peak	No Peak	No Peak	No significant reduction tail
	No Peak	No Peak	No Peak	No Peak	
10	No Peak	No Peak	No Peak	No Peak	Extremely similar to PAni/PAN/TDAB 5 cycled in [Cl⁻]
	No Peak	No Peak	No Peak	No Peak	
	No Peak	No Peak	No Peak	No Peak	
	No Peak	No Peak	No Peak	No Peak	
	No Peak	No Peak	No Peak	No Peak	

Table 5.13 Redox potentials of PAni/PAN/TDAB electrospun electrodes cycled in acetate buffer/Cl⁻

According to Lukachova et al. [43] the sum of the area of the two PAni redox peaks at low pH is equal to the area of the single redox peak at high pH. It was previously mentioned that the pH of the 10^{-1} M/acetate buffer was only 0.06 pH units lower than the acetate buffer alone. This is a very small change in pH and it would not be expected to significantly alter the electrochemical response of PAni, however these decreases in peak current with the evolution of a second redox peak are consistent with a change in

solution pH. As this was not consistent for all three compositions, again it appears the presence of TDAB has altered the electrochemical response of PAni. These responses were also observed for PAni/PVC/TDAB electrodes, and there it was suggested that the protonation of the PAni had increased due to interactions between the ionophore and PAni.

[TDAB] (%)	[BF_4^-] (M)	Oxidation Peak 1		Reduction Peak 1	
		V, vs. Ag/AgCl	Current (mA)	V, vs. Ag/AgCl	Current (mA)
0.5	0	0.22	0.09	0.14	-0.15
	0.0001	0.22	0.10	0.13	-0.17
	0.001	0.24	0.15	0.13	-0.24
	0.01	0.27	0.16	0.16	-0.26
	0.1	0.07	0.08	0.28	-0.25
5	0	0.40	0.07	0.00	-0.10
	0.0001	0.37	0.07	0.01	-0.10
	0.001	0.32	0.09	0.05	-0.11
	0.01	0.30	0.15	0.11	-0.18
	0.1	0.21	0.12	0.23	-0.15
10	0	0.34	0.03	0.04	-0.05
	0.0001	0.30	0.03	0.05	-0.04
	0.001	0.30	0.04	0.07	-0.05
	0.01	0.30	0.05	0.11	-0.06
	0.1	0.22	0.05	0.24	-0.05
[TDAB] (%)	**Oxidation Peak 2**		**Reduction Peak 2**		**Comparison of Voltammograms**
	V, vs. Ag/AgCl	**Current (mA)**	**V, vs. Ag/AgCl**	**Current (mA)**	
0.5	No Peak	No Peak	No Peak	No Peak	Growth in reduction tail with increasing [BF_4^-] Structurally similar to Figure 5.22
	No Peak	No Peak	No Peak	No Peak	
	No Peak	No Peak	No Peak	No Peak	
	No Peak	No Peak	No Peak	No Peak	
	0.37	0.15	No Peak	No Peak	
5	No Peak	No Peak	No Peak	No Peak	Broad redox peaks that sharpened with increasing [BF_4^-] Increase in reduction tail with increased [BF_4^-]
	No Peak	No Peak	No Peak	No Peak	
	No Peak	No Peak	No Peak	No Peak	
	No Peak	No Peak	No Peak	No Peak	
	0.35	0.13	0.02	-0.11	
10	No Peak	No Peak	No Peak	No Peak	Similar structure to Figure 5.23 Sharper redox peaks
	No Peak	No Peak	No Peak	No Peak	
	No Peak	No Peak	No Peak	No Peak	
	No Peak	No Peak	No Peak	No Peak	
	0.34	0.05	-0.02	-0.04	

Table 5.14 Redox potentials of PAni/PAN/TDAB electrospun electrodes cycled in acetate buffer/BF_4^-

For analysis of one PAni/PAN/TDAB 0.5% electrode, replacing NO_3^- with Cl^- produced a stable response in that the oxidation/reduction peak currents only changed from 0.07/-0.11 mA when cycled in the acetate solution to 0.06/-0.11 mA in 10^{-4} M Cl^-. The current then varied only slightly with increasing concentration of chloride.

On increasing the TDAB level to 5% in the PAni/PAN/TDAB electrode, the oxidation/reduction peak currents remained constant at 0.09/-0.02 mA for 10^{-4} M Cl^- in acetate buffer, and subsequently decreased to 0.07/-0.01 mA when cycled in 10^{-3} M Cl^- in acetate buffer. Further increases in Cl^- increased the peak currents, however these increases were not proportional to [Cl^-]. The third electrode in this group, PAni/PAN/TDAB 10%, exhibited relatively unchanged oxidation/reduction peak currents of 0.09/-0.15 mA until it was cycled in 10^{-2} M Cl^-/acetate buffer where the peak currents increased significantly to 0.18/-0.21 mA, and further increased to 0.20/-0.26 mA with the addition of 10^{-1} M Cl^-. At this concentration the oxidation peak current plateaued, and the peak possibly exhibited initial signs of two redox processes. This is also supported by the significant shift in the reduction peak potential to 0.09 V compared with the previous peak at -0.03 V for the 10^{-2} M Cl^- solution.

Cycling PAni/PAN/TDAB 0.5% in BF_4^-/acetate buffer produced cyclic voltammograms similar to those obtained when the sample was cycled in NO_3^-. In this case, the oxidation/reduction peak currents increased after the addition of 10^{-4} M BF_4^- in comparison to the acetate buffer, from 0.09/-0.15 mA to 0.10/-0.17 mA, with further increases in the concentration producing increases in the peak currents until 10^{-1} M BF_4^-. Cycling of the fibres in the 10^{-1} M BF_4^-/acetate buffer solution produced what appeared to be two individual oxidation peaks and a significant positive shift in the peak potentials. However, there was only one clear reduction peak, although the large

reduction tail may have overlapped any secondary reduction peak with shifts in the peak potentials supporting this.

An increase in the concentration of TDAB to 5% in PAni/PAN produced fibre electrodes that exhibited cyclic voltammograms similar to the PAni/PAN/TDAB 0.5% electrode analysed in BF_4^-/acetate buffer, including increasing peak currents with increasing [BF_4^-]. This was also the case for PAni/PAN/TDAB 10%, however neither electrode displayed peak current increases proportional to BF_4^- concentration. The PAni/PAN/TDAB 5% and 10% electrodes also exhibited growth of two oxidation peaks, decline in overall peak currents and shifts in the peak potentials when cycled in 10^{-1} M BF_4^-/acetate buffer, similar to the PAni/PAN/TDAB 0.5% cyclic voltammograms. If these decreases in the peak current were solely related to ion diffusion then it would have been expected the oxidation peak would have simply broadened not exhibit a second oxidation peak. Considering that the evolution of secondary redox peaks were not observed for other analyses, except PAni/PAN/TDAB 0.5% cycled in Cl^- and PAni/PAN/TDAB 10% cycled in NO_3^-, it is likely that these electrodes lacked uniformity.

In terms of other electrochemical characteristics, the hysteresis of the electrodes also differed with the PAni/PAN/TDAB 0.5% exhibiting less peak separation than both PAni/PAN/TDAB 5% and 10%.

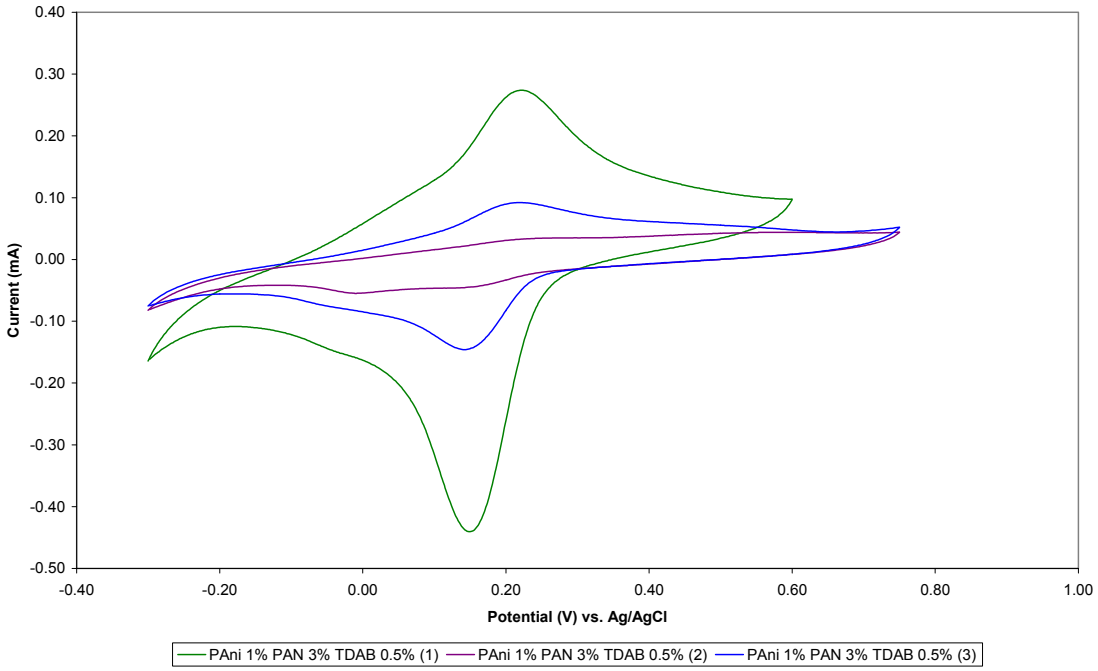

Figure 5.24 Cyclic voltammograms (10th cycle) of replicate electrodes electrospun from PAni 1% PAN 3% TDAB 0.5% in DMSO/DMF/THF and scanned at 50 mV/s in acetate buffer.

The cyclic voltammograms of three replicate PAni/PAN/TDAB 0.5% electrodes cycled in acetate buffer (Figure 5.24) show the electrochemical responses were very different for the three electrodes, again indicating that the electrospun electrodes were quite variable. This may have been a result of the morphology of the electrospun fibres, the degree of contact with the underlying substrate electrode, or the chemical properties of the electrospun electrodes. From Section 3.3.10 it was observed that the fibre morphology of PAni/PAN/TDAB electrodes exhibited beads and globules throughout the mat, possibly leading to these inconsistent electrochemical responses. An increase in the degree of contact with the underlying gold-coated Mylar® electrode would also expected to increase the overall redox response. Similarly, the degree of dispersion of PAni or TDAB throughout the fibre mats could affect conductivity and electroactivity of these electrodes.

Figure 5.25 and Figure 5.26 present the cyclic voltammograms of replicate electrodes of PAni/PAN/TDAB 5% and 10%, respectively. The overall current responses of both sets of electrodes were again quite variable with one PAni/PAN/TDAB 10% electrode revealing a particularly flat cyclic voltammogram. This was most likely a result of the higher concentration of TDAB in the sample, in essence decreasing the electroactive contribution of PAni within the fibres. From Figures 5.24 it can be observed that the overall peak currents were higher for PAni/PAN/TDAB 0.5% than both the 5% and 10% samples, indicating further that the higher concentration of TDAB led to decrease in the electroactivity of these samples. Thus it appears that the ionophore influence was quite unpredictable due to variability between the electrospun electrodes, the hydrophobicity of the electrodes and the intrinsic properties of the fibres, such as dispersion of PAni and the ionophore.

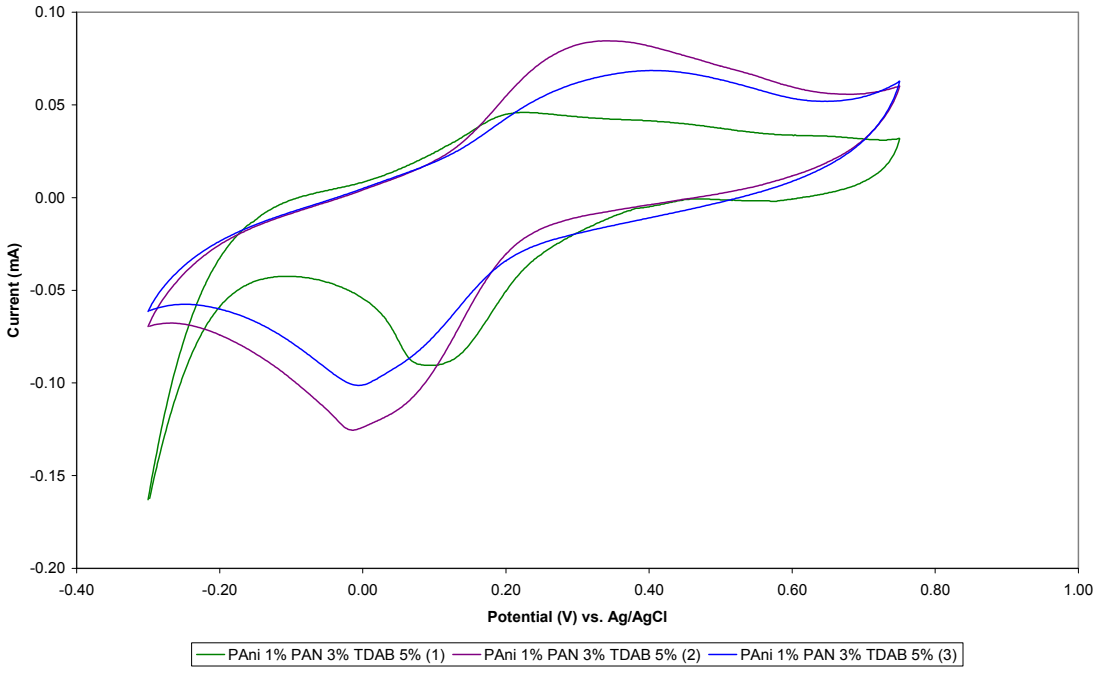

Figure 5.25 Cyclic voltammograms (10th cycle) of replicate electrodes electrospun from PAni 1% PAN 3% TDAB 5% in DMSO/DMF/THF and scanned at 50 mV/s in acetate buffer.

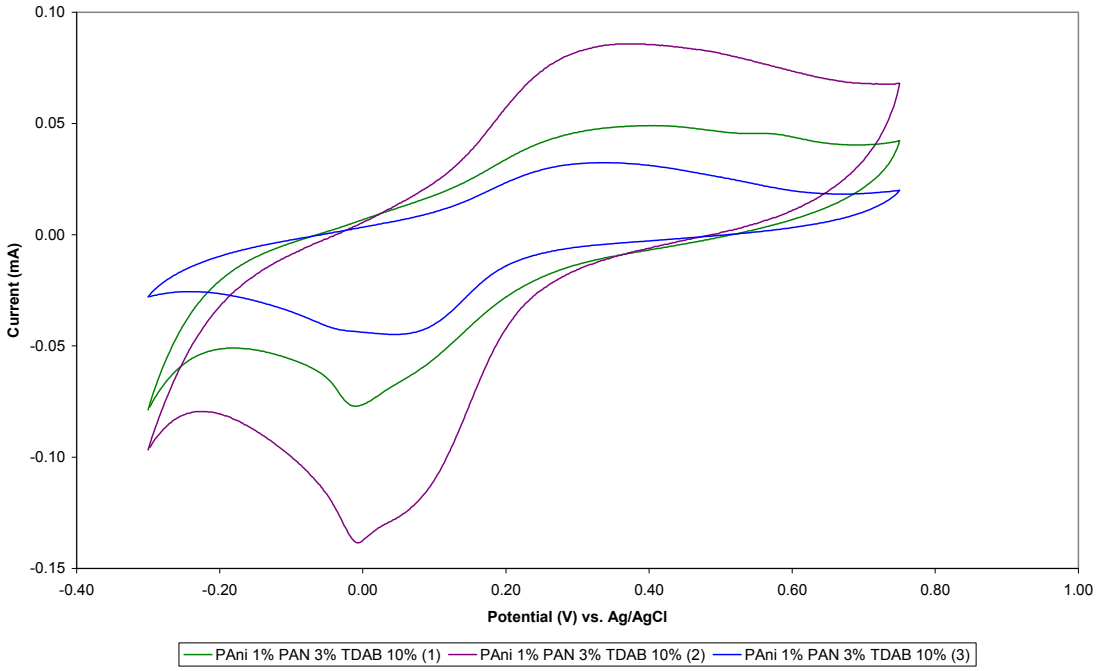

Figure 5.26 Cyclic voltammograms (10^{th} cycle) of replicate electrodes electrospun from PAni 1% PAN 3% TDAB 10% in DMSO/DMF/THF and scanned at 50 mV/s in acetate buffer.

Overall the electrospun electrodes of PAni/PAN/TDAB exhibited little specificity for NO_3^- even though increases in the peak currents were larger than those reported for BF_4^- and Cl^-, but this can be related to the original electroactivity of the electrospun fibres. In terms of response, the evolution of secondary redox couples for electrodes cycled in 10^{-1} M BF_4^-, as well as a consistent increase in peak currents with concentration indicates that BF_4^- interacted with PAni and TDAB in a reliable fashion, unlike NO_3^-, and that an inherent variability existed between, and within the electrospun electrodes.

5.3.9 PAni/PVC/TAEAB Electrospun Fibres

Cyclic voltammetry of an electrode electrospun from PAni 1% PVC 10% TAEAB 0.5% (triallylethylammonium bromide, a documented nitrate ionophore) THF/DMF cycled in increasing concentration of nitrate and spiked with BF_4^- is given in Figure 5.27. Due to

the limited dissolution of TAEAB in the solvent blend of THF/DMF no other blends of PAni/PVC/TAEAB could be prepared for analysis. Table 5.15 provides the peak currents and peak potentials for this blend cycled in NO_3^-, 10^{-1} M NO_3^- spiked with BF_4^- and BF_4^-.

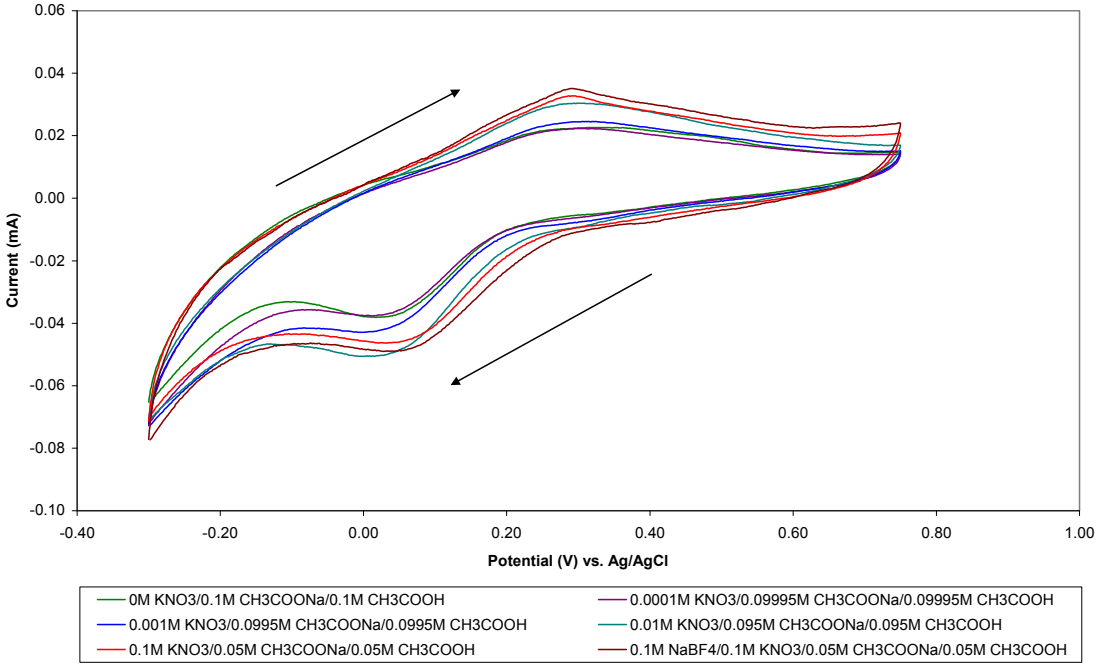

Figure 5.27 Cyclic voltammograms (10^{th} cycle) of an electrode electrospun from PAni 1% PVC 10% TAEAB 0.5% in THF/DMF and scanned at 50 mV/s in NO_3^-/acetate buffer and spiked with 10^{-1} M BF_4^-.

Cycling the electrospun electrode in the acetate buffer resulted in relatively small oxidation/reduction peak currents of 0.02/-0.04 mA with a broad oxidation peak at 0.33 V and a corresponding reduction peak located at 0.02 V. The addition of 10^{-4} M NO_3^- to the acetate buffer resulted in no change to the redox peak currents, but the addition of 10^{-3} M led to an increase in the oxidation peak current to 0.03 mA, whilst the reduction peak current remained constant. A further increase in $[NO_3^-]$ to 10^{-2} M increased the reduction peak current to -0.05 mA, but in this case the oxidation peak current remained

constant, and an increase to 10^{-1} M produced no change to either peak currents. The spike to 10^{-1} M BF_4^- increased the oxidation peak current to 0.04 mA, but did not alter the reduction peak. Overall all analyses showed increases in the peak current with increasing concentration of either NO_3^- or BF_4^-, however these were small, indicating that there was little if any selectivity towards NO_3^-.

[TAEAB] (%)	$[NO_3]$ (M)	Oxidation Peak 1		Reduction Peak 1		Comparison of Voltammograms
		Potential (V) (vs. Ag/AgCl)	Current (mA)	Potential (V) (vs. Ag/AgCl)	Current (mA)	
0.5	0	0.33	0.02	0.02	-0.04	Voltammogram In Figure 5.27
	0.0001	0.31	0.02	0.00	-0.04	
	0.001	0.31	0.03	0.00	-0.04	
	0.01	0.31	0.03	0.00	-0.05	
	0.1	0.29	0.03	0.03	-0.05	
	0.1 BF_4^-	0.29	0.04	0.04	-0.05	
[TAEAB] (%)	$[BF_4^-]$ (M)	Oxidation Peak 1		Reduction Peak 1		Comparison of Voltammograms
		Potential (V) (vs. Ag/AgCl)	Current (mA)	Potential (V) (vs. Ag/AgCl)	Current (mA)	
0.5	0	0.33	0.02	0.00	-0.04	Tilting of voltammogram with increasing concentration
	0.0001	0.33	0.04	No Peak	No Peak	
	0.001	0.33	0.04	No Peak	No Peak	
	0.01	0.37	0.05	No Peak	No Peak	
	0.1	0.42	0.07	No Peak	No Peak	

Table 5.15 Redox potentials of PAni/PVC/TAEAB electrospun electrodes cycled in acetate buffer/NO_3^- and acetate buffer/BF_4^-

Figure 5.28 presents an overlay of replicate electrospun electrodes prior to analysis. Clearly the electrodes electrospun from this blend were much more uniform, at least from an electrochemical point of view, than those electrospun from most other blends.

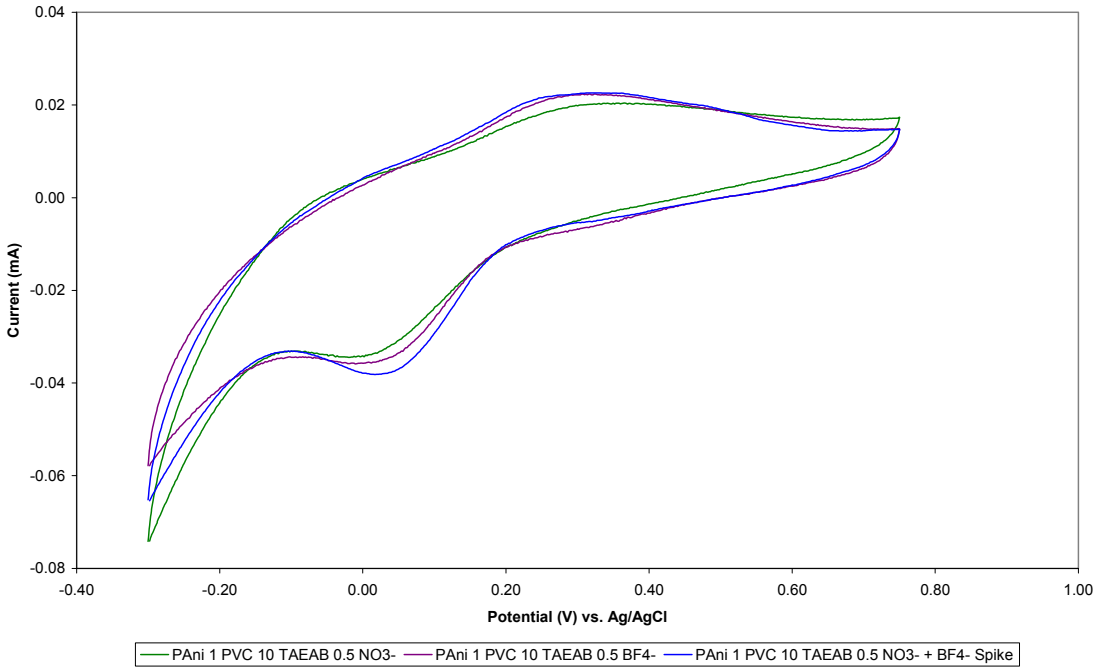

Figure 5.28 Cyclic voltammograms (10^{th} cycle) of replicate electrodes electrospun from PAni 1% PVC 10% TAEAB 10% in THF/DMF and scanned at 50 mV/s in acetate buffer.

5.3.10 PAni/PAN/TAEAB Electrospun Fibres

Cyclic voltammograms of PAni/PAN fibres incorporating TAEAB also exhibited relatively poor responses and electroactivity. Figure 5.29 presents cyclic voltammograms of an electrode electrospun from PAni 1% PAN 3% TAEAB 0.5% and cycled in increasing [NO_3^-] in acetate buffer, and then spiked to 10^{-1} M BF_4^-. These cyclic voltammograms will be used as a typical electrochemical response for comparison of PAni/PAN/TAEAB samples with peak currents and peak potentials given in Table 5.16 and 5.17.

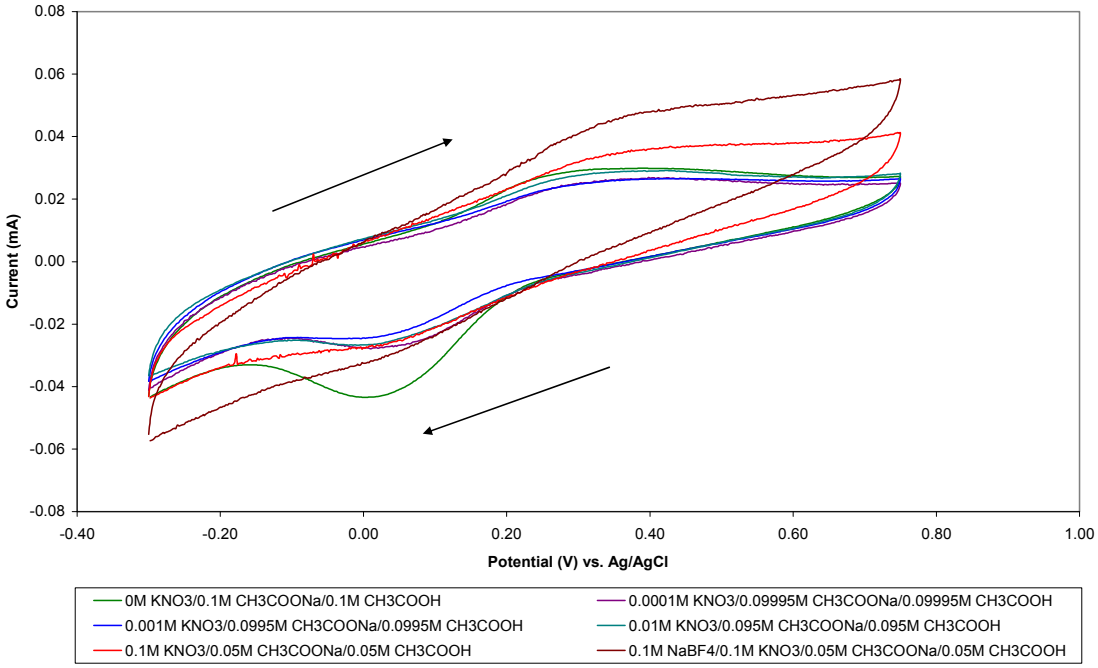

Figure 5.29 Cyclic voltammograms (10^{th} cycle) of an electrode electrospun from PAni 1% PAN 3% TAEAB 0.5% in DMSO/DMF and scanned at 50 mV/s in a NO_3^-/acetate buffer and spiked with 10^{-1} M BF_4^-.

The first cycle of PAni/PAN/TAEAB 0.5% in the acetate buffer produced a broad oxidation peak at ~ 0.38V and a large reduction peak at 0 V with oxidation/reduction peak currents of 0.03/-0.04 mA. After the addition of 10^{-4} M NO_3^- the oxidation peak current remained stable whilst the reduction peak current decreased to -0.03 mA. An increase in [NO_3^-] to 10^{-3} M produced the same oxidation peak current but a further decrease in the reduction peak current to -0.02 mA. Subsequent increases in the concentration of NO_3^- increased the reduction peak current to -0.03 mA with no change to the oxidation peak current. After this solution the peaks barely changed on spiking to 10^{-1} M BF_4^- to produce 0.04/-0.03 mA oxidation/reduction peak currents. The electrode appeared to become far more resistive with increasing [NO_3^-] and cycle numbers, tilting as a result.

[TAEAB] (%)	[NO_3] (M)	Oxidation Peak 1		Reduction Peak 1	
		Potential (V) (vs. Ag/AgCl)	Current (mA)	Potential (V) (vs. Ag/AgCl)	Current (mA)
0.5	0	0.38	0.03	0.00	-0.04
	0.0001	0.36	0.03	0.04	-0.03
	0.001	0.36	0.03	0.03	-0.02
	0.01	0.36	0.03	0.03	-0.03
	0.1	0.34	0.03	0.03	-0.03
	0.1 BF_4^-	0.33	0.04	0.05	-0.03
5	0	0.30	0.02	0.24	-0.01
	0.0001	0.29	0.02	0.24	-0.01
	0.001	0.31	0.03	0.26	-0.01
	0.01	0.29	0.03	0.19	-0.02
	0.1	0.27	0.03	0.27	-0.01
	0.1 BF_4^-	0.34	0.05	0.25	-0.01
10	0	0.24	0.03	0.31	-0.03
	0.0001	0.24	0.03	0.29	-0.04
	0.001	0.24	0.03	0.29	-0.04
	0.01	0.24	0.03	0.29	-0.03
	0.1	0.27	0.03	0.31	-0.03
	0.1 BF_4^-	0.27	0.03	0.22	-0.03
[TAEAB] (%)	Oxidation Peak 2		Reduction Peak 2		Comparison of Voltammograms
	Potential (V) (vs. Ag/AgCl)	Current (mA)	Potential (V) (vs. Ag/AgCl)	Current (mA)	
0.5	No Peak	No Peak	No Peak	No Peak	Voltammogram in Figure 5.29
	No Peak	No Peak	No Peak	No Peak	
	No Peak	No Peak	No Peak	No Peak	
	No Peak	No Peak	No Peak	No Peak	
	No Peak	No Peak	No Peak	No Peak	
	No Peak	No Peak	No Peak	No Peak	
5	No Peak	No Peak	No Peak	No Peak	Similar to Figure 5.29, although further broadening of the reduction peak
	No Peak	No Peak	No Peak	No Peak	
	No Peak	No Peak	No Peak	No Peak	
	No Peak	No Peak	No Peak	No Peak	
	No Peak	No Peak	No Peak	No Peak	
	No Peak	No Peak	No Peak	No Peak	
10	0.45	0.04	0.65	-0.01	Indication of capacitance in sample Presence of secondary redox pair not consistent with PAni
	0.44	0.04	0.64	-0.01	
	0.43	0.04	0.64	-0.01	
	0.44	0.03	0.63	-0.01	
	0.51	0.03	0.68	0.00	
	0.50	0.03	0.67	0.00	

Table 5.16 Redox potentials of PAni/PAN//TAEAB electrospun electrodes cycled in acetate buffer/NO_3^- vs. Ag/AgC land spiked with BF_4^-.

Cycling an electrode of the same composition in increasing concentrations of BF_4^- again led to only slight increases in peak current, though the voltammogram indicated that this electrode was somewhat more electroactive. In this case the oxidation/reduction peak

currents recorded from cycling in the acetate buffer decreased from 0.06/-0.14 to 0.05/-0.12 mA for the 10^{-4} M solution and did not increase until cycled in the 10^{-2} M BF_4^- solution. From Figure 5.30 the cyclic voltammograms of replicate electrodes of PAni/PAN/TAEAB 0.5% again show appreciable variability between electrodes, particularly in the size of the reduction peaks.

[TAEAB] (%)	[BF_4^-] (M)	Oxidation Peak 1		Reduction Peak 1		Comparison of Voltammograms
		Potential (V) (vs. Ag/AgCl)	Current (mA)	Potential (V) (vs. Ag/AgCl)	Current (mA)	
0.5	0	0.39	0.06	0.02	-0.14	Sharper oxidation and reduction peaks.
	0.0001	0.37	0.05	0.01	-0.12	
	0.001	0.35	0.05	0.02	-0.12	
	0.01	0.34	0.07	0.04	-0.12	
	0.1	0.43	0.08	0.12	-0.11	
5	0	0.38	0.03	0.22	-0.02	Similar to Figure 5.29, but growth in reduction tail at 10^{-1} M
	0.0001	0.38	0.03	0.22	-0.03	
	0.001	0.38	0.03	0.22	-0.03	
	0.01	0.38	0.03	0.22	-0.02	
	0.1	0.37	0.03	0.29	-0.02	
10	0	0.48	0.06	0.22	-0.02	Similar to Figure 5.29, but growth in reduction tail at 10^{-1} M
	0.0001	0.47	0.05	0.22	-0.03	
	0.001	0.47	0.55	0.29	-0.03	
	0.01	0.48	0.05	0.29	-0.03	
	0.1	0.40	0.07	0.40	-0.01	

Table 5.17 Redox potentials of PAni/PAN//TAEAB electrospun electrodes cycled in acetate buffer/BF_4^-

The increased ionophore content in PAni 1% PAN 3% TAEAB 5% in DMSO/DMF reduced the electrochemical response of the electrode as its cyclic voltammogram in acetate buffer had very little in the form of PAni redox peaks. A small broad oxidation peak occurred at ~0.30 V, with the corresponding small broad reduction peak at 0.24 V. Subsequent increases in [NO_3^-] for this electrode increased the peak currents only slightly, from 0.02/-0.01 mA for the oxidation/reduction peak currents in the acetate buffer to 0.03/-0.01 mA for 10^{-1} M NO_3^-. Spiking the solution to 10^{-1} M [BF_4^-] produced an increase in the peak currents to 0.05/-0.01mA, however the voltammogram tilted indicating a loss of electroactivity. Thus the presence of TAEAB produced an electrode

that was not selective towards NO_3^-, and also possessed only a small measure of electroactivity related to PAni. This was also evident in the voltammogram for BF_4^- analysis with no significant increase in the peak currents with increasing [BF_4^-].

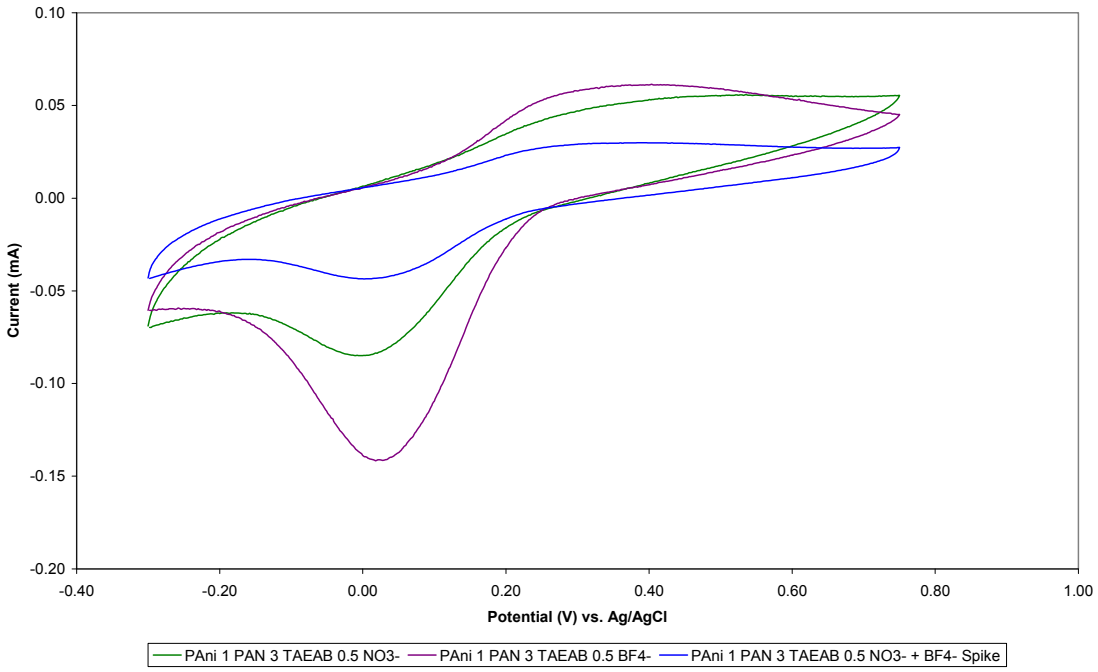

Figure 5.30 Cyclic voltammograms (10th cycle) of replicate electrodes electrospun from PAni 1% PAN 3% TAEAB 0.5% in THF/DMF and scanned at 50 mV/s in acetate buffer.

Increasing the ionophore concentration further to TAEAB 10% produced an electrode possessing electrochemical responses consistent with degradation, and is given in Figure 5.31. Initially, it appeared that two oxidation peaks occurred at ~0.24 V and ~0.45 V (vs Ag/AgCl) and two corresponding reduction peaks at ~0.31 V and ~0.65 V respectively. Clearly the reduction peak at 0.65 V could not be part of this process as it is a more positive than both oxidation peaks, indicating the normal oxidation and reduction processes of PAni were only partially responsible for these peaks, and that redox peaks corresponding to the degradation productions were responsible [292].

Furthermore, the response of the electrode is decreasing with increasing cycle numbers, indicative of degrading PAni [317].

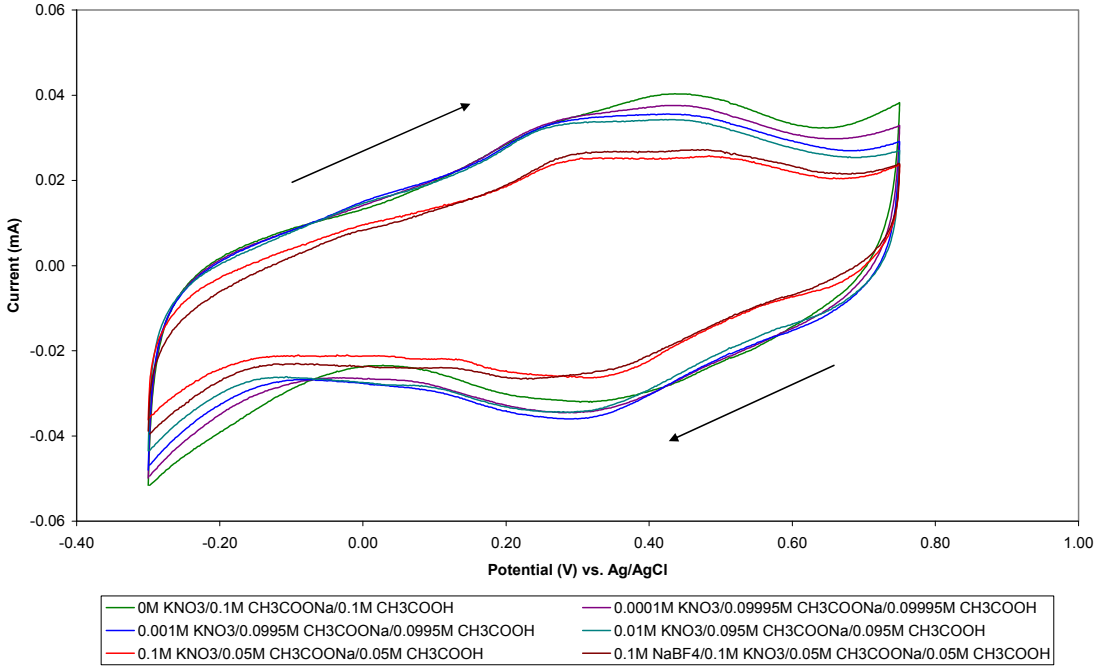

Figure 5.31 Cyclic voltammograms (10^{th} cycle) of an electrode electrospun from PAni 1% PAN 3% TAEAB 10% in DMSO/DMF and scanned at 50 mV/s in a NO_3^-/acetate buffer and spiked with 10^{-1} M BF_4^-.

Cyclic voltammetry of the sample in BF_4^- led to a response quite similar to PAni/PAN/TAEAB 5% in BF_4^-. Overall the presence of TAEAB in PAni/PAN led to low PAni electroactivity and no specificity for NO_3^- in solution.

5.3.11 MWNT/PVC Electrospun Fibres

Electrospun electrodes containing MWNT were also analysed by cyclic voltammetry to study their electrochemical characteristics. Figure 5.32 is an overlay of cyclic voltammograms of an electrode electrospun from MWNT 0.5% PVC 10% THF/DMF and cycled in 0.05 M HCl/0.15 M KCl solution.

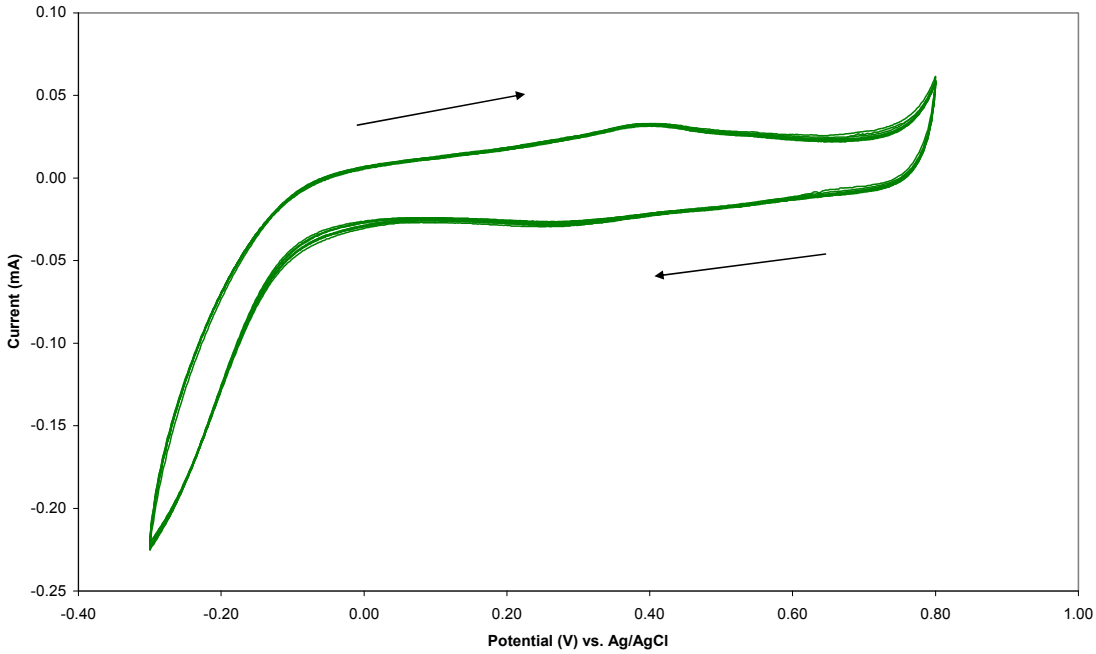

Figure 5.32 Cyclic voltammograms (10 cycles) of an electrode electrospun from MWNT 0.5% PVC 10% in THF/DMF and scanned at 50 mV/s in a 0.05M HCl/0.15M KCl solution.

The overlay indicates that the MWNT formed a conductive network throughout the PVC by the relatively horizontal aspect of the voltammogram, which is surprising considering that the low conductivity of the MWNT blends discussed in Section 2.6.7 and poor quality of the MWNTs in Section 4.3.10. In addition the voltammogram changed very little over the course of these cycles indicating that the electrochemical properties of the electrospun fibres were quite stable. The rectangular aspect of the voltammogram, indicated some degree of capacitance similar to observations by Xiao and Zhou [318]. The cyclic voltammogram in Figure 5.32 also exhibited oxidation and reduction peaks, at 0.41 V and 0.28 V (vs. Ag/AgCl) with peak currents of 0.03 mA and -0.03 mA respectively, similar to that observed by Barisci et al. [319] for SWNT cycled in 1.0M H_2SO_4. Barisci et al. concluded that these peaks were due to surface redox reactions by oxygen-containing functional groups generated during NT purification, and

that changes in pH led to shifts in the response. It is also possible that these peaks were from the oxidation and reduction of metallic impurities present in the MWNT product from the catalytic chemical vapour deposition used to produce nanotubes [320, 321]. The MWNT samples used in the current work were not purified before use and it is unknown what purification methods they were subjected to prior to delivery. However, the certificate of analysis shows the presence of amphorous carbon, as well as nickel and lithium impurities.

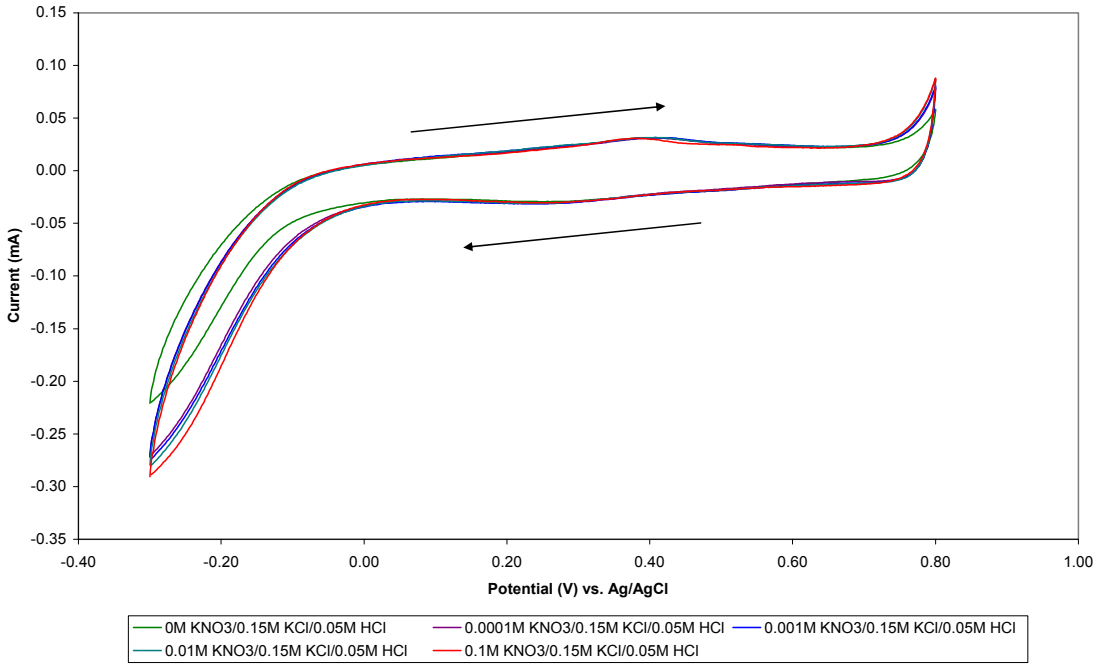

Figure 5.33 Cyclic voltammograms (10th cycle) of an electrode electrospun from MWNT 0.5% PVC 10% in THF/DMF and scanned at 50 mV/s in a 0.05M HCl/0.15M KCl solution with increasing [NO_3^-].

Furthermore, the oxidation of water appears to have been taking place at ~0.8V and a significant reduction tail commenced at approximately -0.07V. These two 'tails' occurred at potentials less positive for the oxidation response, and more positive for the reduction response in comparison to Barisci et al. [319], who report these peaks at

varied potentials depending on the supporting electrolyte. Considering these tails were previously observed in some of the PAni/polymer/ionophore electrodes it that these were due to the oxidation and reduction of water.

The addition of NO_3^- to the HCl/KCl supporting electrolyte produced very little change in the voltammogram apart from an increase in the size of the reduction tail with increasing [NO_3^-]. This can be observed in Figure 5.33. Again, this is consistent with the observations of Barisci et al. [319] who studied the voltammetry of the SWNT in solutions with various anions. They observed little change in the current response and overall shape of the voltammograms with increasing cycles.

5.3.12 MWNT/PAN Electrospun Fibres

An overlay of 10 cycles of an electrode electrospun from MWNT 0.5% PAN 3% DMSO/DMF and cycled in 0.05M HCl/0.15M KCl are presented in Figure 5.34.

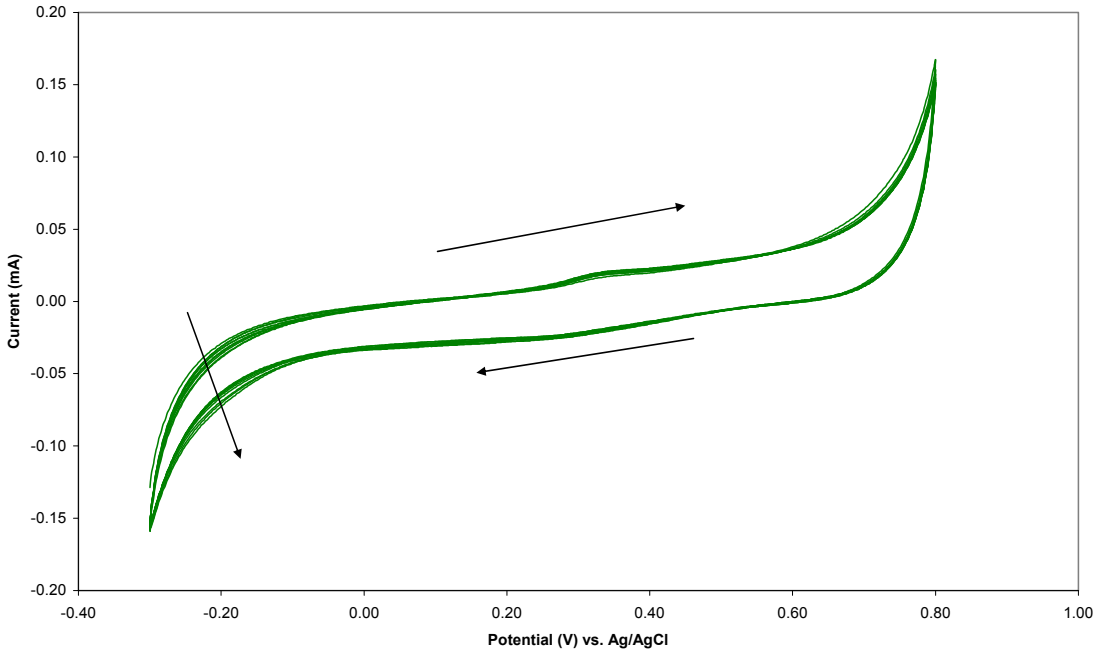

Figure 5.34 Cyclic voltammograms (10 cycles) of an electrode electrospun from MWNT 0.5% PAN 3% in DMSO/DMF and scanned 50 mV/s in 0.05M HCl/0.15M KCl solution.

The cyclic voltammograms were similar to that observed for MWNT/PVC electrospun fibres in that they also possessed oxidation and reduction peaks at 0.33 V and 0.26 V with peak currents of 0.02 mA and -0.03 mA, respectively. The lower redox potentials may indicate easier oxidation of a species within the fibres, possibly due to differences in the support polymers leading to differences in the hydrophobicity of the electrospun fibres. In addition the electrochemical response of the fibrous electrode was slightly unstable as the overlay shows tilting of the voltammograms with increasing cycles.

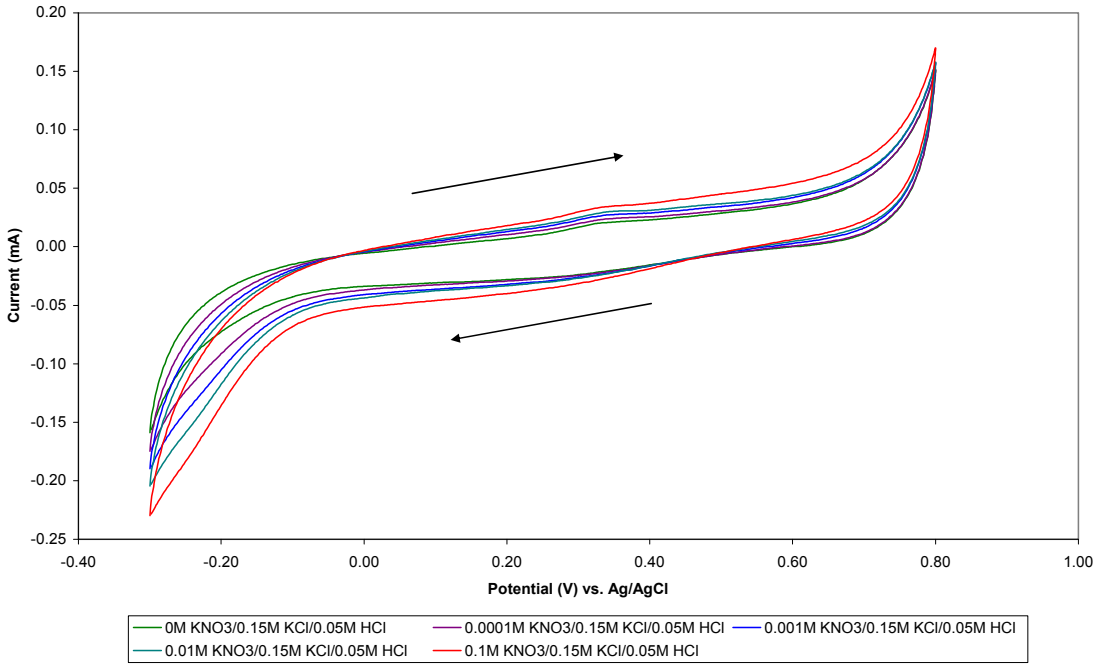

Figure 5.35 Cyclic voltammograms (10th cycle) of an electrode electrospun from MWNT 0.5% PAN 3% in DMSO/DMF and scanned at 50 mV/s in a 0.05M HCl/0.15M KCl solution with increasing [NO_3^-].

This electrode was also somewhat more resistive than MWNT/PVC as it was slightly tilted with respect to the horizontal axis. In real terms the content of MWNT present within the MWNT/PAN fibres was much larger than the MWNT/PVC blend, though

this did not translate into a greater current capacity overall. As indicated by Raman spectra in Section 4.3.13, the MWNT were reasonably dispersed throughout the mat.

Cycling in increasing [NO_3^-] in HCl/KCl produced tilting of the electrode away from the horizontal with increasing concentration and cycle number. The drift in the electrode towards resistance indicates that the conducting network within the fibres is becoming less stable, possibly due to the presence of PAN, changes in the physical properties of the fibres with increasing number of cycles, or the electrode not achieving a steady-state during the analysis. However, overall there is no major change in the electrochemical response in the increased concentration that indicates any specifity towards NO_3^-, or a response proportional to its increased concentration.

5.4 Conclusions

Fibre electrodes electrospun from PAni 1% PVC 10% THF/DMF and PAni 1% PAN 3% DMSO/DMF solutions were electroactive during cyclic voltammetry, exhibiting the characteristic redox response of the three forms of PAni at low pH.

Regardless of the ionophore employed, selectivity towards nitrate ion in an acetate buffer proved minimal. In the case of PAni/PVC/2-NPOE 5% and PAni/PAN/2-NPOE 5% electrodes there was some proportionality between current and increasing NO_3^- concentration. This was only at relatively high concentrations of 10^{-3} M NO_3^- and greater, and a similar proportionality was exhibited with Cl^- acetate buffer. The quaternary ammonium salts of TOAB, TDAB and TAEAB also exhibited little, if any, selectivity towards NO_3^-, and TAEAB was also detrimental to the electrochemical characteristics of the electrodes.

More significantly, the electrochemical responses of the electrospun electrodes varied significantly between compositions. For example, electrodes electrospun from PAni/polymer/2-NPOE solutions exhibited very consistent cyclic voltammograms, however PAni/PVC/TOAB electrodes exhibited very different profiles to PAni/PAN/TOAB. Within each concentration of TDAB (0.5%, 5%, 10%) the electrochemical response of the PAni/polymer/TDAB electrodes were similar. However, the cyclic voltammograms changed with increasing TDAB concentration, indicting changes in the electrochemical properties of the electrodes.

These differences in electrochemical responses between the various electrode compositions appear to be a product of the inherent properties of the electrodes, such as

hydrophobicity, degree of dispersion and homogeneity of PAni and/or the ionophore, and the permeability of the fibres, as well as the physical properties of the electrospun electrodes such as fibre morphology, contact with the underlying electrode and uniformity in the electrospun coating.

Overall, replicate electrospun electrodes of PAni/polymer/ionophore blends showed that not only is electrospinning highly variable, but that this variability translates into a lack of consistency in the background electrochemical response of the electrodes. Consistently, the background cyclic voltammogram peak currents of electrodes cycled in acetate buffer differed between electrodes, including electrodes with the same composition. In addition, increasing the concentration of ionophore within the electrospinning solution produced fibre electrodes that exhibit a decrease in electroactivity, in affect reducing the concentration of the electroactive component (PAni), while increasing the hydrophobicity of the fibres.

One recurring issue throughout this work was the decrease in cyclic voltammogram peak current after the addition of 10^{-4} M NO_3^-, Cl^- or BF_4^- to the supporting electrolyte (acetate buffer), followed by an increase in peak current after cycling in higher test ion concentrations. It was postulated that this decrease-increase response was a product of changes in the degree of doping of PAni, or the result of the ionophore binding the with the test ion, changing the ion-exchange processes. Furthermore, the evolution of two redox couples for some samples when cycled in 10^{-1} M test ion concentrations was also observed, indicating that the degree of protonation of PAni had changed. The pH of the original acetate buffer was recorded as 4.62, and in the case of a 10^{-1} M NO_3^-/acetate buffer solution the pH was 4.56. Thus, either this small change in pH affected the electrochemical properties of PAni, or the presence of high ion concentrations in

conjunction with the ionophore, PAni and support polymer, interacted to increase the protonation of PAni.

Electrospun electrodes containing MWNT produced capacitive cyclic voltammograms that also possessed a small, broad redox couple, possibly derived from metallic impurities from the MWNT or redox reactions of oxygen-containing functional groups.

Chapter 6 – General Conclusion

"A conclusion is the place where you got tired of thinking"

Harold Fricklestein

The process of electrospinning commodity polymer (PVC or PAN) was found to be dependant on a number of parameters, such as solution viscosity, surface tension and conductivity. These parameters were significantly influenced by the polymer employed, the composition of the polymer solution and addition of non-polymer additives, such as QAS. Addition of the conducting polymer PAni to these polymer solutions also led to noticeable changes in these parameters.

Specifically a change in the viscoelastic properties was observed with the addition of PAni to a solution, in turn allowing solutions with much lower concentrations of support polymer to be electrospun successfully. It was postulated that the interaction between PAni and PVC differed to that between PAni and PAN, with PAN providing a supporting scaffold-type structure due to the molecular dipole on the cyano-groups. This was supported by Raman spectra of the electrospun PAni/PAN fibres that suggested PAni had undergone some degree of 'secondary doping', where the PAN support structure had initiated a change in the conformation of PAni to an uncoiled state. In the case of PVC it would appear that PAni was actively lubricating the PVC chains, or that PVC was shielding the PAni chains from each other. This was supported by rheological analysis that showed the PAni/PVC solution possessed a higher viscosity than the PVC-only solution at PVC concentrations less than 15%. Conversely, at a PVC concentration of 20% w/w, the PVC-only solution had a higher viscosity than the PAni/PVC solution. Additionally, Raman analysis also showed that the PAni/PVC electrospun fibres did not exhibit any 'secondary doping', indicating less interaction between PAni and PVC compared with PAni and PAN.

The addition of a quaternary ammonium salt (TDAB) to the PAni/PVC solution led to a significant increase in viscosity, indicating that TDAB actively participates in the

interaction between the solution components. This was also supported by a significant increase in the surface tension of a PAni/PVC/TDAB solution, and differences consistent with conformation changes of PAni in the Raman spectra for PAni/PVC/TDAB compared with PAni/PVC.

Replacing PAni with MWNT also provided evidence that PVC and PAN were inherently different in their interaction with other solution components. Though PAN 3% w/w in DMSO/DMF originally possessed a higher viscosity than PVC 10% w/w in THF/DMF, there was a significant increase in viscosity with the addition of MWNT to PVC 10%, but less so for their addition to PAN 3%. This indicated that it was not simply MWNT entanglement with the polymer in both instances. However, it was discovered by Raman spectroscopy that the MWNT were of poor quality, containing a significant amount of contaminant, and this may have reduced any MWNT/PVC interactions. Conversely, cyclic voltammetry of MWNT/polymer electrospun electrodes showed the MWNT did impart a capacitive response, indicating that whilst the quality of the MWNT was poor, they did retain their characteristic electrochemical properties.

Scanning electron microscopy (SEM) of a wide range of electrospun mats showed that PVC or PVC blend fibres were consistently smoother in appearance than PAN or PAN blend fibres. This was due to the high surface tension of these PAN-based solutions which led to the formation of beads-on-string morphology and larger amounts of electrosprayed polymer. In comparison, the lower surface tension of PAni/PVC solutions produced fibres that did not exhibit this extent of beads and electrospray.

The variation in morphology between PAni/PVC and PAni/PAN blends was unexpected as according to particle size analysis, there were large aggregates throughout all

PAni/polymer solutions. Though these aggregates were not evident in the fibre morphology from SEM, Raman dispersion maps of the electrospun fibres showed areas of high PAni concentration, consistent with electrospray, but the underlying fibres were a uniform dispersion of PAni throughout the fibrous mats of both blends.

SEM also revealed that PVC fibres electrospun from THF/DMF were significantly larger in diameter than fibres of PAN electrospun from DMSO/DMF. Taking into account that the viscosities of the PAN solutions were notably higher than those of PVC solutions, which would be expected to lead to PAN fibres having a greater diameter than PVC fibres, these differences in fibre diameter could only be a result of the higher conductivity of the PAN solutions compared with PVC. It was also determined that the surface tension of the spinning solution had little, if any, influence on fibre diameters. This higher conductivity led to an increase in the extension of the whipping jet, and the consistent production of true electrospun nanofibres, i.e. those below 100 nm for PAni 1% PAN 1% and PAni 1% PAN 3% w/w solutions, as well as extremely low diameters for a number of other PAN based samples. Increasing the concentration of the support polymer led to an increase in the average fibre diameter, a product of the reduced stretching ability of the whipping polymer jet and greater polymer chain entanglement, in addition to an increase in the uniformity of the electrospun fibres and a decrease in the presence of beads and electrospray. This trend was also observed for the PAni/polymer fibres, except those containing 2-NPOE or QAS.

More generally, the addition of plasticisers or ionophores to the electrospinning solution led to changes in the morphology compared with simple blends of PAni/PVC and PAni/PAN. The use of 2-NPOE as a plasticiser prevented the production of electrospun fibres, leading to a complete collapse in the fibre structure at concentrations of 20%

w/w 2-NPOE in solution. Considering plasticiser concentrations of up to 60% w/w are used in ion-selective electrodes (ISEs), this creates difficulty in producing an electrospun ISE with the necessary physical and chemical properties.

At low concentrations of ionophore, PAni/PVC/ionophore fibre morphology was not significantly affected, suggesting that the ionophore, whilst significantly altering solution viscosity, surface tension and conductivity, leads to a balance of these properties such that there was no net change to the electrospinning process and the resultant fibres. At higher ionophore concentrations, notable changes which detrimentally affected the morphology of the electrospun fibres did occur. These led to electrospraying and, in some cases, to a partial collapse of fibre structure, and an increase in the point-bonding of fibres. This point-bonding suggested solvent was retained in the fibres after electrospinning, allowing the polymer fibres to 'flow' and bind with underlying fibres.

Contrary to expectations, point-bonding did not increase the mechanical strength of the samples, although other studies have shown it to significantly contribute to the mechanical strength of fibrous mats. Both PAni/PVC/TDAB and PAni/PVC/TOAB electrospun fibres showed extensive point-bonding, however PAni/PVC/TOAB exhibited significantly lower tensile strength than either PAni/PVC/TDAB or a simple PAni/PVC blend. Thus the presence of TOAB negated the mechanical contribution of PAni to the strength of the electrospun fibres. Furthermore, there was evidence to suggest the higher mechanical strength of PAni/PVC/TDAB fibres was a result of anti-plasticisation. Also contrary to expectations, the point-bonding of the electrospun fibres did not lead to a more electroactive PAni network. Even though more point-bonding was evident, cyclic voltammetry of electrodes with higher concentrations of ionophore

indicated less electroactivity of the fibre electrodes. This was directly related to the relative decrease in PAni levels in the fibres with increasing ionophore concentration.

In the case of PAni/PAN/ionophore solutions, the resultant fibres were quite poor compared with PAni/PAN fibres, as they exhibited significantly more beads and electrosprayed polymer globules. It was postulated that these beads and globules were derived from a higher solution surface tension, and any increase in solution conductivity from the presence of ionophore was negated by this surface tension increase. It was also suggested that droplets on the surface of some fibres may have been aggregates of undissolved ionophore, or possibly undissolved PAni, supported by observations from particle size analysis, however the size of these droplets was not consistent with the diameters produced from particle size analysis. Raman micrographs of the fibre samples did show the presence of large particles throughout the fibre structure, as expected from particle size analysis, but the PAni was well dispersed throughout the underlying fibrous mat.

The addition of MWNT to PVC or PAN solutions led to a decrease in globule and bead formation in the fibre morphology for MWNT/PVC samples, and a degree of porosity in addition to a rough texture for MWNT/PAN fibres. It was postulated that these differences were a result of aggregations of MWNT within the fibres rather than a physico-chemical contribution, again supported by observations from particle size analysis. However, Raman analysis indicated that the MWNT was well dispersed through both MWNT/PVC and MWNT/PAN.

Whilst SEM analysis indicated that the morphology of the electrospun fibres was relatively uniform, cyclic voltammetry of replicate electrodes of

PAni/polymer/ionophore blends showed that the electrochemical responses were quite variable. It was found the electrospun fibres of PAni/PVC and PAni/PAN exhibited electroactivity typical of low and high pH regimes. In 0.1 M HCl/KCl the fibres exhibited two redox pairs indicative of the electrochemical response of PAni: the oxidation of leucoemeraldine to emeraldine, followed by the oxidation of emeraldine to pernigraniline and the corresponding reverse processes. In an acetate buffer solution (pH of ~4.62) the electrochemical properties changed significantly such that the two redox couples coalesced into a single couple. Whilst some studies have indicated that PAni at this pH should exhibit no electroactivity this was not the case as the single redox couple was retained throughout cycling.

Whilst the fabrication of a nitrate selective electrode proved difficult, the electrochemical characterisation and evaluation of electrospun fibre electrodes provided further evidence on the affect of plasticisers and ionophores on PAni/PVC and PAni/PAN fibre electrodes. Different additives resulted in different degrees of electroactivity and responses to anion concentration, with electrodes incorporating the solvent mediator/plasticiser 2-NPOE recording the largest peak currents of any electrospun fibre electrode when cycled in acetate buffer. Additionally, the response to NO_3^- for electrodes containing 2-NPOE indicated some degree of proportional response at concentrations greater than 10^{-3} M NO_3^-, though this also occurred with increasing chloride concentration. The presence of a QAS such as TOAB or TDAB led to a decrease in the electrochemical response, and in the case of some solutions, an increase in the resistivity and change in the electrochemical characteristics. Spiking an acetate buffer/Cl^- solution with NO_3^- to 10^{-3} M NO_3^- did not lead to a significant increase in current response for electrodes containing 5% TOAB. Differences in the peak currents when electrodes containing TDAB were cycled in different test ions was a direct result

of the electroactivity of the electrode, rather than any selectivity to nitrate. Furthermore, TAEAB was found to be severely detrimental to the electrochemical response of the electrodes regardless of the test solution they were cycled in, leading to relatively constant responses with increasing test ion concentration and an increase in resistivity of the electrode. Thus it appears that fibre homogeneity and contact with the underlying electrode, and the influence of the blend composition, through its impact on permeability and hydrophobicity, were responsible for these differences.

One perplexing aspect exhibited by the majority of electrospun fibre mats when cycled in the presence of various test ions (NO_3^-, Cl^-, BF_4^-) was the initial reduction in peak current when cycled in 10^{-4} M anion compared with the peak current recorded for the same electrode cycled in the acetate buffer alone. In some cases peak current decreased further when the electrode was cycled at 10^{-3} M test ion concentration in acetate buffer, before increasing when cycled in 10^{-2} M. Furthermore at 10^{-1} M test ion concentration, some fibre electrodes exhibited the evolution of two oxidation peaks, a feature often associated with cycling PAni at a lower pH. It was postulated that these observations were a result of changes in the degree of protonation of PAni due to the fibre electrode composition and affect of the ionophore on the chemical properties of PAni. An alternative theory for the decrease-increase phenomenon was that the ionophore preferentially 'bound' the test ion, leading to changes in the ion-exchange process. As the concentration of test ion increased, ion-exchange between the PAni and test ion were able to take place, leading to a change in the electrochemical properties of the electrode.

A number of electrospun PAni/polymer/ionophore electrodes exhibited large reduction tails at the lower potential limit, indicative of the reduction of water or, less likely, some

other species. These tails were also present in electrospun MWNT/polymer electrodes, and appear to be a result of the chemical composition and possibly the physical morphology of the fibres.

Morphologically reproducible fibre mats electrospun from solutions containing electroactive PAni/dopant/commodity polymer/ionophore blends or MWNT/commodity polymer blends were successfully fabricated. These fibres were shown to contain well dispersed PAni (and MWNT in separate experiments) and an electrochemical response characteristic of doped PAni. However, the electrochemical properties of these fibre mats remained extremely variable. Unfortunately, electrospun fibre mats produced by simple blending of any ionophore with PAni and a commodity plastic is very unlikely to work as a selective NO_3^- sensor.

"You gain strength, courage and confidence by every experience in which you really stop to look fear in the face. You are able to say to yourself, 'I have lived through this horror. I can take the next thing that comes along.' You must do the thing you think you cannot do."

Eleanor Roosevelt (1884 - 1962)

References

1. Wallace, G.G., G. Spinks, and P.R. Teasdale, *Conductive Electroactive Polymer: Intelligent Materials Systems*. 1997, Lancaster, (Pennsylvania, USA): Technomic Publishing Company.

2. Shirakawa, H., *The discovery of polyacetylene film: the dawning of an era of conducting polymers (Nobel Lecture).* Angewandte Chemie, International Edition, 2001. **40**(14): p. 2575-2580.

3. MacDiarmid, A.G., *Synthetic metals: a novel role for organic polymers.* Synthetic Metals, 2002. **125**(1): p. 11-22.

4. Gomez-Romero, P. and M. Lira-Cantu, *From conducting polymers to electroactive hybrid materials.* Materials Research Society Symposium Proceedings, 2002. **726**(Organic/Inorganic Hybrid Materials--2002): p. 355-368.

5. Diaz, A.F. and J.A. Logan, *Electroactive polyaniline films.* Journal of Electroanalytical Chemistry and Interfacial Electrochemistry, 1980. **111**(1): p. 111-14.

6. Negi, Y.S. and P.V. Adhyapak, *Development in polyaniline conducting polymers.* Journal of Macromolecular Science, Polymer Reviews, 2002. **C42**(1): p. 35-53.

7. Chen, W.-C. and T.-C. Wen, *Electrochemical and capacitive properties of polyaniline-implanted porous carbon electrode for supercapacitors.* Journal of Power Sources, 2003. **117**(1-2): p. 273-282.

8. Fusalba, F., et al., *Electronically conducting polymers as active electrode material for electrochemical supercapacitors.* Proceedings - Electrochemical Society, 1999. **98-15**(Selected Battery Topics): p. 651-660.

9. Hu, C.-C., E. Chen, and J.-Y. Lin, *Capacitive and textural characteristics of polyaniline-platinum composite films.* Electrochimica Acta, 2002. **47**(17): p. 2741-2749.

10. Belanger, D., et al., *Characterization and long-term performance of polyaniline-based electrochemical capacitors.* Journal of the Electrochemical Society, 2000. **147**(8): p. 2923-2929.

11. El-Sherif, M.A., J. Yuan, and A. MacDiarmid, *Fiber optic sensors and smart fabrics.* Journal of Intelligent Material Systems and Structures, 2001. **11**(5): p. 407-414.

12. de Souza, S., et al., *Polyaniline based acrylic blends for iron corrosion protection.* Electrochemical and Solid-State Letters, 2001. **4**(8): p. B27-B30.

13. Barisci, J.N., et al., *Conducting polymers as a basis for responsive materials systems.* Journal of Intelligent Material Systems and Structures, 1999. **9**(9): p. 723-731.

14. Wallace, G.G. and P.C. Innis, *Inherently conducting polymer nanostructures.* Journal of Nanoscience and Nanotechnology, 2002. **2**(5): p. 441-451.

15. Kulkarni, V.G., *Polyanilines: progress in processing and applications.* ACS Symposium Series, 1999. **735**(Semiconducting Polymers): p. 174-183.

16. Aussawasathien, D., J.H. Dong, and L. Dai, *Electrospun polymer nanofiber sensors.* Synthetic Metals, 2005. **154**(1-3): p. 37-40.

17. Aytac, A., et al., *Ion-Selective Electrodes Prepared with Polyaniline Membranes.* Russian Journal of Electrochemistry (Translation of Elektrokhimiya), 2004. **40**(7): p. 732-735.

18. Karyakin, A.A., et al., *Potentiometric biosensors based on polyaniline semiconductor films.* Sensors and Actuators, B: Chemical, 1996. **B33**(1-3): p. 34-38.

19. Lindfors, T., S. Ervela, and A. Ivaska, *Polyaniline as pH-sensitive component in plasticized PVC membranes.* Journal of Electroanalytical Chemistry, 2003. **560**(1): p. 69-78.

20. Shishkanova, T.V., et al., *Ion-selective electrodes: polyaniline modification and anion recognition.* Analytica Chimica Acta, 2005. **553**(1-2): p. 160-168.

21. Virji, S., et al., *Polyaniline nanofiber gas sensors: examination of response mechanisms.* Nano Letters, 2004. **4**(3): p. 491-496.

22. Ye, J. and R.P. Baldwin, *Flow-injection analysis for electroinactive anions at a polyaniline electrode.* Analytical Chemistry, 1988. **60**(18): p. 1979-82.

23. Huang, J., et al., *Nanostructured polyaniline sensors.* Chemistry--A European Journal, 2004. **10**(6): p. 1314-1319.

24. Gerard, M., A. Chaubey, and B.D. Malhotra, *Application of conducting polymers to biosensors.* Biosensors & Bioelectronics, 2002. **17**(5): p. 345-359.

25. Anderson, M.R., et al., *Conjugated polymer films for gas separations.* Science (Washington, DC, United States), 1991. **252**(5011): p. 1412-15.

26. Pellegrino, J., *The use of conducting polymers in membrane-based separations: A review and recent developments.* Annals of the New York Academy of Sciences, 2003. **984**(Advanced Membrane Technology): p. 289-305.

27. Pickup, P.G., *Electrochemistry of electronically conducting polymer films.* Modern Aspects of Electrochemistry, 1999. **33**: p. 549-597.

28. Huang, W.S., B.D. Humphrey, and A.G. MacDiarmid, *Polyaniline, a novel conducting polymer. Morphology and chemistry of its oxidation and reduction in aqueous electrolytes.* Journal of the Chemical Society, Faraday Transactions 1: Physical Chemistry in Condensed Phases, 1986. **82**(8): p. 2385-400.

29. Pud, A.A., *Stability and degradation of conducting polymers in electrochemical systems.* Synthetic Metals, 1994. **66**(1): p. 1-18.

30. MacDiarmid, A.G. and A.J. Epstein, *The polyanilines: a novel class of conducting polymers.* Materials Research Society Symposium Proceedings, 1990. **173**(Adv. Org. Solid State Mater.): p. 283-91.

31. Manohar, S.K., A.G. MacDiarmid, and A.J. Epstein, *Polyaniline: pernigraniline, an isolable intermediate in the conventional chemical synthesis of emeraldine.* Synthetic Metals, 1991. **41**(1-2): p. 711-14.

32. Ayad, M.M. and M.A. Sheneshin, *Effect of acids on in situ polyaniline film formation.* Polymer International, 2004. **53**(8): p. 1180-1184.

33. Adams, P.N. and A.P. Monkman, *Characterization of high molecular weight polyaniline synthesized at -40 DegC using a 0..25:1 mole ratio of persulfate oxidant to aniline.* Synthetic Metals, 1997. **87**(2): p. 165-169.

34. Kang, E.T., K.G. Neoh, and K.L. Tan, *Polyaniline: a polymer with many interesting intrinsic redox states.* Progress in Polymer Science, 1998. **23**(2): p. 277-324.

35. Cao, Y., et al., *Influence of chemical polymerization conditions on the properties of polyaniline.* Polymer, 1989. **30**(12): p. 2305-11.

36. Lux, F., *Properties of electronically conductive polyaniline: a comparison between well-known literature data and some recent experimental findings.* Polymer, 1994. **35**(14): p. 2915-36.

37. Chiang, J.C. and A.G. MacDiarmid, *'Polyaniline': protonic acid doping of the emeraldine form to the metallic regime.* Synthetic Metals, 1986. **13**(1-3): p. 193-205.

38. Bredas, J.L. and G.B. Street, *Polarons, bipolarons, and solitons in conducting polymers.* Accounts of Chemical Research, 1985. **18**(10): p. 309-15.

39. Heeger, A.J., *Self-assembled networks of conducting polyaniline: a new class of conducting polymer blends.* Trends in Polymer Science (Cambridge, United Kingdom), 1995. **3**(2): p. 39-47.

40. Kang, X., et al., *Surface Plasmon Resonance Studies on the Electrochemical Doping/Dedoping Processes of Anions on Polyaniline-Modified Electrode.* Langmuir, 2002. **18**(26): p. 10305-10310.

41. Ping, Z., et al., *Protonation and electrochemical redox doping processes of polyaniline in aqueous solutions: investigations using in situ FTIR-ATR (attenuated total reflection) spectroscopy and a new doping system.* Journal of the Chemical Society, Faraday Transactions, 1997. **93**(1): p. 121-129.

42. Raffa, D.L., K.T. Leung, and F. Battaglini, *Electrochemical copolymerization of aniline and ortho-aminobenzylamine. Studies on its conductivity and chemical derivatization.* Journal of Electroanalytical Chemistry, 2006. **587**(1): p. 60-66.

43. Lukachova, L.V., et al., *Electroactivity of chemically synthesized polyaniline in neutral and alkaline aqueous solutions Role of self-doping and external doping.* Journal of Electroanalytical Chemistry, 2003. **544**: p. 59-63.

44. Epstein, A.J., et al., *Insulator-to-metal transition in polyaniline.* Synthetic Metals, 1987. **18**(1-3): p. 303-9.

45. McCall, R.P., et al., *Spectroscopy and defect states in polyaniline.* Physical Review B: Condensed Matter and Materials Physics, 1990. **41**(8): p. 5202-13.

46. Focke, W.W., G.E. Wnek, and Y. Wei, *Influence of oxidation state, pH, and counterion on the conductivity of polyaniline.* Journal of Physical Chemistry, 1987. **91**(22): p. 5813-18.

47. Travers, J.P., et al., *Is granularity the determining feature for electron transport in conducting polymers?* Synthetic Metals, 1999. **101**(1-3): p. 359-362.

48. Kaiser, A.B., *Electronic transport properties of conducting polymers and carbon nanotubes.* Reports on Progress in Physics, 2001. **64**(1): p. 1-49.

49. Kaiser, A.B., et al., *Comparison of electronic transport in polyaniline blends, polyaniline and polypyrrole.* Synthetic Metals, 1997. **84**(1-3): p. 699-702.

50. Genies, E.M., J.F. Penneau, and E. Vieil, *The influence of counteranions and pH on the capacitive current of conducting polyaniline.* Journal of Electroanalytical Chemistry and Interfacial Electrochemistry, 1990. **283**(1-2): p. 205-19.

51. Stejskal, J. and R.G. Gilbert, *Polyaniline. Preparation of a conducting polymer (IUPAC technical report).* Pure and Applied Chemistry, 2002. **74**(5): p. 857-867.

52. Cao, Y., J. Qiu, and P. Smith, *Effect of solvents and co-solvents on the processibility of polyaniline: I. Solubility and conductivity studies.* Synthetic Metals, 1995. **69**(1-3): p. 187-90.

53. Cao, Y., P. Smith, and A.J. Heeger, *Counter-ion induced processibility of conducting polyaniline and of conducting polyblends of polyaniline in bulk polymers.* Synthetic Metals, 1992. **48**(1): p. 91-7.

54. Avlyanov, J.K., et al., *Polyaniline: conformational changes induced in solution by variation of solvent and doping level.* Synthetic Metals, 1995. **72**(1): p. 65-71.

55. MacDiarmid, A.G. and A.J. Epstein, *The concept of secondary doping as applied to polyaniline.* Synthetic Metals, 1994. **65**(2-3): p. 103-16.

56. Formhals, A., *Process and Apparatus for Preparting Artificial Threads*. 1934, Formhals, Anton: Germany.

57. Subbiah, T., et al., *Electrospinning of nanofibers.* Journal of Applied Polymer Science, 2005. **96**(2): p. 557-569.

58. Norris, I.D., et al., *Electrostatic fabrication of ultrafine conducting fibers: polyaniline/polyethylene oxide blends.* Synthetic Metals, 2000. **114**(2): p. 109-114.

59. Zhang, Y., et al., *High surface area chemosensor material by electrospinning of fluorescent conjugated polymer.* Polymeric Materials Science and Engineering, 2001. **85**: p. 622-623.

60. Wang, X., et al., *Fluorescent electrospun polymer films for the detection of explosives.* Polymer Preprints (American Chemical Society, Division of Polymer Chemistry), 2002. **43**(1): p. 130-131.

61. Gouma, P.I., *Nanostructured polymorphic oxides for advanced chemosensors.* Reviews on Advanced Materials Science, 2003. **5**(2): p. 147-154.

62. Ding, B., M. Yamazaki, and S. Shiratori, *Electrospun fibrous polyacrylic acid membrane-based gas sensors.* Sensors and Actuators, B: Chemical, 2005. **B106**(1): p. 477-483.

63. Sawicka, K., P. Gouma, and S. Simon, *Electrospun biocomposite nanofibers for urea biosensing.* Sensors and Actuators, B: Chemical, 2005. **B108**(1-2): p. 585-588.

64. Wang, X., et al., *Biochemical sensor via combination of electrospinning with electrostatic layer-by-layer assembly.* Polymeric Materials Science and Engineering, 2003. **88**: p. 35-36.

65. Fong, H. and D.H. Reneker, *Electrospinning and the formation of nanofibers.* Structure Formation in Polymeric Fibers, 2001: p. 225-246.

66. Lee, S.-W. and A.M. Belcher, *Virus-Based Fabrication of Micro- and Nanofibers Using Electrospinning.* Nano Letters, 2004. **4**(3): p. 387-390.

67. Boland, E.D., et al., *Tailoring tissue engineering scaffolds using electrostatic processing techniques: a study of poly(glycolic acid) electrospinning.* Journal of Macromolecular Science, Pure and Applied Chemistry, 2001. **A38**(12): p. 1231-1243.

68. Matthews, J.A., et al., *Electrospinning of Collagen Nanofibers.* Biomacromolecules, 2002. **3**(2): p. 232-238.

69. Duan, B., et al., *Electrospinning of chitosan solutions in acetic acid with poly(ethylene oxide).* Journal of Biomaterials Science, Polymer Edition, 2004. **15**(6): p. 797-811.

70. Katti, D.S., et al., *Bioresorbable nanofiber-based systems for wound healing and drug delivery: Optimization of fabrication parameters.* Journal of Biomedical Materials Research, Part B: Applied Biomaterials, 2004. **70B**(2): p. 286-296.

71. Casper, C.L., et al., *Controlling Surface Morphology of Electrospun Polystyrene Fibers: Effect of Humidity and Molecular Weight in the Electrospinning Process.* Macromolecules, 2004. **37**(2): p. 573-578.

72. Spasova, M., et al., *Preparation of chitosan-containing nanofibers by electrospinning of chitosan/poly(ethylene oxide) blend solutions.* e-Polymers, 2004: p. o54.

73. Belcheva, N., et al., *Crosslinked poly(ethylene oxide) for drug release systems.* Macromolecular Symposia, 1996. **103**(Polymers and Medicine): p. 193-211.

74. Wang, X., et al., *Electrospun nanofibrous membranes for optical sensing.* Polymeric Materials Science and Engineering, 2001. **85**: p. 617-618.

75. Wang, X., et al., *Electrospinning technology: a novel approach to sensor application.* Journal of Macromolecular Science, Pure and Applied Chemistry, 2002. **A39**(10): p. 1251-1258.

76. Wang, X., et al., *Synthesis and electrospinning of a novel fluorescent polymer PMMA-PM for quenching-based optical sensing.* Journal of Macromolecular Science, Pure and Applied Chemistry, 2002. **A39**(10): p. 1241-1249.

77. Madhugiri, S., et al., *Electrospun MEH-PPV/SBA-15 Composite Nanofibers Using a Dual Syringe Method.* Journal of the American Chemical Society, 2003. **125**(47): p. 14531-14538.

78. Drew, C., et al., *Electrospun nanofibers of electronic and photonic polymer systems.* Annual Technical Conference - Society of Plastics Engineers, 2000. **58th**(Vol. 2): p. 1477-1481.

79. MacDiarmid, A.G., et al., *Electrostatically-generated nanofibers of electronic polymers.* Synthetic Metals, 2001. **119**(1-3): p. 27-30.

80. Shin, Y.M., et al., *Experimental characterization of electrospinning: the electrically forced jet and instabilities.* Polymer, 2001. **42**(25): p. 09955-09967.

81. Feng, J.J., *The stretching of an electrified non-Newtonian jet: A model for electrospinning.* Physics of Fluids, 2002. **14**(11): p. 3912-3926.

82. Hohman, M.M., et al., *Electrospinning and electrically forced jets. I. Stability theory.* Physics of Fluids, 2001. **13**(8): p. 2201-2220.

83. Yarin, A.L., S. Koombhongse, and D.H. Reneker, *Taylor cone and jetting from liquid droplets in electrospinning of nanofibers.* Journal of Applied Physics, 2001. **90**(9): p. 4836-4846.

84. Lee, K.H., et al., *Mechanical behavior of electro spun fiber mats of poly(vinyl chloride)/polyurethane polyblends.* Journal of Polymer Science, Part B: Polymer Physics, 2003. **41**(11): p. 1256-1262.

85. Hayati, I., *Eddies inside a liquid cone stressed by interfacial electrical shear.* Colloids and Surfaces, 1992. **65**(1): p. 77-84.

86. Scuador, A.E., Jr., M.T. Shaw, and P.T. Mather, *Electrospinning of polymeric nanofibers: analysis of jet formation.* Materials Research Society Symposium Proceedings, 2001. **661**(Filled and Nanocomposite Polymer Materials): p. KK5.9/1-KK5.9/6.

87. Yarin, A.L. and E. Zussman, *Upward needleless electrospinning of multiple nanofibers.* Polymer, 2004. **45**(9): p. 2977-2980.

88. Hohman, M.M., et al., *Electrospinning and electrically forced jets. II. Applications.* Physics of Fluids, 2001. **13**(8): p. 2221-2236.

89. Shin, Y.M., et al., *Electrospinning: A whipping fluid jet generates submicron polymer fibers.* Applied Physics Letters, 2001. **78**(8): p. 1149-1151.

90. Bousfield, D.W., et al., *Nonlinear analysis of the surface tension driven breakup of viscoelastic filaments.* Journal of Non-Newtonian Fluid Mechanics, 1986. **21**(1): p. 79-97.

91. Fridrikh, S.V., et al., *Non-linear whipping behavior of electrified fluid jets.* Polymer Preprints (American Chemical Society, Division of Polymer Chemistry), 2003. **44**(2): p. 55-56.

92. Zuo, W., et al., *Experimental study on relationship between jet instability and formation of beaded fibers during electrospinning.* Polymer Engineering and Science, 2005. **45**(5): p. 704-709.

93. Reneker, D.H., et al., *Bending instability of electrically charged liquid jets of polymer solutions in electrospinning.* Journal of Applied Physics, 2000. **87**(9, Pt. 1): p. 4531-4547.

94. Fridrikh, S.V., et al., *Controlling the Fiber Diameter during Electrospinning.* Physical Review Letters, 2003. **90**(14): p. 144502/1-144502/4.

95. Wu, X., et al., *Effect of solvent on morphology of electrospinning ethyl cellulose fibers.* Journal of Applied Polymer Science, 2005. **97**(3): p. 1292-1297.

96. Liu, H. and Y.-L. Hsieh, *Ultrafine fibrous cellulose membranes from electrospinning of cellulose acetate.* Journal of Polymer Science, Part B: Polymer Physics, 2002. **40**(18): p. 2119-2129.

97. Kattamuri, N., J. Shawon, and C. Sung, *Electrospinning of polycarbonate nanofibers with THF and DMF.* Polymer Preprints (American Chemical Society, Division of Polymer Chemistry), 2003. **44**(1): p. 763-764.

98. Shawon, J. and C. Sung, *Electrospinning of polycarbonate nanofibers with solvent mixtures THF and DMF.* Journal of Materials Science, 2004. **39**(14): p. 4605-4613.

99. Frenot, A. and I.S. Chronakis, *Polymer nanofibers assembled by electrospinning.* Current Opinion in Colloid & Interface Science, 2003. **8**(1): p. 64-75.

100. Theron, A., E. Zussman, and A.L. Yarin, *Electrostatic field-assisted alignment of electrospun nanofibres.* Nanotechnology, 2001. **12**: p. 384-390.

101. Theron, S.A., E. Zussman, and A.L. Yarin, *Experimental investigation of the governing parameters in the electrospinning of polymer solutions.* Polymer, 2004. **45**(6): p. 2017-2030.

102. Deitzel, J.M., et al., *The effect of processing variables on the morphology of electrospun nanofibers and textiles.* Polymer, 2001. **42**(1): p. 261-272.

103. Jaeger, R., et al., *Electrospinning of ultrathin polymer fibers.* Macromolecular Symposia, 1998. **127**(Rolduc Polymer Meeting 10: \"Petro\" Polymers vs. \"Green\" Polymers, 1997): p. 141-150.

104. Reneker, D.H. and I. Chun, *Nanometer diameter fibers of polymer, produced by electrospinning.* Nanotechnology, 1996. **7**(3): p. 216-223.

105. Reneker, D.H., et al., *Nanofiber garlands of polycaprolactone by electrospinning.* Polymer, 2002. **43**(25): p. 6785-6794.

106. Srinivasan, G. and D.H. Reneker, *Structure and morphology of small diameter electrospun aramid fibers.* Polymer International, 1995. **36**(2): p. 195-201.

107. Demir, M.M., et al., *Electrospinning of polyurethane fibers.* Polymer, 2002. **43**(11): p. 3303-3309.

108. Krishnappa, R.V.N., C. Sung, and H. Schreuder-Gibson, *Electrospinning of polycarbonates and their surface characterization using the SEM and TEM.* Materials Research Society Symposium Proceedings, 2002. **702**(Advanced Fibers, Plastics, Laminates and Composites): p. 235-240.

109. Bognitzki, M., et al., *Submicrometer shaped polylactide fibers by electrospinning.* Polymeric Materials Science and Engineering, 2000. **82**: p. 115-116.

110. Yao, L. *Electrospinning of poly(vinyl alcohol) nanofibers*. in *American Chemical Society Division of Industrial & Engineering Chemistry - Abstracts*

223rd ACS National Meeting. 2002. Orlando, Florida.

111. Sung, C., H. Gibson, and R. Varma. *Electrospinning of polycarbonates and their surface characteristics*. in *New Frontiers in Fiber Science; I*. 2001: The Fiber Society.

112. Jun, Z., et al., *Poly-L-lactide nanofibers by electrospinning - Influence of solution viscosity and electrical conductivity on fiber diameter and fiber morphology.* e-Polymers, 2003: p. No pp. given, Paper No. 9.

113. Kim, J.-S. and D.H. Reneker, *Polybenzimidazole nanofiber produced by electrospinning.* Polymer Engineering and Science, 1999. **39**(5): p. 849-854.

114. Lee, K.H., et al., *Characterization of nano-structured poly(e-caprolactone) nonwoven mats via electrospinning.* Polymer, 2003. **44**(4): p. 1287-1294.

115. Ding, B., et al., *Preparation and characterization of a nanoscale poly(vinyl alcohol) fiber aggregate produced by an electrospinning method.* Journal of Polymer Science, Part B: Polymer Physics, 2002. **40**(13): p. 1261-1268.

116. Wang, Y., S. Serrano, and J.J. Santiago-Aviles, *Conductivity measurement of electrospun PAN-based carbon nanofiber.* Journal of Materials Science Letters, 2002. **21**(13): p. 1055-1057.

117. Deitzel, J.M., et al., *Controlled deposition of electrospun poly(ethylene oxide) fibers.* Polymer, 2001. **42**(19): p. 8163-8170.

118. Inai, R., M. Kotaki, and S. Ramakrishna, *Structure and properties of electrospun PLLA single nanofibres.* Nanotechnology, 2005. **16**(2): p. 208-213.

119. Gupta, P., et al., *Electrospinning of linear homopolymers of poly(methyl methacrylate): exploring relationships between fiber formation, viscosity, molecular weight and concentration in a good solvent.* Polymer, 2005. **46**(13): p. 4799-4810.

120. Jun, Z., et al., *Poly(vinyl alcohol) nanofiber by electrospinning: Influence of molecular weight on fiber shape.* e-Polymers, 2005: p. No pp given.

121. Li, L. and Y.-L. Hsieh, *Ultra-fine polyelectrolyte fibers from electrospinning of poly(acrylic acid).* Polymer, 2005. **46**(14): p. 5133-5139.

122. Seoul, C., Y.-T. Kim, and C.-K. Baek, *Electrospinning of poly(vinylidene fluoride)/dimethylformamide solutions with carbon nanotubes.* Journal of Polymer Science, Part B: Polymer Physics, 2003. **41**(13): p. 1572-1577.

123. Yang, Q., et al., *Influence of solvents on the formation of ultrathin uniform poly(vinylpyrrolidone) nanofibers with electrospinning.* Journal of Polymer Science, Part B: Polymer Physics, 2004. **42**(20): p. 3721-3726.

124. Choi, S.W., et al., *Electrochemical and spectroscopic properties of electrospun PAN-based fibrous polymer electrolytes.* Journal of the Electrochemical Society, 2005. **152**(5): p. A989-A995.

125. Bergshoef, M.M. and G.J. Vancso, *Transparent nanocomposites with ultrathin, electrospun nylon-4,6 fiber reinforcement.* Advanced Materials (Weinheim, Germany), 1999. **11**(16): p. 1362-1365.

126. Fennessey, S.F. and R.J. Farris, *Fabrication of aligned and molecularly oriented electrospun polyacrylonitrile nanofibers and the mechanical behavior of their twisted yarns.* Polymer, 2004. **45**(12): p. 4217-4225.

127. Huang, Z.-M., et al., *Electrospinning and mechanical characterization of gelatin nanofibers.* Polymer, 2004. **45**(15): p. 5361-5368.

128. Schreuder-Gibson, H., et al., *Characteristics of electrospun fibers containing carbon nanotubes.* Proceedings - Electrochemical Society, 2000. **2000-12**(Fullerenes 2000--Volume 10: Chemistry and Physics of Fullerenes and Carbon Nanomaterials): p. 210-221.

129. Desai, K. and C. Sung, *Electrospinning nanofibers of PANI/PMMA blends.* Materials Research Society Symposium Proceedings, 2002. **736**(Electronics on Unconventional Substrates--Electrotextiles and Giant-Area Flexible Circuits): p. 121-126.

130. Fong, H., et al., *Generation of electrospun fibers of Nylon 6-montmorillonite nanocomposite.* Polymer Preprints (American Chemical Society, Division of Polymer Chemistry), 2001. **42**(2): p. 63-64.

131. Diaz-de Leon, M.J. *Electroctrospinning Nanofibers of Polyaniline and Polyaniline/(Polystyrene and Polyethylene Oxide) Blends*. in *Proceeding of The National Conference On Undergraduate Research*. 2001. University of Kentucky, Lexington.

132. Hou, H., et al., *Poly(p-xylylene) Nanotubes by Coating and Removal of Ultrathin Polymer Template Fibers.* Macromolecules, 2002. **35**(7): p. 2429-2431.

133. Hou, H. and D.H. Reneker, *Carbon nanotubes on carbon nanofibers: A novel structure based on electrospun polymer nanofibers.* Advanced Materials (Weinheim, Germany), 2004. **16**(1): p. 69-73.

134. Hong, J.H., et al., *Electrospinning of polyurethane/organically modified montmorillonite nanocomposites.* Journal of Polymer Science, Part B: Polymer Physics, 2005. **43**(22): p. 3171-3177.

135. Kim, S.J., C.K. Lee, and S.I. Kim, *Effect of ionic salts on the processing of poly(2-acrylamido-2-methyl-1-propane sulfonic acid) nanofibers.* Journal of Applied Polymer Science, 2005. **96**(4): p. 1388-1393.

136. Wang, M., A.J. Hsieh, and G.C. Rutledge, *Electrospinning of poly(MMA-co-MAA) copolymers and their layered silicate nanocomposites for improved thermal properties.* Polymer, 2005. **46**(10): p. 3407-3418.

137. Wutticharoenmongkol, P., et al., *Electrospinning of polystyrene/poly(2-methoxy-5-(2'-ethylhexyloxy)-1,4-phenylene vinylene) blends.* Journal of Polymer Science, Part B: Polymer Physics, 2005. **43**(14): p. 1881-1891.

138. Jiang, H., et al., *Preparation and characterization of ibuprofen-loaded poly(lactide-co-glycolide)/poly(ethylene glycol)-g-chitosan electrospun membranes.* Journal of Biomaterials Science, Polymer Edition, 2004. **15**(3): p. 279-296.

139. Zhang, Y., et al., *Electrospinning of gelatin fibers and gelatin/PCL composite fibrous scaffolds.* Journal of Biomedical Materials Research, Part B: Applied Biomaterials, 2005. **72B**(1): p. 156-165.

140. Wannatong, L. and A. Sirivat, *Electrospun fibers of polypyrrole/polystyrene blend for gas sensing applications.* PMSE Preprints, 2004. **91**: p. 692-693.

141. Doshi, J. and D.H. Reneker, *Electrospinning process and applications of electrospun fibers.* Journal of Electrostatics, 1995. **35**(2&3): p. 151-60.

142. Lee, K.H., et al., *Influence of a mixing solvent with tetrahydrofuran and N,N-dimethylformamide on electrospun poly(vinyl chloride) nonwoven mats.* Journal of Polymer Science, Part B: Polymer Physics, 2002. **40**(19): p. 2259-2268.

143. Kang, Y.-S., et al., *The Effect of Processing Parameters on the Diameter of Electrospun Polyacrylonitrile (PAN) Nano Fibers.* Polymer (Korea, In Korean Language), 2002. **26**(3): p. 360-366.

144. Lee, K.H., et al., *The change of bead morphology formed on electrospun polystyrene fibers.* Polymer, 2003. **44**(14): p. 4029-4034.

145. Lee, S.-H., J.-W. Yoon, and M.H. Suh, *Continuous nanofibers manufactured by electrospinning technique.* Macromolecular Research, 2002. **10**(5): p. 282-285.

146. Wei, M., et al., *Preparation of core-sheath nanofibers from conducting polymer blends.* Macromolecular Rapid Communications, 2005. **26**(14): p. 1127-1132.

147. MacDiarmid, A.G., et al., *Polyaniline based chemical transducers with sub-micron dimensions.* Polymeric Materials Science and Engineering, 2000. **83**: p. 544-545.

148. Dong, H., et al., *Polyaniline/poly(methyl methacrylate) coaxial fibers: The fabrication and effects of the solution properties on the morphology of electrospun core fibers.* Journal of Polymer Science, Part B: Polymer Physics, 2004. **42**(21): p. 3934-3942.

149. Hong, K.H. and T.J. Kang, *Polyaniline-nylon 6 composite nanowires prepared by emulsion polymerization and electrospinning process.* Journal of Applied Polymer Science, 2006. **99**(3): p. 1277-1286.

150. Zhu, Y., et al., *Stable, superhydrophobic, and conductive polyaniline/polystyrene films for corrosive environments.* Advanced Functional Materials, 2006. **16**(4): p. 568-574.

151. Li, M., et al., *Electrospinning polyaniline-contained gelatin nanofibers for tissue engineering applications.* Biomaterials, 2006. **27**(13): p. 2705-2715.

152. Pinto, N.J., P. Carrion, and J.X. Quinones, *Electroless deposition of nickel on electrospun fibers of 2-acrylamido-2-methyl-1-propanesulfonic acid doped polyaniline.* Materials Science & Engineering, A: Structural Materials: Properties, Microstructure and Processing, 2004. **A366**(1): p. 1-5.

153. Bouchard, D.C., M.K. Williams, and R.Y. Surampalli, *Nitrate contamination of groundwater: sources and potential health effects.* Journal - American Water Works Association, 1992. **84**(9): p. 85-90.

154. Elmi, A.A., C. Madramootoo, and C. Hamel, *Influence of water table and nitrogen management on residual soil NO3- and denitrification rate under corn production in sandy loam soil in Quebec.* Agriculture, Ecosystems & Environment, 2000. **79**(2-3): p. 187-197.

155. Eichler, F. and D. Schulz, *The nitrogen reduction program in the Federal Republic of Germany.* Environmental Pollution, 1998. **102**(Suppl. 1): p. 609-617.

156. Bolger, P., et al., *Contamination of Australian Groundwater Systems with Nitrate*, in *Occasional Paper Series*. 1999, Land & Water Resources: Research & Development Corporation: Canberra, ACT.

157. *Nitrates: An Environmental Assessment*. 1978, The National Research Council: Washington DC. p. 723.

158. Van Maanen, J.M.S., et al., *Does the risk of childhood diabetes mellitus require revision of the guideline values for nitrate in drinking water?* Environmental Health Perspectives, 2000. **108**(5): p. 457-461.

159. *Standard Methods for the Examination of Water and Wastewater*. 17 ed, ed. L.S. Clesceri, A.E. Greenburg, and R.R. Trussell. 1989, Washington, DC: American Public Health Association, American Water Works Association, & Water Pollution Control Federation.

160. Horvai, G., K. Toth, and E. Pungor, *Theoretical models of ion-selective electrode membranes.* Analytica Chimica Acta, 1989. **216**(1-2): p. 163-76.

161. Pungor, E. and K. Toth, *Ion selective electrodes. A review.* Analytical Sciences, 1987. **3**(5): p. 387-93.

162. Simon, W., et al., *Ion-selective sensors.* Angewandte Chemie, International Edition in English, 1970. **9**(6): p. 445-55.

163. Skoog, D.A., F.J. Holler, and T.A. Nieman, *Principles Of Instrumental Analysis*. 5th ed. 1998, Florida, USA: Harcourt Brace College Publishers.

164. Feng, D., *Ion-selective electrodes based on ion associates.* Ion-Selective Electrode Reviews, 1987. **9**(1): p. 95-121.

165. Johnson, R.D. and L.G. Bachas, *Ionophore-based ion-selective potentiometric and optical sensors.* Analytical and Bioanalytical Chemistry, 2003. **376**(3): p. 328-341.

166. Akl, M.A., A.K. Ghoneim, and M.H. Abd El-Aziz, *Novel plastic chromium(III)-ion selective electrodes based on different ionophoric species and plasticizing solvent mediators.* Electroanalysis, 2006. **18**(3): p. 299-306.

167. Orion, T., *Nitrate Electrode: Instruction Manual*. 2001. p. 69.

168. Braven, J., et al., *Mechanistic aspects of nitrate-selective electrodes with immobilized ion exchangers in a rubbery membrane.* Analyst (Cambridge, United Kingdom), 2003. **128**(8): p. 1067-1072.

169. Ebdon, L., J. Braven, and N.C. Frampton, *Nitrate-selective electrodes with polymer membranes containing immobilized sensors*, in *Analyst (Cambridge, United Kingdom)*. 1990. p. 189-93.

170. Ebdon, L., J. Braven, and N.C. Frampton, *Nitrate-selective electrodes containing immobilized ion exchangers within a rubbery membrane with controlled cross-link density*, in *Analyst (Cambridge, United Kingdom)*. 1991. p. 1005-10.

171. Nielsen, H.J. and E.H. Hansen, *New nitrate ion-selective electrodes based on quaternary ammonium compounds in nonporous polymer membranes.* Analytica Chimica Acta, 1976. **85**(1): p. 1-16.

172. Quan, D.P., et al., *A Conductive Polypyrrole Modified Microelectrode for Selective Amperometric Detection of Nitrate in a Flow Injection System.* Anal Sci, 2001. **17**(Supplement): p. i745 - i748.

173. Arada Perez, M.d.l.A., et al., *Influence of different plasticizers on the response of chemical sensors based on polymeric membranes for nitrate ion determination.* Sensors and Actuators, B: Chemical, 2003. **B89**(3): p. 262-268.

174. Santos, E.M.G., et al., *Use of tin (IV) porhyrins as ionophores for the construction of phthalate-selective electrodes: Influence of the structure and membrane composition on their response properties.* Electroanalysis, 2005. **17**(21): p. 1945-1951.

175. Elmosallamy, M.A.F., et al., *Potentiometric Membrane Sensor for Determination of Saccharin.* Microchimica Acta, 2005. **151**(1-2): p. 109-113.

176. Lu, W.-Y., Y.-H. Chang, and W.-H. Li, *Preparation of poly(vinyl chloride) membrane ionic electrode for nitrate determination.* Fenxi Huaxue, 1980. **8**(1): p. 48-51.

177. Baro-Roma, J., et al., *Construction and development of ion-selective electrodes responsive to anionic surfactants.* Sensors and Actuators, B: Chemical, 1993. **15**(1-3): p. 179-83.

178. Wegmann, D., et al., *Anion-selective liquid membrane electrodes based on lipophilic quaternary ammonium compounds.* Mikrochimica Acta, 1984. **3**(1-2): p. 1-16.

179. Fluka. *Selectophore Application Notes - Nitrate*. 2006 [cited 2006 20/4/05]; Available from: http://www.sigmaaldrich.com.

180. Miles, D.C. and J.H. Briston, *Polymer Technology*. 2nd ed. 1979, New York, N.Y.: Chemical Publishing Co., Inc.

181. Moody, G.J., *Role of Polymeric Materials in the Fabrication of Ion-Selective Electrodes and Biosensors*, in *Biosensors and Chemical Sensors: Optimizing Performance Through Polymeric Materials*, P.G. Edelman and J. Wang, Editors. 1992, American Chemical Society: Washington, DC.

182. Rosen, S.L., *Fundamental Principles of Polymeric Materials*. 2nd ed. 1993, New York, N.Y.: John Wiley & Sons, Inc.

183. Fong, H., I. Chun, and D.H. Reneker, *Beaded nanofibers formed during electrospinning.* Polymer, 1999. **40**(16): p. 4585-4592.

184. Lin, T., et al., *The charge effect of cationic surfactants on the elimination of fibre beads in the electrospinning of polystyrene.* Nanotechnology, 2004. **15**(9): p. 1375-1381.

185. Son, W.K., et al., *The effects of solution properties and polyelectrolyte on electrospinning of ultrafine poly(ethylene oxide) fibers.* Polymer, 2004. **45**(9): p. 2959-2966.

186. Geng, X., O.-H. Kwon, and J. Jang, *Electrospinning of chitosan dissolved in concentrated acetic acid solution.* Biomaterials, 2005. **26**(27): p. 5427-5432.

187. Jain, R. and R.V. Gregory, *Solubility and rheological characterization of polyaniline base in N-methyl-2-pyrrolidinone and N,N'-dimethylpropyleneurea.* Synthetic Metals, 1995. **74**(3): p. 263-7.

188. Lizymol, P.P. and S. Thomas, *Miscibility studies of polymer blends by viscometry methods.* Journal of Applied Polymer Science, 1994. **51**(4): p. 635-41.

189. Yang, D. and B.R. Mattes, *Investigation of Gel Inhibitor Assisted Dissolution of Polyaniline: A Case Study for Emeraldine base, 2-Methyl-Aziridine and N-Methyl-Pyrrolidone.* Synthetic Metals, 1999. **101**(1-3): p. 746-749.

190. Tan, S.H., et al., *Systematic parameter study for ultra-fine fiber fabrication via electrospinning process.* Polymer, 2005. **46**(16): p. 6128-6134.

191. Zong, X., et al., *Structure and process relationship of electrospun bioabsorbable nanofiber membranes.* Polymer, 2002. **43**(16): p. 4403-4412.

192. Xia, H. and Q. Wang, *Synthesis and characterization of conductive polyaniline nanoparticles through ultrasonic assisted inverse microemulsion polymerization.* Journal of Nanoparticle Research, 2001. **3**(5/6): p. 401-411.

193. Pron, A., et al., *Flexible, highly transparent, and conductive polyaniline-cellulose acetate composite films.* Journal of Applied Polymer Science, 1997. **63**(8): p. 971-977.

194. Park, C., et al., *Dispersion of single wall carbon nanotubes by in-situ polymerization under sonication.* Chemical Physics Letters, 2002. **364**(3,4): p. 303-308.

195. Hilding, J., et al., *Dispersion of carbon nanotubes in liquids.* Journal of Dispersion Science and Technology, 2003. **24**(1): p. 1-41.

196. Jin, Z., et al., *Nonlinear optical properties of some polymer/multi-walled carbon nanotube composites.* Chemical Physics Letters, 2000. **318**(6): p. 505-510.

197. King, B., *Nitrate-selective electrodes with covalently bound sensors*. 1985, Sheffield City Polytechnic: Sheffield City.

198. Wilkinson, W.L., *Non-Newtonian Fluids: Fluid Mechanics, Mixing and Heat Transfer*. International Series of Monographs on Chemical Engineering, ed. P.V. Danckwerts and R.F. Baddour. Vol. 1. 1960, London: Pergamon Press Ltd. 138.

199. Mikolajczyk, T. and M. Bogun, *Effect of ceramic nanoparticles on the rheological properties of spinning solutions of polyacrylonitrile in dimethylformamide.* Fibres & Textiles in Eastern Europe, 2005. **13**(1): p. 28-31.

200. Geller, B.E., et al., *Structural-mechanical properties of mixtures of polyacrylonitrile and cellulose triacetate.* Khimicheskie Volokna, 1976(3): p. 28.

201. Abu-Sharkh, B.F., et al., *Viscosity behavior and surface and interfacial activities of hydrophobically modified water-soluble acrylamide/N-phenyl acrylamide block copolymers.* Journal of Applied Polymer Science, 2003. **89**(8): p. 2290-2300.

202. Fredrickson, A.G., *Principles and Applications of Rheology*, ed. N.R. Amundson. 1964, Englewood Cliffs, New Jersey: Prentice-Hall International. 326.

203. Hwo, C.-H. and J.F. Johnson, *Flow properties of poly(vinyl chloride).* Polymer Engineering and Science, 1973. **13**(5): p. 322-36.

204. Benrraou, M., B. Bales, and R. Zana, *Effect of the nature of the counterion on the interaction between cesium and tetraalkylammonium dodecylsulfates and poly(ethylene oxide) or poly(vinylpyrolidone).* Journal of Colloid and Interface Science, 2003. **267**(2): p. 519-523.

205. Choe, H.S., et al., *Characterization of Some Polyacrylonitrile-Based Electrolytes.* Chemistry of Materials, 1997. **9**(1): p. 369-379.

206. Croce, F., et al., *Lithium-7 NMR and ionic conductivity studies of gel electrolytes based on polyacrylonitrile.* Chemistry of Materials, 1993. **5**(9): p. 1268-72.

207. Chen-Yang, Y.W., et al., *Polyacrylonitrile electrolytes 1. A novel high-conductivity composite polymer electrolyte based on PAN, LiClO4 and a-Al2O3.* Solid State Ionics, 2002. **150**(3,4): p. 327-335.

208. Iovleva, M.M., V.N. Smirnova, and G.A. Budnitskii, *The solubility of polyacrylonitrile.* Fibre Chemistry (Translation of Khimicheskie Volokna), 2001. **33**(4): p. 262-264.

209. Pornsopone, V., et al., *Electrospinning of methacrylate-based copolymers: Effects of solution concentration and applied electrical potential on morphological appearance of as-spun fibers.* Polymer Engineering and Science, 2005. **45**(8): p. 1073-1080.

210. Campanella, L., et al., *Sensitive membrane ISFETs for nitrate analysis in waters.* Sensors and Actuators, B: Chemical, 1995. **B27**(1-3): p. 329-35.

211. Alexander, P.W., T. Dimitrakopoulos, and D.B. Hibbert, *A six sensor array of coated-wire electrodes for use in a portable flow injection analyzer.* Electroanalysis, 1998. **10**(10): p. 707-712.

212. House, H.O., E. Feng, and N.P. Peet, *Comparison of various tetraalkylammonium salts as supporting electrolytes in organic electrochemical reactions.* Journal of Organic Chemistry, 1971. **36**(16): p. 2371-5.

213. Ajayan, P.M. and O.Z. Zhou, *Applications of carbon nanotubes.* Topics in Applied Physics, 2001. **80**(Carbon Nanotubes): p. 391-425.

214. Andrews, R. and M.C. Weisenberger, *Carbon nanotube polymer composites.* Current Opinion in Solid State & Materials Science, 2004. **8**(1): p. 31-37.

215. Yu, J.H., S.V. Fridrikh, and G.C. Rutledge, *Effect of fluid elasticity on the morphology of electrospun fiber.* Abstracts of Papers, 230th ACS National Meeting, Washington, DC, United States, Aug. 28-Sept. 1, 2005, 2005: p. PMSE-571.

216. Yu, J.H., S.V. Fridrikh, and G.C. Rutledge, *The role of elasticity in the formation of electrospun fibers.* Polymer, 2006. **47**(13): p. 4789-4797.

217. Entov, V.M. and L.E. Shmaryan, *Numerical modeling of the capillary breakup of jets of polymeric liquids.* Fluid Dynamics (Translation of Izvestiya Akademii Nauk, Mekhanika Zhidkosti i Gaza), 1998. **32**(5): p. 696-703.

218. Jung, H.W., H.-S. Song, and J.C. Hyun, *Draw resonance and kinematic waves in viscoelastic isothermal spinning.* AIChE Journal, 2000. **46**(10): p. 2106-2111.

219. Newman, N., *Development of a Nitrate Selective Electrode Employing Conducting Fibres Fabricated by Electrospinning*, in *School of Chemistry*. 2002, University of Tasmania: Launceston. p. 115.

220. Chen, D.-R., D.Y.H. Pui, and S.L. Kaufman, *Electrospraying of conducting liquids for monodisperse aerosol generation in the 4 nm to 1.8 mm diameter range.* Journal of Aerosol Science, 1995. **26**(6): p. 963-77.

221. Kaufman, S.L., F. Zarrin, and F. Dorman, *Electrospray apparatus for producing uniform submicrometer droplets*. 1993, (Tsi Incorporated, USA). Application: WO. p. No pp given.

222. Efremova, A., A. Regis, and L. Arsov, *Electrochemical formation and deposition of polyaniline on electrode surface; in situ Raman spectroscopical study.* Electrochimica Acta, 1994. **39**(6): p. 839-45.

223. Lapkowski, M., et al., *Electrochemical Oxidation of Polyaniline in Nonaqueous Electrolytes: \"In Situ\" Raman Spectroscopic Studies.* Macromolecules, 1995. **28**(4): p. 1233-8.

224. Liu, C., et al., *Doping level change of polyaniline film during its electrochemical growth process.* Journal of Applied Polymer Science, 2004. **92**(1): p. 171-177.

225. Job, A.E., et al., *Effect of natural rubber latex on the conducting state of polyaniline blends determined by Raman spectroscopy.* Journal of Raman Spectroscopy, 2003. **34**(10): p. 831-836.

226. Bernard, M.-C. and A. Hugot-Le Goff, *Raman spectroscopy for the study of polyaniline.* Synthetic Metals, 1997. **85**(1-3): p. 1145-1146.

227. Cochet, M., et al., *Theoretical and experimental vibrational study of polyaniline in base forms: non-planar analysis. Part I.* Journal of Raman Spectroscopy, 2000. **31**(11): p. 1029-1039.

228. Cochet, M., et al., *Theoretical and experimental vibrational study of emeraldine in salt form. Part II.* Journal of Raman Spectroscopy, 2000. **31**(12): p. 1041-1049.

229. Laska, J., A. Pron, and S. Lefrant, *Phosphoric acid diesters protonated polyaniline: preparation, spectroscopic properties, and processability.* Journal of Polymer Science, Part A: Polymer Chemistry, 1995. **33**(9): p. 1437-45.

230. Ohira, M., et al., *Raman and infrared spectra of polyaniline.* Synthetic Metals, 1987. **18**(1-3): p. 347-52.

231. Quillard, S., et al., *Vibrational analysis of the reduced form of polyaniline: the leucoemeraldine base.* Synthetic Metals, 1992. **50**(1-3): p. 525-30.

232. Pereira da Silva, J.E., et al., *Raman characterization of polyaniline induced conformational changes.* Synthetic Metals, 1999. **101**(1-3): p. 834-835.

233. Lindfors, T. and A. Ivaska, *Raman based pH measurements with polyaniline.* Journal of Electroanalytical Chemistry, 2005. **580**(2): p. 320-329.

234. Felbeck, D.K. and A.G. Atkins, *Strength and Fracture of Engineering Solids*. 2nd ed. 1996, New Jersey, USA: Prentice-Hall Inc.

235. Gordon, J.E., *The Science and Structures of Materials*. 1988, New York, USA: Scientific American Books Inc.

236. Hannah, J. and M.J. Hillier, *Applied Mechanics*. 3rd ed. 1995, Essex, England: Pearson Education Limited.

237. Bolton, W., *Mechanical Science*. 1993, Oxford, England: Blackwell Scientific Publications.

238. Mills, N.J., *Plastics: Microstrucutre & Engineering Applications*. 2nd Edition ed. Metallurgy and Materials Science, ed. R.W.K. Honeycombe and P. Hancock. 1993, New York, NY: John Wiley & Sons, Inc.

239. Nissan, A.H. and G.L. Batten, *The link between the molecular and structural theories of paper elasticity.* TAPPI Journal, 1997. **80**(4): p. 153-158.

240. Voyiatzis, G.A., et al., *Polarized Resonance Raman and FTIR Reflectance Spectroscopic Investigation of the Molecular Orientation in Industrial Poly(vinyl chloride) Specimens.* Macromolecules, 2000. **33**(15): p. 5613-5623.

241. Robinson, M.E.R., et al., *Raman spectroscopic study of poly(vinyl chloride) particles.* Polymer, 1978. **19**(10): p. 1225-9.

242. Robinson, M.E.R., D.I. Bower, and W.F. Maddams, *Molecular orientation in poly(vinyl chloride) studied by Raman spectroscopy and birefringence measurements.* Journal of Polymer Science, Polymer Physics Edition, 1978. **16**(12): p. 2115-38.

243. Ellahi, S. and R.E. Hester, *Waveguide resonance Raman spectroscopy of degraded PVC.* Spectrochimica Acta, Part A: Molecular and Biomolecular Spectroscopy, 1995. **51A**(4): p. 549-53.

244. Liebman, S.A., et al., *Laser Raman studies of poly(vinyl chloride).* Macromolecules, 1971. **4**(1): p. 134-8.

245. Reyes-Labarta, J., et al., *Wet-chemical surface modification of plasticized PVC. Characterization by FTIR-ATR and Raman microscopy.* Polymer, 2003. **44**(8): p. 2263-2269.

246. Robinson, M.E.R., D.I. Bower, and W.F. Maddams, *A study of the carbon-chlorine stretching region of the Raman spectrum of PVC.* Polymer, 1978. **19**(7): p. 773-84.

247. Gerrard, D.L. and W.F. Maddams, *Resonance Raman spectrum of thermally degraded poly(vinyl chloride).* Macromolecules, 1975. **8**(1): p. 54-8.

248. Maddams, W.F., *Some applications of Raman spectroscopy in structural studies on poly(vinyl chloride).* Journal of Macromolecular Science, Physics, 1977. **B14**(1): p. 87-100.

249. Williams, K.P.J. and D.L. Gerrard, *The degradation of poly(vinyl chloride) studied using Fourier-transform Raman spectroscopy.* European Polymer Journal, 1990. **26**(12): p. 1355-8.

250. Bowley, H.J., D.L. Gerrard, and W.F. Maddams, *Resonance Raman spectroscopic studies on dehydrochlorinated stretched poly(vinyl chloride).* Makromolekulare Chemie, 1987. **188**(4): p. 899-906.

251. Koenig, J.L. and D. Druesedow, *Raman spectra of extended-chain syndiotactic poly(vinyl chloride).* Journal of Polymer Science, Polymer Physics Edition, 1969. **7**(6): p. 1075-84.

252. Schrader, B., ed. *Infrared and Raman Spectroscopy: methods and applications*. 1995, VCH Publishers, Inc.: Weinheim, Germany.

253. Liang, C.Y. and S. Krimm, *Infrared spectra of high polymers. VII. Polyacrylonitrile.* Journal of Polymer Science, 1958. **31**: p. 513-22.

254. Huang, Y.S. and J.L. Koenig, *Raman spectra of polyacrylonitrile.* Applied Spectroscopy, 1971. **25**(6): p. 620-2.

255. Beevers, R.B., *The physical properties of polyacrylonitrile and its copolymers.* Macromolecular Reviews, 1968. **3**: p. 113-254.

256. Mathieu, D., et al., *Insight into polyacrylonitrile molecular structure from calculated vibrational frequencies and infrared intensities of model oligomers.* Chemical Physics, 1994. **188**(2,3): p. 183-95.

257. Wang, Z., et al., *Experimental evidence of the interaction between polyacrylonitrile and ethylene carbonate plasticizer by Raman spectroscopy.* Journal of Raman Spectroscopy, 1996. **27**(8): p. 609-613.

258. Grassie, N. and J.N. Hay, *Thermal coloration and insolubilization in polyacrylonitrile.* Journal of Polymer Science, 1962. **56**: p. 189-202.

259. Cundall, R.B., D.D. Eley, and J. Worrall, *Anionic polymerization of acrylonitrile.* Journal of Polymer Science, 1962. **58**: p. 869-80.

260. Baibarac, M., et al., *SERS spectra of polyaniline thin films deposited on rough Ag, Au and Cu. Polymer film thickness and roughness parameter dependence of SERS spectra.* Synthetic Metals, 1998. **96**(1): p. 63-70.

261. Pereira Da Silva, J.E., M.L.A. Temperini, and S.I. Cordoba De Torresi, *Secondary doping of polyaniline studied by resonance Raman spectroscopy.* Electrochimica Acta, 1999. **44**(12): p. 1887-1891.

262. Quillard, S., et al., *Vibrational spectroscopic studies of the isotope effects in polyaniline.* Synthetic Metals, 1997. **84**(1-3): p. 805-806.

263. Arsov, L.D., W. Plieth, and G. Kossmehl, *Electrochemical and Raman spectroscopic study of polyaniline; influence of the potential on the degradation of polyaniline.* Journal of Solid State Electrochemistry, 1998. **2**(5): p. 355-361.

264. Osswald, S., et al., *Elimination of D-band in Raman spectra of double-wall carbon nanotubes by oxidation.* Chemical Physics Letters, 2005. **402**(4-6): p. 422-427.

265. Thomsen, C. and S. Reich, *Double Resonant Raman Scattering in Graphite.* Physical Review Letters, 2000. **85**(24): p. 5214-5217.

266. Ajayan, P.M. and T.W. Ebbesen, *Nanometer-size tubes of carbon.* Reports on Progress in Physics, 1997. **60**(10): p. 1025-1062.

267. Benoit, J.M., et al., *Low-frequency Raman studies of multiwalled carbon nanotubes: Experiments and theory.* Physical Review B: Condensed Matter and Materials Physics, 2002. **66**(7): p. 073417/1-073417/4.

268. Jorio, A., et al., *Characterizing carbon nanotube samples with resonance Raman scattering.* New Journal of Physics, 2003. **5**: p. 1-17, Paper No 139.

269. Li, M.-W., et al., *Low temperature synthesis of carbon nanotubes using corona discharge plasma reaction at atmospheric pressure.* Journal of Materials Science Letters, 2003. **22**(17): p. 1223-1224.

270. Rao, A.M., et al., *Polarized Raman study of aligned multiwalled carbon nanotubes.* Physical Review Letters, 2000. **84**(8): p. 1820-1823.

271. Rey, I., et al., *Infrared and Raman study of the PEO-LiTFSI polymer electrolyte.* Electrochimica Acta, 1998. **43**(10-11): p. 1505-1510.

272. Sardanopoli, A.A., *Thermoplastic Polyurethanes (TPUR)*, in *Engineered Materials Handbook: Engineering Plastics*, J.N. Epel, et al., Editors. 1988, ASM International: Metals Park, OH.

273. Shah, B.L. and V.V. Shertukde, *Effect of plasticizers on mechanical, electrical, permanence, and thermal properties of poly(vinyl chloride).* Journal of Applied Polymer Science, 2003. **90**(12): p. 3278-3284.

274. Matsubara, Y. and S. Wakabayashi, *Flame-retarding plasticizer for nitrocellulose*. 1955, (Saisei Shono Co.). JP.

275. Pron, A., et al., *Processable conducting polyaniline.* Synthetic Metals, 1993. **57**(1): p. 3520-5.

276. Miyagawa, H., et al., *Biobased Epoxy/Layered Silicate Nanocomposites: Thermophysical Properties and Fracture Behavior Evaluation.* Journal of Polymers and the Environment, 2005. **13**(2): p. 87-96.

277. Miyagawa, H., M.J. Rich, and L.T. Drzal, *Thermophysical properties of anhydride-cured epoxy/nano-clay composites.* Polymer Composites, 2005. **26**(1): p. 42-51.

278. Jacobsen, S. and H.G. Fritz, *Plasticizing polylactide-the effect of different plasticizers on the mechanical properties.* Polymer Engineering and Science, 1999. **39**(7): p. 1303-1310.

279. Matuana, L.M., C.B. Park, and J.J. Balatinecz, *The effect of low levels of plasticizer on the rheological and mechanical properties of polyvinyl chloride/newsprint-fiber composites.* Journal of Vinyl & Additive Technology, 1997. **3**(4): p. 265-273.

280. Pita, V.J.R.R., E.E.M. Sampaio, and E.E.C. Monteiro, *Mechanical properties evaluation of PVC/plasticizers and PVC/thermoplastic polyurethane blends from extrusion processing.* Polymer Testing, 2002. **21**(5): p. 545-550.

281. Guerrero, S.J., *Antiplasticization and crystallinity in poly(vinyl chloride).* Macromolecules, 1989. **22**(8): p. 3480-5.

282. Lourdin, D., H. Bizot, and P. Colonna, *\"Antiplasticization\" in starch-glycerol films?* Journal of Applied Polymer Science, 1997. **63**(8): p. 1047-1053.

283. Tiemblo, P., et al., *On a novel interpretation of PVC antiplasticization based on some local chain conformations.* Polymer Bulletin (Berlin, Germany), 1994. **32**(3): p. 353-9.

284. Jung, Y.C., N.G. Sahoo, and J.W. Cho, *Polymeric nanocomposites of polyurethane block copolymers and functionalized multi-walled carbon nanotubes as crosslinkers.* Macromolecular Rapid Communications, 2006. **27**(2): p. 126-131.

285. Breuer, O. and U. Sundararaj, *Big returns from small fibers: A review of polymer/carbon nanotube composites.* Polymer Composites, 2004. **25**(6): p. 630-645.

286. Gong, X., et al., *Surfactant-Assisted Processing of Carbon Nanotube/Polymer Composites.* Chemistry of Materials, 2000. **12**(4): p. 1049-1052.

287. Ruan, S.L., et al., *Toughening high performance ultrahigh molecular weight polyethylene using multiwalled carbon nanotubes.* Polymer, 2003. **44**(19): p. 5643-5654.

288. Ye, H., et al., *Reinforcement and rupture behavior of carbon nanotubes-polymer nanofibers.* Applied Physics Letters, 2004. **85**(10): p. 1775-1777.

289. Dominis, A.J., et al., *A de-doping/re-doping study of organic soluble polyaniline.* Synthetic Metals, 2002. **129**(2): p. 165-172.

290. Bhadani, S.N., M.K. Gupta, and S.K. Sen Gupta, *Cyclic voltammetry and conductivity investigations of polyaniline.* Journal of Applied Polymer Science, 1993. **49**(3): p. 397-403.

291. Yamamoto, K., M. Yamada, and T. Nishiumi, *Doping reaction of redox-active dopants into polyaniline.* Polymers for Advanced Technologies, 2000. **11**(8-12): p. 710-715.

292. Pruneanu, S., et al., *Characterization of polyaniline by cyclic voltammetry and UV-Vis absorption spectroscopy.* Journal of Materials Science, 1999. **34**(11): p. 2733-2739.

293. Motheo, A.J., et al., *Influence of different types of acidic dopant on the electrodeposition and properties of polyaniline films.* Polymer, 1998. **39**(26): p. 6977-6982.

294. Patil, R.C., et al., *Effect of protonation media on chemically and electrochemically synthesized polyaniline.* Polymer International, 2000. **49**(2): p. 189-196.

295. Brett, C.M.A., et al., *Properties of polyaniline formed at tin dioxide electrodes in weak acid solution: effect of the counterion.* Journal of Applied Electrochemistry, 1993. **23**(4): p. 332-8.

296. Park, Y.H. and C.R. Park, *Preparation of conducting polyacrylonitrile/polyaniline composite films by electrochemical synthesis and their electroactivity.* Synthetic Metals, 2001. **118**(1-3): p. 187-192.

297. Namazi, H., R. Kabiri, and A. Entezami, *Determination of extremely low percolation threshold electroactivity of the blend polyvinyl chloride/polyaniline doped with camphorsulfonic acid by cyclic voltammetry method.* European Polymer Journal, 2002. **38**(4): p. 771-777.

298. Hosseini, S.H. and A.A. Entezami, *Preparation and characterization of polyaniline blends with polyvinyl acetate, polystyrene and polyvinyl chloride for toxic gas sensors.* Polymers for Advanced Technologies, 2001. **12**(8): p. 482-493.

299. Andrieux, C.P., et al., *Fast scan rate cyclic voltammetry for conducting polymers electropolymerized on ultramicroelectrodes.* Journal of Electroanalytical Chemistry and Interfacial Electrochemistry, 1991. **305**(1): p. 153-62.

300. Nunziante, P. and G. Pistoia, *Factors affecting the growth of thick polyaniline films by the cyclic voltammetry technique.* Electrochimica Acta, 1989. **34**(2): p. 223-8.

301. Genies, E.M., M. Lapkowski, and J.F. Penneau, *Cyclic voltammetry of polyaniline. Interpretation of the middle peak.* Journal of Electroanalytical Chemistry and Interfacial Electrochemistry, 1988. **249**(1-2): p. 97-107.

302. Trivedi, D.C., *Dopant induced solubilization of conducting polyaniline.* Indian Journal of Chemistry, Section A: Inorganic, Bio-inorganic, Physical, Theoretical & Analytical Chemistry, 1994. **33A**(6): p. 552-7.

303. Grzeszczuk, M. and R. Szostak, *Redox switching hysteresis in polyaniline-acetate systems: a search of molecular factors important for the dynamics of the polymer reaction.* Journal of Electroanalytical Chemistry, 2004. **571**(1): p. 51-57.

304. Grzeszczuk, M. and R. Szostak, *Electrochemical and Raman studies on the redox switching hysteresis of polyaniline.* Solid State Ionics, 2003. **157**(1-4): p. 257-262.

305. Yang, K.Y., Y.H. Park, and K.C. Go, *Comparison of Electrochemical Properties of Poly(vinyl phenylmethylamine)/Polyaniline Composite with those of Poly(vinyl benzylmethylamine)/Polyaniline Composite.* Molecular Crystals and Liquid Crystals, 2006. **445**: p. 71-80.

306. Nguyen, T.A., et al., *The use of cyclic voltammetry and principal component analysis for the rapid evaluation of selectivity of conductive polymer sensors.* Electroanalysis, 2000. **12**(2): p. 89-95.

307. Thompson, L.A., et al., *Label-Free DNA Hybridization Probe Based on a Conducting Polymer.* Journal of the American Chemical Society, 2003. **125**(2): p. 324-325.

308. Dersch, R., et al., *Nanoprocessing of polymers: applications in medicine, sensors, catalysis, photonics.* Polymers for Advanced Technologies, 2005. **16**(2-3): p. 276-282.

309. Ding, B., et al., *Electrospun nanofibrous membranes coated quartz crystal microbalance as gas sensor for NH3 detection.* Sensors and Actuators, B: Chemical, 2004. **B101**(3): p. 373-380.

310. Wang, X., et al., *Electrospun Nanofibrous Membranes for Highly Sensitive Optical Sensors.* Nano Letters, 2002. **2**(11): p. 1273-1275.

311. Aussawasathien, D. and L. Dai, *LiClO4-doped poly (ethylene oxide) electrospun nanofiber humidity sensors.* Polymer Preprints (American Chemical Society, Division of Polymer Chemistry), 2003. **44**(2): p. 106-107.

312. Liu, H., et al., *Polymeric Nanowire Chemical Sensor.* Nano Letters, 2004. **4**(4): p. 671-675.

313. Genies, E.M. and M. Lapkowski, *Polyaniline films. Electrochemical redox mechanisms.* Synthetic Metals, 1988. **24**(1-2): p. 61-8.

314. Park, Y. and K. Yang, *Comparison of electrical and electrochemical properties between poly(vinyl chloride) and poly(vinyl methylaniline) composites with polyaniline.* Molecular Crystals and Liquid Crystals, 2004. **425**: p. 223-229.

315. Jones, B.J.S. and M. Kalaji, *Influence of electrode geometry on the redox switching characteristics of conducting polymers.* Electrochimica Acta, 2005. **50**(22): p. 4505-4512.

316. Volkov, A.G., S. Paula, and D.W. Deamer, *Two mechanisms of permeation of small neutral molecules and hydrated ions across phospholipid bilayers.* Bioelectrochemistry and Bioenergetics, 1997. **42**(2): p. 153-160.

317. Fenelon, A.M. and C.B. Breslin, *An investigation into the degradation of polyaniline films grown on iron from oxalic acid.* Synthetic Metals, 2004. **144**(2): p. 125-131.

318. Xiao, Q. and X. Zhou, *The study of multiwalled carbon nanotube deposited with conducting polymer for supercapacitor.* Electrochimica Acta, 2003. **48**(5): p. 575-580.

319. Barisci, J.N., G.G. Wallace, and R.H. Baughman, *Electrochemical characterization of single-walled carbon nanotube electrodes.* Journal of the Electrochemical Society, 2000. **147**(12): p. 4580-4583.

320. Dresselhaus, M.S. and P. Avouris, *Introduction to carbon materials research.* Topics in Applied Physics, 2001. **80**(Carbon Nanotubes): p. 1-9.

321. Thostenson, E.T., Z. Ren, and T.W. Chou, *Advances in the science and technology of carbon nanotubes and their composites: a review.* Composites Science and Technology, 2001. **61**(13): p. 1899-1912.